GRAPHENE OXIDE GOLD NANOSTRUCTURE BASED SURFACE ENHANCED RAMAN SCATTERING DNA BIOSENSOR FOR THE DETECTION OF MEAT SPECIES

MD. IBRAHIM KHALIL

INSTITUTE FOR ADVANCED STUDIES
UNIVERSITY OF MALAYA
KUALA LUMPUR

2020

GRAPHENE OXIDE GOLD NANOSTRUCTURE BASED SURFACE ENHANCED RAMAN SCATTERING DNA BIOSENSOR FOR THE DETECTION OF MEAT SPECIES

MD. IBRAHIM KHALIL

THESIS SUBMITTED IN FULFILMENT OF THE REQUIREMENTS FOR THE DEGREE OF DOCTOR OF PHILOSOPHY

INSTITUTE FOR ADVANCED STUDIES
UNIVERSITY OF MALAYA
KUALA LUMPUR

2020

UNIVERSITY OF MALAYA

ORIGINAL LITERARY WORK DECLARATION

Name of Candidate: **Md. Ibrahim Khalil**

Matric No: **HHC150006**

Name of Degree: **Doctor of Philosophy**

Title of Project Paper/Research Report/Dissertation/Thesis ("this Work"):

GRAPHENE OXIDE GOLD NANOSTRUCTURE BASED SURFACE ENHANCED RAMAN SCATTERING DNA BIOSENSOR FOR THE DETECTION OF MEAT SPECIES.

Field of Study: **Biotechnology (Nanobiotechnology)**

I do solemnly and sincerely declare that:

(1) I am the sole author/writer of this Work;
(2) This Work is original;
(3) Any use of any work in which copyright exists was done by way of fair dealing and for permitted purposes and any excerpt or extract from, or reference to or reproduction of any copyright work has been disclosed expressly and sufficiently and the title of the Work and its authorship have been acknowledged in this Work;
(4) I do not have any actual knowledge nor do I ought reasonably to know that the making of this work constitutes an infringement of any copyright work;
(5) I hereby assign all and every rights in the copyright to this Work to the University of Malaya ("UM"), who henceforth shall be owner of the copyright in this Work and that any reproduction or use in any form or by any means whatsoever is prohibited without the written consent of UM having been first had and obtained;
(6) I am fully aware that if in the course of making this Work I have infringed any copyright whether intentionally or otherwise, I may be subject to legal action or any other action as may be determined by UM.

Candidate's Signature Date: 07.07.2020

Subscribed and solemnly declared before,

Witness's Signature Date:

Name:

Designation:

GRAPHENE OXIDE GOLD NANOSTRUCTURE BASED SURFACE ENHANCED RAMAN SCATTERING DNA BIOSNESOR FOR THE DETECTION OF MEAT SPECIES

ABSTRACT

Authentication, detection and quantification of the ingredients, and adulterant in the food, meat and meat products are of high importance in current days. However, the conventional meat species detection techniques based on lipid, protein and DNA biomarkers have been confronting challenges due to the poor selectivity, sensitivity, and unsuitability for processed food products or complex food matrices. Hence, nanoparticle-based DNA biosensing strategies have attracted the most interests and considered as one of the best alternatives to conventional strategies. Among these, surface enhanced Raman scattering (SERS) has gained the substantial acceptance as an excellent, fast and ultrasensitive sensing technique due to its ability to produce molecule specific distinct spectra, narrow spectral bandwidth and multiplexing ability. However, the performance of the SERS DNA biosensor relies on the DNA probe length, platform composition, presence and position of Raman tags and the chosen sensing strategy. Herein, it was demonstrated for the first time SERS DNA sensing for the detection meat species using short-length DNA probe and two different strategies of Raman tag attachment either co-adsorbed with or intercalated in the DNA probe sequences. Moreover, SERS-active dual platforms comprising of graphene oxide-gold nanoparticles (GO-AuNPs), graphene oxide-gold nanorod (GO-AuNR), and AuNPs were used in different combinations. At the first sensing strategy, GO-AuNP functionalized with capture probe 1 (CP1) and AuNPs with co-adsorbed CP2 and Cy3 were used to fabricate the SERS biosensor for the quantitative detection of the Malayan Box Turtle (MBT). Hybridization mediated coupling of the two platforms generated the huge amplified SERS signal which in consequence facilitated to achieve a greater sensitivity with a limit of detection (LOD) of

10 fM (synthetic target DNA) and 100 fM (real sample). In the second strategy, a uniquely designed Raman tag (ATTO Rho6G) integrated signal probe (SP) sequence immobilized AuNPs and the CP DNA functionalized GO-AuNR were utilized to detect the pig species. This biosensing approach showed an outstanding sensitivity with an LOD of 100 aM as well as validated with DNA extracted from pork sample (LOD – 1fM). Finally, a duplex SERS DNA biosensor was fabricated following the same strategy using Cy3 and ATTO Rho6G intercalated SP sequences specific to MBT and pig species respectively as well as GO-AuNPs and AuNPs as sensor platforms for the simultaneous detection of both species. In the presence of the target DNA sequences, covalent linking of the CP functionalized GO-AuNPs and SP functionalized AuNPs triggered the huge SERS signal enhancement due to the multi-component agglomeration. The duplex DNA biosensor exhibited an excellent sensitivity with an LOD of 10 fM for the synthesized target DNA and 100 fM for real sample. Moreover, the fabricated SERS biosensors showed an outstanding selectivity and specificity to differentiate the DNA sequences of the closely related non-target species and the target DNA sequences with single and three nucleotide base-mismatches. The developed short-length DNA conjugated dual platforms based SERS biosensors proved as a selective, sensitive and convenient technology for the detection of single and dual species, hence could be universally applicable for the versatile applications and opted for the simultaneous multiplex detection.

Keywords: Biosensors, Surface enhanced Raman Scattering, Graphene oxide, DNA biosensor, Meat adulteration.

NANOSTRUKTUR GRAPHENE OKSIDA EMAS BERDASARKAN PERMUKAAN MENINGKATKAN PENYERAKAN RAMAN BIOSENSOR DNA UNTUK MENGESAN SPESIS DAGING

ABSTRAK

Pengesahan, pengesanan dan kuantifikasi bahan-bahan, dan bahan noda dalam produk makanan berasaskan daging adalah sangat penting pada masa kini. Walau bagaimanapun, teknik konvensional pengesanan spesies daging berasaskan lipid, protein dan penanda bio DNA telah menghadapi cabaran disebabkan oleh pemilihan dan kepekaan yang kurang baik, dan tidak sesuai untuk produk makanan yang diproses atau matriks makanan yang kompleks. Oleh itu, strategi penderiaan bio DNA berasaskan nanopartikel telah menarik minat yang paling banyak dan dianggap sebagai salah satu alternatif terbaik untuk strategi konvensional. Di antaranya, penyebaran Raman yang dipertingkatkan permukaan (SERS) telah dapat diterima dengan baik sebagai teknik penginderaan yang cemerlang, cepat dan ultrasensitif kerana keupayaannya menghasilkan spektrum berbeza molekul yang khusus, jalur lebar spektrum sempit dan keupayaan pemultipleksan. Walau bagaimanapun, prestasi penderia bio DNA SERS bergantung pada panjang proba DNA, komposisi pelantar, kehadiran dan kedudukan tag Raman dan strategi penderiaan yang dipilih. Di sini, ia telah ditunjukkan untuk pertama kalinya pengesanan DNA SERS bagi mengesan spesies daging menggunakan proba DNA pendek dan dua strategi yang berbeza lampiran tag Raman sama ada secara serapan atau berinterkalat dalam urutan proba DNA. Selain itu, pelantar dwi-aktif SERS yang terdiri daripada partikel nano emas – grafin oksida (GO-AuNPs), batang nano emas – grafin oksida (GO-AuNR), dan partikel nano emas (AuNPs) digunakan dalam kombinasi yang berbeza. Pada strategi pengesan pertama, GO-AuNP difungsikan dengan perangkap proba 1 (CP1) dan AuNPs dengan CP2 dan Cy3 yang diserap bersama digunakan untuk memasang siap penderia bio SERS bagi pengesanan kuantitatif Penyu Kotak Malaya (MBT). Gabungan penghibridan kedua-dua

pelantar menghasilkan isyarat SERS teramplifikasi dengan besarnya yang kemudiannya dipermudahkan untuk mencapai sensitiviti yang lebih besar dengan had pengesanan (LOD) 10 fm (DNA sasaran sintetik) dan 100 fM (sampel sebenar). Dalam strategi kedua, AuNPs diselaraskan dengan isyarat bersepadu Raman (ATTO Rho6G) yang disusun secara unik dan CP DNA difungsikan GO-AuNR telah digunakan untuk mengesan spesies babi. Pendekatan penderiaan bio ini menunjukkan kepekaan sangat luar biasa dengan LOD 100 aM yang 100 kali lebih besar daripada strategi yang disebutkan di atas. Pendekatan penderiaan bio ini menunjukkan sensitiviti yang luar biasa dengan LOD 100 aM serta disahkan dengan DNA yang diekstrak dari sampel babi (LOD - 1fM). Akhir sekali, biosensor DNA SERS dupleks dipasang dengan menggunakan strategi yang sama mengikut urutan SP Cy3 dan ATTO Rho6G berinterkalat SP spesifik bagi spesies MBT dan babi masing-masing serta GO-AuNPs dan AuNPs sebagai pelantar deria untuk mengesan kedua-dua spesies secara serentak. Dengan kehadiran urutan DNA sasaran, pemautan kovalen CP difungsikan GO-AuNPs dan AuNP diprogramkan SP mencetuskan peningkatan isyarat SERS yang besar disebabkan oleh aglomerasi pelbagai komponen. Penderia bio DNA dupleks mempamerkan sensitiviti yang sangat baik dengan LOD 10 fM untuk DNA sasaran disintesis dan 100 fM untuk sampel sebenar. Lebih-lebih lagi, ketiga-tiga penderia bio DNA SERS menunjukkan selektiviti dan kekhususan yang luar biasa untuk membezakan urutan DNA spesies bukan sasaran yang berkait rapat dan juga urutan DNA sasaran dengan satu dan tiga nukleotida berasaskan salah padanan. Penghasilan ukuran-pendek DNA yang dikonjugasikan dwi pelantar berasaskan penderia bio SERS terbukti sebagai teknologi terpilih, sensitif dan mudah untuk mengesan spesies tunggal dan kembar, oleh itu ianya boleh digunakan secara umum untuk aplikasi yang serba boleh dan dipilih bagi pengesanan multipleks serentak.

Kata kunci: Penderia bio, Penyebaran Raman yang Dipertingkatkan Permukaan, Grafin oksida, Penderia bio DNA, Pengadukan makanan.

ACKNOWLEDGEMENTS

All praises to Almighty Allah (SWT), the most merciful, the most gracious and the supreme powerful, who has given me the ability and strength to carry out my research works presented in this dissertation.

First of all, I would like to express my heartfelt gratitude and deepest respect to my supervisors at the University of Malaya, **Dr. Wageeh Abdulhadi Yehya Dabdawb, Dr. Nurhidayatullaili Binti Muhd Julkapli and Professor Dr. Wan Jefrey Basirun** for their utmost guidance, encouragement, and supports throughout my research journey. My sincere acknowledgement for their valuable time, and efforts to supervise me to be successful in my research works. I am remembering with deep respect to Late Professor Dr. Sharifah Bee Abd Hamid and praying peace for her departed soul. I would also like to extend my deepest gratitude to Professor Dr. Mohd Rafi Johan, Director, NANOCAT, University of Malaya for his intellectual supports.

I am very much thankful to Associate Professor Dr. Eaqub Ali for providing the lab facilities in NANOCAT, Dr. Motalib Hossian, Dr. Asing, Dr. Ziaul Karim, Dr. Subrata Saha, and Dr. Emy Marlina for their encouragement, guidance and supports. Special thanks to my fellow lab-members Amit Ranjan Nath, Shahrooz Rahmati, Syed Tawab Shah, Hafiz Ahmed, Lina Al-Ani, Syuhada Abas, Syabilah Sazeli, Muhammad Ariff, Mohammad Shalauddin and others for their cordial assistance, worth sharing of their experiences and creating a wonderful lab environment. I also would like to thank all NANOCAT staffs and faculties for being helpful throughout my research tenure.

I would like appreciate and thank to my respected parents, my siblings and my family members for their sacrifice, support and inspiration. My special acknowledgment to my lovely wife for her unlimited sacrifice, encouragement and love. Finally, lots of love to my two princess, Inshirah Ibrahim and Inayah Ibrahim. Their smiling faces energize me to cross the hurdles and be successful. Thank you very much to all of you.

TABLE OF CONTENTS

Abstract iii

Abstrak v

Acknowledgements vii

Table of Contents viii

List of Figures xiv

List of Tables xix

List of Symbols and Abbreviations xx

List of Appendices xxii

CHAPTER 1: INTRODUCTION 1

1.1 Research Overview 1

1.2 Problem Statement 5

1.3 Scope of the Research 8

1.4 Project Novelty and Hypothesis 9

1.5 Objectives 11

1.6 Outline of the Thesis 11

CHAPTER 2: LITERATURE REVIEW 14

2.1 Overview 14

2.2 Animal Meat and Meat Products in the Food Chain 14

2.3 Prevalence, Pattern and Intensity of Adulteration, Mislabeling and Fraud in Meat and Meat Products 17

2.4 Impact of Adulteration, Mislabeling and Fraud of Meat and Meat Products 19

2.5 Religious Belief and Social Issues 22

2.6 Importance of Malayan Box Turtle in the Food Chain 23

2.7 Importance of Pork in the Food Chain 26
2.8 Current Meat Species Detection Techniques 29
2.8.1 Lipid Based Detection Techniques 29
2.8.2 Protein Based Detection Techniques 31
2.8.3 DNA Based Detection Methods 34
2.8.3.1 Species-Specific PCR Assay 35
2.8.3.2 PCR-Restriction Fragment Length Polymorphism 38
2.8.3.3 Real-Time PCR 38
2.8.3.4 Randomly Amplified Polymorphic DNA 39
2.8.3.5 DNA Sequencing 40
2.9 Nanomaterial Based DNA Biosensors 40
2.9.1 Electrochemical DNA Biosensors 42
2.9.1.1 Fundamental of Electrochemical Biosensing 42
2.9.1.2 Strategies of Electrochemical DNA Biosensing 44
2.9.1.3 Graphene and Graphene-Nanocomposite as Electrochemical DNA Biosensor platform 46
2.9.2 Optical Biosensors 53
2.9.2.1 Fluorescence Based DNA Biosensors 54
2.9.2.2 Colorimetry Based DNA biosensors 56
2.9.2.3 Surface Plasmon Resonance DNA Biosensors 59
2.9.2.4 SERS Based DNA Biosensors 65

CHAPTER 3: SELECTION, VERIFICATION AND MODIFICATION OF THE DNA PROBE SEQUENCES 80

3.1 Influences of DNA Probe Design, Modification and Immobilization in Biosensing Application 80

3.1.1 DNA Probe Design 80
3.1.2 DNA Probe Immobilization Strategies 81
3.1.3 Spacer linked to DNA Probe Sequences 83
3.2 Selection, Verification, Design and Modification of the DNA Probe Sequences for this study 84
3.2.1 Selection of the DNA probes 84
3.2.2 In-silico Analysis of Biomarkers using Bioinformatics Tools 84
3.2.3 DNA Probe Design and Modification - 1 88
3.2.4 DNA Probe Design and Modification - 2 89
3.3 Selection of the Raman labels 91

CHAPTER 4: DUAL PLATFORM AND SHORT-LENGTH DNA PROBE BASED SERS DNA BIOSENSOR FOR THE QUANTITATVIE DETECTION OF MALAYAN BOX TURTLE 94
4.1 Introduction 94
4.2 Materials and Methods 96
4.2.1 Chemicals and Instruments 96
4.2.2 Probe, Target and Non-Target DNAs 97
4.2.3 Collection of the Meat Samples and Extraction of Genomic DNA 98
4.2.4 Synthesis of Graphene Oxide 99
4.2.5 Synthesis of AuNPs 100
4.2.6 Synthesis of GO-AuNP nanocomposites 102
4.2.7 Attachment of thiol-modified DNA probe to AuNPs and GO-AuNPs 102
4.2.8 Attachment of Cy3-cysteamine to Oligo-functionalized AuNPs 105
4.2.9 Fabrication of GO-AuNPs DNA Biosensor 106
4.2.10 Preparation of Samples for SERS Experiment 106

4.3 Results and Discussion 107
4.3.1 Design and Principle of the Biosensor 107
4.3.2 Characterization of GO, AuNPs, and GO-AuNPs nanocomposite 109
4.3.3 Attachment of Capture DNA Probes and Raman Tag to Nanoparticles 112
4.3.4 Justification of the Biosensing Strategy 115
4.3.5 Optimization of Cy3-Cysteamine concentration 118
4.3.6 Analytical Performance of the Biosensor 118
4.3.6.1 Selectivity of the Biosensor 118
4.3.6.2 Sensitivity of the Biosensor 120
4.3.6.3 Dynamic Detection Range of the Biosensor 122
4.3.6.4 Application of the SERS DNA Biosensor for Real Sample Analysis 125
4.4 Conclusion 126

CHAPTER 5: DUAL PLATFORM AND RAMAN TAG INTERCALATED SHORT-LENGTH DNA PROBE BASED SERS DNA BIOSENSOR FOR THE QUANTITATIVE DETECTION OF PIG SPECIES 128

5.1 Introduction 128
5.2 Materials and Methods 131
5.2.1 Chemicals and Instruments 131
5.2.2 Probe sequences, Complementary and Non-complementary Target DNA 132
5.2.3 Collection of Meat Samples and Extraction of Genomic DNA 133
5.2.4 Synthesis of Graphene Oxide 133
5.2.5 Synthesis of AuNPs 133
5.2.6 Synthesis of AuNRs and GO-AuNR composite 133

5.2.7 Preparation of Signal Probe conjugated AuNPs..... 134
5.2.8 Preparation of Capture Probe conjugated GO-AuNR 135
5.2.9 Fabrication of the Sandwich Biosensor and acquisition of SERS Spectra 136
5.3 Results and Discussion 137
5.3.1 Characterization of GO, AuNPs, AuNRs and GO-AuNR..... 137
5.3.2 Attachment of the DNA Probe Sequences onto Sensor Platforms..... 140
5.3.3 Principle and Justification of the SERS DNA Biosensing Technique ... 141
5.3.4 Performance of the Dual Platform based SERS DNA Biosensor 145
5.3.5 Selectivity, Specificity and Reproducibility study of the Biosensor..... 148
5.3.6 Application of the Biosensor for Real Sample Analysis 151
5.4 Conclusion 153

CHAPTER 6: SERS BASED DUPLEX DNA BIOSENSOR FOR THE SIMULTANEOUS QUANTITATIVE DETECTION OF MALAYAN BOX TURTLE AND PIG SPECIES..... 155

6.1 Introduction..... 155
6.2 Materials and Methods 158
6.2.1 Chemicals and Instruments 158
6.2.2 Probe sequences, Complementary and Non-complementary Target DNA. 158
6.2.3 Collection of Meat Samples and Extraction of Genomic DNA 160
6.2.4 Synthesis of AuNPs..... 160
6.2.5 Synthesis of GO-AuNPs..... 161
6.2.6 Preparation of Signal Probe conjugated AuNPs..... 161
6.2.7 Preparation of Capture Probe conjugated GO-AuNP..... 163

6.2.8 Fabrication of the Sandwich Biosensor and acquisition of SERS spectra 164

6.3 Results and Discussion 165

6.3.1 Principle of the SERS Duplex Biosensor 165

6.3.2 Characterization of GO, AuNPs, and GO-AuNPs nanocomposite 167

6.3.3 Attachment of DNA Probe Sequences onto the Sensor platform..... 171

6.3.4 Justification of the Duplex Biosensing strategy 172

6.3.5 Analytical Performance of the Duplex SERS DNA Biosensor..... 177

6.3.5.1 Reproducibility, Selectivity and Specificity of the Biosensor 177

6.3.5.2 Sensitivity of the Biosensor..... 181

6.3.5.3 Application of the SERS DNA Biosensor for Real Sample Analysis 185

6.4 Conclusion 187

CHAPTER 7: CONCLUSION AND RECOMMENDATIONS 188

References 192

List of Publications and Papers Presented 229

Appendix A: Front pages of publications 231

Appendix B: Poster presentation..... 235

LIST OF FIGURES

Figure 2. 1: World meat and poultry consumption shares in 2018. Sources: USDA Foreign Agricultural Service, OECD. Adopted from the Reference (USDA-FAS, 2018a).....16

Figure 2. 2: (a) Top 10 pork-producing countries in 2018, and (b) World pork export shares in 2018. Source: USDA Foreign Agricultural Service. Adopted from the Reference (USDA-FAS, 2018b). 28

Figure 2. 3: General scheme of a Biosensor. Adapted with permission from the Reference (Martins et al., 2013). 41

Figure 2. 4: Classification of the biosensor based on the type of biological signaling and signal transduction mechanism. 42

Figure 2. 5: Strategies for optical sensing of DNA. Adapted with permission from Reference (Vikrant et al., 2019). 53

Figure 2. 6: In the Rayleigh and Raman Scattering process where an amount of energy is exchanged with the sample as shown schematically in the quantum energy level. Here, V_0 and V_1 indicates the incident and transmitted beam intensity respectively. Rayleigh scattering has the same frequency as the incident beam and Raman scattering the frequency is equivalent to $V_0 \pm V_1$. Therefore, $V_0 - V_1$ = Stokes and $V_0 + V_1$ = anti-Stokes. 65

Figure 2. 7: Schematic representation of SERS effect in: (A) an individual nanoparticle. (B) An interparticle gap, hot-spot area with further enhanced Raman signal. Adapted with permission from the Reference (Abalde-Cela et al., 2016). 68

Figure 2. 8: (a) Molecular sentinel-on-chip 'on-to-off', the figure is adopted with permission from reference (Ngo et al., 2013); and (b) inverse molecular sentinel-on-chip 'off-to-on' SERS DNA biosensors, the figure is adopted with permission from reference (Ngo et al., 2014a).....74

Figure 2. 9: Different biosensing strategies. (a) Co-adsorption of Raman tag and DNA probe onto sensor platform; (b) Intercalation of Raman dye in DNA probe sequence for dual platform based biosensor, adopted with permission from the Reference (Kang et al., 2010); and (c) Integrated Raman tag in Reporter DNA for single platform based biosensor, adopted with permission from the Reference (He et al., 2012). 77

Figure 3. 1: Structure of the C6 spacer and C3 spacer. 88

Figure 3. 2: Schematic presentation of the synthesis and modification of the probe sequences. (a) Amino modifier serinol, the core structure of chemically synthesized oligo probe sequence, (b) Synthesis of crude intermediate product containing oligo probe

sequences with an amino group and a C6 S-S at 5′ terminal, and (c) Final crude product comprising of oligo sequences with integrated Raman dye with 5′ C6 S-S. 90

Figure 3. 3: Final structure of the chemically modified oligo probe sequences of (a) MBT with intercalated Cy3, and (b) pig intercalated with ATTO Rho6G.....91

Figure 3. 4: Chemical structure of the (a) Raman dyes Cy3, (b) ATTO Rho6G, (c) Cysteamine, and (d) Cy3 functionalized with cysteamine.....92

Figure 3. 5: UV-vis absorption spectra of (a) the Cy3 and ATTO Rho6G, and (b) the corresponding Raman label intercalated oligo probe sequences. Distinct Raman spectra of the selected Raman labels - (c) Cy3 and (d) ATTO Rho6G.....93

Figure 4. 1: AuNP synthesis using the Turkevich method. The figure was adopted with permission from Reference (Zhao et al., 2013).....102

Figure 4. 2: Synthesis of thiolated oligo-functionalized AuNP. Thiol-terminated oligo sequences displaces citrate ions and forms strong Au–S bond on the AuNP surface. Subsequent addition of NaCl solution minimize the repulsion between the oligo strands and AuNPs, leading to the formation of a dense monolayer of oligonucleotides. The figure was redrawn with permission from the Reference (Giljohann et al., 2010). 105

Figure 4. 3: Schematic presentation of SERS sample preparation. 107

Figure 4. 4: The schematic illustration of SERS sandwich biosensor based on GO-AuNPs and AuNPs dual platforms. 108

Figure 4. 5: (a) XRD patterns, (b) UV-vis spectra and (c) Raman spectra of GO, and AuNP and GO-AuNP.....110

Figure 4. 6: HR-TEM images of (a) GO, (b) AuNP and (c) GO-AuNP on lacy carbon coated copper grid. (d-f) HR-TEM images of hybridized composites by the coupling of two platforms, GO-AuNPs and AuNPs via the hybridization of the CP sequences with the complementary target sequence. As hybridization happened, AuNPs were found mostly aggregated or linked to each other on GO sheets.....112

Figure 4. 7: UV-vis absorption spectra of (a) AuNP, AuNPs-ssDNA and AuNP-ssDNA-Cy3 and (b) GO-AuNPs, GO-AuNPs modified with thiolated CP2, followed by corresponding Target and finally the hybridized composite.....113

Figure 4. 8: AFM topography 2D and 3D images of AuNPs (a-b), AuNPs-DNA (c-d), GO-AuNPs (e-f), and GO-AuNPs-DNA (g-h) adsorbed on mica surface.....114

Figure 4. 9: Raman spectra of AuNPs functionalized with DNA, Cy3 and both DNA and Cy3 (a), GO-AuNP and GO-AuNP functionalized with DNA, Cy3 and both DNA and Cy3 (b). 116

Figure 4.10: (a) SERS spectra of the hybridized composites, representing D and G band of GO at 1355 cm^{-1} and 1590 cm and Cy3 representing peak at 1468 cm^{-1}. (b) Variation of the SERS spectra of Cy3 Raman dye with variable concentration (1 nM to 10 μM). (c) Photographs of the hybridized composites prepared for SERS experiment, in inset the representative spots are marked with black circles, and (d) the corresponding SERS spectra of the hybridized composites 117

Figure 4.11: (a) SERS spectra of the selectivity study using complementary, non-complementary, negative control (blank) and non-target sequences. (b) SERS spectra of the hybridized composites with corresponding (red), single-base mismatch (dark blue) and three-base mismatches (black) target sequences. (c) Stacked SERS spectra for hybridized composites by 10 μM to 1 fM dilutions of MBT target DNA. (d) SERS spectra of the hybridized composites chopped from 1450 to 1480 cm^{-1} to magnify and distinguish the intensity of 1468 cm^{-1} peak. (e) Linear plot of SERS intensities of 1468 cm^{-1} band vs corresponding target DNA concentration. Error bars represent standard deviations of peak intensities from n=3 repeated measurements. 121

Figure 4.12: (a) SERS spectra of GO-AuNPs (red), coupled dual platforms via hybridization without Cy3 (GO-AuNPs-CP1-T-CP2-AuNP) (red) and hybridized composite with Cy3 (GO-AuNPs-CP1-T-CP2-AuNP-Cy3) (blue), and (b) SERS intensity of D-band and G-band value of bare GO-AuNPs, hybridized composite in absence and presence of Cy3. 123

Figure 4.13: (a) The SERS spectra of the hybridized composites coupled by the target DNA extracted from the MBT muscle tissue. The SERS peak at 1468 cm^{-1} dictated the target DNA concentration and observed a gradual decline of the peak intensity with the increment of the target DNA dilution. (b) The linear curve of SERS intensity at 1468 cm^{-1} vs target DNA concentration for the real sample. Error bars represent standard deviations of peak intensities from n=3 repeated measurements. 126

Figure 5. 1: (a) XRD spectra of GO, AuNP and GO-AuNR. UV-vis absorption spectra of (b) AuNPs, AuNPs functionalized with thiolated SP DNA, and AuNP linked SP with partially hybridized target DNA; and (c) GO, AuNR, GO-AuNR, and GO-AuNR functionalized with the CP DNA. 138

Figure 5. 2: HR-TEM images of (a) AuNPs, (b) GO, (c) AuNR, and (d) GO-AuNR samples prepared on lacy carbon coated copper grid. 139

Figure 5. 3: AFM topography 2D and 3D images of AuNPs (a-b), GO (c-d) and GO-AuNR (e-f) adsorbed on mica surface. 140

Figure 5. 4: Schematic representation of the SERS DNA biosensing strategy using GO-AuNR and AuNP platforms. 142

Figure 5. 5: Raman spectra of (a) pure ATTO Rho6G, AuNPs functionalized with SP DNA intercalated with ATTO Rho6G followed by partial hybridization with the

corresponding target DNA, and (b) GO-AuNR, GO-AuNR functionalized with SP DNA and the hybridized composite (GO-AuNR-CP-Target- SP-AuNP). 144

Figure 5. 6: HR-TEM images of the hybridized composites (GO-AuNR-CP-Target- SP-AuNP) at 100 nm (a) and 50 nm (b-d) magnification. The hybridized composites were formed via probe-target hybridization mediated coupling of AuNPs onto the GO-AuNR. In the images, the AuNPs are mostly found attaching to the AuNRs of GO-AuNRs hybrid, indicates the successful hybridization. 145

Figure 5. 7: (a) The stacked SERS spectra of the hybridized composites obtained from the target DNA of pork species from 1 μM to 10 aM, (b) the chopped spectra (1490 to 1520 cm^{-1}) of the hybridized composites (1 μM to 10 aM) to magnify and distinguish the intensity of the peak at 1508 cm^{-1} (c) The linear curve of SERS intensity at 1508 cm^{-1} vs target DNA concentration. Error bars represent standard deviations of peak intensities from n=3 repeated measurements. 148

Figure 5. 8: (a) SERS spectra of the selectivity study of the fabricated biosensors using different DNA sequences -complementary (1 μM), LOD concentration (100 aM), 1 μM concentration of blank sample, single mismatch, triple mismatches and interference samples (non-target sequence of goat, rat, sheep, cow, horse and buffalo), and (b) the corresponding intensity of the SERS fingerprint signal at peak position 1508 cm^{-1}. Error bars represent standard deviations of peak intensities from n=3 repeated measurements. (c) SERS spectra of the hybridized composite (100 pM target DNA) from six different spots, and (d) the RSD of the SERS peak intensity at 1508 cm^{-1} for 6 different spots. 151

Figure 5. 9: (a) The SERS spectra for the hybridized composites by target DNA (100 aM to 10 nM) from real pork sample. (b) The linear curve of SERS intensity at 1508 cm^{-1} vs target DNA concentration for the real sample. Error bars represent standard deviations of peak intensities from n=3 repeated measurements. 153

Figure 6. 1: Functionalization of citrate capped AuNPs with thiol-active probe sequences and the impact of salt aging process. Addition of NaCl in small increments facilitate the attachment of DNA strands and provides stability of AuNPs from irreversible aggregation. Reproduced with permission from the Reference (Liu & Liu, 2017). 163

Figure 6. 2: The schematic illustration of dual platform (GO-AuNP and AuNP) and Raman tag intercalated probe sequence based duplex SERS DNA biosensor..... 167

Figure 6. 3: (a) UV-vis absorption spectra of AuNP, GO and GO-AuNPs. (b) Raman spectra of GO, GO-AuNPs and GO-AuNPs functionalized with CP DNA. TEM images of (c) AuNP, (d) GO, and (e-f) GO-AuNP at 2 μM and 200 nm on lacy carbon copper grid. 170

Figure 6. 4: AFM topography 2D and 3D images of (a-b) AuNPs and (c-d) GO-AuNP adsorbed on mica surface. 171

Figure 6. 5: (a) UV-vis absorption spectra of AuNP, AuNPs functionalized with Raman tag integrated SP sequences and AuNP-SP with partially hybridized target DNA. (b) UV-vis spectra of GO-AuNP, GO-AuNPs modified with both MBT and pig CP sequences and the hybridized composite.....172

Figure 6. 6: SERS spectra of (a) AuNPs functionalized with SP sequences of MBT, pig and both MBT and pig species; (b) GO-AuNP immobilized with MBT SP DNA; (c) GO-AuNP functionalized with Pig SP sequences; and (d) the stacked SERS spectra of GO-AuNP, GO-AuNP functionalized with SP sequences of MBT and pig, and the hybridized composite. 175

Figure 6. 7: TEM images of the hybridized composites at 2 μM (a), 1 μM (b-c) and 200 nm (d) magnifications. The hybridized composites were formed via probe-target hybridization mediated coupling of AuNPs onto the GO-AuNP. In the images, the AuNPs are found onto GO sheets as well as mostly linked to each other, dictates the successful hybridization. 177

Figure 6. 8: (a) SERS spectra of the hybridized composite (10 pM target DNA concentration) from five different spots, and (b) the RSD of the intensity of SERS peaks at 1478 cm^{-1} and 1508 cm^{-1} for the five different spots. (c) SERS spectra of the selectivity study of the fabricated biosensors using different DNA sequences - 1 μM concentration of complementary, single base-mismatch, triple base-mismatches, interference samples (non-target DNA sequences of cow, buffalo, goat, horse and sheep) and blank sample; and the corresponding intensity of the SERS fingerprint peak at (d) 1478 cm^{-1} and (e) 1508 cm^{-1}. Error bars in (d) & (e) represent standard deviations of peak intensities from n=3 repeated measurements. 179

Figure 6. 9: (a) The SERS spectra representing all the produced peaks of the hybridized composite obtained from the serially diluted target DNA (1 μM to 1 fM) of both MBT and pig species. (b) The SERS spectra were chopped from 1460 to 1525 cm^{-1} to reveal and magnify the fingerprint peaks of Cy3 at 1478 cm^{-1} and ATTO Rho6G at 1508 cm^{-1}. Linear curve of SERS intensities at (c) 1478 cm^{-1} and (d) 1508 cm^{-1} band vs corresponding target DNA concentration. Error bars in (c) & (d) represent standard deviations of peak intensities from n=3 repeated measurements. 183

Figure 6. 10: (a) The SERS spectra of the hybridized composite obtained by the addition of a gradually diluted (10 nM to 10 fM) extracted target DNA of both MBT and pork samples. The Cy3 and ATTO Rho6G representing peaks at 1478 cm^{-1} and 1508 cm^{-1} perhaps confirming the presence of both species, showed a steady downward trend with the decreasing target DNA concentration. (b) The linear curve of SERS intensity at 1478 cm^{-1} and 1508 cm^{-1} vs the target DNA concentrations where error bars represent standard deviations of peak intensities from n=3 repeated measurements. 186

LIST OF TABLES

Table 2.1: Protein based techniques for the identification of origin of meat species. 33

Table 2.2: PCR based DNA detection techniques used for the identification of origin of meat species. 37

Table 2. 3: Compositions of the electrochemical DNA biosensors and their application, detection range and limit of detection. 51

Table 2. 4: Optical biosensing strategies, application, detection range and limit of detection. 62

Table 3. 1: The mismatch comparison of the MBT probe sequence against multiple aligned region of cytb gene of MBT and non-target species. 86

Table 3. 2: The mismatch comparison of the pig probe sequence against multiple aligned region of cytb gene of pork and other non-target species. 87

Table 3. 3: MBT DNA Probe sequences and the modifications 88

Table 3. 4: DNA Probe sequences and the modifications 89

Table 4. 1: List of oligonucleotide sequences 98

Table 5. 1: List of the oligo nucleotide sequences 132

Table 6. 1: List of the oligo nucleotide sequences 159

Table 6. 2: SERS peak profiles of the signal probes immobilized onto AuNP, GO-AuNP and hybridized composite. 173

LIST OF SYMBOLS AND ABBREVIATIONS

aM	:	Attomolar
a.u	:	Arbitrary Unit
bp	:	Base pair
cfu	:	Colony Forming Unit
cm	:	Centimeter
DNA	:	Deoxyribonucleic acid
EU	:	European Union
FAM	:	6-Carboxyfluorescein
FAO	:	Food and Agriculture Organization
FDA	:	Food and Drug Administration
fM	:	Femtomolar
g	:	Gram
ID	:	Identification/Identity
lb	:	Pound
h	:	Hour
L	:	Liter
mer	:	The number of nucleotide bases in the oligonucleotide sequence
mL	:	Milliliter
µm	:	Micrometer
µm	:	Micrometer
µM	:	Micromolar
M	:	Molar
min	:	Minute
ng	:	Nanogram

NIR	:	Near-infrared
nm	:	Nanometer
nM	:	Nanomolar
OECD	:	The Organization for Economic Co-operation and Development
pg	:	Picogram
pM	:	Picomolar
Rho6G	:	Rhodamine 6G
RNA	:	Ribonucleic acid
s	:	Second
ss	:	Single stranded
UK	:	United Kingdom
UV-vis	:	Ultraviolet-visible
USA	:	United States of America
USDA	:	The United States Department of Agriculture
vs	:	Versus
w/w	:	Weight/weight
2D	:	Two dimensional
3D	:	Three dimensional
°C	:	degree Celsius
Å	:	Angstrom
%	:	Percent
≤	:	Less than equal to
$	:	United States Dollar

LIST OF APPENDICES

Appendix A: Front Pages of Publications…….. 231

Appendix B: Certificates of Poster Presentation…… 235

CHAPTER 1: INTRODUCTION

1.1 Research Overview

Since the first report of an oxygen electrode ('true' Biosensor) by Professor Leland Qlark in 1956 (Qlark Jr, 1956), and launching of the first commercial glucose biosensor by Yellow Springs Instruments for the direct determination of glucose in 1975 (Yoo & Lee, 2010), researches on sensing technology have been advancing exponentially. Biosensing technologies are of increasing importance in diverse fields such as healthcare, agri-foods, environmental and security sectors, industrial processes which reflects in the continued growth of global markets for such technologies. Fabrication of the biosensors using DNA as the biological recognition element is of immense important for the selective, sensitive and quantitative detection of specific genes, pathogenic microorganisms (Tondro et al., 2018), cancer biomarkers (Huang et al., 2018b; Shahrokhian & Salimian, 2018), trace elements, environmental hazards, drug screening, and the analysis of gene sequences (Li et al., 2005b; Saidur et al., 2017), forensic applications (Yáñez-Sedeño et al., 2014), food safety (Ha et al., 2017) and many more.

Among the technologies available, nanoparticle based DNA biosensing features have attracted the most interests in recent days as excellent screening technique and being considered as cost-effective, sensitive, and potential alternatives to the existing conventional strategies (Merkoçi, 2010). In this regard, DNA biosensors with different sensing principles such as fluorescence (Li et al., 2005b; Zhao et al., 2012), colorimetry (Thavanathan et al., 2014), surface plasmon resonance (SPR) (Diao et al., 2018; Wang et al., 2016a; Zhou et al., 2017), electrochemistry (Khalil et al., 2018; Wang et al., 2015a), SERS (Khalil et al., 2016; Sun et al., 2007) and surface enhanced resonance Raman scattering (SERRS) (Faulds et al., 2008; Faulds et al., 2004) have been reported. SERS is a robust and sophisticated approach which enables single molecule identification by

providing molecule specific vibrational spectra, therefore, considered as one of the most powerful analytical technique for the fast and ultra-sensitive detection of DNA (Kneipp et al., 2006; Nie & Emory, 1997; Pan et al., 2015). SERS has certain advantages over fluorescence, spectroscopy, electrochemistry and some other techniques. For instance, no photo-bleaching from the Raman tags or Raman scattering compound, availability of large number of Raman labels which have broaden up the scope to select the right one according to the experimental design and intended applications, unique spectral fingerprint from the Raman tag upon laser excitation and the narrow spectrum peak widths that opens up the opportunity of high level multiplex detection (Kneipp et al., 2006; Zhang et al., 2010). It is used for both qualitative and quantitative molecular information of the biological samples (Hering et al., 2008). Owing to its low detection limits, narrow spectral bandwidths, ability to quench fluorescence and the capacity to be used with or without optical labels make it an ideal choice for DNA or RNA analysis (Barhoumi et al., 2008; Ni et al., 1990; Vo-Dinh, 2008), genetics and proteomics (Chou et al., 2008), and medical diagnostics (Jarvis & Goodacre, 2008) etc.

SERS phenomenon can be explained by the two enhancement mechanisms, electromagnetic and chemical enhancement. Electromagnetic enhancement is due to the enhanced electromagnetic fields localized to the few nanometers of a nanostructured metallic surface formed by the SPR while chemical enhancement results from the electronic resonance–charge transfer between a metal and the molecule that is strongly chemically adsorbed onto its surface (Khalil et al., 2016; Maher, 2012), consequently increasing the polarizability of the molecule as well as Raman scattering cross section (Tiwari et al., 2007). Moreover, nanoparticle-based SERS signaling is mostly dependent on the hot spots which are the highly localized regions of intense local field enhancement caused by SPR and usually originated in the nanoscale junctions and interstitial crevices of the two or more interacting SERS substrates and consequently provide extraordinary

enhancements of up to 10^{15} orders of magnitude to the SERS signal (Hao & Schatz, 2004; Maher, 2012; Qian et al., 2008; Shiohara et al., 2014). Therefore, metallic nanostructures (NS) of different forms such as nanoparticles, nanorods, nanogaps, nanoshells, nanostars, dimers, and many more as well as combination of different materials have been utilized to explore the hot spots and employed in DNA sensing as it could greatly increase the Raman cross section of the immobilized biomolecules, leading to the amplified SERS intensity and consequently to a low detection limit (Khalil et al., 2016; Lu et al., 2011).

Several metals (such as gold, silica, silver, cadmium etc.) are used either in single, bi-metallic or in combination with other component for the preparation of nanostructures with better surface enhancement and in conjugation with short-length DNA biomarkers to detect species in complex background and even to distinguish single molecule differences. AuNPs are one of the most studied nanomaterials, due to their ease of preparation, remarkable surface chemical properties (Zhong et al., 2004), higher chemical stability and excellent catalytic activity (Han et al., 2009), biocompatibility (Connor et al., 2005) and other notable properties. AuNPs possess unique physiochemical properties such as optical absorption of specific wavelength of light, high electrical conductance with rich surface electrons, and ease surface modification with different chemical groups including sulfhydryl groups. These properties of AuNPs make it a suitable substrate for the attachment of thiolated DNA by the well-established Au-S linkage (Kim et al., 2016), hence, a model component for the detection of DNA (Elghanian et al., 1997; Khan et al., 2013; Li & Rothberg, 2004), proteins (Wei et al., 2007), microorganisms (Phillips et al., 2008) and so on. At present, lots of experiments have been conducted for the detection of DNA using AuNPs as SERS substrate for single or multiplex detection (Cao et al., 2002; Hou et al., 2015; Sun et al., 2007).

On the other hand, graphene (Gr) or the oxidized form of Gr, i.e., graphene oxide (GO), which is the single-atom thick, two-dimensional sheet of sp^2 bonded carbon, is of prime attraction as biosensing element due to its availability, low price, biocompatibility, excellent conductivity, electrocatalytic activity and for the preparation of SERS-active platform (Chen et al., 2008; Chuang et al., 2014; He et al., 2012). Hence, it is highly expected that combination of GO and AuNS to fabricate GO-AuNS hybrid composites will exhibit enhanced SERS signals and lead to excellent responses in diverse biosensing application. It is to be noted that GO-AuNPs showed a SERS enhancement factor up to 10–100 times more than the AuNPs alone (Kong et al., 2013). Moreover, GO-AuNPs have been shown to be the most effective SERS platform by the combination of unique electronic, mechanical and thermal properties of GO and plasmonic properties of AuNPs compared to the individual components (Prinz et al., 2016). In addition, GO-AuNR composites were also used as the sensor platform where AuNRs display two separate SPR bands known as transverse and longitudinal plasmon bands, therefore, contribute in strong SERS activity due to combined electromagnetic and chemical enhancement mechanism, consequently enhance the weak Raman signal. GO-AuNS have been proved as a SERS stable platform (Vianna et al., 2016) for the detection of DNA (Lin et al., 2015) due to easy attachment of the thiolated DNA onto AuNS via popular Au-S bonding, immunoassay of hepatitis B surface antigen (Liu et al., 2018), transferrin (Zhang et al., 2013a), and pesticides (Nguyen et al., 2014).

Till date, lots of SERS based DNA biosensing approaches have been experimented to have better outputs in terms of sensitivity, selectivity and multiplexity of the biosensors (Prinz et al., 2016). A key step in fabricating SERS DNA biosensor is the construction of SERS label either by co-adsorption of Raman Tag (chromophores) and DNA probe on the nanoparticles (Qian et al., 2008) or adsorption of Raman dye conjugated probe DNA (Cao et al., 2002). Moreover, in case of Raman tag conjugated DNA sequence in SERS

biosensor, Raman tags are normally inserted at the terminal end of the capture/reporter DNA sequences and upon hybridization with the corresponding target sequences, the signal carrying molecule (Raman tag) are therefore being positioned a bit far from the sensor platform for single nanoparticle platform based SERS DNA biosensors (He et al., 2012) or kept position at the interstices/junctions of the coupled duplex platforms of sandwich biosensors and enhances the Raman signal dramatically due to the hot-spot generation (Kang et al., 2010). However, the distance of the Raman tag in the intercalated probe sequences to the nanostructure platform has significant role in the SERS intensity, the closer the Raman tag the greater the amplification, hence improved sensitivity of the sandwich assay sensing strategy (Sun et al., 2011; Zou & Schatz, 2006). Therefore, there are few factors that influence the performance of the SERS sensing system such as electromagnetic effect induced by the nanoparticles-aggregated hot-spots, chemical enhancement which is distance-dependent between Raman tag and the corresponding nanoparticles as well as structure, shape, arrangement and composition of the sensor platform. This doctoral work therefore, focuses on the research gap on the SERS based DNA detection techniques and propose a novel idea in designing of short-length probe DNA sequences and the use of dual platforms for the quantitative detection of single and dual species and the sensing strategies could be guided to multiplex meat species detection by a single laser shot.

1.2 Problem Statement

Morphological diagnostic features do not applicable for the degraded or highly treated products, therefore making the microscopic identification tools obsolete for the food forensic studies (Nejad et al., 2014). In addition, lipid and protein biomarker based detection schemes are also proved as less effective because these biomarkers are degraded or denatured at high temperatures, unstable under physico-chemical shocks,

environmental harsh conditions, could be extensively modified during food processing, as well as could not provide the exact source information in a mixed background samples (Ali et al., 2015a; Ali et al., 2012a; Murugaiah et al., 2009; Rahmati et al., 2016). However, some techniques such as liquid extraction surface analysis mass spectrometry got success in the identification of heat-stable peptide markers from raw and cooked meat products (Montowska et al., 2014). Initially, many tests were directed towards the identification of protein fractions in foods using isoelectric focusing (IEF) and Enzyme Linked Immunosorbent Assay (ELISA) (Bottero & Dalmasso, 2011). However, these techniques have also gradually proven less effective due to the low specificity under complex matrices and vigorous processing steps such as chilling, salting, seasoning and heating which induces marked structural modification of proteins (Dooley et al., 2004). Therefore, the limitations experienced by the protein and lipid biomarkers, urge to find the alternative DNA marker based procedures for the detection of meat species or traceability of adultering agents in food products.

DNA is highly stable at high temperature including oven temperature or the sterilization cycle (121°C for 15 min at 15 lb/inch^2 pressure). Therefore, DNA based detection techniques have shown a greater success and been considered as the most acceptable alternative due to the high stability, accuracy and efficiency even in environmentally compromised and highly processed samples (Kang & Tanaka, 2018; Zhang et al., 2007). Among the DNA based detection procedures, polymerase chain reaction (PCR) is the most accepted technique and being considered as the current gold standard (Ngo et al., 2016). PCR based methods include species-specific PCR (Lee et al., 2016), PCR-restriction fragment length polymorphism (PCR-RFLP) (Hossain et al., 2016), randomly amplified polymorphic DNA (RAPD) (Saez et al., 2004), and real time PCR assays with species-specific primers allows qualitative and quantitative detection of single to multiple species present in the meat products (Ahamad et al., 2017; Kang &

Tanaka, 2018; Xu et al., 2018a). However, PCR is quite laborious, time-consuming, and requires relatively bulky and expensive equipment, as well as skilled workers. Moreover, use of short-length DNA biomarker in PCR based techniques is often very challenging for the detection of DNA (Ngo et al., 2016). Usually, the smaller the amplicon length, the better the recovery (Aboud et al., 2010; Ali et al., 2012b; Ali et al., 2012c). High sensitivity in the PCR-RFLP assay for the detection of pork adulteration in commercial products and species detection of marine turtle achieved with the reduction of amplicon length (Ali et al., 2012c; Turna et al., 2010). Short-length amplicons typically ≤150 bp in length improve the better recovery of the detection from the degraded DNA specimens or compromised forensic evidences (Turna et al., 2010), however reduction of amplicon length often limits the PCR based technique by the low specificity, producing artifacts in the final results (Ali et al., 2012a; Hird et al., 2006). Furthermore, utilization of long PCR amplicon limits the detection process specially processed food samples as the DNA are broken down into smaller parts due to the treatments. To overcome these limitations, development of short-length DNA biomarkers unique to species would be a smart choice due to the withstanding capacity even at the harsh food processing treatments and other environmental stresses (Ali et al., 2015a). Hence, nanoparticle-based DNA biosensors are being considered as the best alternative to conserve the specificity and sensitivity at very high level using very short segment of DNA as the detection probe (Merkoçi, 2010).

Nanoparticle based DNA sensing strategies include colorimetric detection by UV-vis spectrophotometry (Ali et al., 2012d), electrochemical (Roy et al., 2016), fluorescence (Li et al., 2019a) and SPR (Muench et al., 2019) biosensors which could be considered as well-replacement techniques to PCR for the high sensitivity but are still limited to the single species detections with very few exceptions (Zhang et al., 2019). On the other hand, SERS which provides intrinsic chemical information and single molecule specific vibrational fingerprints (Nie & Emory, 1997; Pan et al., 2015), has advantages over

colorimetry, fluorescence, spectroscopic, and electrochemistry in terms of multiplex detection (Kang et al., 2010; Kim et al., 2019). Different nanoparticles or nanostructure composites have already been reported as the SERS biosensor platforms such as noble metal nanoparticles, Gr, and Gr-metallic composites. However, Gr alone as sensing platform exhibits some limitations such as Gr in solution is self-agglomerated and it is also unable to covalent attachment of thiolated probe DNA which is the fundamental step in the biosensing fabrication. Therefore, addition of AuNS with GO to form GO-AuNS not only prevents the self-agglomeration by acting as the nano-spacer between the Gr sheets, but also ensure easy attachment of thiolated DNA probe sequences on AuNS by Au-S bonding as well as contribute in SERS signal enhancement. Hence, considering all of the above-mentioned issues and to resolve the research gaps, herein short-length DNA probe based SERS biosensors were approached using GO-AuNS and AuNP as the sensor platforms for the single as well as duplex detection of meat species with greater selectivity and sensitivity.

1.3 Scope of the Research

The title of the thesis dictates the focus of the research works to develop GO-AuNS based SERS DNA biosensors for the sensitive detection of meat species. The key motivation behind this doctoral work is to overcome the limitations experienced by other DNA based detection techniques in terms of stability, selectivity and LOD as well as to establish multiplex detection strategy. Hence, the biosensor fabrication takes favor to resolve these issues by introducing short-length ssDNA markers, dual sensor platforms, sandwich assay strategy and SERS as the detection technique. Short-length DNA markers are of enormous significance in biosensors (Jung et al., 2008), biochip (Iwobi et al., 2011) and forensic applications (Aboud et al., 2010). SERS has emerged as the most powerful analytical technique for the prompt and ultra-sensitive detection of oligonucleotides as

well as capable of doing structural characterization of DNA by providing intrinsic chemical information and vibrational fingerprints of single molecules (Nie & Emory, 1997; Xu et al., 2015). Moreover, utilization of the dual platforms such as GO-AuNS and AuNPs, followed by the aggregation due to the presence of the corresponding target DNA sequences would advances the generation of hot spots which in consequent contribute to enhance the SERS signal. Therefore, combining all of these features – short-length DNA markers as probe sequence, GO-AuNS and AuNPs as sensor platforms and SERS as the detection strategy, could be the best alternative for the fabrication of SERS DNA biosensors. Moreover, selection and design of the probe sequences, availability of the wide range of Raman tags, use of Raman tags either co-adsorption with or intercalated in probe DNA are of remarkable for broadening the scope as well as better performance of the DNA sensors. Therefore, in this doctoral research works, both strategies including Raman tag co-adsorbed with DNA probe sequences onto AuNPs and Raman label intercalated probe DNA sequences linked to AuNPs were implemented for the detection of two different meat species. This work also features an effort to fabricate dual platform based DNA biosensors for the detection of two different target species simultaneously by a single laser shot which in consequent could definitely provide guidelines for the multiplex detection by SERS. In addition, the fabricated biosensors were validated to detect the corresponding target species from the DNA samples extracted from the different real meat samples.

1.4 Project Novelty and Hypothesis

The acceptability, reliability, selectivity and sensitivity of the biosensor devices are solely dependent on the few issues such as the composition of the platform substrate itself, length and orientation of the probe DNA sequences, easiness of the attachment of DNA probe sequences on sensor platform, easy availability of the target DNA for the

hybridization and the detection technique followed. In this study, a novel and efficient dual platform and split DNA probe based SERS biosensor was proposed for the detection of different meat species. The novelty in designing of the probe sequence is that the selected DNA probe sequences were split into two fractions and immobilized onto the two different nanostructure platforms. Presence of the corresponding target sequences, two platforms are coupled via covalent hybridization of probe-target sequences to form sandwich structure, thereby generates locally enhanced electromagnetic field 'hotspot' which therefore significantly enhance the SERS intensity. In the DNA sensing strategies, Raman tag with different fingerprint spectra were either co-adsorbed with probe sequence onto sensor platforms or intercalated in different probe sequences in such a way that could produce Raman dye specific fingerprint signal without any hindrance after DNA hybridization. Moreover, in designing the Raman tag intercalated probe DNA sequences, a unique and novel approach was considered where the Raman tag was inserted at the 5′-terminal of split DNA probe sequences, just immediate after the spacer molecule which ensures no steric hindrance in DNA hybridization rather provide Raman tag specific spectra, signatory for a specific DNA probe. It is also anticipated that Raman tag in probe sequence upon attachment over sensor platforms remain within the few nanometers from the surface, therefore contribute to the SERS intensity by chemical charge transfer mechanism between the nanoparticles and adsorbed Raman tagged probe sequences. Moreover, the concept of using dual platforms is also unique, where coupled two platforms by DNA hybridization facilitate to generate hotspots at the junctions/interstices of nanostructures, consequently contribute significantly to enhance the SERS signal and lead to a greater sensitivity. Therefore, the proposed protocols describe two different biosensing strategies for single and dual species detection with greater selectivity and sensitivity. The research works belong to this thesis are therefore unique and novel as using short-length DNA split probe sequences, two different SERS active nanocomposite

as the biosensor platform, and the expected outcomes would be extraordinary in terms of sensitivity, selectivity and applicability in wide-range of sample formulations. To the best of our knowledge, for the first time herein, the DNA based SERS biosensors are reported for the detection of meat species.

1.5 Objectives

The aim of this study is to develop a short-length ssDNA and two different platform component based SERS biosensor for the sensitive detection of meat species. Theoretical and experimental works are combined to investigate the performance of the biosensor. The specific objectives of this study include:

1. To develop dual platforms (GO-AuNP and AuNP) and co-adsorption of short-length DNA probe and Raman tag based SERS DNA biosensor for the quantitative detection of Malayan Box Turtle.
2. To develop dual platforms (GO-AuNR and AuNP) and Raman tag integrated short-length DNA probe based SERS DNA biosensor for the quantitative detection of pig species.
3. To evaluate GO-AuNP and AuNP platforms and Raman tag integrated short-length DNA probe based SERS DNA biosensor for the simultaneous and quantitative detection of Malayan Box Turtle and pig species.

1.6 Outline of the Thesis

The thesis is written in the article style format and consists of seven chapters briefly described in the following:

Chapter 1 provides a brief overview of the research background, problem statements, addresses the research gap, scope of the research, project novelty and hypothesis of the research study. The chapter is ended with the objectives of this thesis.

Chapter 2 discusses about the importance of meat and meat products as protein sources, provides a detailed review on the food adulterations, prevalence and impact of food fraud, and influence of pork and MBT in the food chain. This chapter also provides a brief review on the conventional meat species detection techniques with advantages and limitations. In addition, the currently available nanoparticles based DNA sensor technologies for the detection of meat species are also discussed. Finally a brief discussion on the background and principles of SERS and a comprehensive literature review on SERS based DNA biosensing in terms of the sensor components, use of single or dual platforms, as well as different amplification strategies with very recent experimental evidences are highlighted. Moreover, the importance of the GO-AuNS as electrochemical and SERS biosensor platform were also discussed in details.

Chapter 3 describes about the selection, design and further modification of the DNA probe sequences of the MBT and pig species for SERS sensing application.

Chapter 4 presents the reaction protocols adopted for the synthesis of GO, AuNPs, and *in situ* synthesis of GO-AuNPs and their characterization techniques including X-ray diffraction (XRD), UV-vis absorption spectroscopy, Atomic Force Microscopy (AFM), Raman, and transmission electron microscopy (TEM). This chapter also explains the design and fabrication of the SERS biosensor for the detection of MBT. In the fabrication process, GO-AuNP and AuNP were used as the platforms and AuNPs were functionalized by the co-adsorption of DNA probe and Raman tag (Cy3).

Chapter 5 describes the synthesis and characterization of GO-AuNR along with GO and AuNPs. In biosensor fabrication, dual platforms – GO-AuNR and AuNP as well as Raman tag (ATTO Rho6G) intercalated probe sequences were utilized for the detection of pig species. Here the influence of Raman tag integration in the probe sequence as well as use of GO-AuNR as sensor platform were evaluated by the sensing strategies.

Chapter 6 demonstrates the fabrication of the biosensor for the simultaneous detection of MBT and pig species. Here, in the biosensor fabrication, GO-AuNPs and AuNPs as the platforms and MBT and pork specific DNA probe sequences functionalized with two different Raman tag, Cy3 and ATTO Rho6G respectively were used. This chapter therefore, highlights the simultaneous detection of two species using dual platforms and Raman tagged probe sequences with simple fabrication process as well as exhibits the validation of the detection technique with real sample analysis.

Chapter 7 summarizes the entire doctoral works that have been presented in this thesis. This chapter includes the conclusion drawn from the findings of the thesis, existing challenges, and suggestions for the possible future works to improve the sensitivity as well as applicability in multiplex detection.

CHAPTER 2: LITERATURE REVIEW

2.1 Overview

This chapter provides an introductory discussion on the importance of meat and meat products as protein sources in the food menu. This chapter also discusses comprehensively about the patterns, occurrences, intensity and the impact of adulteration, mislabeling and fraud in meat and meat products. Moreover, it also highlights the importance of the two meat species such as MBT and pig in the natural ecosystem as well as their existence in the food chain and usage in traditional Chinese medicine (TCM). This chapter therefore presents an overview of the pros and cons of the currently available conventional techniques to recently invented sensor technologies for the detection of meat species in the food ingredients. Moreover, the principles and mechanisms of nanoparticle based DNA detection strategies following different transduction mechanisms in reference to the most relevant and recent research works were also discussed. Next, a brief description of the fundamental principles of SERS, and most importantly the SERS based DNA biosensing in terms of compositions and arrangement of sensor platforms, fabrication strategies and sensitivity were emphasized in reference to the concurrent studies. Considering the various sensor platforms and strategies available, herein this study focuses mainly on the GO and AuNS based dual platforms and SERS sandwich assay detection techniques.

2.2 Animal Meat and Meat Products in the Food Chain

Meat and meat products are generally consumed throughout the world as one of the dietary sources of protein. Of the total global protein consumption, animal protein contributes 40% of the total share. As a consequence, overall global meat consumption is rising simultaneously with the rapidly increasing populations in the world (Leinonen et al., 2019; Lynch et al., 2019). From 1961 to 2011, meat consumption was increased

globally from 23.1 to 42.20 kg/person and the consumption growth rate is expected to be ranked second (1.7% per year) next to vegetable oil (2% per year) by 2021 (Henchion et al., 2014; Sans & Combris, 2015). In addition, it is also predicted that by 2050, global meat consumption will raise by 76%, spurred by population growth, rising income, urbanization, and shifting of dietary intake to protein and calorie-rich Westernized diets in emerging and developing countries (Happer & Wellesley, 2019). Global meat trade was increased by 5% to 30 Metric tons in 2016 in comparison to 2015, where pig meat contributed the highest percentage (9%) (OECD-FAO, 2017). Moreover, the global meat production is also projected to be 13% more in 2026 relative to the base period (2014-2016) (OECD-FAO, 2017). Therefore, the world's livestock sector is also growing faster to meet the growing demand for high-value animal protein. The main sources of animal proteins for human consumption include poultry, pigs, cattle, sheep, buffaloes, and goats; to a lesser extent camels, yaks, deer, ostriches, and game animals while in very limited extent the exotic animals such as turtle, crocodiles, snakes and lizards are also considered as meat sources and have regional preferences as well (FAO, 2014). Among all protein sources, pork is the most widely consumed meat across the countries in the world which accounts for over 40% of the world's meat intake in 2018, followed by chicken and beef with more than 33 % and 21%, respectively (Figure 2.1) (USDA-FAS, 2018a). Unlike bovine meat, pork is generally consumed at little quantities as well as in processed form rather than fresh meat. As a consequence, animal meats in different formulations, forms or compositions have been getting entry into the commercial food chain such as minced meat, sausages, meatballs and burger patty which are the most commonly and widely consumed around the world regardless of the brands, geographical and ethical preferences (Qiu & Hou, 2020; Laestadius & Wolfson, 2019). Moreover, processed meat products are popular due to their distinct flavor, tastes and high nutritional values as well as have

preferences of the customers due to the ready-made, ready-to-heat or ready-to-consume with less effort and time-saving features (Laestadius & Wolfson, 2019).

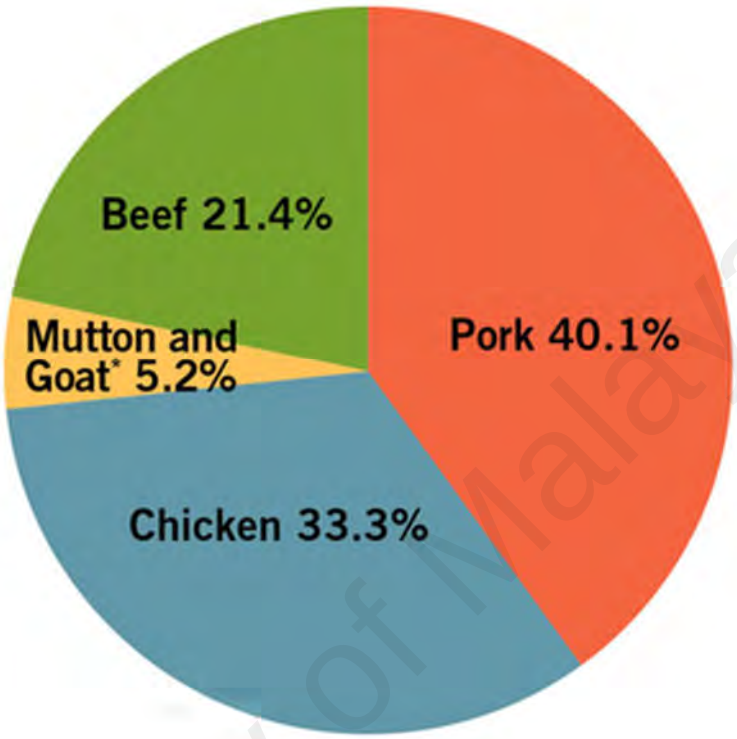

Figure 2. 1: World meat and poultry consumption shares in 2018. Sources: USDA Foreign Agricultural Service, OECD. Adopted from the Reference (USDA-FAS, 2018a).

The demand of meat and meat products are increasing very rapidly across the globe. To cope with huge demand for the vast population, especially in developing countries, the food manufactures are also facing challenges to support the market demand for both raw and processed products (Delgado, 2003; Henchion et al., 2014). Therefore, escalating prices of commercial meat products, globalization of food trade, and processing of meat into value-added products in large extent; the incidences of species substitution, adulteration and fraud-labeling of meat products have become a commonplace to get illegal financial benefits. Though substituting or admixing of undeclared species in the meat products is illegal and not acceptable by the food safety regulatory authorities of almost every country of the world, lots of species substitution, particularly beef and

mutton substitution by pork, buffalo and horse meat in many instances have been reported (Cawthorn et al., 2013; Hossain et al., 2017a).

2.3 Prevalence, Pattern and Intensity of Adulteration, Mislabeling and Fraud in Meat and Meat Products

Food adulteration is defined as the act of degrading the quality of food products by fraudulent admixing or substitution of low-grade ingredients by its higher value counterparts for financial or other additional benefits (Rahman, 2015). Meat adulteration may be intentional which involves the addition or substitution of high value meat species with cheaper one or addition of undeclared plant proteins. On the other hand, unintentional entry of undeclared meat species occur in some instances due to the ignorance, inadequate hygiene or cross-contamination from improperly cleaned equipment used to process multiple meat species at the same time (Cawthorn et al., 2013; Flores-Manguia et al., 2000). According to the Food Standards Agency (FSA) UK, food fraud is the deliberate placement on the market for financial gain, with the intention of deceiving the consumers either by selling unfit and potentially harmful food or by providing intentionally the misleading or misdescription of the foods (Johnson, 2014; Rahman, 2015).

Food adulteration or fraud, specifically meat and meat products, has therefore become a common issue in the world nowadays. Lots of cases on mislabeling of meat and meat products have been reported and the trends reflect that the practice is ongoing extensively throughout the world, even in the highly regulated markets of the developed countries. For example, it was reported that 68% meat products in South Africa, 19.4% in the USA, 33% in the Gulf countries, 22% in Turkey and 8% in the U.K were mislabeled (Hossain et al., 2017a). An investigation on the 143 prepacked beef and poultry products sold at local and international supermarket chains in Malaysia, was conducted by multiplex PCR

experiment. 78.3% of the samples were found mislabeled, attributed by the false declaration of species and/or presence of undeclared meat species (Chuah et al., 2016). A market surveys on the labeling of meat and meat products in Mexico, Turkey and South Africa dictates the mislabeling rate was about 20-70%, while another lab testing of processed meat products in South Africa indicates 68% of the samples were adulterated with non-declared species (Kane & Hellberg, 2016).

In China, mutton products are very popular food items all the year round, therefore adulteration of mutton with low cost meat are very frequent and lots of incidents were reported in recent years. For example, adulteration of mutton samples with duck meat and pork was reported in Suzhou market in 2013 while mutton admixed with pork, duck and chicken (40.8%) was reported in Beijing market in 2014 (Jin et al., 2014; Li et al., 2016a; Li et al., 2019b). Moreover, few incidents such as rat meat sold as lamb; fox, mink, and rat meats processed with gelatin to comply as lamb; fake beef prepared by chemically treating the pork were reported in China (Ali et al., 2014), therefore intensify the level of adulteration/fraud of meat and meat products. However, meat adulteration/mislabeling/ substitution is not only confined to the conventional meat species but also includes some unconventional species in very low extent such as donkey, goat and water buffalo (Cawthorn et al., 2013), game meat species and near-threatened or vulnerable species (Quinto et al., 2016). A recent survey conducted by Clear Labs at northern California in USA, using burgers of 79 brands from 22 retailers and fast food chains, reports that around 14% of the samples were adulterated by either pork DNA in beef burger or beef DNA in ground lamb, 4% of samples were found contaminated with food-borne illness causing pathogenic microorganisms and surprisingly in few instances positive for human and rat DNA (Kowitt, 2016).

The EU meat scandal which had shaken the world in sense of food safety and security, due to the presence of undeclared horse meat in 61% of the tested lasagna products claimed and labeled as 100% beef by a survey conducted by FSA in 2013 (Brown, 2013; Kane & Hellberg, 2016). Similarly in the same year, FSA of Ireland published a small survey report on the testing a number of beef burger products, and salami where 37% of the products were found positive for horsemeat and 85% of the products contained pork. This horse meat scandal therefore spreads to many EU countries and consequently become a global issue (Walker et al., 2013). Aftermath of this horse meat scandal, countries particularly dependent on the imported meat products as well as where the meat consumption patterns are based on cultural preferences and religious beliefs, testing of processed meat products became a must do. As part of it, raw and processed meat products imported in the Arabian Gulf region were checked for adulteration by DNA based detection technique and results showed the presence of 7% of horse and 26% of pork DNA of the total 105 tested samples (Bourguiba-Hachemi & Fathallah, 2016). Another remarkable report which received global media attention and intense public outrage specifically from the Muslim countries, was the presence of pork DNA in the Cadbury chocolates in Malaysia in 2014 (Ahmad et al., 2018; Jaques, 2015). The above mentioned incidents are only very few among the thousands of reported studies on animal meat adulteration, food-forgery or mislabeling, have been happening throughout the world but sufficient enough to understand the intensity of ill-acts.

2.4 Impact of Adulteration, Mislabeling and Fraud of Meat and Meat Products

Deceiving consumers by selling adulterated, mislabeled or fraud foods is not a current issue. In spite of getting some instant economic benefits, food fraud has both short term and long term impacts, affects not only the consumers but also the manufacturers, regulators, industry, and local or international trading partners by imposing mistrust the

food supply chain, and consequently lead to market and trade disruptions (Esteki et al., 2019). The most common form of corrective action after getting confirmation about the adulteration or food fraud is the recall of the products from the retail shops. For example, according to U.S. Department of Agriculture's Food Safety and Inspection Service (FSIS), a fully Hazard Analysis and Critical Control Points (HACCP) implemented company in USA, had to recall approximately 12,566 pounds of beef, pork, and poultry products in 2015 due to misbranded of undeclared ingredients (FSN, 2015). Ranch Foods Direct of Colorado Springs CO., USA recalled about 2600 pounds of non-intact beef products due to the contamination of pathogenic *Escherichia coli* O157:H7 as announced by the FSIS in 2016 (FSN, 2016). Another report by FSIS in 2018 on the recall of 65,000 pounds of various ready-to-eat and raw meat and poultry products which was due to not listing the allergens on the finished product label (FSN, 2018). Recently, more than 3,300 pounds of ready-to-eat meat and poultry products were recalled in Texas by the Great American Marketing Inc. of Houston, USA due to the presence of *Listeria monocytogenes* which was found on a shared FSIS and FDA processing area in the established production facility (Mackin, 2019).

Moreover, food adulteration also put consumer on serious health risks due to the presence of certain undeclared ingredient which is allergic to certain people, or presence of harmful microorganisms in meat products which are the causes of zoonotic diseases such as food-borne illness and certain chronic disorders (cancer, and cardiovascular diseases), therefore even lead to the death in few instances (Nizar et al., 2018; Bansal et al., 2017). It was reported that approximately 75% of the new and emerging human diseases have been caused by pathogens originating from animals or from products of animal origin (Formenty et al., 2011; Karesh & Machalaba, 2012). A comprehensive literature survey on 1415 infectious human pathogenic organisms, 868 (61%) were identified as zoonotic and of the total, 177 were considered as emerging (Taylor et al.,

2001). Another study based on the database of emerging infectious diseases (EID) from 1940 to 2004, concluded that EID is dominated by zoonoses (60.3% of EIDs) while the majority of the zoonoses (71.8%) are originated from wildlife (severe acute respiratory virus, Ebola virus) and are increasing significantly over time (Jones et al., 2008).

In this context, meat and meat products are the potential carriers of several pathogenic organisms in addition to some chemical agents which are the cause of serious threats to public health, and lead to regional to global emergency (Scallan et al., 2011). Such as, a major food crisis, known as 'Belgian polychlorinated biphenyls (PCBs)/dioxin crisis' which was caused by the accidental introduction of PCBs and dioxins to a stock of recycled fat using for the animal feed production in Belgium in 1999 (Covaci et al., 2008). The extent of poisonous effect was so severe that more than 2500 poultry and pig farms were affected, exerted restriction to slaughter and transport of poultry, cattle and pigs nationally. The country had experienced economic adverse effects due to the import ban imposed by many countries while USA banned imports of all sort of poultry and pork even from all European countries for a short period of time (Covaci et al., 2008). It is estimated that the incident costs more than 1 billion Euro from the Belgian Treasury, and the worst consequences was the resigning of the Minister of Agriculture, followed by the Minister of Health and eventually collapse of the whole Belgian government (Kennedy et al., 2009). Few other dioxin incidents include the presence of elevated levels of dioxin in milk in Netherland in 2004, in animal feed due to the contaminated fat used in feed production in the Netherlands in 2006, and the latest one is the Irish pork contamination in 2008 which forced to decide the authority a global recall of Irish pork as a precautionary measure and public health concern (Kennedy et al., 2009).

2.5 Religious Belief and Social Issues

Religions have strong influence on the consumer's attitude and behavior in general, selection of food ingredients, menu, and purchasing and consumption habits in particular throughout the human civilization (Bonne & Verbeke, 2008). Almost every religion has its own proclamation regarding the human food consumption, food ingredients of either allowed or non-allowed. According to Islamic Law, Muslims are not allowed to eat pork or pork derived products, non-permissible body parts such as blood and plasma from halal (permissible) animals and even meat of the halal animals which are not slaughtered ritually (Karahalil, 2020; Nakyinsige et al., 2012). Similarly, for Jewish the animal's ingredient must need to conform the kosher laws (Regenstein, 2020). According to both Muslim and Jewish laws, pig meat and pork derivatives are strongly prohibited as pig does not fulfill the criteria of an animal to be permissible such as features of split hooves and chew the cud (Regenstein et al., 2003). On the other hand, beef and beef-derived food products are legal for Muslim, Jewish and Christian communities while strongly restricted to the followers of Hinduism though milk is allowed to take (Meyer-Rochow, 2009). Halal animals includes cows, sheep, goats, poultry, buffaloes, camel, ostrich, turkey etc. if they are slaughtered according to the Muslim Sharia law while major non-halal species include pork, dog, cat and many more. In fact, most of the religious guidelines promote healthy lifestyle and restrict to consume the foods that cause illness. For example, 'Halal' in current days, is a concept of a product or food-catering service which ensures hygiene and cleanliness of production environment, safety for consumption and next benchmark for quality. Halal foods, nowadays, are not the foods from religious concept rather representing a global sign of healthy and quality products (Mathew, 2014). Consequently, Halal food market is expanding very rapidly and integrating with the mainstream market due to the increasing Muslim populations globally as well as its huge appeal to other non-Muslim communities too (Hanzaee & Ramezani, 2011). Likewise, culture and social

lifestyle also has significant role in food selection or consumption patterns. Therefore, meat adulteration or fraud or substitution is a sensitive issue in terms of cultural, social and religious perspectives which may provoke to destroy the social harmony (Al Amin et al., 2020). It is immense important to ensure that meat and meat products are not adulterated, rightly packaged, labeled and marketed for the well-being of public health, to conform religious integrity, and fair-trade economic practices in food businesses.

2.6 Importance of Malayan Box Turtle in the Food Chain

Turtles and tortoises have existed on the earth for around 300 million years, since the Triassic Era, long before many dinosaurs walked through. They belong to the reptile umbrella and include nearly 460 different varieties around the world. At present, turtles are being considered as the most endangered clade of vertebrates on earth and according to International Union for Conservation of Nature and Natural Resources (IUCN), out of 293 Red-listed freshwater turtles and tortoises, 88 species are found in Asia. Among the total turtle species in the world, 3% are already extinct, 9% are critically threatened, 18% are threatened, and 2% are at high risk in different habitats. However, In Asia the percentages of turtles are as already extinct 1%, critically endangered 20%, endangered 31%, and vulnerable 25% (Ali et al., 2016; Asing et al., 2016; Fund, 2002). Regardless of high volume exploitation by local and international illegal traders in combination with its slow reproductivity, the other causes of extinction particularly in Malaysia include rapid and extensive destruction of tropical forests, drainage and irrigation works, unregulated chemicals and pesticides in the paddy field. The MBT which belongs to the genus *Cuora*, is a mostly distributed hard-shelled turtle species in South Asia and South East Asian countries (Schoppe, 2008). MBT has been categorized as vulnerable by the IUCN and also enlisted as endangered species in Appendix II of the Convention on International Trade in Endangered Species of Wild Fauna and Flora (CITES). As a

consequence, Department of Wildlife and National Parks of Malaysia and the Malaysian government have jointly banned the export of MBT and other turtle species to other countries (Ali et al., 2015a; Schoppe, 2008).

Since long before, animal tissues of various wildlife such as tiger bones, antelope, buffalo or rhino horns, deer antlers, dog testicles, bear or snake bile as well as different body parts of turtles are being used as active ingredient in TCM. One study based on genetic analysis of TCM samples revealed that 50% of the samples contained undeclared pharmaceutical agents, plant or animal species including an endangered species of *Panthera* (snow leopard), and high level of heavy metals (Coghlan et al., 2015). This traditional medication has been continued from generation to generation based on the belief and rituals though have almost very little scientific evidences. It is believed that the bones, shells, skins and eggs of turtle and tortoise species possess active healing powers and stimulating agent for the long-term restoration of youth and sexual life (Graham-Rowe, 2011). Both meat and shells of the turtles have high demand in international markets as well due to their use in tonics and foods and in antipyretic, analgesic and invigorating medicines. Moreover, MBT has huge appeal as pets in Europe and North America, and an exotic food item. As a consequence, MBT species is extensively captured by local hunters for the meat, shells and bones for illegal trades in local and international markets. Therefore, this huge demand in local and international markets, MBT and other turtles are the lucrative items, encourage for the illegal trafficking (Ali et al., 2015b).

In 2002, a report indicated that every year more than 10 million of live Asian box turtles (*Cuora*) are imported into southern China from Southeast Asian countries (Fund, 2002). A statistical report on customs trade from 1999 to 2008 in Taiwan reported that 1989 metric tons shells of hard-shelled turtles with an average of 198.9 metric tons/year

and 290 metric tons soft-shell turtle shells, averaging 29.0 metric tons/year have been imported to fulfill the demand for TCM market. This huge consumption dictates that millions of turtles and tortoises have been killed annually for TCM market in Taiwan only (Chen et al., 2009). In 2008, a record haul of 10000 eggs of endangered turtles were seized by Malaysia police in Sabah state while 4.3 metric tons of reptiles including lizards, snakes, freshwater turtles and tortoises at the Thailand–Malaysia border area in 2010 (Asing et al., 2016). In 2015, a huge shipment of illegal freshwater turtle meat labelled as fish meat from more than 4,000 turtles valued at US$6 million bound for Hong Kong was seized at Karachi port in Pakistan (Woodhouse, 2015). In 2016, Wildlife Crime Unit of Malaysia seized 1,070 tortoises and turtles of two different species in two raids (Bernama, 2016). Moreover, a report entitled "Operation Dragon: Revealing new evidence of the scale of corruption and trafficking in the turtle and tortoise trade" in a press release by the Wildlife Justice Commission (WJC) in the Netherlands, had brought to the light the multi-million-dollar illegal trade of endangered reptile species in South and Southeast Asia. WJC had exploited an illegal turtle trade network over the period of 2 years long investigations (2016-2018) which led to the seizure of more than 6,000 live turtles and tortoises ranging from vulnerable to critically endangered, worth $3 million wholesale value, hence break down the chain of eight wildlife trafficking networks, and arrested 30 traffickers (WJC, 2018).

Turtles are the natural scavengers and they eat vegetable, fallen fruits and soft invertebrates such as worms and slugs, and waste materials in wetland, hence its temporary or permanent removal from its natural habitats is not only threat for their extinction but also lead to an imbalance in the ecosystem. On contrary, as a natural scavenger of waste materials, turtles are the carrier of several pathogenic bacteria, parasites, various biotoxins and heavy metals, hence consumption of or contact with turtles and/or turtle-derived materials in food chains and medicines have significant

health concerns (Green et al., 2010). There are some incidents over foodborne illness due to the consumption of turtle meats such as a chelonitoxism outbreak caused from consuming turtle meat and turtle meat soup among the residents of a coastal village in Eastern Samar, Philippine in 2013 and as a consequence 4 person of different age group were died (Ventura et al., 2015). Besides, consumption of turtle-derived materials has a significant religious and social impact as it is forbidden by certain religions specifically in Islam (Asing et al., 2016). It therefore, urges for the reliable authentication technique to detect this turtle species whether substitution of or adulterated by turtle ingredients in common foods to restrict the health hazards and consequently to prevent or reduce illegal trades.

2.7 Importance of Pork in the Food Chain

The ancestor of the domestic pig is the wild boar (*Sus scrofa*). An extensive zooarcheological record suggests that pigs were first domesticated around 9000 years ago in the Near East and another archaeological and genetic evidences indicate a second major independent domestication centre in East Asia (China). However, another study based on mitochondrial DNA diversity data reveal that the origin of wild boar was in South East Asia and the domestication was followed by multiple centers across the Eurasia and Europe. It is also considered that the wild boars are the principal source of modern European domestic pigs (Larson et al., 2005; Rischkowsky & Pilling, 2007). Pigs are very versatile and spreading very quickly in the areas in which they have been (re)-introduced, hence now they are available throughout the world. The scientific name of the wild and domestic pigs belong to the same species (*Sus scrofa*) although some scientists classified the domestic pig under the subspecies *Sus scrofa domesticus*. According to the data provided by the USDA Foreign Agricultural Service in 2018, China is the topmost pork producing country (54,040,000 metric tons), followed by the European Union (EU) and

USA (Figure 2.2a) while EU contributed to the highest share (35%) of pork export over the world and USA hold the 2nd position (31%) (Figure 2.2b) (USDA-FAS, 2018b). According to OECD-FAO, EU is the highest pork consuming country (34.8 kg/capita), is Vietnam is the second (32.8 kg/capita) and China ranked the third position (32.1 kg/capita), followed by Korea (31.5 kg/capita) and USA (23.6 kg/capita) (OECD, 2020).

However, feral pigs are being included among the "100 of the world's worst invasive alien species" by the World Conservation Union's Invasive Species Specialist Group, because they are recognized as major contributor of extinction and ecosystem change. They are also considered as the potential carrier/source of the exotic diseases in human and animals such as Aujeszky's disease, a viral swine disease followed by infecting cattle mostly but also Rats, dogs, horses and wild animals like panthers as secondary hosts results in the disease named mad itch (Anonym, 2018; Gingerich, 2006). They also represent a potential source of other diseases like pseudo rabies, trichinosis, swine brucellosis, and leptospirosis which are fatal to humans. Some other diseases such as leptospirosis, Japanese encephalitis, toxoplasmosis and foot and mouth disease (FMD) causing agents are also shaded by the feral pigs (Anonym, 2018; Gauss et al., 2005). In California in 2006, an *E. coli* outbreak due to spinach contamination was led to the death of three people and the followed by investigation identified the root cause, the transmission of pathogenic *E. coli* strain from feral pigs to spinach fields from the nearby cattle pastures. These parasitic infections are normally transmitted to humans by eating undercooked pork or through contact (Anonym, 2018). Moreover, consumption of pork and pork meat products has also religious restriction for the Muslim, Jewish, and certain Christian denomination.

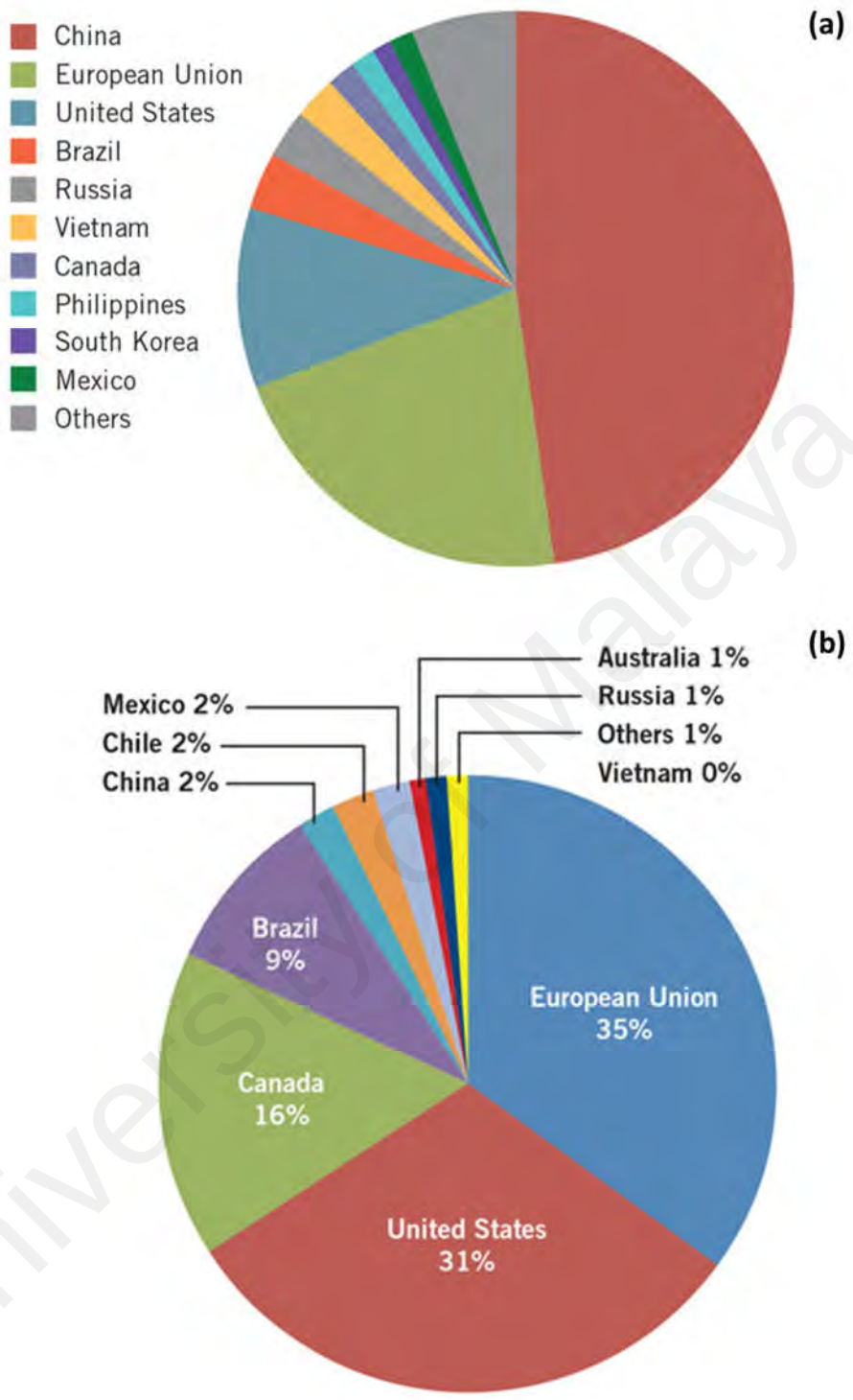

Figure 2. 2: (a) Top 10 pork-producing countries in 2018, and (b) World pork export shares in 2018. Source: USDA Foreign Agricultural Service. Adopted from the Reference (USDA-FAS, 2018b).

From the above literature, it is summarized that adulteration and/or mislabeling is a common issues since many years to dill date and possibly a never ending issue. However, consumers are now concern about the food adulteration/fraud/substitutions, to know the composition and origin of meat and meat products, about the appropriate labelling of the products with exact descriptions. These are therefore highly demanded in today's world to secure the individual's food choice, public health safety, reserve the traditional, cultural and religious coherences, to conserve social harmony and finally fair trade and smooth business growth. Therefore, irrespective of manufacturing methods and practices, authentication of the food ingredients would be the key criteria to satisfy the consumers which in fact depends of the technology we adhere.

2.8 Current Meat Species Detection Techniques

Lots of researches have been conducted throughout the world for the development of an ideal, facile, selective and sensitive technique for the qualitative and/or quantitative detection of animal species due to ever-increasing meat and meat products fraudulent issues (Ali et al., 2014). Morphological and microscopic tests are currently being considered as obsolete/inappropriate for the detection of meat species particularly in processed meat products as well as the incompetence to determine the exact animal species in food staff (Ali et al., 2012a; Cammà et al., 2012). However, lipid, protein and DNA biomarkers based different analytical techniques have been reported for the authentication of species origin in meat and meat products.

2.8.1 Lipid Based Detection Techniques

Lipid based meat species detection techniques are generally based on the analysis of positional distribution of fatty acids in triacylglycerols (TAGs) and 2-monoacylglycerol (2-MAG). All the species except pigs generally conserve monoenoic and n-6 polyenoic

fatty acids in TAGs and possess long chain length and unsaturation at the sn-2 position. In contrary, lard contains greater percentage of saturated fatty acids in the 2-position of the TAGs in compare to other animal fats, therefore, considered as a lipid biomarker for the differentiation of animal fats (Jaswir et al., 2003; Szabo et al., 2007). Admixture of foreign fat in lard were determined by Boemer number method which relies on the differentiation of melting points of TGA and fatty acids, is large for lard and small for other fats such as beef tallow (Jaswir et al., 2003). Numerous analytical methods such as differential scanning calorimetry (Nakyinsige et al., 2012), gas chromatography (GC) (Indrasti et al., 2010), high pressure liquid chromatography (HPLC) (Marikkar et al., 2005) and Fourier transform infrared spectroscopy method (FTIR) (Rohman et al., 2011) have been used for the detection of lard contaminated by other animal fats and vice versa as well as analysis of lard in different food products (Nurrulhidayah et al., 2015).

FTIR spectroscopy combined with chemometrics of partial least square was applied for detecting and quantifying of pork adulteration in some vegetable oils (Rohman et al., 2011), body fats of lamb, cow, and chicken (Rohman & Che Man, 2010) and beef meatballs (Rohman et al., 2011). Nizar et al. (2013) conducted a study to discriminate lard from poultry and other animal fat using Gas Chromatography Mass Spectrometry (GC-MS) and Elemental Analyzer–Isotope Ratio Mass Spectrometry (EA-IRMS). In a study, it was proved that the ratios of carbon isotope in the bulk carbon is a better indicator to discriminate the animal fats than the direct comparisons among the fatty acids (Nizar et al., 2013). However, some of these methods are laborious, time consuming, expensive and sophisticated instrumentation dependent. Though the positional distribution of fatty acids in TAGs and 2-MAGs have shown success for the identification of species, the content and varieties of TGAs and 2-MAGs are generally modified by the food processing or cooking treatments. Therefore, lipid biomarkers based specifies detection techniques in food and food stuff have limitations due to its reliability.

2.8.2 Protein Based Detection Techniques

Protein or peptide biomarkers are most commonly used for the detection or differentiation of animal species using different sophisticated instrumentations such as GC-MS (Estévez et al., 2003), liquid chromatography (LC) (Chou et al., 2007), HPLC (De Mey et al., 2012), liquid chromatography–electrospray ionisation–mass spectrometry (Armenteros et al., 2009), liquid chromatography-mass spectroscopy (LC-MS) (von Bargen et al., 2013), ultra-performance liquid chromatography tandem mass spectrometry (UPLC-MS/MS) (Scheijen et al., 2016), liquid extraction surface analysis mass spectrometry (LESA-MS) (Montowska et al., 2014; Montowska, Alexander, Tucker, & Barrett, 2015), and mass spectrometry (MS) (Marbaix et al., 2016). Moreover, vibrational spectroscopy (Abbas et al., 2018; Ellis et al., 2005), electrophoretic methods (Montowska & Pospiech, 2007), capillary electrophoresis (CE) (Cota-Rivas & Vallejo-Cordoba, 1997; Papetti & Colombo, 2019; Vallejo-Cordoba et al., 2005), and immunoassay techniques such as enzyme-linked immunosorbent assay (ELISA) (Asensio et al., 2008; Nhari et al., 2019; Thienes et al., 2019) have also been used for the identification of meat adulteration using protein biomarkers. Protein based techniques for the identification of origin of species in meat samples are summarized in the Table 2.1.

Histidine dipeptides such as carnosine (ß-alanyl-Lhistidine), anserine (ß-alanyl-L-1 methylhistidine), and balenine (ß-alanyl-L-3 methylhistidine) which occur naturally in organ specific tissues of some vertebrates and are absent in plant sources, therefore, is a characteristic component of the animal species as well as differentiating marker between mammals and nonmammals (Aristoy & Toldrá, 2004). Theses peptide biomarkers have shown better stability to heat treatment and exposure to high temperature (120°C for 20 min), therefore used as marker to differentiate the processed meat products by knowing the ratio of these dipeptides employing cation exchange HPLC method (Aristoy & Toldrá,

2004). HPLC which is mostly based on the differentiation of the profiles of proteins, peptide and/or amino acids, proved as comparatively sensitive and reproducible technique for the routine analysis of meat identification.

Immunological methods, such as ELISA has been proved as suitable and popular techniques for the species authentication studies due to its low cost, simplicity, high selectivity and sensitivity (Asensio et al., 2008). Until now, various studies have been reported for the authentication of food products by using both monoclonal antibodies (MAbs) and polyclonal antibodies (PAbs) based on structural and soluble muscle proteins. For example, sandwich ELISA was applied using PAbs as biomarker for the detection of adulterated raw pork in raw beef mixture with the quantification limit up to 1% (Martin et al., 1988), quantification of pork in heat treated meat products using MAbs against heat-stable muscle protein of pig with LOD 0.5% (w/w) which was further verified by the commercial PAbs test kit (Chen & Hsieh, 2000), evaluation of porcine material in thermal-treated (132°C for 2 h) meat samples using MAbs based quantitative sandwich ELISA for the detection of pork with LOD of 0.05% in adulterated mixture (Liu & Lu, 2006). Currently, ELISA test kits are commercially available for the detection of different meat species from raw, processed, cooked meat, meat products and feedstuff with greater reliability (Asensio et al., 2008). By principle, ELISA depends on the reaction of antibody with the corresponding soluble protein which is susceptible to heat treatments, therefore limits the applicability of the method for the highly processed food products (Hsu et al., 1999). Moreover, cross-species reactions among the closely related species as well as the inability of differentiating species particularly of closely related species from mixed sample matrices, also limits the applications (Di Pinto et al., 2005). Protein based detection methods have promising sensitivity and selectivity, however, limits the applicability due to the requirement of sophisticated instruments, specialized skilled personnel for the operation and data interpretation, and most importantly the

instability of protein biomarkers at high temperature or heat treatment process (Rady & Adedeji, 2018).

Table 2.1: Protein based techniques for the identification of origin of meat species.

Techniques	Sub classes	Justification of Analysis	References
Chromatography & Mass spectroscopy	LC	To differentiate meat products of 15 different animal species	(Chou et al., 2007)
	GC-MS	To differentiate pork and pork products from beef, mutton and chicken	(Nurjuliana et al., 2011)
	HPLC	To detect biogenic amines in dry fermented meat samples	(De Mey et al., 2012)
	LC-MS	To determine trace contamination of horse and pork meat against chicken, lamb, and beef	(von Bargen et al., 2013)
	LESA-MS	To differentiate beef, pork, horse, chicken, and turkey from heat treated meat samples	(Montowska et al., 2014)
	MS	To determine the exact origin of processed animal proteins	(Marbaix et al., 2016)
	UPLC-MS/MS	To determine advanced glycation end products in food products	(Scheijen et al., 2016)
Spectroscopy	Vis/NIR	To detect contamination of fishmeal with meat and bone meal	(Murray et al., 2001)
	Vis/NIR	To authenticate and quantify adulteration in crab meat samples	(Gayo & Hale, 2007)
	UV-vis, NIR & mid infrared	To detect minced beef adulteration with turkey meat	(Alamprese et al., 2013)
	Vis/NIR	To determine plant and animal proteins in minced beef and pork	(Rady & Adedeji, 2018)

Table 2.1: continued.

Techniques	Sub classes	Justification of Analysis	References
Electrophoretic method	AUT-PAGE/SDS electrophoresis	To detect water-soluble proteins in fresh pork and dry-cured products	(Picariello et al., 2006)
	IEF	To identify animal species from three component mixtures	(Skarpeid et al., 1998)
	IEF	To analyze three different sources of meat originating from cattle	(Skarpeid et al., 2001)
	IEF-Western blot	To verify the quality of chicken meat	(Saud et al., 2019)
	CE-SDS-filled CGE	To establish meat profile for the identification of meat species	(Vallejo-Cordoba & Cota-Rivas, 1998)
	CE	To determine the collagen level in processed meat	(Mazorra-Manzano et al., 2012)
	CZE	To identify the non-protein nitrogen from salted herring meat	(Felisiak, et al., 2019)
Immunoassays	Agar Gel Immunodiffusion	To identify the meat species in meat products	(Ahmed et al., 2011)
	Radioimmuno-assay	To differentiate animal species using bone fragments and blood stains	(Lowenstein et al., 2006)
	Lateral flow	To detect beef/sheep meat from different meat products	(Rao & Hsieh, 2007)
	ELISA	To quantitate beef in cooked mixed meat sample	(Thienes et al., 2019)

Vis/NIR: visible and near-infrared spectroscopy, AUT-PAGE: acetic acid-urea-triton polyacrylamide gel, SDS: sodium dodecyl sulfate, CGE: capillary gel electrophoresis, CE: capillary electrophoresis, CZE: capillary zone electrophoresis.

2.8.3 DNA Based Detection Methods

Nowadays, DNA based detection strategies have been considered as the leading species identification and differentiation techniques. This widely acceptance is due to the inherent properties of DNA molecules such as high stability, ubiquitous presence in most

of the biological tissues along with intra-species conserved and inter-species polymorphic fingerprint etc. (Ali et al., 2014; Mafra et al., 2008; Manikandan et al., 2014; Murugaiah et al., 2009; Rahmati et al., 2016). Therefore, the greater stability even at compromised conditions as well as easy extraction and requirement of very small amount of DNA sample, have made the DNA based approaches ideal for the detection, quantification, and tracing of adulteration even in highly processed meat and meat products (Darling & Blum, 2007; Hellberg & Morrissey, 2011; Mane et al., 2012). Among the DNA based assays, PCR has been gaining immense popularity due to its better accuracy, sensitivity and reliability. PCR is an *in vitro* process where a specific fragment of DNA sequence is amplified to several orders of magnitudes, generating thousands to million copies within a short time (Joshi & Deshpande, 2010; Rahmati et al., 2016). PCR amplified product is therefore treated for DNA visualization by either agarose gel electrophoresis or SDS-PAGE system using a DNA staining dye and DNA ladder followed by a gel image documentation system to obtain the gel image or on an automatic CE system for both gel image and electroferogram (Dooley et al., 2005). Some of the most commonly used PCR techniques for meat authenticity verification and/or quantification are discussed in below and several experimental evidences are enlisted in Table 2.2.

2.8.3.1 Species-Specific PCR Assay

Species-specific PCR involves routine laboratory techniques such as DNA extraction, amplification of short-length amplicon to multiple copies using a set of species-specific primers (forward and reverse) and the enzymatic addition of the nucleotides by DNA polymerase, followed by conventional gel electrophoresis and staining with ethidium bromide or other non-carcinogenic dye (Zhang et al., 2016). This simplex assay technique is so unique that exclusively designed primer sequences are selectively and specifically anneal with the target sequences of the selected species. In addition, there is no

requirement of further sequencing or digestion of the PCR amplified products, hence received huge attention for the detection of species adulteration (Girish et al., 2004). Till date, lots of simplex PCR experiments were reported due to its superior sensitivity, accuracy and robustness in detecting various species with distinct amplicon size (Table 2.2). Though PCR is being considered as the current gold standard of DNA detection owing to its greater sensitivity, it is time consuming, laborious, necessitates relatively huge and costly instrument, trained personnel as well as limited to the lab-based operation, and not applicable for the point of care purpose (Ngo et al., 2016; Niemz et al., 2011; Rahmati et al., 2016).

On the other hand, multiplex PCR which involves the simultaneous amplification of the multiple target DNA fragments in a single assay mixture, is also a highly useful and efficient method. Here, multiple copies of target DNA fragments with different lengths are amplified, and detected by gel staining by a single PCR assay. Though this approach reduces both cost and time, it has some limitations such as inherent complexity, and unequal amplification of different-length templates, therefore is less suited and sensitive for the target DNA quantification in comparing to the simplex procedure (Ahamad et al., 2017; Hou et al., 2015). However, to achieve better recovery and avoid cross-specificity reaction in highly processed foods, the amplicon length should be less than 150 bp because larger amplicons are more susceptible to breakdown into smaller fragments under harsh environments (Rojas et al., 2010).

Table 2.2: PCR based DNA detection techniques used for the identification of origin of meat species.

Techniques	Amplicon/ Probe size (bp)	Detected Species	References
Simplex PCR	513	Raw, processed and autoclaved beef and beef products	(Mane et al., 2012)
	271	Heat treated beef	(Arslan et al., 2006)
	482	Buffalo	(Girish et al., 2013)
	387	Pork in commercial products	(Che Man et al., 2007)
Multiplex PCR	256, 292, 401, & 835	Chicken, duck, pigeon and pig	(Haunshi et al., 2009)
	131, 283, & 387	Chicken, duck and goose	(Hou et al., 2015)
	172, 163, 141, 129, & 108	Cat, dog, pig, monkey and rat meats	(Ali et al., 2015c)
	123, 108, & 243	Rabbit, rat and squirrel	(Ahamad et al., 2017)
	148, 226, 148, & 91	Chicken, duck, pork and beef	(Qin et al., 2019)
PCR-RFLP	109	Pork DNA in commercial meat products	(Ali et al., 2012c)
	360	Pork and lard samples	(Aida et al., 2005)
	120	MBT in food chain and TCM	(Ali et al., 2016)
	609	Cattle, buffalo, goat, sheep and pig	(Kumar et al., 2014)
	123, 108, & 243	Rabbit, rat and squirrel	(Ali et al., 2018)
Real-time PCR	120	MBT	(Asing et al., 2016)
	142	Goat	(Papetti & Colombo, 2019)
	106, 90, & 146	Cattle, buffalo, and porcine	(Hossain et al., 2017b)
	134, 169, & 120	Red, fallow and roe deer	(Fajardo et al., 2008)
	Probe: cow-26, pork-23	Beef and pork in minced food	(Iwobi et al., 2015)
	Probe: goat-30, cow-30	Cow and goat meat, milk and cheese	(Guo et al., 2019)

2.8.3.2 PCR-Restriction Fragment Length Polymorphism

In PCR-RFLP, the amplified products of the conserved region using species specific primers are digested with the selective restriction endonuclease enzymes by incubating for certain period at specific temperature. The enzyme cleaves at specific recognition sites of the PCR product, thereby producing set of DNA fragments of variable lengths which are separated and visualized by gel electrophoresis (Ballin et al., 2009). Therefore, using the restriction fingerprints within a defined region of DNA, verification of the individual species (Nizar et al., 2019; Ali et al., 2015a; Ali et al., 2016) as well as discrimination between the closely related species (Ali et al., 2018; Maede, 2006; Sultana et al., 2018) have been reported. Though there are some false results due to random point mutations in restriction sites, PCR-RFLP in broad sense is a very simple, inexpensive and easy applicable routine analysis technique. Moreover, it also removes the ambiguities in the amplified products of single specific PCR assay by verifying the artifacts formed due to the presence of very minute amount of foreign DNA.

2.8.3.3 Real-Time PCR

Real-time PCR has been getting greater acceptance due to its fast, automated, highly sensitive and sequence-specific features. It offers both detection and quantification at real-time, has no post amplification processing such as electrophoresis (Asing et al., 2016). Real-time PCR identification generally involves two types of fluorescence chemistries; firstly, fluorescent labelled sequence specific DNA probe-based approach such as TaqMan (Hossain et al., 2017a) or molecular beacon; and secondly, non-specific fluorescent dyes intercalated dsDNA chemistry such as SYBR Green and Eva Green (Asing et al., 2016). Probe based assays such as TaqMan real-time PCR allows the use of very short-length amplicon, as well as offers dual checking as both probe and primers bind with their corresponding sites of the amplicon target, hence enhances the assay

specificity and reliability (Ali et al., 2012b). When the DNA probe sequences are completely hybridized with its complementary target sequences, fluorescent dye specific signal is obtained, therefore used as the real-time signatory data to correlate between the intensity of the fluorescent dye and the quantity of PCR products (Fajardo et al., 2010). On the other hand, intercalation of SYBR Green dye to the minor groove of the dsDNA gives greater fluorescence under UV and being considered as the simple, least expensive and direct fluorescent detection technique, however limits its sensitivity due to the non-specific binding of the dye with any dsDNA including primer-dimers, therefore detecting false positive (Arya et al., 2005). In addition multiplex quantitative PCR is also greatly promising as it simultaneously detects and quantitate the multiple target DNA samples in a single assay as well as saves both time and analytical expenses. In duplex or multiplex experiments, different dyes integrated with the different DNA probes followed by hybridization with the corresponding target DNA sequences produce the unique signal to discriminate individual PCR reactions. Few experimental results based on simplex and multiplex real-time PCR for the qualitative and quantitative detection of meat species are summarized in Table 2.2.

2.8.3.4 Randomly Amplified Polymorphic DNA

RAPD are the segments of DNA amplified by the short arbitrary PCR primers and produce ranged of amplified products. It is therefore simultaneous amplification of many distinct segments of DNA via binding of short arbitrary primers at the different positions on the genomic DNA, followed by gel electrophoresis and visualization of the amplified products according to their size (Ballin et al., 2009). Though the reproducibility of the RAPD-PCR is poor, investigation of the adulteration of different meat and processed meat products were reported (Calvo et al., 2004).

2.8.3.5 DNA Sequencing

DNA sequencing is the most straightforward and informative tool to identify species by comparing the obtained target sequence with the known sequences at Gene bank database at the National Center for Biotechnology databases (Genbank: http://www.ncbi.nlm.nih.gov/). DNA sequencing is also used to identify unknown species in samples of having a unique DNA sequence, even if no reference material is available (Shendure & Ji, 2008). The DNA sequencing technique provides more information without further actions such as gel electrophoresis or digestion with restriction endonuclease enzymes or further data analysis. It is the confirmative step to analyze the PCR amplicons following the results obtained by gel electrophoresis and real-time PCR (Ballin et al., 2009). However, in spite of extensive use of PCR based DNA detection techniques in analytical or clinical laboratories, on site or point of care application is still in its infancy. Moreover, lack of simple transduction mechanism for the detection of generated signal, as well as requisite of sophisticated and costly instrumentation are the major hindrances of the DNA based detection techniques (Vikrant et al., 2019).

2.9 Nanomaterial Based DNA Biosensors

With the advancement of the nanotechnology, the optical, electrical, or electromagnetic properties of the nanomaterials as well as the surface to volume ratio, surface reactivity have continuously been explored and improved. This advantageous features have therefore been prompted for the fabrication of nanoparticles/nanocomposites based biosensors with simple miniaturization, easy operation, fast response, greater intensity, and finally economically viable (Vikrant et al., 2019). Basically, a biosensor consists of a biological recognition element, a signal transducer, and a signal processing unit or reader device (Figure 2.3). The biological

recognition element interacts with the target analyte to generate a signal which is the consequence of either alteration in proton concentration; release or uptake of gases; emission, absorption or reflectance of light; release of heat or changes of the mass. This signal is thus converted by the transducer into another easily-measurable or detectible signal and the signal processing unit displays a graphical, numerical or comparative information (Asal et al., 2018; Martins et al., 2013).

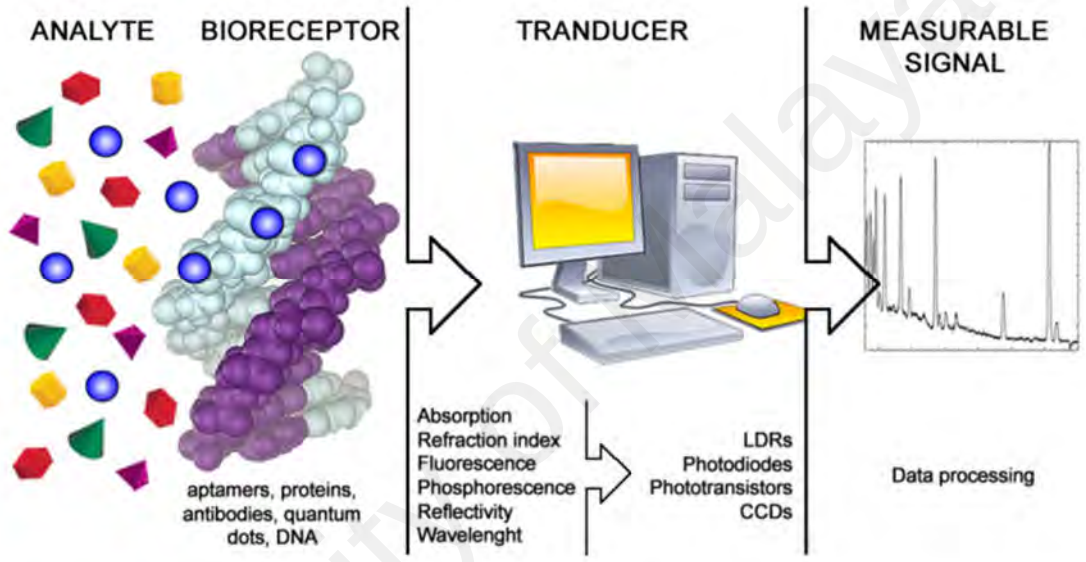

Figure 2. 3: General scheme of a Biosensor. Adapted with permission from the Reference (Martins et al., 2013).

Biosensors are therefore categorized according to either the biological recognition elements or the type of signal transduction mechanisms (Figure 2.4). However, the transducer elements should have some properties such as chemical inertness, uniformity, robustness, easy accessibility to the target analytes, and enough sensitivity to generate a reproducible, stable signal which is detectable even for minor modulation to achieve a low LOD (Vikrant et al., 2019). A wide range of transduction approaches have been approached over the decade (Figure 2.4) and among them electrochemical and optical methods are the mostly used, and accepted, hence described here in brief. Different inorganic nanostructures (nanoparticles, nanorods, nanotubes and nanowires) or nanocomposites provide a promising and diverse way of electrochemical/optical

biosensor fabrications for the fast, selective and sensitive detection of biomolecules in diverse field of applications. A DNA biosensor thus comprise of a transducer immobilized with a species-specific short oligonucleotide probe sequence as a biological recognition element to recognize the corresponding target DNA sequences, followed by the conversion of this biorecognition event via transducer element into a measurable signal.

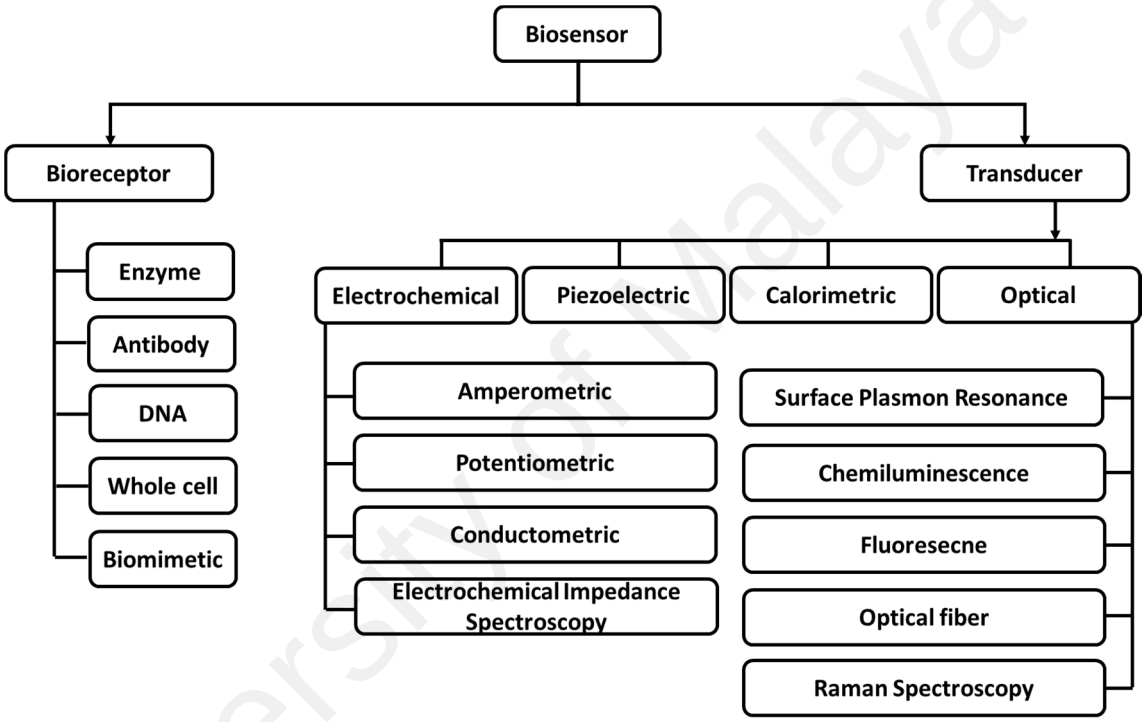

Figure 2. 4: Classification of the biosensor based on the type of biological signaling and signal transduction mechanism.

2.9.1 Electrochemical DNA Biosensors

2.9.1.1 Fundamental of Electrochemical Biosensing

According to the International Union of Pure and Applied Chemistry (IUPAC) an electrochemical biosensor is "a self-contained integrated device, which is capable of providing specific quantitative or semi-quantitative analytical information using a biological recognition element (biochemical receptor) retained in direct spatial contact with an electrochemical transduction element" (Thévenot et al., 2001). In electrochemical

biosensor, an electrode is used as the transducer element which measures the changes of the electrons or ions concentration as a reaction output between recognition element and the target analyte. Electrochemical biosensors have been sub-classified into amperometric, potentiometric, conductometric and impedimetric based on the nature of electrochemical changes occur during a biorecognition event (Perumal & Hashim, 2014; Pohanka & Skládal, 2008). In electrochemical biosensing, the target analyte in reaction with the bioreceptor either generates a measureable current (amperometric), a potential or charge accumulation (potentiometric) or change the conductive properties of a medium (conductometric) between electrodes (Chaubey & Malhotra, 2002). Electrochemical biosensor generally comprises of a reference, a working and a counter or auxiliary electrode which should be conductive and chemically stable. The working electrode acts as the transduction surface for the biorecognition event between the bioreceptor and target molecule while the counter electrode initiates a connection with electrolytic solution so that a current is applied to the working electrode (Grieshaber et al., 2008).

In amperometric biosensors, the current produced by the oxidation or reduction of an electroactive analyte is measured while the potential is kept fixed. The produced current is linearly correlated to the analyte concentration (Chaubey & Malhotra, 2002). In potentiometric biosensors, the signal is generated due to the variation of ion concentration or charge accumulation between the ion-selective electrodes, hence converting the recognition process into a potential signal which is correlated to the concentration of the target molecules. In addition, **c**onductometric sensors determine the ability of an analyte or electrolyte solution to conduct an electrical current between electrodes (Grieshaber et al., 2008; Perumal & Hashim, 2014). In voltammetric technique, a magnitude relative to an analyte is obtained by measuring the current produced due to the variation of a potential. The particular chemical is correlated to the peak current while the concentration of the corresponding species is related to the intensity of the peak current. The

voltammogram, the current vs potential graph, shows the behavior of the chemical reaction. Various forms of voltammetry includes linear sweep, hydrodynamic, differential pulse, square wave, stripping, and cyclic voltammetry (Di Pietrantonio et al., 2019). The electrochemical impedance spectroscopy (EIS) which measures the changes of electrical impedance (both resistance and reactance) resulting from the interfacial properties of the electrode due to the interactions of analyte and probe molecule, is calculated as voltage vs current ratio. The EIS comprises of three electrode system, a potentiostat and a frequency response analyzer (Grieshaber et al., 2008; Perumal & Hashim, 2014).

2.9.1.2 Strategies of Electrochemical DNA Biosensing

Numerous strategies adopting different chemistries have been employed for the electrochemical detection of DNA. The approaches are based on the direct or indirect electrochemical oxidation or reduction of DNA, DNA based charge transport chemistry, electrochemistry at polymer-modified electrodes, electrochemistry of DNA-specific redox reporters, and nanoparticles facilitated signal amplification (Drummond et al., 2003). However, the basic, facile, well-recognized and straight forward approach of fabricating an electrochemical DNA sensor involves the attachment of a short DNA probe sequence onto the electrode, followed by hybridization with a complementary target sequence and consequent transduction of the hybridization event into a measurable signal (Drummond et al., 2003). Various transduction strategies have therefore been reported using either electro-active indicator or indicator free approaches. DNA-mediated charge transport chemistry is generally based on the electrostatic attachment of electroactive indicator on the DNA strands (Steel et al., 1998) or intercalated redox probe molecules to report on perturbations in base stacking (Boon & Barton, 2002). In the former approach, the electroactive dye normally binds more firmly to dsDNA than to ssDNA, therefore

hybridization of immobilized probe DNA with the corresponding target DNA sequences, proportionally facilitates the binding of more electrostatically bound dye molecules and consequently yielding a higher signal (Hajihosseini et al., 2016; Pan et al., 2015; Steel et al., 1998). Therefore, this strategy provides a reliable and robust assay for the quantitative measurement of DNA sample present on the electrode surface. On the other hand, intercalative redox probe molecules provide information on perturbations in base stacking, therefore facilitate to know the changes in DNA strands due to the base bulges, single base-mismatches or protein induced distortions (Boon & Barton, 2002; Drummond et al., 2003). Tris(2,2'- bipyridyl)cobalt(III), Co(bpy)33+; metal complexes (e.g., tri(1,10-phenanthroline) cobalt(III), Co(phen)33+), Ru(NH3)63+; and organic molecules (e.g., Hoechst 33258, daunomycin, methylene blue, oracet blue, and 2,6-disulfonic acid anthraquinone) have been most commonly reported as hybridization indicators (Hajihosseini et al., 2016; Lee, 2008; Pan et al., 2015; Steel et al., 1998).

Electrochemical DNA detection using sequence-specific redox-active molecules have been done following different strategies, including labelling of the target DNA sequences with redox-active dye followed by the hybridization with the immobilized CP sequences and the appearance of hybridization confirmative characteristic electrochemical response of the redox reporter (Fojta et al., 2003). Another strategies based on three-component sandwich assay involves an immobilized CP, a redox-active molecule labelled SP sequence, and corresponding target DNA sequence. Therefore, in the presence of target DNA, both CP and SP sequences hybridize with the target DNA sequences and produce electroactive mediator mediated electrochemical signal which in fact dependent on the target DNA concentration (Immoos et al., 2004). In another approach, a SP labelled with electroactive dye hybridizes with the complementary portions of each of the two target DNA sequences, therefore produces a supersandwich architecture with longer DNA concatamers containing multiple target DNA and signal label which in consequent leads

to huge signal amplification in a voltammetric measurement with greater sensitivity (Wang et al., 2014; Xia et al., 2010). In this strategy, multiple copies of SP sequences and target DNA are spared, hence limits the sensitivity. In another supersandwich strategy, an auxiliary probe sequence with complementary sequence profile for two different area of SP is used to obtain a hybridized long DNA concatamers containing only single target DNA with many times of SP sequences (Chen et al., 2011; Wang et al., 2015a).

2.9.1.3 Graphene and Graphene-Nanocomposite as Electrochemical DNA Biosensor platform

Numerous types of conductive nanomaterials such as quantum dots, noble metal, metal oxides, magnetic nanoparticles, semiconductor and nanoparticles composite have been used as the electrode material in the fabrication of electrochemical biosensors. Nanoparticles perform some basic roles such as immobilization of biomolecules, catalysis of electrochemical reactions, enhancement of electron transfer, labeling of biomolecules and acting as a reactant (Abalde-Cela et al., 2016). Moreover, nano-carbon materials such as GO, Gr, reduced graphene oxide (rGO), single and multi-walled carbon nanotube are also used as lucrative electrode material in the electrochemical biosensor and now at the forefront of the research (Khalil et al., 2018). Gr is a single layer of carbon atoms in a closely packed honeycomb two-dimensional lattice with some extraordinary properties such as large surface area, high thermal conductivity, fast electron transport, easy of functionalizing (Yola et al., 2014), and good biocompatibility (Kung et al., 2014). Therefore, integration of graphitic or CNT based component with different nano-scale inorganic materials, noble metals, transition metals, metal oxides, and metal alloys, and conducting polymers have been using to obtain a promising electro-conductive features due to the synergistic influences of the dual or multi composites relative to the individual nanoparticles (Li et al., 2015a). Moreover, addition of a second component increases the

inter-planar space of the Gr nano-sheets, inhibits the Gr sheets from aggregating by acting as spacer molecule, and in some instances creates a 3D nano structure for the attachment or adhesion of analytes at maximal level. Consequently increases the bioactive surfaces as well as improves their electrical conductivity and electron mobility, thereby enhancing the achievable selectivity and sensitivity of the fabricated biosensors (Liu et al., 2014a). Besides, the structure, shape and orientation of Gr sheets as well as the morphology, form, composition, alignment, and distribution of the other component added to Gr to obtain a composite, have been tailoring for better oxidative catalytic activity, suitability of binding of the target analytes and improved electrochemical signal (Khalil et al., 2018; Li et al., 2016b).

Therefore, Gr and Gr-nanoparticle composites have recently paved more attention toward their electrochemical sensing capability for the detection of diverse compounds. However, Gr-AuNPs hybrid among the composites synthesized till date is one of the best studied composite in electrochemical biosensing of wide range of applications. AuNPs is the mostly favored co-element in Gr nanohybrid biosensors due to its superior electronic conductivity, high stability, greater catalytic properties and versatile surface functionalization chemistry for the easy attachment of different biomolecules. Gr-AuNPs thus in different composition/orientations have been used for the electrochemical sensing of different biological compounds such as glucose, H_2O_2, ascorbic acid, folic acid, dopamine; biomolecules such as DNA, RNA; growth hormones; antibiotics; environmental pollutants; food adulterants and different pathogenic microorganisms (Khalil et al., 2016; Khalil et al., 2018).

However, electrochemical biosensors considering DNA as a bioreceptor and using wide range of transducer material have also been reported for wide range of applications including detection of pathogenic microorganisms, cancer biomarkers, heavy metals and

many more (Khalil et al., 2016; Khalil et al., 2018; Saidur et al., 2017). For example, GO/Nickel oxide (NiO) hybrid modified with carbon ionic liquid electrode (CILE) as the electrode substrate in electrochemical DNA biosensor fabrication for the detection of *Salmonella enteritidis* gene sequence. ssDNA probe was attached to the NiO of the NiO/Gr/CILE electrode via terminal 5′-phosphate group, which in turn hybridize with the corresponding target ssDNA sequences and confirmed by the methylene blue indicator. This biosensor showed a good discrimination to single or triple-base mismatch ssDNA sequences (Sun et al., 2015a). Among the thousands of experimental evidences, some of the electrochemical DNA biosensors based on GO and AuNP components in different sensing fields are discussed in below as well as summarize in the Table 2.3.

Electrochemical DNA biosensors based on the immobilization of ss CP DNA on Gr-Au nanocomposites by thiol bridging, followed by subsequent addition of either complementary target with redox indicator or target plus signal/auxiliary probe DNA with electroactive dye have been explored as the sensitive DNA detection tool for the detection of pathogenic bacteria, viruses or even gene mutation e.g., *BRCA1* from early-stage breast cancer patients (Benvidi et al., 2015; Hajihosseini et al., 2016; Huang et al., 2015; Pan et al., 2015). Wang et al. (2012) showed that nano electrode ensembles (GCE–GO–AuNP) can be easily modified by thiolated DNA probe through strong Au-S bonding. Addition of the target DNA or single-mismatch target DNA facilitates the hybridization of DNA probe with intercalation of methylene blue into the DNA duplex specifically by binding with guanine in DNA molecules (Wang et al., 2012a). In contrary, Wang et al. (2015) fabricated a super-sandwich electrochemical biosensor using a methylene blue-labelled SP for sequence-specific DNA detection with ultra-sensitivity and single-base mismatch target DNA detection (Wang et al., 2015a). Peng et al. (2015) constructed AuNPs/toluidine blue-GO based (AuNPs/TB-GO) label free biosensor for the detection of the multidrug resistant 1 (MDR1) gene responsible for the resistance to

chemotherapeutic drugs used in the treatment of human cancer. The developed sensor showed very low LOD with a wide linear range as well as an ability to differentiate between single-base mismatched DNA sequences among the MDR1-related DNA sequences (Peng et al., 2015). Sun et al. (2015) reported an electrochemical DNA biosensor made up of multilayer Gr-AuNPs immobilized with dual-labelled (50-SH and 30-biotin) stem-loop DNA probe. This DNA biosensor is extremely effective in the detection of the peanut allergen-Ara h1 gene from peanut milk beverages as well as highly sensitive and selective to the target DNA sequence with great recovery (86.8% to 110.4%) (Sun et al., 2015b).

Some pathogenic bacterial species are very difficult to isolate and identify due to their low growth rate and fastidious nature. Hence, their rapid and sensitive detection are crucial to laboratory diagnosis and appropriate patient management. *Mycobacterium tuberculosis* is one of the most problematic bacteria worldwide to public health concern. Hence, the fabrication of an electrochemical DNA biosensor to identify *M. tuberculosis* is a pressing need to public health and society. Liu et al. (2014) immobilized a specific sequence of the IS6110 gene (CP) on rGO-AuNPs and a probe-label (AuNPs-PANI) as a tracer label for amplification. The sensor exhibits ultra-sensitive detection of *M. tuberculosis* DNA as low as fM level (Liu et al., 2014b). On the other hand, Wang *et al.* (2015) fabricated DNA based electrochemical biosensor using TiO_2NW/ERGO/CS/ CILE as the electrode substrate and immobilizing 23-base long *tlh* gene sequence, specific for *Vibrio parahaemolyticus.* The electrochemical responses of the methylene blue were recorded by DPV where the reduction current of MB decreases with concentration of complementary target DNA sequence (Wang et al., 2015b). In overall, though electrochemical biosensor has lots of advantages such as fast, simple, low cost, high sensitivity, and relatively simple instrumentation**,** one of the major drawbacks is that

it can generally be used for the detection of single target analyte, unless an array of electrodes are employed.

Table 2. 3: Compositions of the electrochemical DNA biosensors and their application, detection range and limit of detection.

Sensor composition	**Detected Analyte**	**Linear Range of Detection**	**Detection Limit (LOD)**	**References**
ssDNA/AuNP-GO/GCE	*Helicobacter pylori*	60.0 to 600.0 pM	27.0 pM	(Hajihosseini et al., 2016)
ssDNA/AuNPs–Gr/GCE	*Klebsiella pneumoniae* carbapenemase	1×10^{-12} to 1×10^{-7} M	2×10^{-13} M	(Pan et al., 2015)
CP/AuNPs–rGO/GCE	DNA	0.1 μM to 1.0 fM	0.35 fM	(Wang et al., 2014)
CP/AuNPs–rGO/GCE	DNA	0.1 μM to 0.1 fM	35 aM	(Wang et al., 2015a)
CP/Au electrode	DNA	1 nM to 100 aM	100 aM	(Chen et al., 2011)
ssDNA/GO–AuNP/GCE	DNA	10^{-9} to 10^{-12} M	100 fM	(Wang et al., 2012a)
ssDNA/AuNPs–ATPGO/GCE	DNA	1.0×10^{-13} to 1.0×10^{-9} M	1.13×10^{-14} M	(Gupta et al., 2013)
ssDNA/AuNPs/TB–GO/GCE	MDR gene	1.0×10^{-11} to 1.0×10^{-9} M	2.95×10^{-12} M	(Peng et al., 2015)
stem-loop DNA/Au film/multi-layered Gr-Au nanocomposite/GCE	*Ara h1* gene	10^{-16} to 10^{-13} M	0.041 fM	(Sun et al., 2015b)

Table 2.3: continued.

Sensor composition	Detected Analyte	Linear Range of Detection	Detection Limit (LOD)	References
ssDNA/Au NPs/rGO/GCE	DNA	1.0×10^{-8} to 1.0×10^{-13} M	3.5×10^{-14} M	(Zhang & Jiang, 2012)
CP/AuNR/Polythione /Gr/GCE	DNA (Human papillomavirus)	1.0×10^{-13} to 1.0×10^{-10} M	4.03×10^{-14} M	(Huang et al., 2015)
CP/AuNPs/rGO/GCE	BRCA1 5382 insC mutation	3.0×10^{-20} to 1.0×10^{-12} M, 1.0×10^{-12} to 1.0×10^{-7} M	1.0×10^{-20} M	(Benvidi et al., 2015)
CP/AuNPs/rGO/GCE & AuNP/polyaniline (as a tracer label)	*M. tuberculosis*	1.0×10^{-15} to 1.0×10^{-9} M (1 fM to 1 nM)	-	(Liu et al., 2014b)
GCE/GO-AuNR	Cancer biomarker (plasma mRNA, Mir-155)	2.0 fM to 8.0 pM	0.6 fM	(Azimzadeh et al., 2016)

*CP- capture probe; DPV – differential pulse voltammetry; ATPGO - p-aminothiophenol (ATP) functionalized GO, EIS – electrochemical impedance spectroscopy; TB – toluidine blue; MDR – multidrug resistance.

2.9.2 Optical Biosensors

An optical biosensor is a miniaturized device containing a biodetector integrated with an optical-based transducer. Optical biosensor measures the changes in the optical properties on the surface of a sensor platform upon binding of a target analyte and generates an identifiable output signal which is proportional to the analyte concentration. Therefore, optical attributes of the various nanomaterials have been explored for the development of DNA detection procedures. Optical DNA detection methods are mostly based on the hybridization process and measurement of the consequent changes in plasmonic properties, resonance, or fluorescence of the nanomaterials (Vikrant et al., 2019). Nanomaterial based optical DNA biosensors are thus classified as fluorescence, SPR, colorimetric, and SERS depending on the different transduction methods, summarized in Figure 2.5 and discussed in below.

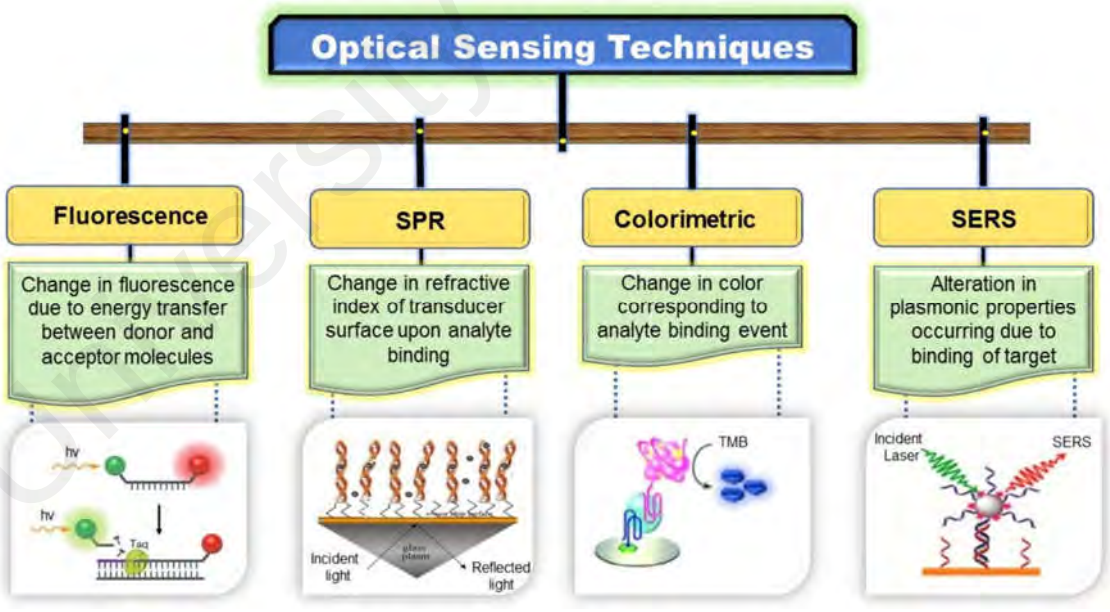

Figure 2. 5: Strategies for optical sensing of DNA. Adapted with permission from Reference (Vikrant et al., 2019).

2.9.2.1 Fluorescence Based DNA Biosensors

The fluorescence based optical biosensor records the differences of fluorescence intensity upon analyte recognition to a transducer element. Therefore, the change of the fluorescence intensity due to the hybridization event between DNA probe conjugated to transducer element and the corresponding target DNA, is measured by a fluorescence spectrophotometer. Several fluorescent DNA biosensors have been reported based on the Fluorescence Resonance Energy Transfer (FRET) which is an energy transfer mechanism between fluorophore as the energy donor and quencher molecules as the energy acceptor. FRET process causes either an upsurge or reduction in fluorescence intensity which is directly proportional to the analyte DNA concentration (Vikrant et al., 2019). For example, an aptamer based FRET biosensor was reported for the fast, sensitive and selective detection of *E. coli* in real food and water samples. Here, AuNPs were functionalized with aptamers and upconversion nanoparticles (UCNPs) were functionalized with corresponding target DNA. Hybridization of the probe-target DNA resulted in the spectral overlap between UCNPs and AuNPs, hence causing upconversion fluorescence quenching via FRET. In the presence of target bacteria, the aptamers preferentially bind to bacteria forming a three-dimensional structure and thereby dissociate UCNPs-cDNA from AuNPs-aptamers, causing the recovery of upconversion fluorescence (Jin et al., 2017).

Some nanomaterials such as CNT, AuNPs, GO and metal organic frameworks (MOFs) have been reported for their fluorescence quenching properties and used for the fabrication of turn OFF/ON type DNA biosensors. For example, a fluorophore (FAM) tagged DNA probe sequence was conjugated to MOF [N,N′-bis(2-hydroxyethyl)dithiooxamidatocopper(II)] via hydrophobic and π-stacking interactions which caused the fluorescence quenching of FAM due to FRET. In the presence of

corresponding target DNA, hybridization occurred between the probe and target DNA sequences which causes the conformational change of DNA and subsequently leads to release from the MOF and the restoration of FAM fluorescence that has been applied for the quantitative measurement of the target DNA (Zhu et al., 2013). Similar strategy was followed for the fabrication of fluorescence DNA biosensors by utilizing the fluorescence quenching ability of TiO_2NWs as well as the variable affinities of TiO_2NWs to ssDNA, dsDNA and triplex DNA. ssDNA has strong affinity to TiO_2NWs, hence fluorescence of the FAM-labelled ssDNA is strongly quenched, however, addition of ssDNA or dsDNA targets, FAM-labelled ssDNA probe hybridized with and form dsDNA or triplex DNA complex, and are dissociated from the TiO_2NWs due to weaker binding affinity. Therefore, high fluorescence intensity was achieved, which was directly correlated with the corresponding target DNA (Ding et al., 2019). Adhering the same principle, few other OFF/ON fluorescence biosensors based on quenching effect as well as preferential binding of the transducer to ssDNA over dsDNA were fabricated using different transducer component for diverse applications. For example, GO was used for the detection of apolipoprotein encoding short DNA sequence (Manzanares et al., 2019), poly(l-lysine)-graft-dextran functionalized GO for the verification of single nucleotide polymorphism (Han et al., 2019), Au/Ag nanocluster for the detection of *Campylobacter jejuni* DNA spiked in milk sample (Dehghani et al., 2019), and transition-metal carbides (Ti_3C_2 MXenes) nanosheets for the selective analysis of human papillomavirus (Peng et al., 2019).

A fluorescent aptasensor based on dsDNA/GO as the SP, a dye labeled competitor and actions of exonuclease I (Exo I) were used for the detection of adenosine. In the absence of adenosine, the competitor sequence hybridized with the aptamer to form dsDNA, protecting competitor from digestion by Exo I and adsorbed on GO surface. However, addition of target, aptamer favored to form aptamer/target complex due to the stronger

binding affinity, hence Exo I acted on the competitor sequences and release the fluorophore molecule. In consequent, addition of GO into the reaction system, a little change in fluorescent intensity is observed. This study helped to achieve LOD as low as 3.1 μM which is very lower in compare to traditional dye-labeled aptamer/GO based platform (LOD=21.2 μM) (Xing et al., 2016).

Moreover, lots of efforts have been invested to enhance the signal intensity for the sensitive detection of trace amounts of analytes present in the sample. Hence numerous non-nanomaterial based amplification strategies have been adopted such as cyclic signal amplification, dual recycling amplification, strand displacement-target recycling amplification, hybridization chain reaction (HCR), rolling circle amplification (RCA) for the sensitive detection of nucleic acid, bacteria, cancer biomarkers, and miRNA (Table 2.4) (Cai et al., 2019; Li et al., 2019a; Li et al., 2019b; Liang et al., 2019; Ma et al., 2019). In addition, amplification strategies along with several nanomaterials, more specifically GO, rGO have been used to improve the sensitivity of the fluorescence biosensors for diverse application (Krishnan et al., 2019).

2.9.2.2 Colorimetry Based DNA biosensors

Colorimetry is one of the simplest and convenient instantaneous sensing strategy, depends on the change of absorbance that is sensed by naked eye via color change. Colorimetric DNA sensor generally involves functionalization of the nanomaterials with nucleic acid and the consequent color changes is applicable for the visual detection in real time, hence promoted this facile and convenient sensor for commercial applications (Vikrant et al., 2019). AuNPs among the different signal-conversion nanomaterials, is the most commonly used nanoparticles in colorimetric biosensors fabrication for diverse applications. AuNPs in particular offer to utilize the color shift from red to purple/blue/violet by the aggregation event due to the aggregation effects of some

reagents, hence provides a simple mechanism of manipulation in developing a biosensor with a visual read out. For example, a simple and facile technique was reported for the direct detection of *Brucella* species using plasmonic properties of AuNPs. In this experiment, AuNPs were functionalized with thiolated oligonucleotide probe sequences, specific to an insertion sequence (IS711) (Sattarahmady et al., 2015) and the outer membrane protein encoded BCSP31 gene (Chuong et al., 2017), followed by hybridization with the corresponding complementary sequences and the consequent plasmonic shifting observed by visually and UV-vis spectrophotometer were used to detect and quantify the target DNA. Similarly, DNA aptamer-based sandwich type capillary detection platform was fabricated for the visual detection of food borne illness causing bacteria *S. enteritidis*. Here, the two highly specific aptamers were developed by Cell Systematic Evolution of Ligands by Exponential Enrichment (Cell-SELEX) system, therefore the sensitivity of the fabricated biosensor was increased to detect *S. enteritidis* as low as 10^3 cfu/mL (Bayraç et al., 2017).

Moreover, some other colorimetric biosensors using AuNPs platform but different fabrication strategies were also reported. For example, Park et al. (2019) fabricated an isothermal and colorimetric DNA assay method by dual amplification steps using Klenow fragment and nicking enzyme for selective amplification of DNA, followed by optical signal amplification due to catalytic hairpin assembly mediated aggregation of AuNPs and the resulting color shift from red to blue. However, the degree of AuNPs aggregation was dependent on the target DNA concentration and quantified by measuring the ratio of the intensity of UV-vis absorbance spectra for agglomerated AuNPs (620 nm) and bare AuNPs (524 nm) (Park et al., 2019). In another strategy, AuNPs were self-assembled onto glass surface via functionalization with 3-(mercaptopropyl) trimethoxysilane, followed by immobilization of ssDNA probe onto AuNPs. Application of methylene blue interacted with the free guanine bases of ssDNA probe and consequently absorbed onto

glass surface. Addition of target DNA solution decreased the free quinine concentration due to hybridization mediated coupling of probe and target DNA. Therefore, the change of UV-vis absorbance peak for methylene blue before and after target addition was the indicative of hybridization which was investigated by naked eye and sensed by spectrophotometric method. The developed biosensor showed a wide linear range (1 to 300 nM) for the detection of complementary target DNA sequence with LOD of 0.6 nM (Talemi & Mousavi, 2017).

Irrespective of AuNPs, some other nanoparticles such as AuNRs, AgNPs, and GO have been used in colorimetric sensor fabrication. AuNRs along with the HCR amplification strategy of hairpin DNA probe in the presence of target DNA to form a nicked double-helix DNA and the consequent electrostatic adsorption of HCR product with AuNRs was used to establish a colorimetric DNA detection method. In the presence of high salt concentration and target DNA, the AuNRs were stable and well dispersed while absence of target DNA, AuNRs aggregated due to the weak protection of hairpin DNA. The biosensor exhibited a good range of target DNA detection (0–60 nM), with high sensitivity (LOD - 1.47 nM) and selectivity to discriminate even a single base-mismatch DNA (Xu et al., 2018b). Likewise, AgNPs modified with DNA tetrahedron via amino-silver chemistry was used as a colorimetric biosensing strategy for the detection of HIV related DNA with excellent specificity and sensitivity (Ma & Miao, 2019). Moreover, dual nanoparticle based colorimetric DNA assay was developed by the functionalization of AuNPs and GO with DNA probe and target DNA respectively. The two platforms were coupled via hybridization and produced an obvious color change from pinkish-red to purplish blue, hence a spectrophotometric wavelength shift (22 nm) to achieve an LOD of 8 nM (Thavanathan et al., 2014).

2.9.2.3 Surface Plasmon Resonance DNA Biosensors

SPR is a direct, label free technique usually used to sense the biomolecular interactions happened on the transducer surface. In SPR system, a plane-polarized light is passed through a glass prism which is in contact at the bottom with the transducer surface functionalized with the bioreceptor. Upon analyte binding with bioreceptor, the refractive index of the transducer surface is changed due to the shifted SPR angle. This refractive index change is therefore measured and is directly proportional to the biomolecule concentration (Khansili et al., 2018; Vikrant et al., 2019). Different nanomaterials such as metal nanoparticles, Gr have been reported in the fabrication of SPR-based optical DNA biosensors. For example, an SPR DNA biosensor of portable operation was reported to detect *M. tuberculosis* where Gr was used as the transducer element and dropcasted over the SPR chip, followed by immobilization of the ssDNA probe over Gr layers via noncovalent interactions. In presence of target DNA, the DNA probes are detached from the Gr surface and hybridized with the complementary target sequences and the changed refractive index is measured to quantify the DNA concentration (Prabowo et al., 2016).

However, to improve the efficiency of SPR DNA biosensors, different nanomaterials as well as sensing strategies have been opted for the detection of miRNA, microorganisms, cancer biomarkers and many more biomedical applications (Table 2.4) (Bhardwaj et al., 2019; Li et al., 2007; Nguyen et al., 2015; Vikrant et al., 2019; Xue et al., 2019). For example, Wang et al. (2016) fabricated a SPR biosensor, by immobilizing ss CP DNA onto Au film, followed by hybridization with part of the target miRNA and the subsequent addition of assistant DNA-linked GO-AuNPs to bind with the unhybridized portion of the target miRNA sequence. This strategy resulted in a huge amplification of the SPR signal for the sensitive and selective detection of miRNA from large pool of miRNA members (Wang et al., 2016a). Similarly, based on multiple signal

amplification strategies, stem–loop structure of hairpin CP DNA immobilized on Au film was unfolded in the presence of target miRNA, facilitated to bind the assistant DNA linked to AuNPs with the terminus of the unfolded hairpin probe. Therefore, AuNPs acted here not only as a primary amplification component but also initiated DNA supersandwich formation adding two or more reporter DNA sequences. Hence, an enhanced shift of resonance angle was obtained due to the electronic coupling of localized plasmon of AuNPs and surface plasmon wave of Au film as well as DNA supersandwich structure mediated enhancement of refractive index of the medium next to the metal film (Wang et al., 2016b). Moreover, to achieve a further enhancement of SPR response in consequent to improve the sensitivity, Liu et al. (2017) added positively charged AgNPs to be absorbed onto long range DNA supersandwich structure homogenously (Liu et al., 2017). Similar way, a dual AuNP amplified SPR aptasensor was fabricated for the detection of exosomes by preparing Au film functionalized with CP DNA, followed by addition of target exosomes, aptamer/T30 linked AuNPs and finally A30 coated AuNPs where T30 and A30 are the complementary sequences and linked the two AuNPs composite (Wang et al., 2019). A recent and very interesting application of SPR is the remote detection via microstructured optical arrays of conical nanotips or micropillars. Micropillar coated with a thin Au layer increased up to 10^{-4} refractive index units. Therefore, this Au thin film coated micropillar arrays were functionalized with probe and kinetics of hybridization with corresponding target DNA was monitored remotely (Vindas et al., 2019).

The SPR based biosensing is therefore rapid, label-free, highly sensitive, reproducible and amenable for real-time analysis. However, false positive results are encountered due to the fluctuations in refractive index, owing to variation in temperature or composition of the sample. In addition, non-specific interactions of non-target or structurally similar molecules to sensor surface also limit the usage of SPR-based biosensors. Further,

currently available commercial SPR instruments, such as Biacore TM series are expensive and bulky which also limits the extent of their application (Bhardwaj et al., 2019; Nguyen et al., 2015).

Table 2. 4: Optical biosensing strategies, application, detection range and limit of detection.

Types of Sensors/Detection Principle	Target Analyte	Linear Range of Detection	Detection Limit (LOD)	References
UCNPs based FRET aptasensor	*Escherichia coli*	5 to 10^6 cfu/mL	3 cfu/mL	(Jin et al., 2017)
MOFs based FRET biosensor	HIV DNA	10 to 100 nM	3 nM	(Zhu et al., 2013)
TiO_2NWs based fluorescence biosensor	ds target DNA	2 to 150 nM	1.6 nM	(Ding et al., 2019)
TiO_2NWs based fluorescence biosensor	ss target DNA	2 to 200 nM	1.4 nM	(Ding et al., 2019)
Au/Ag nanocluster based OFF/ON fluorescence biosensor	*C. jejuni*	10 to 300 pM	4.4 pM	(Dehghani et al., 2019)
DNA polymerase-mediated chain displacement amplification fluorescence aptasensor	*S. paratyphi A*	10^2 to 10^8 cfu/mL	10^2 cfu/mL	(Liang et al., 2019)
Entropy-driven strand displacement and DNAzyme mediated dual cycling amplification based fluorescence biosensor	Human cancer biomarker (P53 gene)	500 fM to 10 nM	220 fM	(Li et al., 2019a)
Molecular beacon and strand displacement target recycling amplification fluorescence biosensor	*S. aureus*	80 to 8×10^6 cfu/mL	39 cfu/mL	(Cai et al., 2019)
Hyper-branched RCA fluorescence biosensor	Hepatitis B virus	0.1 to 40 nM	0.05 nM	(Li et al., 2019c)
Branched RCA based fluorescence biosensor	miRNA	50 to 500 fM	25 fM	(Ma et al., 2019)

Table 2.4: continued.

Types of Sensors/Detection Principle	Target Analyte	Linear Range of Detection	Detection Limit (LOD)	References
AuNP based colorimetric DNA biosensor	(DNA)*Brucella* spp.	-	31.75[a] pg/µL & 1.09[b] pg/µL	(Sattarahmady et al., 2015)
AuNP based colorimetric DNA biosensor	(DNA)*Brucella* spp.	-	102.5[a] pg/µL & 1.36[b] pg/µL	(Sattarahmady et al., 2015)
AuNP-probe-target DNA hybridization mediated visual detection	*Brucella* spp.	-	10^3 cfu/mL	(Pal et al., 2017)
Cell-SELEX and sandwich aptamer-based colorimetric detection	*S. enteritidis*	-	10^3 cfu/mL	(Bayraç et al., 2017)
Double amplification based colorimetric DNA detection	DNA	-	3.1 fM	(Park et al., 2019)
AuNPs self-assembly oriented colorimetric DNA biosensor	DNA	1 to 300 nM	0.6 nM	(Talemi & Mousavi, 2017)
AuNRs and HCR amplification assisted colorimetric biosensor	DNA	0 to 60 nM	1.47 nM	(Xu et al., 2018b)
DNA tetrahedron-modified AgNPs based colorimetric biosensor	HIV-related DNA	1 to 1.5×10^4 nM	0.84 nM	(Ma & Miao, 2019)
Dual platform (GO & AuNP) based spectrophotometric detection	DNA	Optimum: 63 nM	8 nM	(Thavanathan et al., 2014)

[a] LOD with naked eye. [b] LOD based on absorbance measurement.

Table 2.4: continued.

Types of Sensors/Detection Principle	Target Analyte	Linear Range of Detection	Detection Limit (LOD)	References
Gr based portable SPR sensor	*M. tuberculosis* DNA	-	28 fM	(Prabowo et al., 2016)
SPR DNA biosensor based on biotin-streptavidin binding system	DNA (*Salmonella* spp.)	5 to 1000 nM	0.5 nM	(Zhang et al., 2012a)
	S. typhimurium	10^2 to 10^{10} cfu/mL	10^2 cfu/mL	
Dual AuNP assisted signal amplification based SPR aptasensor	Cancerous exosomes	-	5×10^3 exosomes/mL	(Wang et al., 2019)
GO-AuNP hybrids-based SPR biosensor	miRNA (prostate cancer)	-	1 fM	(Wang et al., 2016a)
AuNP coupled DNA supersandwich based SPR biosensor	miRNA	-	8 fM	(Wang et al., 2016b)
AgNPs aided multiple signal amplification based SPR biosensor	miRNA	-	0.6 fM	(Liu et al., 2017)
Antimone and AuNR originated SPR sensor	miRNA-21 & miRNA-155)	-	10 aM	(Xue et al., 2019)

2.9.2.4 SERS Based DNA Biosensors

*(a) **Fundamental of SERS Biosensing***

Upon light exposure to a sample, a very tiny fraction of the scattered light of a changed frequency is obtained due to its energy changed by the interaction of photon with the laser induced molecular vibrations. This is the Raman scattering effect, and only about 1 part in 10 million of the scattered light has a shifted color. When a light energy or radiation energy is incident on a molecule, a small percentage of radiation is elastically scattered known as Rayleigh scattering while a very minor fraction of the radiation is inelastically scattered known as the Raman scattering. However, in Raman scattering, either the scattered radiation energy from molecules in ground state back to the excited level with the energy $h(v_0-v_1)$ (Figure 2.6) which is known as the Stokes Raman scattering; or scattered light from the vibrationally excited state inelastically back to the ground state, giving rise to Raman effect with energy $h(v_0+v_1)$ (Figure 2.6), is known as the anti-Stokes Raman scattering (Grasselli et al., 1981).

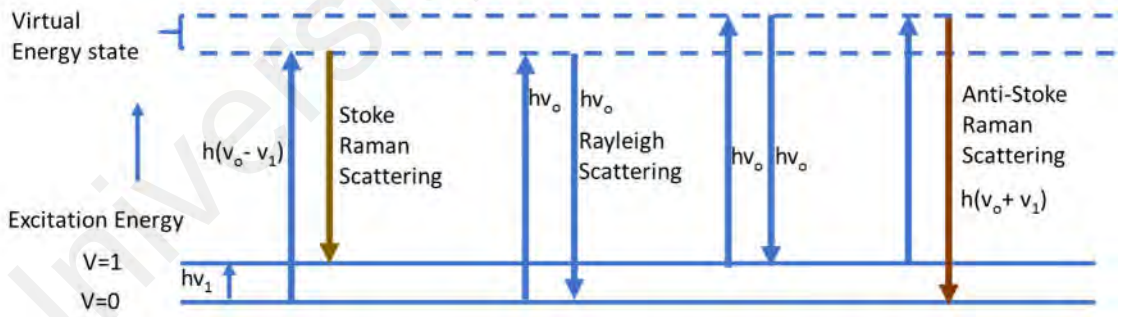

Figure 2. 6: In the Rayleigh and Raman Scattering process where an amount of energy is exchanged with the sample as shown schematically in the quantum energy level. Here, V_0 and V_1 indicates the incident and transmitted beam intensity respectively. Rayleigh scattering has the same frequency as the incident beam and Raman scattering the frequency is equivalent to $V_0 \pm V_1$. Therefore, $V_0 - V_1$ = Stokes and $V_0 + V_1$ = anti-Stokes.

In conventional Raman spectroscopy, the obtained Raman signal is very weak to see with the naked eye, therefore reduces the sensitivity of the tests and limits the applications range. This shortcomings urges to explore the surface enhancement effect due to surface

features of the materials in Raman studies. SERS which combines the laser spectroscopy and optical features of material, is the best suited for the amplification of the obtained Raman signal. SERS was first observed in adsorbed pyridine molecules onto the roughened Ag electrodes by Fleischman et al. in 1974 (Fleischmann et al., 1974), and verified by Albrecht et al. in 1977 (Albrecht & Creighton, 1977). SERS provides greatly enhanced signal from the Raman active analyte adsorbed onto the material surface (Kandjani et al., 2014; O'Mullane et al., 2009; Pearson et al., 2012; Plowman et al., 2009; Selvakannan et al., 2013; Sharma et al., 2011). SERS is a very useful to determine the conformational changes or structural differences or preferred orientation of the molecules (Hicks, 2001). However, the SERS enhancement is strongly dependent on the type, size, shape, composition of the metallic nanostructure and the nature of the molecular analytes (Abalde-Cela et al., 2016). For example, noble metals such as Ag and Au, and the alkali metals are the substrates of choice for visible Raman excitation (Ferraro, 2003).

The overall SERS effect is due to the two different enhancement mechanisms – the long-range electromagnetic and short-range chemical enhancement. The electromagnetic enhancement is due to the enhancement of the local electromagnetic field at the surface of the metals by the excitation of light which excites the conduction electrons and causes collective oscillations of the surface electrons of the nanoparticles termed as SPR (Ferraro, 2003). This enhancement is based on the interaction between the exposed laser induced electric field of surface plasmons on the metals and transition moment of an adsorbed molecule (Kiefer & Schlücker, 2011). Electromagnetic enhancement is therefore dependent on surface roughness features of metals (Hicks, 2001) and is the major contributor of the overall SERS enhancement. However, when the frequency of incident light is resonant with a plasmon, the metal nanoparticles radiate a dipolar field and be coherent with the exciting electric field. This process leads to redistribution of the local field and a great enhancement of the electromagnetic field at a specific position

around the nanoparticles called 'hot spot'. A molecule near or adsorbed at the hot spot experiences much-enhanced incident intensity (Figure 2.7). When both the incident light and the scattered signal of molecules are in resonance with the plasmon frequency, then the SERS signal is maximized (Stiles et al., 2008; Wang et al., 2012a; Wang et al., 2012b). Electromagnetic enhancement also has a strong analyte distance-dependence feature: only molecules on or very close to the metal surface experience the enormous field enhancement (Schlücker, 2009; Wang et al., 2012b). In this mechanism the enhancement factor E at each molecule is (approximately) given by $E = |\boldsymbol{E}(\omega)|^2|\boldsymbol{E}(\omega')|^2$, where $\boldsymbol{E}(\omega)$ is the local electric-field enhancement factor at the incident frequency ω, and $E(\omega')$ is the corresponding factor at the Stokes-shifted frequency ω' (Schatz, 2006). On the other hand, chemical enhancement is due to the charge-transfer mechanism between the metal surface and the adsorbed molecules, resulting in increase in the Raman cross-section for the adsorbed molecule (Kiefer & Schlücker, 2011). Interaction between the adsorbed molecules and metal surface, perturbs the electronic structure, hence the optical properties of the molecule is changed compare to its unbound state. Specifically, the interaction between the molecular orbitals of the adsorbed molecules and the electronic band structure of the metal allows the charge (electron) between the molecule and the metal surface. It is s short-range effect, restricted to the first layer of adsorbed molecules and enhance the scattering cross section only one or two of magnitude (10-100) (Figure 2.7) (Kambhampati et al., 1998; Kosuda et al., 2010).

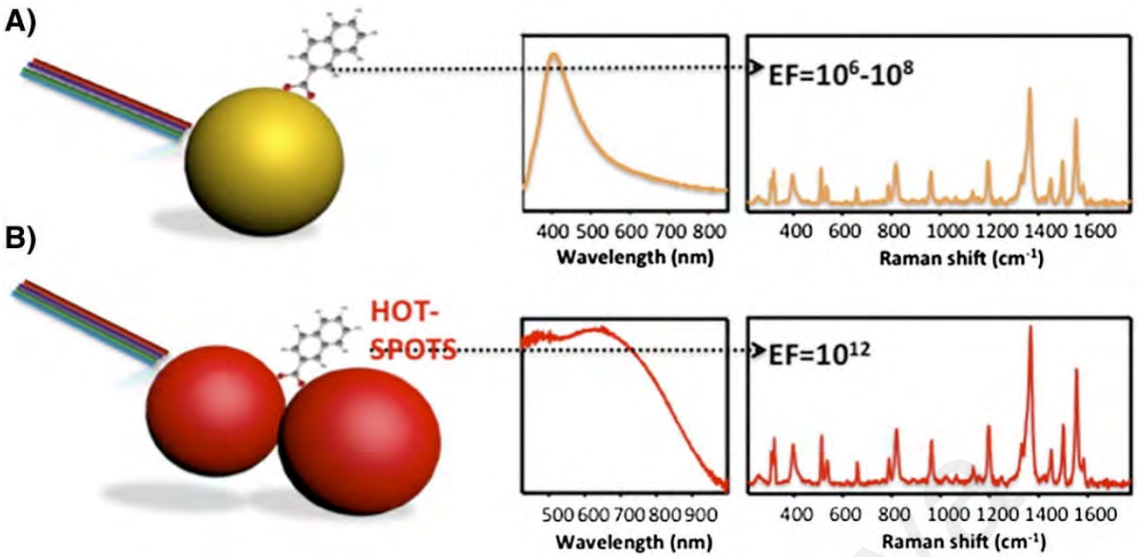

Figure 2. 7: Schematic representation of SERS effect in: (A) an individual nanoparticle. (B) An interparticle gap, hot-spot area with further enhanced Raman signal. Adapted with permission from the Reference (Abalde-Cela et al., 2016).

(b) ***Graphene and Graphene based Nanocomposite as SERS substrates***

Nanoparticles are the artificially synthesized structures with dimensions between 1 and 100 nm. Metal nanoparticles with size ranges from 10-100 nm possess specific SPR property in compare to the bulk materials. However, metal nanoparticles in colloidal form have been used most commonly as SERS substrate due to easy preparation, and functionalization. With the progress of nanoscience, metal nanoparticles from spherical to various other shapes with wide size distribution, single or alloy nanoparticle to multicomponent composites have been used to improve the SERS signal. In addition, metal nanoparticles in aggregated form is more important, as the hot spots are generated at the junctions of nanoparticles, therefore strongly influence the SERS signal. As SERS intensity strongly relies on the excitation light wavelength as well as the strength of the plasmons propagating on the surface of the metal nanoparticles, it is therefore immense important to engineer the SPR of the nanoparticles to maximize the signal strength (Kiefer, 2011). To date, lots of SERS experiments have been reported using colloidal metal nanoparticles specifically AuNPs and AgNPs or roughened metal surfaces as the substrate. Though these substrates support high SERS enhancement, for practical

applications it urges the engineered SERS substrate with tunable and reproducible features. It is noted that maximum SERS intensity is observed by tuning the laser excitation wavelength near the localized surface plasmon resonance (LSPR) maximum of the SERS substrate. Therefore, nanostructure with different morphology including nanospheres, nanoshells, nanogaps, nanoholes, nanotips, nanowires for tailoring the optical properties have been fabricated following different procedures such as nanospheres lithography, e-beam lithography, spin coating, electrochemical deposition, electrochemical etching and many more (Bantz et al., 2011).

The 2D planar Gr sheet holds some outstanding chemical, electrical, material, optical, and physical properties which make it as the key component for diverse applications in SERS biosensing and imaging arena. Furthermore, addition of another nanoparticle to form a nanocomposite minimize the self-agglomeration of Gr sheets, thus increases the effective surface area, catalytic activity and the electrical conductivity (Khalil, 2016; Si & Samulski, 2008; Tien, 2011). Gr-nanoparticle composites offer a number of highly desirable and markedly advantageous additional unique physicochemical properties and functions in bio-applications in comparison to either material alone (Wu et al., 2012). It is well known that noble metal nanoparticles (e.g. Cu, Ag or Au) are more commonly used in SERS-based experiments due to their electromagnetic properties which enhance the Raman signal (Huang et al., 2010). On the other hand, Gr or GO have the potentiality to enhance the Raman signals via the chemical enhancement mechanism which is independent from that of noble metal nanoparticles (Ling et al., 2009; Wang et al., 2013; Xu et al., 2013a). Therefore, as anticipated, Gr-metal nanocomposites acted synergistically for further magnification of the weak Raman signals by many orders of magnitude via electromagnetic and chemical enhancement when compared to using either Gr or metal nanoparticles alone (Huang et al., 2010; Jasuja & Berry, 2009; Jasuja et al., 2010). Hu et al. (2013) provided a clear dictation in this context by comparing the Raman

signals of adsorbed aromatic dye molecule, crystal violet onto Silica oxide (SiO_2)/silica (Si), GO, AuNRs and GO-AuNRs separately and validated the boosted SERS signal of GO-AuNRs nanohybrids (Hu et al., 2013). This enhancement is the summation of electromagnetic enhancement based on local electromagnetic field by the AuNRs and chemical mechanism based on the charge transfer and chemical bonding of GO-AuNR and crystal violet dye molecules (Hu et al., 2013). Zhang et al. (2013) fabricated SERS-active substrates in newer dimension based on GO embedded Au@AgNPs sandwich nanostructures (Au@Ag-NPs/GO/Au@Ag-NPs) to achieve a higher sensitivity, reproducibility and reliability of the Raman readout and obtained dramatic enhancements of the Raman signals (R6G with an enhancement factor of $7.0x10^7$) due to abundant hot spots on their surfaces and distinctive edifice of the GO sheets (Zhang et al., 2013b). It is experimentally proved that the degree of SERS enhancement was fine-tuned by the quantity (Lee et al., 2014), size and shape (Jasuja & Berry, 2009; Qiu et al., 2013; Zhu et al., 2014), type (Wang et al., 2010) of AuNS on the Gr sheets, morphological arrangement of Gr and AuNPs (Xu et al., 2013b) as well as the excitation wavelength of the laser (Lee et al., 2011). For example, GO-AuNRs have been proved as strong SERS substrates by using a model molecule (cresyl violet perchlorate) that unveiled very large SERS enhancement factors (10^6) with very low molecular detection limits (10^{-11}M) (Caires et al., 2015).

On the other hand, corresponding enhancement factors rely on the volume of Gr and consequentially its thickness (Li et al., 2015b), layer numbers such as single layer Gr provides larger SERS enhancement in comparison to fewer layer Gr (Lee et al., 2011), and type of defects of Gr sheets. All of these extraordinary advantageous properties make Gr-Au nanocomposites the perfect substrate for SERS measurements as it has been extensively investigated in versatile applications including sensing and molecular diagnostics, biomedical applications, agriculture, food adulteration (Nguyen et al., 2014),

intracellular bioimaging (Ma et al., 2013), detection of pathogenic microorganisms (Fan et al., 2013) and biomolecules (Das et al., 2012; Li et al., 2012), nucleic acids (He et al., 2012), cancer cells (Manikandan et al., 2014), and even in the detection of explosives and chemical warfare agents (Hakonen et al., 2015).

(c) SERS Based DNA Biosensing

SERS is being considered as a powerful analytical tool for surface and interfacial analysis as it can unveil molecular fingerprint information and ultrahigh surface sensitivity (Zong et al., 2015). It is one of the best techniques for molecular analysis with very low sensitivities (Lu et al., 2011) and the detection of single molecules (Kneipp et al., 1997; Le Ru & Etchegoin, 2012; Nie & Emory, 1997; Sonntag et al., 2014) as well. In this context, researchers are continuously trying to explore the new designs/techniques for rapid, reliable and sensitive detection of DNA which is helpful for the early diagnosis and prevention of diseases in some instances. SERS is a reliable and non-destructive tool which has been successfully using for the detection of DNA sequences from a trace amount of sample or differentiation of DNA from large pool of DNA or RNA sequences or even to distinguish the single nucleotide polymorphism (Bell & Sirimuthu, 2006; Xu et al., 2015). Therefore, employing the basic DNA hybridization principle and the advantageous features of SERS, numerous SERS DNA sensing strategies either label or label free have been developed.

Though theoretically label-free SERS DNA detection scheme is feasible, it is very difficult to achieve the SERS spectral reproducibility of DNA sequences. It is also very challenging in label free techniques to obtain a specific and distinguishing SERS signal for the hybridized ds DNA sequences by simple probe-target hybridization as both of the strands consist of the same four nucleotides, though some successful studies reported (Barhoumi & Halas, 2010). For example, Au nanoshells bound to glass substrates was

employed to obtain intrinsic SERS spectra of DNA, which was dominated by the adenine vibrational bands at 729 cm^{-1} (Barhoumi et al., 2008). The presence of adenine in the DNA sequences is considered as an endogenous marker. Therefore, based on the concept, using adenine free probe sequences by substituting with 2-aminopurine (2-AP), label-free SERS based detection of DNA hybridization was achieved. In this experiment, the distinguishing feature between the ssDNA probe and ds hybridized strands was the presence of adenine peak at 736 cm^{-1}. Hence the hybridization efficiency was determined by the peak intensity ratio of 736 cm^{-1} (adenine peak)/807 cm^{-1} (2-AP peak) and the value 0 indicates for no hybridization and maximum value corresponds to complete hybridization (Barhoumi & Halas, 2010). Another label-free method involving *in situ* DNA-metallization was followed to increase the SERS signal. Here, a glass slide surface was modified with peptide nucleic acid (PNA) sequences as the recognition probe, followed by hybridization with the target DNA sequences and a silver enhancement step. Ag+ were adsorbed on negatively charged phosphate skeleton of target DNA and the subsequent chemical reduction by hydroquinone, AgNPs of 10 nm in size were grown along the DNA skeleton which therefore aided to obtain a good quality SERS signal dominating adenine peak at 736 cm^{-1} and LOD of 34 pM (Qian et al., 2018). Some other label-free SERS DNA detection strategies include head-flocked Au nanopillar substrate based biosensor for the multiplex detection of cancer-associated miRNA (Kim et al., 2019), and GO functionalized popcorn shaped AuNPs hybrid platform for the detection of HIV DNA at fM level and methicillin-resistant *S. aureus* bacteria with LOD 10 cfu/mL (Jin et al., 2014).

Hence, to overcome the limitations of label-free detection techniques, Raman labeled biosensors of different fabrication strategies have been attempted and being continued. One of the techniques is the molecular sentinel-on-chip. In the molecular sentinel, the architecture of the probe DNA is like a step-loop structure, where probe sequence is

attached to a SERS-active nanostructure by thiol-linkage of the terminal end of an arm and a Raman label is attached to the end of another arm. Therefore, the Raman tag resides in close proximity of the SERS-active sensor platform and generates a strong SERS signal. However, the hybridization between the target DNA with the complementary loop part of the molecular sentinel disrupts the stem-loop configuration which then forces the two arms to be far apart, therefore Raman label is physically moved away from the metal surface, leading to a decreased SERS signal intensity (Ngo et al., 2013; Wabuyele & Vo-Dinh, 2005). This is also termed as "On-to-Off" SERS signal process (Figure 2.8a). On the other hand, in inverse molecular sentinel-on-chip, also named as "Off-to-On" signaling technique, where in the absence of target DNA, the placeholder and probe sequences forms partial duplex structure, keep away the Raman tag from the chip's metal surface, resulting in weak SERS signal due to the increase of Raman dye-sensor platform distance (Off state). When the target DNA is introduced into the system, the target sequence binds to the complementary overhanging region of the previously partially hybridized probe-placeholder conjugate, followed by complete hybridization with the placeholder, thus the reporter probes become free to form hairpin structure as of their by-design nature and bring the Raman label to close proximity of chip's metal surface and inducing a strong SERS signal (On state) (Figure 2.8b) (Ngo et al., 2014a; Wang et al., 2015c). Therefore, based on the molecular sentinel and using different plasmonic sensor platforms, different DNA biosensors have been fabricated for the diagnosis of disease biomarkers, viral infections, HIV-1, and breast cancers either in simplex (Ngo et al., 2014a; Ngo et al., 2013; Ngo et al., 2016; Wabuyele & Vo-Dinh, 2005; Wang et al., 2015c) or multiplex form (Ngo et al., 2014b; Wang & Vo-Dinh, 2009).

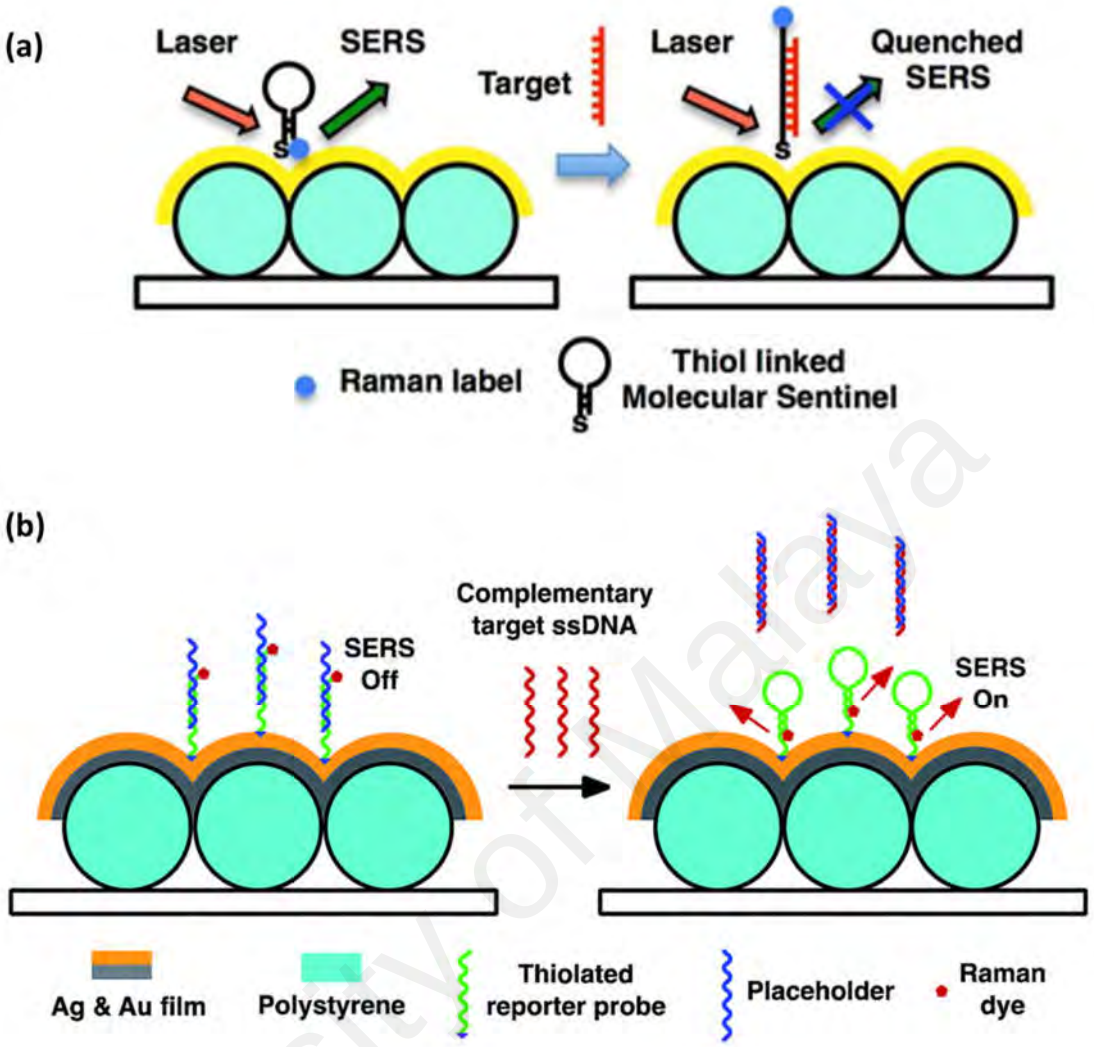

Figure 2. 8: (a) Molecular sentinel-on-chip 'on-to-off', the figure is adopted with permission from reference (Ngo et al., 2013); and (b) inverse molecular sentinel-on-chip 'off-to-on' SERS DNA biosensors, the figure is adopted with permission from reference (Ngo et al., 2014a).

A very common SERS detection strategy involves single or dual platforms based three component sandwich assay. In dual platform based sandwich assay, CP sequences are immobilized onto a SERS-active or SERS-inactive platform and SP sequences are either co-adsorbed with Raman reporter molecules (Figure 2.9a) (Khalil et al., 2019; Zhang et al., 2015) or Raman dye intercalated SP sequences are immobilized onto another nanoparticles platform (Figure 2.9b) (Kang et al., 2010). Hence addition of the corresponding target DNA sequence complementary to both of the SP and CP sequences, results in the hybridization mediated covalent linking of the two platforms to form a

sandwich structure. However, sandwich biosensor based on the dual platforms where either one is SERS-inactive, need further treatment with another metallic solution to coat the metallic platform and form a layer to enhance the SERS signal and facilitated to obtain the Raman label specific fingerprint spectra (Cao et al., 2002; Jin et al., 2006). For example, Cao et al. fabricated a microarray sandwich assay biochip for the multiplexed detection of DNA by functionalizing glass slide surface with the CP strands, followed by partial hybridization with the corresponding target sequences and finally addition of the AuNP functionalized with Raman dye tagged oligo probes to hybridize with the overhanging region of target sequences. Finally the chip was treated with Ag enhancement solution where AuNPs probes catalyze the formation of a Ag layer to enhance the SERS signal and aided to obtain LOD as low as 20 fM (Cao et al., 2002). Another method was reported following the same strategy replacing the glass slide by glass beads functionalized with CP, followed by hybridization with target sequences and Raman dye labeled probe sequences linked AuNP which acts as catalysts for developing a Raman-enhancing Ag layer and hence the SERS intensity (Jin et al., 2006).

On the other hand, dual SERS-active platform based sandwich biosensor facilitates the Raman signal to be greatly enhanced due to the hot spot generation by the agglomeration of two different platforms. Therefore, the SERS-based sandwich detection method provides a special hybridization event which is useful for the single as well as multiple detection of target analytes using different Raman labels of avoiding overlapping characteristic signals. For example, Zhang et al. (2015) fabricated a dual species SERS biosensor for the simultaneous detection of *S. typhimurium* and *S. aureus* in pork samples with detection limits of 35 cfu/mL and 15 cfu/mL respectively. In the fabrication process, organism specific aptamer sequences and Raman molecules - mercaptobenzoic acid and 5,5′-dithiobis(2-nitrobenzoic acid) specific for *S. typhimurium* and *S. aureus* respectively were co-adsorbed on AuNPs but at two different reaction solutions, while Fe_3O_4 magnetic

AuNPs were functionalized with CP sequences of both species. Therefore, addition of both target bacteria, CP sequence specifically captured the respective bacteria, followed by the addition of SP immobilized AuNPs also connected with the target bacteria through the specific binding effect of aptamer to form the sandwich like detection structure (Zhang et al., 2015). Similarly, Braun et al. (2007) fabricated a sandwich biosensor by the immobilization of CP onto Ag film labeled with 5-((2-(and-3)-*S*-(acetylmercapto) succinoyl)amino) fluorescein, followed by coupling with another CP sequence functionalized on AgNPs via corresponding target DNA mediated hybridization (Braun et al., 2007). Kang et al. (2010) reported the sensing technique where AuNWs were functionalized with DNA probe and AuNPs were modified with Raman dye intercalated reporter DNA and finally aggregation of AuNPs on AuNW via target DNA-probe-reporter DNA linking (Kang et al., 2010). An interesting sandwich biosensor was reported for the detection of West Nile Virus genome via hybridization with complementary probe sequences covalently linked to silica shell-coated paramagnetic nanoparticles (MNP) and dye-labeled AuNP functionalized with reporter probes to form AuNP-WNB target-MNP complex. The hybridized complex was subsequently separated from the solution by the application of an external magnet and the obtained concentrated pellet was examined under laser treatment. The obtained LOD for target sequences in buffer was 10 pM (Zhang et al., 2010).

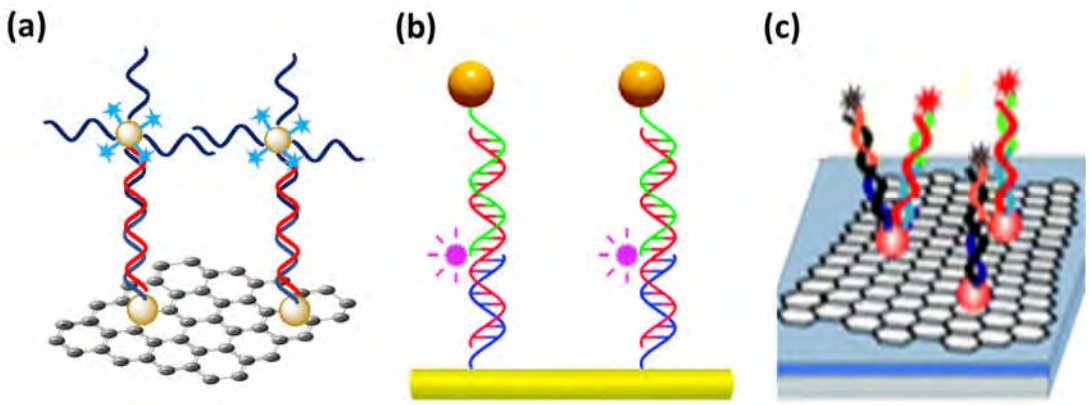

Figure 2. 9: Different biosensing strategies. (a) Co-adsorption of Raman tag and DNA probe onto sensor platform; (b) Intercalation of Raman dye in DNA probe sequence for dual platform based biosensor, adopted with permission from the Reference (Kang et al., 2010); and (c) Integrated Raman tag in Reporter DNA for single platform based biosensor, adopted with permission from the Reference (He et al., 2012).

In contrary, in single platform based sandwich assay technique, generally the CP sequences are immobilized onto a sensor platform and the Raman dye intercalated SP sequences are kept free without immobilizing onto any surface, hence presence of the corresponding target DNA couples the CP and SP strands (Figure 2.9c) (Duan et al., 2016a; He et al., 2012). A SERS aptasensor was fabricated for the detection of *S. typhimurium* from food samples, where Au@Ag core/shell nanoparticles was functionalized with aptamer 1 acting for the capture of target bacteria and X-rhodamine (ROX)-modified aptamer 2 was used as the recognition element and Raman reporter. Presence of *S. typhimurium*, two aptamers were interacted with the bacteria to form Au@Ag-apt1-target-apt 2-ROX sandwich-like complexes (Duan et al., 2016a). Similarly, SiO_2@Au core/shell nanoparticles-Apt1 and Apt 2-Cy3 were used to form sandwich complex in presence of the *V. parahaemolyticus* which leads to an LOD of 10 cfu/mL (Duan et al., 2016b). A portable SERS biosensor based on sandwich assay principle and magnetic separation has been developed for the fast and simultaneous detection of food borne bacteria such as *E. coli* O157:H7 and *S. enterica.* In the fabrication process, target sequences were first hybridized with CP attached to magnetic beads and biotinylated detection probes, followed by separation of the hybridized composite with external

magnet application and finally binding of the NeutrAvidin coated Nanoplex^{TM} biotags (Si-coated AuNPs) (Xu et al., 2012). Moreover, single platform based sandwich biosensor for the contemporaneous multiplex DNA examination with a single excitation light source was also reported where AuNPs-GO-SiO_2/Si substrate was functionalized with two different thiolated capture DNA sequences, followed by addition of corresponding target DNAs and two different reporter DNAs with integrated Raman labels – Cy3 and TAMRA at the terminal end. The hybridized composite produced the SERS spectra with unique fingerprint spectra for the two Raman labels specified the two different DNA sequences, such as the peaks at 1239 cm^{-1} and 1480 cm^{-1} for Cy3 and 1649 cm^{-1} for TAMRA, therefore distinguished the two different target DNA sequences with the LOD 10 pM (He et al., 2012).

However, to trace the minute of amount of DNA in the samples, sometimes amplification strategy is also attempted which is either amplification of the target DNA samples to increase the total number of DNA fragments or signal amplification by amplifying the length of DNA fragment to facilitate the attachment of more Raman label (Chen et al., 2019). Though the target DNA amplification followed by SERS detection is an old strategy and involves two different techniques, justified with greater performances by the inherent molecular specificity of DNA hybridization as well as spectral selectivity and high sensitivity of SERS. For example, in an experiment the target DNA of HIV virus specific *gag* gene was amplified using cresyl fast violet (CFV) labeled primers while the CP sequence complementary to PCR amplified product was bound to polystyrene substrate. Addition of the CFV labeled PCR products to CP tagged polystyrene substrate resulted in the hybridization between the capture and target sequences. The hybridized products were further coated with silver solution to amplify the CFV specific SERS spectra (Isola et al., 1998). Similarly, RCA and SERS technique were combined to develop a system for the detection of 35S promoter gene specifying a

genetically modified organism. In RCA-SERS method, enhanced SERS signal of target molecule was produced due to RCA reaction and the obtained LOD (6.3 fM) was higher than the followed method without RCA reaction (0.1 pM) (Guven et al., 2015). Conversely, target DNA triggered unfolding of immobilized hairpin capture DNA followed by the HCR to form a long DNA nanowire facilitated the self-assembly of AuNPs probes in multiple numbers on DNA nanowire, hence the amplified SERS signal to detect the transgenic sequence of *Bacillus thuringiensis* with an LOD of 50 pM (Chen et al., 2014). Hence, considering the attributes of AuNPs, GO and the GO-AuNPs or GO-AuNRs composites, we have chosen these composites as the SERS sensor platforms for the selective and sensitive detection of single as well as dual species by a single laser shot following sandwich assay strategy.

CHAPTER 3: SELECTION, VERIFICATION AND MODIFICATION OF THE DNA PROBE SEQUENCES

3.1 Influences of DNA Probe Design, Modification and Immobilization in Biosensing Application

3.1.1 DNA Probe Design

Design of the DNA probe sequences is one of the most significant pre-analytical step in biosensing due to their highly specific recognition capabilities to hybridize the corresponding target DNA. Different probe sequences based on the chemical composition and conformational arrangement have been used to construct the DNA biosensors. DNA probe sequence made up of linear oligonucleotides are most commonly used while hairpin-loop structured oligonucleotides are also being used in good frequency. Probe sequences are normally selected and designed from the hypervariable or highly conserved regions of the retrieved genomic sequences of the target species from the data bank followed by their assembly and alignment using dedicated software. Probe sequence of 18-25 nucleotides long usually confers high level of specificity in hybridization reactions than the extremely longer nucleotide sequences (Lucarelli et al., 2008).

On the other hand, hairpin probes are the stem-loop structured DNA sequences comprise of a ds-stem region due to intramolecular base pairing and ss-loop structure containing the oligonucleotide probe sequence (Lucarelli et al., 2008). Hairpin stem-loop structured probes are most commonly used in electrochemical biosensing where one end of the probe sequence is attached to sensor platform and the free end bearing a redox active compound remains in close proximity to the electrode surface due to their structural conformation. Presence of the target sequences, hybridization event take place between the target sequences with the corresponding oligonucleotides in the loop region, hence the conformational change displaces the electroactive label from the platform. The extent

of signal suppression is therefore used as an indicator of the presence and concentration of target DNA (Lucarelli et al., 2008). Moreover, infrequently some sort of the probe sequences such as PNA and locked nucleic acids (LNAs) are also used in biosensor fabrication.

PNAs are a class of DNA mimics in which the nucleobases are linked to a neutral *N*-(2-aminoethyl)-glycine repeating units and hybridize with the target DNA by hydrogen bonding and base stacking. However, due to the neutral properties of PNA, PNA-DNA duplex exhibits higher melting temperature than the homologous DNA-DNA hybrids, stability to nuclease and protease enzyme, and relatively insensitive to ionic strength (Fortunati et al., 2019; Kerman et al., 2006; Lucarelli et al., 2008). LNAs are also DNA mimics where the ribose ring is locked by a methylene bridge between the 2′-O atom and the 4′-C atom, also exhibits greater thermal stability and discriminative ability to distinguish single-base mismatch target sequences.

3.1.2 DNA Probe Immobilization Strategies

Likewise, the sequence profile and orientation of the probe sequences, immobilization of the DNA probes to the sensor platforms while maintaining its biorecognition capability to the corresponding target DNA is also a crucial step. The immobilization step promotes high reactivity, perfect orientation of the probe sequences to be hybridized with its corresponding target DNA (Rashid & Yusof, 2017). Requirement of DNA probes attachment over a wide range of material surfaces thus urges equally to opt broad range of immobilization strategies. The available strategies can generally be classified as physisorption or physical adsorption, covalent immobilization and non-covalent molecular recognition (affinity coupling) (Tjong et al., 2014). Physisorption of the DNA probes generally occur through electrostatic, van der Waals, hydrogen bond or hydrophobic interaction. In electrostatic physisorption, the negatively charged phosphate

group of DNA is adsorbed onto the positively charged surface of the biosensor platform. Though this immobilization process is rapid, involving simple steps, minimum use of chemical reagents, and do not require further modification of DNA sequences, however exhibits limitations such as desorption of the formed DNA probes monolayer due to the influence of pH buffer, ionic strength and temperature. Moreover, in physisorption method, DNA probes are attached onto sensor platforms in a random orientation at multiple sites which has the negative influence on the hybridization efficiency (Lucarelli et al., 2008; Rashid & Yusof, 2017; Tjong et al., 2014).

On the contrary, immobilization of the DNA probe sequences via covalent bonding to sensor platform ensures a good stability, prevents desorption of DNA probe monolayer and more importantly facilitate a good vertical orientation which enhances the hybridization efficiency (Rashid & Yusof, 2017; Wang et al., 2011). In covalent bonding approach, the synthesized DNA probe is typically functionalized with thiol (SH) or amino (NH_2) group at the 3′ or 5′ terminal end to bind covalently to the metal surfaces or any other functional group introduced onto sensor surface. It thus ensures specific attachment of DNA probe onto sensor platform and prevent non-specific binding. Chemisorption and covalent attachment are commonly used in the covalent immobilization of DNA probe. The chemisorption technique is frequently observed between the thiol-modified probe sequences with AuNS surface via Au-S covalent bonding to form a self-assembled monolayer of DNA probe on sensor composite (Sassolas et al., 2008). Covalent attachment of NH_2-terminated DNA probes with several functional groups such as carboxyl, aldehyde, sulfonic, epoxy and isothiocyanate on the surface of sensor platform have also been reported. It is to be noted that covalent linking between carboxyl group and NH_2-terminated DNA probes is facilitated by the carboxyl group activation via carbodiimide reagents (N-hydroxysuccinimide and 1-ethyl-3-(3-dimethylaminopropyl) carbodiimide) (Rashid & Yusof, 2017; Sassolas et al., 2008).

The non-covalent immobilization (affinity coupling) of DNA probes is another popular strategy of DNA attachment, involves the use of avidin/streptavidin-biotin recognition pairs. The avidin/streptavidin and biotin molecules interact each other with high affinity, hence reported as one of the strongest non-covalent interactions, which is highly stable and resistant to extreme conditions such as high temperature, pH, denatured detergents and organic solvents. In affinity coupling, immobilization of DNA could be done by modifying the 3′ or 5′ terminal of the probe sequence with biotin molecule and avidin/streptavidin modified with the surface of sensor platform. Moreover, avidin/streptavidin represents tetrameric binding sites for biotin thus allow for sandwich-like affinity coupling approach that links biotin modified DNA and a biotin-modified surface via a (strept)avidin bridge (Rashid & Yusof, 2017; Tjong et al., 2014).

3.1.3 Spacer linked to DNA Probe Sequences

There are few key factors that influence the performance of surface-tethered DNA in biosensing applications such as the conformation of the DNA on surfaces, spacer molecules used for DNA attachment, non-specific cross-hybridization of probe DNA with non-target DNA or non-specific adsorption of target DNA directly to sensor surface, and the surface topography (Tjong et al., 2014). However, insertion of spacer molecules between the oligonucleotide probe sequence and solid support, is the most common approach to minimize the steric hindrance and improve the hybridization efficiency of surface-tethered DNA probe with the complementary strands (Milton et al., 2013; Tjong et al., 2014). Therefore, spacer molecules have some effects such as raising the DNA probe from the surface, impacting on the local electrostatic and hydrophilic environment of the DNA probe, influencing the ‘steric’ accessibility of the DNA probe to hybridization. In addition, some spacers, can reduce the non-specific binding of the target DNA sequences on the surface (Halperin et al., 2006; Milton et al., 2013). Common

spacers include alkyl chains and homo-oligonucleotides (poly dA, or poly dT) (Heise & Bier, 2005) and in some instances oligomers of ethylene glycol (Cha et al., 2002).

3.2 Selection, Verification, Design and Modification of the DNA Probe Sequences for this study

3.2.1 Selection of the DNA probes

The MBT DNA probe sequence (31-mer) was selected from the short-length DNA fragment (120 bp) of mitochondrial cytochrome b (cytb) gene of MBT species (*Cuora amboinensis*). The sequence was developed and verified by Ali, et al. (2016) for the detection of MBT species from the complex food matrices by PCR technique (Ali et al., 2016). On the other hand, pig (*Sus scrofa*) DNA probe sequence (24-mer) was selected from cytb gene and verified by Hossain et al. (2017) to discriminate cattle, buffalo and porcine materials in food chain by real-time PCR (Hossain et al., 2017a).

3.2.2 In-silico Analysis of Biomarkers using Bioinformatics Tools

The cytb gene sequences of MBT (*C. amboinensis*, FJ763736.1), pig (*S. scrofa*, AF034253.1) and 26 other potential non-target meat and fish species (buffalo, cow, goat, horse, sheep, donkey, sika deer, dog, cat, rat, rabbit, monkey, crocodile, chicken, pigeon, turkey, quail, duck, ostrich, tuna, tilapia, cod, frog, salmon, rohu, and pangas) were retrieved from the National Centre of Biotechnology Information (NCBI) database (https://www.ncbi.nlm.nih.gov/). The selected DNA probe sequences of MBT and pig species were verified in silico by multiple aligning with cytb gene of both MBT and pig species along with 26 non-target species as mentioned above using Molecular Evolutionary Genetics Analysis version 5 (MEGA5) software. MEGA is a sophisticated and user-friendly software developed for the statistical analyses of DNA and protein sequence data from an evolutionary standpoint. With the time being, the tool has been

integrated for mining online databases, conducting sequence alignment, phylogenetic tree reconstruction and visualization, web-based acquisition of sequenced data, estimating rates of molecular evolution, and testing evolutionary hypotheses. The software is available at free of cost at https://www.megasoftware.net/ (Tamura et al., 2011). In this study, MEGA5 was used to determine the total number of mismatches in DNA probe sequences of target (MBT and pig) and non-target species. The analysis revealed that the selected 31-mer DNA probe sequence was matched 100% only with MBT cytb gene sequence and scored 6-15 nucleotide (19.4 - 48.4%) mismatching with other non-target species (Table 3.1), therefore reflecting huge genetic distance and unlikelihood of cross-species recognition in a real experiment. In contrary, the alignment result showed that 24-mer probe sequence of pork was 100% matching only with pork cytb gene and 3-12 nucleotides (12.5-50%) mismatching with other non-target species (Table 3.2).

Table 3. 1: The mismatch comparison of the MBT probe sequence against multiple aligned region of cytb gene of MBT and non-target species.

Malayan Box Turtle (MBT) probe sequence	G	A	T	C	A	T	T	A	C	T	A	G	G	C	A	C	C	T	G	C	C	T	A	A	T	C	C	T	T	C	A	Mismatch
MBT cytb gene (NC 014769.1)	.	.	.	.	.	.	.	.	.	.	.	.	.	.	.	.	.	.	.	.	.	.	.	.	.	.	.	.	.	.	.	0
Buffalo cytb gene (NC 006295.1)	.	C	.	.	T	C	.	C	.	.	.	.	.	.	.	T	.	.	.	.	.	.	.	.	.	.	.	.	G	.	.	6
Horse cytb gene (KU575247.1)	.	C	.	.	C	C	.	C	.	.	.	.	.	A	.	T	.	.	.	.	.	.	.	.	.	.	.	.	C	.	.	7
Equus asinus donkey/ass cytb gene	.	C	.	.	T	C	.	C	.	.	.	.	.	A	.	T	.	.	.	.	.	.	.	.	.	.	.	.	C	.	.	7
Pork cytb gene (AF034253.1)	.	T	.	.	C	C	.	C	T	.	.	.	.	.	.	T	.	.	.	.	.	.	.	.	.	.	T	.	G	.	.	8
Cow cytb gene (AF492351.1)	.	T	.	.	C	C	.	C	.	.	G	.	.	A	.	T	.	.	.	.	.	.	.	.	.	.	.	.	A	.	.	8
Goat cytb gene (KP271023.1)	.	.	.	.	C	C	.	C	.	.	.	.	.	A	.	T	T	.	.	.	.	.	.	.	.	.	T	.	A	.	.	8
Sika deer cytb gene (NC 006993.1)	.	C	.	.	C	C	.	.	.	.	.	.	.	A	.	T	T	.	.	T	.	.	.	.	.	.	.	.	A	.	.	8
Dog cytb gene (MH891616.1)	.	.	.	.	C	.	.	.	.	.	.	.	.	A	G	T	A	.	.	.	T	.	G	.	.	T	.	.	A	.	.	9
Rabbit cytb gene (NC 001913.1)	.	C	.	.	T	C	.	.	.	.	.	.	.	.	C	T	G	.	.	.	.	.	T	.	.	A	A	.	.	.	.	9
Ostrich cytb gene (NC 002785.1)	.	.	.	.	G	C	.	.	.	.	.	.	.	A	.	T	T	.	.	.	.	.	.	.	.	T	A	C	C	.	.	9
Tuna cytb gene (KF906721.1)	.	C	.	.	.	C	.	.	.	.	T	.	.	.	C	T	T	.	.	.	.	.	T	.	.	T	T	C	.	.	.	10
Tilapia cytb gene (GU238433.1)	.	.	.	.	T	C	.	.	.	.	.	.	.	.	C	T	.	.	.	T	.	.	.	G	C	.	G	C	C	.	.	10
Sheep cytb (KR868678.1)	.	C	.	.	T	C	.	C	.	.	.	.	.	.	.	T	T	.	.	.	T	.	.	.	.	T	T	.	A	.	.	10
Cat cytb gene (NC 001700.1)	.	C	.	.	C	C	.	T	.	.	.	.	.	A	G	T	.	.	.	.	.	.	.	.	C	.	T	.	A	.	.	10
Pigeon cytb gene (KJ722068.1)	.	G	.	.	C	C	.	.	.	.	.	.	.	.	.	T	T	.	.	.	T	.	G	C	.	A	A	C	.	.	.	11
Quail (Japanese) cytb gene (KX712089.1)	.	C	.	.	C	C	.	.	.	.	.	.	C	A	.	T	A	.	.	.	.	.	C	.	.	.	A	C	C	.	.	11
Cod cytb gene (NC 002081.1)	.	C	.	.	T	C	.	T	.	.	.	.	.	.	C	T	T	.	.	.	T	.	.	.	.	T	A	C	.	.	.	11
Rat cytb gene (AC 000022.2)	.	T	.	.	T	C	.	.	.	.	.	.	.	A	G	T	A	.	.	.	.	.	C	.	.	A	G	.	A	.	.	11
Turkey cytb gene (NC 010195.2)	.	C	.	.	C	C	.	.	.	.	.	.	C	A	G	T	A	.	.	.	.	.	C	.	.	.	A	C	.	.	.	11
Duck cytb gene (EU009397.1)	.	.	.	.	T	C	.	G	.	.	C	.	C	.	.	T	.	.	.	.	.	.	G	G	C	.	A	C	A	.	.	12
Frog cytb gene (NC 024548.1)	.	G	.	.	.	C	.	T	.	.	.	.	.	.	T	T	A	.	.	T	T	.	.	.	.	T	G	C	C	.	.	12
Monkey cytb gene (NC 012670.1)	.	C	.	.	.	C	.	T	.	.	C	A	C	A	G	.	.	.	.	T	.	.	.	.	C	.	T	.	A	.	.	12
Crocodylus porosus cytb gene (DQ273698.1)	.	.	.	.	.	C	.	T	.	.	C	.	.	A	T	T	.	A	C	.	.	.	.	T	.	A	A	.	C	.	.	12
Chicken cytb gene (AP003580.1)	.	C	.	.	C	C	.	.	T	.	.	.	C	A	G	T	.	.	.	.	.	.	C	.	.	G	A	C	C	.	.	13
Salmon cytb gene (KF792729.1)	.	C	.	.	.	C	.	C	T	.	.	.	.	.	C	T	A	.	.	T	.	.	.	G	C	.	A	C	C	.	.	13
Rohu cytb gene (NC 017608.1)	.	.	.	.	C	C	.	C	.	.	.	.	.	A	T	T	A	.	.	T	T	.	G	.	.	T	A	C	C	.	.	14
Pangas cytb gene (NC 023924.1)	.	C	.	.	C	C	.	C	.	.	.	C	T	A	C	T	A	.	.	T	.	.	T	.	.	A	G	.	A	.	.	15

Table 3. 2: The mismatch comparison of the pig probe sequence against multiple aligned region of cytb gene of pork and other non-target species.

Pork probe	**C**	**C**	**T**	**G**	**C**	**C**	**A**	**T**	**T**	**C**	**A**	**T**	**C**	**A**	**T**	**T**	**A**	**C**	**C**	**G**	**C**	**C**	**C**	**T**	**Mismatch**
Pork (*Sus scrofa*) cytb gene (AF034253.1)	.	.	.	.	.	.	.	.	.	.	.	.	.	.	.	.	.	.	.	.	.	.	.	.	0
Goat cytb gene (KP271023.1)	C	C	T	C	C	C	A	T	T	C	A	T	C	A	T	C	A	C	A	G	C	C	C	T	3
Horse cytb gene (KU575247.1)	C	C	T	A	C	C	C	T	T	C	A	T	C	A	T	C	A	C	A	G	C	C	C	T	4
Rat cytb gene (AC 000022.2)	C	C	T	C	C	C	A	T	T	C	A	T	T	A	T	C	G	C	C	G	C	C	C	T	4
Monkey cytb gene (NC 012670.1)	.	.	.	A	.	.	C	.	.	.	.	.	.	.	.	C	.	T	.	.	.	.	.	.	4
Sheep cytb gene (KR868678.1)	T	T	T	C	C	C	A	T	T	C	A	T	C	A	T	C	G	C	A	G	C	C	C	T	6
Buffalo cytb gene (NC 006295.1)	.	.	.	C	.	.	.	.	.	.	.	.	T	.	.	C	G	.	A	.	.	A	.	.	6
Rohu cytb gene (NC 017608.1)	A	.	.	A	.	.	.	.	.	T	.	.	.	.	.	.	G	.	.	.	.	.	G	C	6
Dog cytb gene (MH891616.1)	.	.	.	C	.	.	T	.	.	.	.	.	.	.	.	C	G	.	A	.	.	T	.	.	6
Frog cytb gene (NC 024548.1)	T	.	.	C	.	.	.	.	.	T	.	.	T	.	.	.	.	.	.	.	.	T	G	.	6
Equus asinus donkey/ass cytb gene (KT182635.1)	T	.	.	A	.	.	C	.	.	T	.	.	.	.	.	C	.	.	G	.	.	.	.	.	6
Cow cytb gene (AF492351.1)	.	.	.	T	.	.	.	.	.	T	.	.	.	.	.	C	.	T	A	.	.	A	A	.	7
Sika deer cytb gene (NC 006993.1)	T	.	.	T	.	.	.	.	.	T	.	.	.	.	.	C	G	.	A	.	.	A	.	.	7
Rabbit cytb gene (NC 001913.1)	.	T	.	.	.	.	.	.	.	T	.	.	.	.	.	.	G	.	A	A	.	T	T	.	7
Cat cytb gene (NC 001700.1)	T	.	.	T	.	.	.	.	.	.	.	.	T	.	.	C	T	.	A	.	.	.	T	.	7
Pigeon cytb gene (KJ722068.1)	.	.	.	C	.	.	C	.	.	T	.	.	A	.	.	C	G	.	A	.	G	.	.	.	8
Tuna cytb gene (KF906721.1)	A	T	.	C	.	.	.	.	.	.	G	.	.	.	.	C	G	.	A	.	.	.	A	.	8
Tilapia cytb gene (GU238433.1)	.	T	.	C	.	.	C	.	.	.	.	.	.	.	.	.	G	.	A	.	.	T	G	C	8
quail (Japanese) cytb gene (KX712089.1)	.	.	.	C	.	.	.	.	.	.	T	.	A	.	.	C	G	.	A	.	G	A	A	.	9
Pangas cytb gene (NC 023924.1)	A	.	.	C	.	.	.	.	.	.	G	.	A	G	.	.	.	T	.	.	.	A	G	C	9
Crocodylus porosus cytb gene (DQ273698.1)	G	.	.	C	.	.	.	.	.	T	.	.	.	C	.	C	.	T	A	.	.	.	A	C	9
Turkey cytb gene (NC 010195.2)	.	.	.	C	.	.	C	.	.	.	.	.	A	.	.	C	G	.	A	.	G	A	A	.	9
Salmon cytb gene (KF792729.1)	A	T	.	C	.	.	.	.	.	.	G	.	T	.	.	.	G	.	A	.	.	T	G	C	10
MBT cytb gene (FJ763736.1)	A	.	.	C	.	.	C	.	.	.	G	C	T	.	.	C	G	.	T	.	G	T	.	.	10
Ostrich cytb gene (NC 002785.1)	.	.	.	C	.	.	.	.	.	T	G	.	A	.	.	C	G	.	T	.	G	.	A	.	10
Duck cytb gene (EU009397.1)	A	.	.	A	.	.	C	.	.	T	T	.	A	.	.	C	G	.	A	.	G	A	A	.	12
Chicken cytb gene (AP003580.1)	.	.	.	C	.	.	C	.	.	T	G	C	A	.	.	C	G	.	A	.	G	T	A	.	12
Cod cytb gene (NC 002081.1)	A	T	.	C	.	.	C	.	.	T	G	.	T	G	.	.	G	.	T	.	.	T	T	.	12

3.2.3 DNA Probe Design and Modification - 1

As a sensing strategy, the MBT DNA probe sequence was designed to split into two fractions – 16-mer and 15-mer length which were further modified with 5′ thiol modifier with 6-carbon spacer arm (C6 S-S) and 3′ thiol modifier with 3-carbon spacer arm (C3 S-S) respectively (Table 3.3). Structure of the spacer arms are presented in Figure 3.1. The spacer arm separates the thiol group from the nucleotide bases of the oligo sequences to reduce the steric interactions with the end of the oligo. On the other hand, the thiol modification is accomplished into the probe sequence as a disulfide form during oligonucleotide synthesis in order to protect the thiol group from undesirable side reactions. The disulfide bond is generally reduced with TCEP or dithiothreitol (DTT) to generate the fully active thiolated oligo for further use. For this study, the thiol functionalized oligonucleotide sequences were synthesized and purified by the Integrated DNA Technologies (IDT), Singapore (https://sg.idtdna.com/pages).

Table 3. 3: MBT DNA Probe sequences and the modifications

Sequence ID	Sequence Profile
Probe sequence	5'-GATCATTACTAGGCACCTGCCTAATCCTTCA-3'
Probe (16-mer)	5′-S-S-C6-GATCATTACTAGGCAC-3'
Probe (15-mer)	5'-CTGCCTAATCCTTCA-C3-S-S-3′

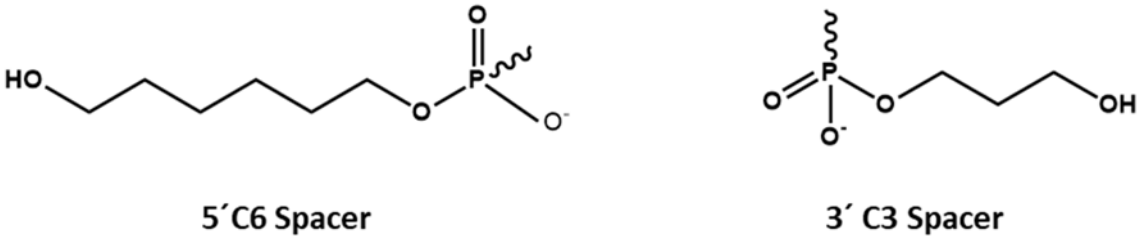

5´C6 Spacer 3´ C3 Spacer

Figure 3. 1: Structure of the C6 spacer and C3 spacer.

3.2.4 DNA Probe Design and Modification - 2

The selected MBT and pig oligonucleotide probe sequences (31-mer and 24-mer respectively) were split into two halves i.e., 16-mer and 15-mer for MBT and 12-mer of two equal halves for pig species. The 5′ end of 16-mer split-probe sequence of MBT was chemically functionalized with a Raman dye (Cy3) while the 5′ terminus of 12-mer length split-probe sequence of pig species was chemically functionalized with the Raman label, ATTO Rho6G. In both cases, the Raman labels were adjacent to the C6 spacer arm preceded by a 5′ thiol modifier. On the other hand, 15-mer part of MBT and another 12-mer length split-probe sequence of pig species were functionalized with 3′ C3 S-S. The DNA probe sequence profile of the two species and the modifications are summarized in the Table 3.4.

Table 3. 4: DNA Probe sequences and the modifications

Species	Sequence ID	Sequence Profile
MBT	Probe sequence	5′-GATCATTACTAGGCACCTGCCTAATCCTTCA-3′
	Probe (16-mer)	5′-S-S-C6-(Cy3)-GATCATTACTAGGCAC-3′
	Probe (15-mer)	5′-CTGCCTAATCCTTCA-C3-S-S-3′
Pig	Probe sequence	5′-CCTGCCATTCATCATTACCGCCCT-3′
	Probe (12-mer)	5′-S-S-C6-(ATTO Rho6G)-CCTGCCATTCAT-3′
	Probe (12-mer)	5′-CATTACCGCCCT-C3-S-S-3′

Herein, in this study a unique structure was designed to functionalize the Raman tag integrated DNA probe sequences. The chemical modification of the oligo probe sequences was performed at the 5′ end of the sequences. The modification was mainly based on the using of a core chemical structure – amino modifier serinol (Figure 3.2a) where oligonucleotide sequences were synthesized at one end and the respective Raman dye was added next to it and finally the 5′ thiol modifier. More specifically, to synthesize

and cleave the oligo (which has an amino group and a thiol-modifier C6 S-S at 5′ but has no dye modification), the manufacturer followed the standard oligo synthesis procedure to obtain the crude intermediate product (Figure 3.2b). The intermediate is synthesized from 3′ to 5′ including the modified serinol and thiol modified C6 spacer. Finally, the intermediate is modified with the insertion of the selected Raman dye to obtain the final crude product (Figure 3.2c). The final structure of the chemically modified probe sequences for both species are presented in the Figure 3.3.

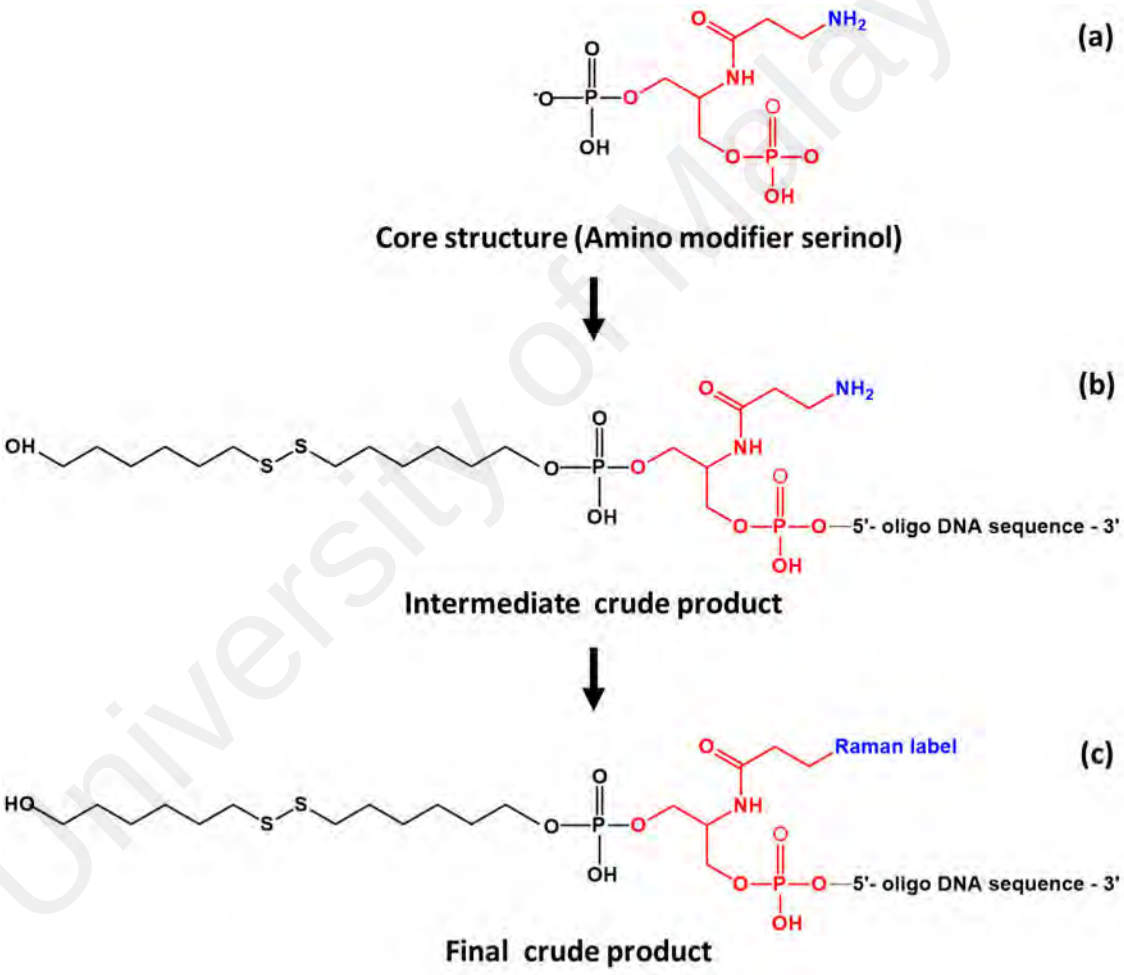

Figure 3. 2: Schematic presentation of the synthesis and modification of the probe sequences. (a) Amino modifier serinol, the core structure of chemically synthesized oligo probe sequence, (b) Synthesis of crude intermediate product containing oligo probe sequences with an amino group and a C6 S-S at 5′ terminal, and (c) Final crude product comprising of oligo sequences with integrated Raman dye with 5′ C6 S-S.

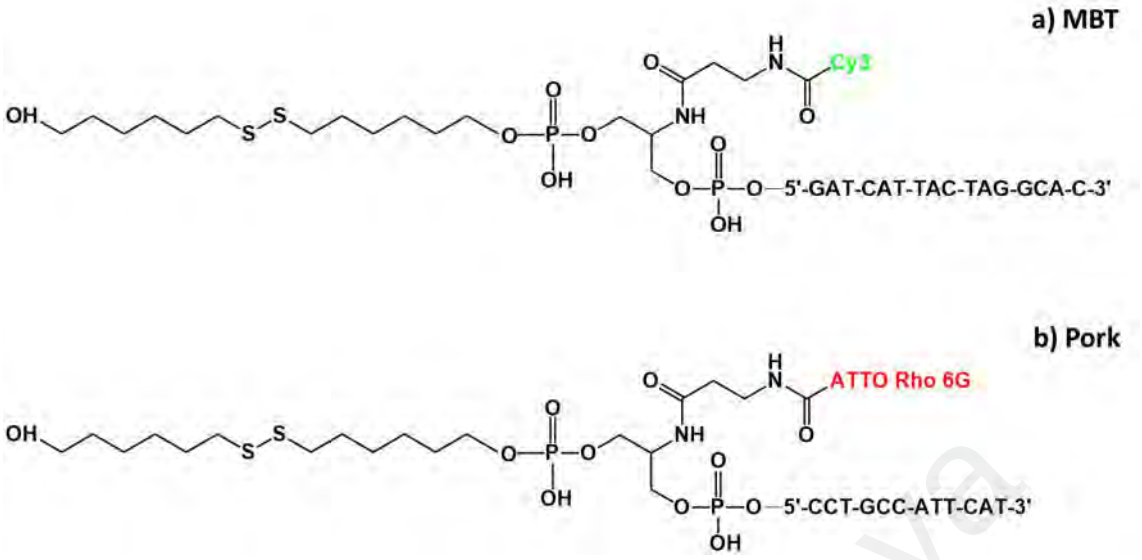

Figure 3. 3: Final structure of the chemically modified oligo probe sequences of (a) MBT with intercalated Cy3, and (b) pig intercalated with ATTO Rho6G.

3.3 Selection of the Raman labels

Cy3 is a fluorescent dye (greenish yellow) that belongs to the cyanine family of synthetic polymethine dyes (Figure 3.4a). It is reactive, water-soluble, and has an absorbance maximum of 550 nm and an emission maximum of 570 nm. It is available both a phosphoramidite and an NHS ester, and is used for direct coupling to oligo sequences at either the 5′ or 3′-end, or internally using automated chemistry. On the other hand, ATTO Dyes are a series of fluorescent labels and dyes manufactured by ATTO-TEC GmbH in Siegen, Germany. The ATTO Rho6G which is a cationic dye closely related to well-known Rho6G, moderately hydrophilic and has an absorbance maximum of 535 nm and an emission maximum of 560 nm (Figure 3.4b). It has a rigid structure, shows high thermal and photo-stability. It does not show any cis-trans isomerization, thus exhibit exceptional intensity with minimal spectral shift on conjugation. However, for direct attachment of Cy3 onto nanoparticles, Cy3 Raman tag were further functionalized with cysteamine which carries amine functional group at one end and thiol group at another end (Figure 3.4c). Therefore, cysteamine is used as the spacer molecule to link

Cy3 at the amino-terminal end and keeping thiolated end in disulfide form to be attached with the nanoparticle surfaces ((Figure 3.4d) (Kahraman et al., 2009).

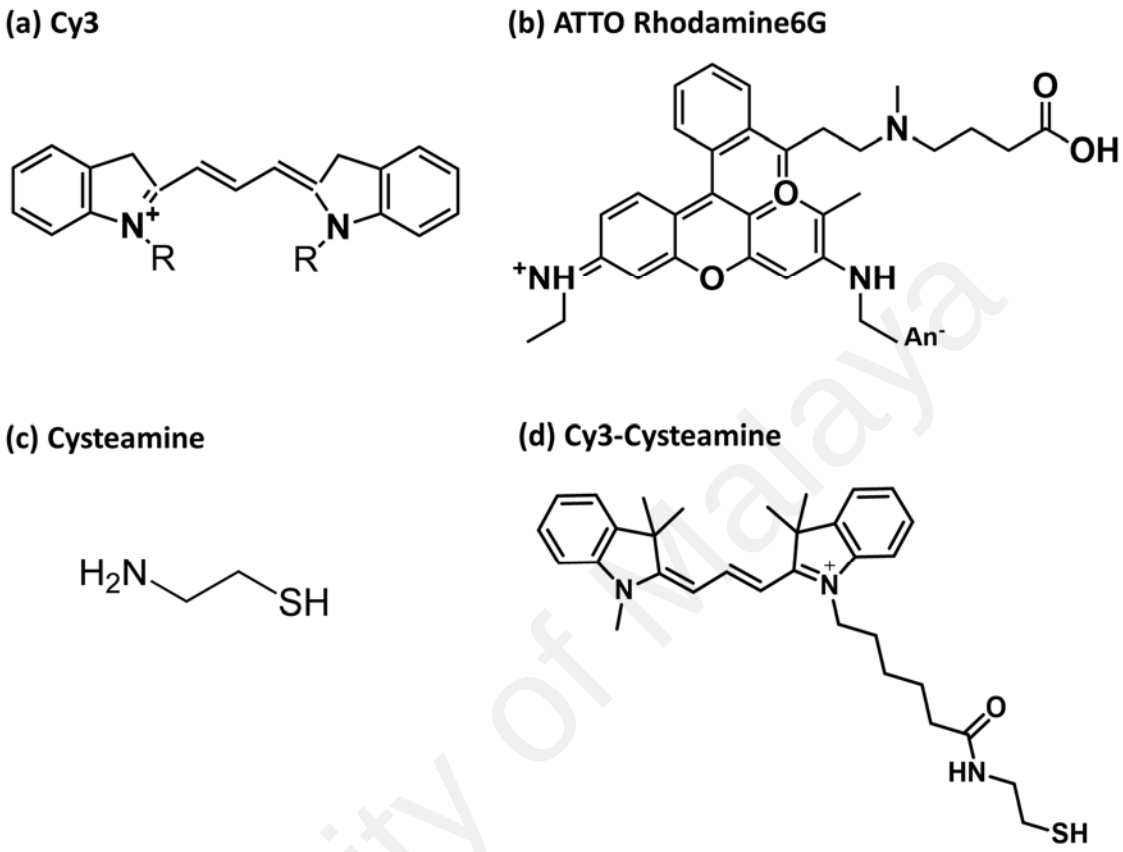

Figure 3. 4: Chemical structure of the (a) Raman dyes Cy3, (b) ATTO Rho6G, (c) Cysteamine, and (d) Cy3 functionalized with cysteamine.

The cysteamine functionalized Cy3 and the chemically modified oligonucleotide probe sequences were synthesized and purified by Biosynthesis, USA (https://www.biosyn.com/index.aspx). The UV-vis spectra of the Cy3 (NHS) and ATTO Rho6G (NHS) showed absorption peaks at 563 nm and 539 nm respectively (Figure 3.5a) which comply the theoretical specifications. Intercalation of Cy3 to the 16-mer oligo probe sequences and ATTO Rho6G to the 12-mer probe sequence also exhibited the UV-vis absorption spectra at 550 and 540 nm respectively, dictating the presence of the corresponding dye while the peak at 260 nm for both of the probe sequences corresponds the DNA structure (Figure 3.5b). The Raman dyes were selected for this study due to their unique Raman spectra and large Raman cross section (Cao et al., 2002). Cy3 exhibited

the unique Raman peaks predominantly at 798, 937, 1121, 1270, 1384, 1470 and 1592 cm^{-1} (Figure 3.5c) correspond to the C–H deformation in (>N)-CH_3, C–H aromatic ring bending, C–H in plane bending in (>N)-CH3), aromatic C–C stretching, methane chain, and C–N stretching modes, respectively (Hart, et al., 2020; Alwan, et al., 2018). On the other hand, Raman spectra of ATTO Rho6G revealed major peaks at 1183, 1357, 1505, 1569 and 1648 cm^{-1} (Figure 3.5d) which are assigned to the C–H in-plane bending of xanthene ring, C–C stretching of xanthene ring/amine group, C–C stretching of xanthene ring/amine group, C=C symmetric stretching motion in phenyl ring, and C=C symmetric stretch of xanthene ring, respectively (Eremina, et al., 2020; Watanabe, et al., 2005).

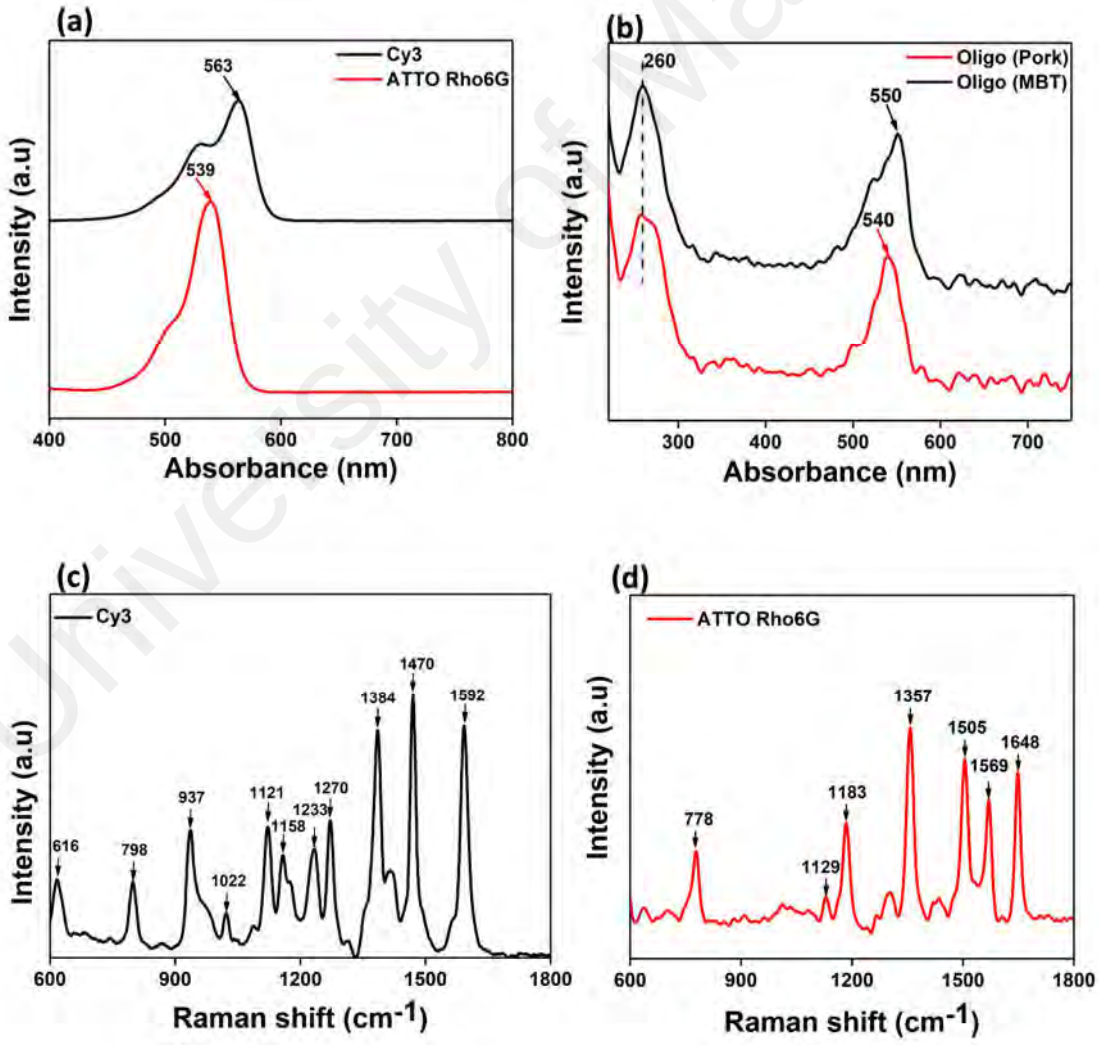

Figure 3. 5: UV-vis absorption spectra of (a) the Cy3 and ATTO Rho6G, and (b) the corresponding Raman label intercalated oligo probe sequences. Distinct Raman spectra of the selected Raman labels - (c) Cy3 and (d) ATTO Rho6G.

CHAPTER 4: DUAL PLATFORM AND SHORT-LENGTH DNA PROBE BASED SERS DNA BIOSENSOR FOR THE QUANTITATVIE DETECTION OF MALAYAN BOX TURTLE

4.1 Introduction

DNA sensing technology has rapidly emerged since last decades to get the biological footprints of every species. Current technologies for DNA identification such as sequencing, microarray and mass spectrometry are labor-intensive, time-consuming and require expensive equipment. In addition, the use of short-length DNA probe in the widely accepted PCR based techniques for the DNA detection is often very challenging (Ngo et al., 2016). Short-length amplicons, typically ≤150 bp in length improve better recovery of the detection from the degraded DNA specimens or compromised forensic evidences (Turna et al., 2010). However, reduction of amplicon length in PCR based technique is limited by the low specificity, and producing artifacts in the final results (Ali, et al., 2012; Hird et al., 2006). Therefore, nanoparticles based DNA sensing has recently considered as one of the best alternatives to the conventional strategies to conserve the high specificity and sensitivity using very short segment of DNA as the detection probe (Merkoçi, 2010). In recent years, nanoparticles based DNA biosensors are employed in diversified applications including identification of pathogenic microorganisms (Tondro et al., 2018), detection of cancer biomarkers (Huang et al., 2018a; Shahrokhian & Salimian, 2018), trace elements, environmental hazards, drug screening, and the analysis of gene sequences (Li et al., 2005b; Saidur et al., 2017) and food safety (Ha et al., 2017). Hence, the nanoparticle based SERS DNA sensing technology could be strategic to identify the endangered and vulnerable turtle – MBT species. MBT is also an attractive item to the illegal wildlife trader due to its huge appeal as an exotic food item as well as in TCM. Moreover, it is a carrier of several pathogenic microorganisms, parasites, various toxins, and heavy metals (Ali et al., 2016; Green et al., 2010). Therefore, consumption of

or contact with this turtle and/or turtle-derived materials in food chains and medicines have significant health concerns which urge for the reliable authentication technique for this turtle species to restrict health hazards, as well as to prevent or reduce illegal trades.

SERS has emerged as the most powerful analytical technique for the fast and ultra-sensitive detection of DNA with single molecule differentiations by providing intrinsic chemical information and vibrational fingerprints of each molecules (Nie & Emory, 1997; Xu et al., 2015). However, nanoparticle-based SERS signaling is mostly dependent on the local electromagnetic field enhancement due to hot spots at the nanoscale junctions and interstitial crevices of the two or more linking SERS-active substrates (Hao & Schatz, 2004; Qian et al., 2008). Till date, lots of SERS-active substrates either in single component or composite form have been employed to achieve enhanced SERS signal, hence to increase the efficiency of the sensing strategy (Khalil et al., 2016; Lu et al., 2011). GO-AuNP hybrid composites have recently been proved as an effective SERS platform due to the synergistic effect of two individual components which can magnify the weak Raman signals (Khalil et al., 2016). However, the integration of GO-AuNP hybrid composites with AuNPs has never been explored which can further enhance the Raman signal of the adsorbed molecules with many order of magnitude via electromagnetic and chemical enhancement in comparison to the individual components (either GO, AuNPs or GO-AuNP hybrid alone). Thus, DNA sensing strategy that uses both GO-AuNP hybrid composite and AuNPs as the sensor platforms, could revolutionize the current biosensing techniques for detecting endangered species as well as DNA biomarkers for many diseases including cancer.

Herein, in this chapter a novel SERS based DNA detection strategy is reported involving dual platforms and short-length DNA probes for the detection of MBT species. In this biosensing feature, the detection is based on the covalent linking of the two

platforms involving GO-AuNP functionalized with CP 1 and AuNP modified with CP 2 and Cy3 via hybridization with the corresponding target sequences. Coupling of the two platforms facilitates covalent agglomeration of the strongly coupled plasmonic AuNPs over GO-AuNPs, thereby exhibits locally enhanced electromagnetic field at the junctions. The use of dual platforms thus significantly enhanced the SERS signal due to the 'hot spot' generation between GO-AuNPs and AuNPs system (Hao & Schatz, 2004; He et al., 2012; Qian et al., 2008). The developed sensing protocol detected the target DNA sequence of endangered MBT species, using a short-length CP sequence, which is a limitation for current PCR based techniques. Moreover, in this study the Raman tag was attached directly onto the AuNPs surfaces which minimizes the distance dependent limitations, and produced intense SERS spectra by the charge transfer mechanism between the Cy3 and AuNP surfaces (Wabuyele & Vo-Dinh, 2005). With this greater amplification of the SERS signal generated by the hybridized sandwich structure, an LOD of 10 fM was achieved. Moreover, the dual platforms showed excellent sequence specificity and sensitivity to discriminate the closely related six non-target DNA sequences as well as single nucleotide base-mismatch in the target DNA sequence. In comparison with other SERS DNA biosensors, this fabricated sandwich biosensor is cost effective and avoids complex manipulation of ssDNA probe. Therefore, this simple but highly selective, specific and sensitive DNA sensing approach would be useful for the wide-range of biosensing applications.

4.2 Materials and Methods

4.2.1 Chemicals and Instruments

Gold chloride trihydrate ($HAuCl_4 \cdot 3H_2O$), sodium citrate dihydrate ($C_6H_5Na_3O_7 \cdot 2H_2O$) (≥99%), graphite powder (<20μm), tris(2-carboxyethyl) phosphine hydrochloride (≥98%) (TCEP) and Tris-EDTA (TE) buffer solution, pH 7.4 were

obtained from Sigma Aldrich. Potassium permanganate ($KMnO_4$), phosphoric acid (H_3PO_4) were purchased from R & M Chemicals Ltd.; sulphuric acid (H_2SO_4) (95-97%), hydrochloric acid (HCl) (37%), and ethanol (99.8%) from Friendemann Schmidt and hydrogen peroxide (H_2O_2) (35%) from Quality Reagent Chemical (Qrec). DPEC treated water (DTW) was purchased from Biobasic Canada Inc. while ultrapure water (UPW) (18.2 MΩ cm) was prepared from CASCADA LS Water, Pall UltraPure Water System and used throughout the study. The rest of the chemicals were of analytical reagent grade and used as per requirement.

Washing and purification of the GO, AuNP and GO-AuNPs were done by using high speed Heraeus Multifuge X3FR Centrifuge, Thermo Scientific. On the contrary, Mini-15K CE High Speed Mini Centrifuge was employed throughout the study for the washing of unbound DNA, washing or separation of nanoparticles/nanocomposites. Ultrasonic homogenizer (TF-650Y) was used for the exfoliation of GO. UV–vis experiments were conducted by using UV-2600 UV–vis spectrophotometer (Shimadzu co., Ltd, Japan). High resolution Transmission electron microscopy (HR-TEM) was performed using lacy carbon coated copper (Cu) grid with FEI Tecnai F20 TWIN 200kV transmission electron microscope (FEI Company, Hillsboro, USA). X-ray diffraction (XRD) was performed by using PANalytical X-ray diffractometer (model - EMPYREAN, Almelo, Netherlands). SERS spectra were recorded using Renishaw Invia Confocal Raman Microscope. AFM was performed using AFM5000II Scanning Probe Microscope (Hitachi) in dynamic force (tapping) mode.

4.2.2 Probe, Target and Non-Target DNAs

The DNA probe sequence (31-mer) was selected from the short-length DNA fragment (120 bp) of mitochondrial cytb gene of MBT species. The sequence was developed and verified by PCR technique for the detection of MBT species from complex food matrices

by Ali, *et al.* (2016) (Md Eaqub Ali et al., 2016). The DNA probe sequence was further split into two fractions – 16-mer and 15-mer length, followed by modification with 5′-C6-S-S and 3′-C6-S-S respectively. All the oligonucleotide sequences (Table 4.1) were synthesized and purified by the IDT, Singapore. The lyophilized oligonucleotides were resuspended in TE buffer (10 mM Tris HCl, 1 mM EDTA, pH 7.4) as per manufacturer instructions and kept at - 40°C as stock solution in 100 µM concentration. To prepare the working standard or dilution from the stock solution, DPEC treated water was used throughout the study.

Table 4. 1: List of oligonucleotide sequences

Name	**Sequence Profile**
CP 1 (16-mer)	: SH-$(CH_2)_6$-5′-GATCATTACTAGGCAC-3′
CP 2 (15-mer)	: 5′-CTGCCTAATCCTTCA 3′-$(CH_2)_3$-SH
Target DNA	: 5′-TGAAGGATTAGGCAGGTGCCTAGTAATGATC-3′
One-base mismatch	: 5′-TGAAGGATTAGGCAAGTGCCTAGTAATGATC-3′
Three-base mismatch	: 5′-TGAAGGATTAGGTGAGTGCCTAGTAATGATC-3′
NC DNA	: 5′-CAGGAAGCCGAATGAACATTCGACGGCAGCT-3′
NT DNA (Buffalo)	: 5′-TGCAGGATTAGGCAGATGCCTAGGAGAGAGC-3′
NT DNA (Horse)	: 5′-TGGAGGATTAGGCAGATTCCTAGGAGGGAGC-3′
NT DNA (Cow)	: 5′-TGTAGGATTAGGCAGATTCCCAGGAGGGAAC-3′
NT DNA (Pork)	: 5′-AGGGCGGTAATGATGAATGGCAGG-3′
NT DNA (Dog)	: 5′-TGGCTGTGTCCGATGTATAGTGCAAGTCCACTT-3'

NC: Noncomplementary, NT: Non-target

4.2.3 Collection of the Meat Samples and Extraction of Genomic DNA

Authentic frozen raw meat samples of MBT species in triplicates were collected from another research team of Nanotechnology and Catalysis Research Centre (NANOCAT), University Malaya who have already identified the supplied meat sample employing different PCR methods (Ali et al., 2015b; Ali et al., 2016; Asing et al., 2016). The total

DNA was extracted from the muscle tissue of MBT using FavorPrep Tissue Genomic DNA Extraction Mini Kit (Favorgen Bitoech Corp, Taiwan) as per supplied instructions. In brief, 25 mg of tissue sample was taken in a microcentrifuge tube, grounded and homogenized with lysis buffer-1 and proteinase K by a micropestle, which was followed by incubation at 60°C for 2-3 h until complete cell lysis and protein degradation. The sample mixture was further treated with lysis buffer-2, vortex mixed and incubated at 70°C for 10 min, followed by adding ethanol (96-100%) and mixing with pulse-vortexing. The sample mixture was then transferred into the mini-column and centrifuged at 14000 rpm for 3 min to bind the DNA onto the glass fiber matrix. The mini column was washed with W1 buffer, centrifuged and discarded the flow-through, repeated the procedure with wash buffer containing ethanol. Finally the purified DNA was collected by adding pre-heated elution buffer to the membrane of the mini column, kept standing for 3 min and centrifuged at high speed for 2 min. The concentration and purity of the extracted DNA were checked by NanoDrop 2000 spectrophotometer (Thermo Scientific, USA). The concentration was determined based on the absorbance at 260 nm and the purity was evaluated by the absorbance ratio at 260 nm and 280 nm (A260/A280), where A260 and A280 indicate the absorbance maxima of nucleic acid and proteins respectively. The obtained purified genomic DNA was stored at -20°C for further use.

4.2.4 Synthesis of Graphene Oxide

GO was synthesized as per protocol described by Marcano, *et al*. (Marcano et al., 2010). In a typical method, a 9:1 mixture of concentrated H_2SO_4/H_3PO_4 (419.4 : 46.6 mL) was added to the graphite powder (3.5 g) in a 1000 mL two-neck round bottom flask placed in oil bath and started to stir slowly. $KMnO_4$ (21.0 g) was added gradually to the mixture, producing a slight exotherm to 35−40°C. The reaction was then heated to 50°C with continuous stirring for 12 h. The reaction was then cooled down to room temperature

and poured onto ice (466 mL). 30% H_2O_2 (3.5 mL) was then added to the suspension until a light-yellow color developed. The suspension was centrifuged at low speed (500 rpm for 10 min) to remove the unoxidized graphite and other large particles (multilayered GO) and kept the supernatant. The filtrate was then washed two times with deionized (DI) water, 30% HCl, and ethanol, respectively by centrifugation at 10000 rpm for 30 min. Every time the supernatant was decanted away and collected the pellet, homogenized with the respective solvent and centrifuged. Finally, the GO suspension was washed with DI water for two times by centrifugation at 10000 rpm for 30 min. The material remaining after this multi-wash process was collected, filled into cellulose membrane dialysis tubing (average diameter: 21 mm, Sigma-Aldrich) and left in continuous stirring for 72 h with regular changing of DI water at 4 h interval. The pH of the suspension was reached around 6. The obtained material was freeze-dried to get the GO powder.

4.2.5 Synthesis of AuNPs

AuNPs were synthesized by Turkevich method as per the described protocol with few modifications (Liu & Lu, 2006). In brief, 350 mL of 1.0 mM $HAuCl_4.3H_2O$ solution was kept in 500 mL Erlenmeyer flask on a stirring hot plate and heated the solution until boiling. To the rapidly-stirred boiling solution, promptly added 35 mL of 38.8 mM sodium citrate solution. The solution was turned to deep red color from light yellow within 2 min. The solution was allowed to reflux for another 20 min. Heating was turned off and the system was allowed to cool to room temperature under stirring and subsequently filtered through 0.45 μm syringe filter. Finally, AuNPs suspension was stored in the cool and dark place (in the refrigerator by wrapping the bottle with aluminum foil).

AuNPs synthesis by Turkevich method is based on the reduction of tetrachloroauric acid by trisodium citrate (Figure 4.1). The AuNPs formation involves multiple chemical

reaction steps occurring in a series and parallel where the initial step is the oxidation of the citrate to yields dicarboxy acetone (Equation 1). The second step is the reduction of the auric salt to aurous salt (Equation 2) and the final step is the disproportionation of aurous species to Au atoms in which three aurous chloride are required to produce to two Au atoms (Equation 3). The overall stoichiometry of the reduction reaction by Turkevich method is represented in Equation 4 (Kumar et al., 2007). However, recently Gao et al. (2019) proposed that Turkevich mechanism involves two consecutive reduction steps (Au^{3+} Au^{+} Au^{0}) rather than a reduction followed by the disproportionation reaction as conventionally believed. Moreover, it was also postulated that second reduction step (Au^{+} Au^{0}) rather than the previously considered first reduction reaction (Au^{3+} Au^{+}) is the rate-limiting step in controlling the size of AuNPs as well as dicarboxy acetone, an intermediate product of citrate oxidation, plays a key role in the electrostatic stabilization of AuNPs (Gao & Torrente-Murciano, 2020).

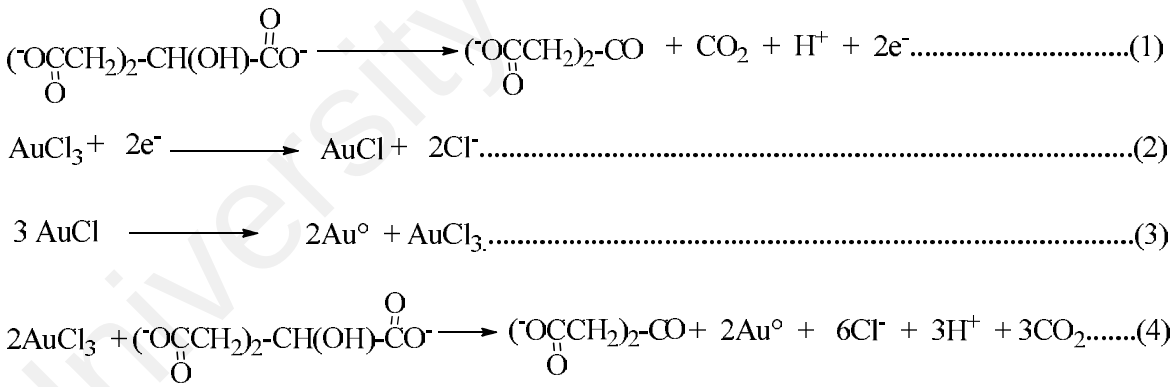

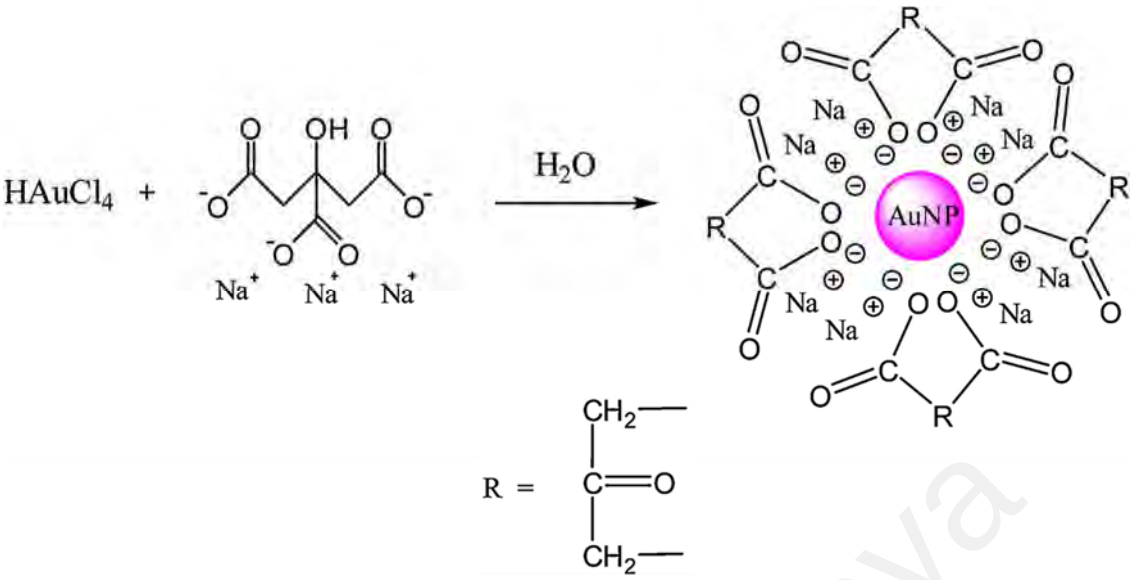

Figure 4. 1: AuNP synthesis using the Turkevich method. The figure was adopted with permission from Reference (Zhao et al., 2013).

4.2.6 Synthesis of GO-AuNP nanocomposites

GO-AuNPs composites were synthesized by the citrate reduction of gold (III) salt as per reported procedure with minor modifications (Goncalves et al., 2009). An aqueous suspension of GO (0.5 mg/mL, 20mL) was prepared by ultrasonication for 2 h, followed by the addition of syringe filtered 100 mL $HAuCl_4 \cdot 3H_2O$ solution (1 mM). The resultant suspension was then aged for 30 min with continuous stirring to promote the interaction of Au ions with GO surface. The suspension was then heated until 80°C and 2 mL of sodium citrate aqueous solution (300 mM) was added promptly into it. The reaction was continued at 80°C with stirring for another 4 h. The resulting GO-AuNPs composite was centrifuged at 6000 rpm for 2 h and washed three times with UPW to eliminate the free AuNPs. The final GO-AuNPs nanocomposite was resuspended in UPW and stored in the refrigerator.

4.2.7 Attachment of thiol-modified DNA probe to AuNPs and GO-AuNPs

To activate the thiol-modified oligo DNA, 100 µL of 1 µM CP1 and CP2 were treated separately with 10 µL of freshly prepared 10 mM TCEP and incubated at room

temperature for 1 h. Thiol-activated ss-oligonucleotide was then bound to the AuNPs and GO-AuNPs following the procedure developed by Sun *et al.* (2007) with little modifications (L. Sun et al., 2007). As-prepared AuNPs (3 mL) and GO-AuNPs (500 µL) suspension into two different Eppendorf tubes were centrifuged at 8000 rpm for 30 min and the pellets were re-dispersed with 0.1 mM PBS (pH 7.4) to produce the final volume of 300 µL and 500 µL respectively. TCEP treated CP1 was added into GO-AuNPs while CP2 into AuNPs tube, mixed well with gentle hand shaking and incubated for 16 h at room temperature in dark environment. After 16 h, 10 mM PBS (pH 7.4) with 0.1% Tween 20 was added to the mixture to result in a solution with a final buffer concentration of 1 mM PBS with 0.01% Tween 20 and kept standing for 30 min. Next, the salt aging of the DNA functionalized nanoparticles was initiated slowly with 1 M NaCl to reach the final NaCl concentration of 100 mM. NaCl was added gradually at 1h interval while the increment rate was such that after first addition of 1 M NaCl it reached to 10 mM.

Upon addition of thiol-terminated oligonucleotides to the citrate-capped AuNPs, the thiol ligand displaces the weakly bonded citrate from the AuNPs through the formation of a stronger Au-S bonding at ambient condition. Moreover, addition of NaCl to the reaction mixture during the salt aging process, the Na^+ moderately minimizes the net charge of both AuNPs and DNA, thus diminishes the strong electrical repulsion force between the AuNPs and DNAs, as well as between the DNA strands on the AuNP, hence leading to a faster adsorption kinetics and resulting in a dense monolayer of oligonucleotides on the AuNPs surface within 1-2 days (Figure 4.2) (Giljohann et al., 2010; Liu & Liu, 2017; Xu et al., 2016; Zhang et al., 2013c). Furthermore, the slow and gradual addition of NaCl protects the AuNPs from the irreversible self-aggregation. Because at each NaCl increment, a certain amount of DNA is attached, allowing the AuNPs and GO-AuNPs to survive the next small increment of salt. Furthermore, the conformation of DNA is also changed from being parallel to an upright arrangement on

the AuNP surface which provides more effective steric stability as well as make easy availability of DNA sequences for hybridization (Cutler et al., 2012; Xu et al., 2013a).

The 100 mM NaCl treated samples were further allowed to age under the same conditions for another 40 h at room temperature. The aged solution was then centrifuged at 8000 rpm for 20 min and pipetted off the supernatant as much as possible to remove the free DNA. Functionalized nanoparticles were again dispersed in 0.1 mM PBS and 100 mM NaCl, pH 7.4 and centrifuged at 8000 rpm for 20 min and the procedure was repeated for 2-3 times. Finally, GO-AuNP immobilized CP1 precipitates (GO-AuNP-CP1) was dispersed in 0.1 mM PBS (pH 7.4) and 100 mM NaCl buffer and stored at refrigerator for further use.

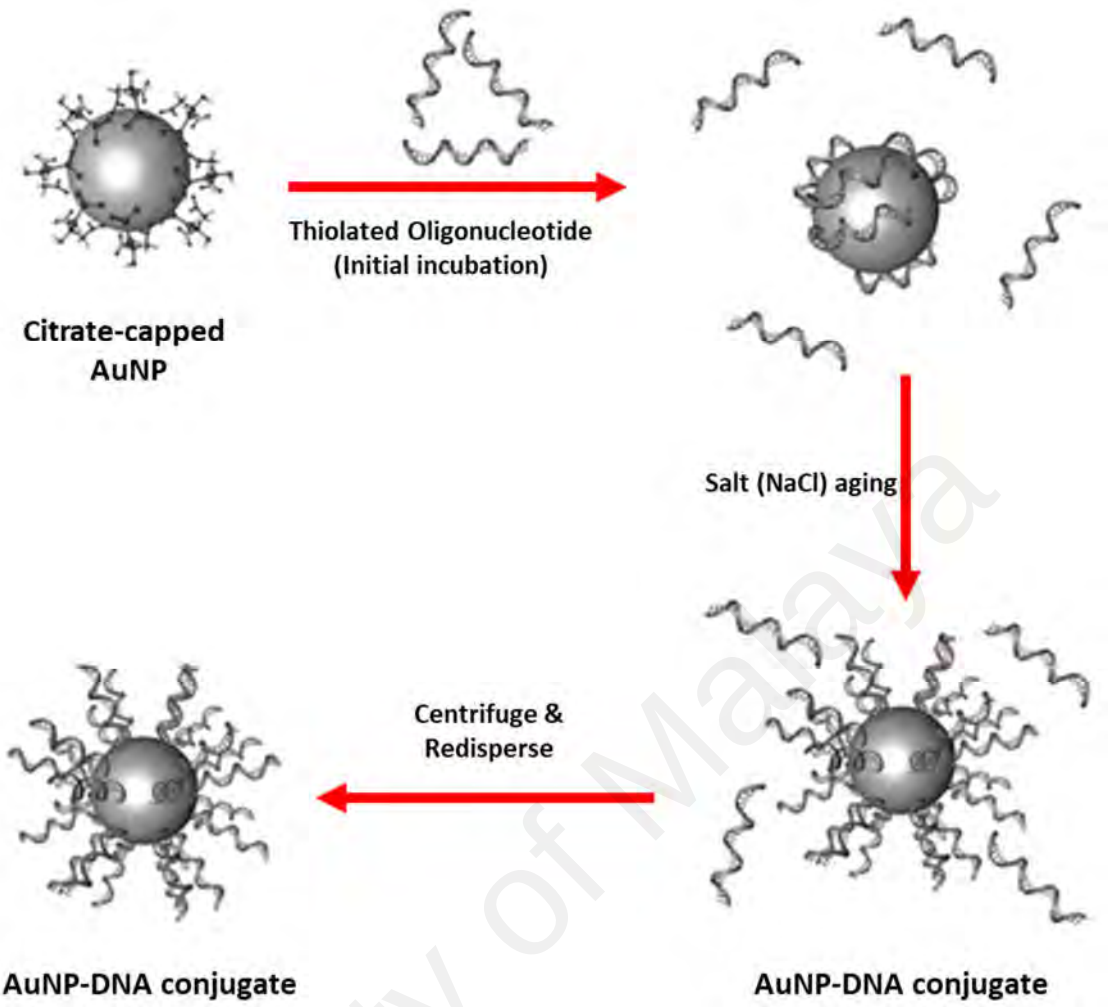

Figure 4. 2: Synthesis of thiolated oligo-functionalized AuNP. Thiol-terminated oligo sequences displaces citrate ions and forms strong Au–S bond on the AuNP surface. Subsequent addition of NaCl solution minimize the repulsion between the oligo strands and AuNPs, leading to the formation of a dense monolayer of oligonucleotides. The figure was redrawn with permission from the Reference (Giljohann et al., 2010).

4.2.8 Attachment of Cy3-cysteamine to Oligo-functionalized AuNPs

Cy3-cysteamine (1000 µL, 1µM) was treated with 100 µL of freshly prepared 10 mM TCEP and incubated for 1 h at room temperature. Due to TCEP treatment, the disulfide bond of the cysteamine was broken down to form thiol-active Cy3 which was therefore added to the red oily precipitate of AuNP-CP2 obtained from the previous step and allowed to keep for 24 h with frequent manual stirring. The solution was then centrifuged at 8000 rpm for 20 min and the supernatant was discarded. The precipitate was washed with DTW by successive centrifugation and re-dispersion. It has already been established

that formation of monolayer of ssDNA after attachment of thiolated DNA onto AuNPs, there were still spaces on AuNPs surface for the subsequent attachment of Raman tags (Sun et al., 2007).

4.2.9 Fabrication of GO-AuNPs DNA Biosensor

GO-AuNP-CP1 (400 µL) was incubated with corresponding target DNA (100 µL) for overnight at room temperature. GO-AuNP-CP1-Target nanocomposite was centrifuged at 8000 rpm for 20 min and washed twice with washing buffer to remove the unhybridized target DNA. The GO-AuNP-CP1-Target nanocomposite was then dispersed into DTW for the subsequent hybridization with equal quantity of AuNP-CP2-Cy3 in the microcentrifuge tube, shaken manually and incubated at room temperature for overnight to facilitate the hybridization of the CP2 with the unbound part of the target DNA. The hybridized compound (GO-AuNP-CP1-Target-CP2-AuNP-Cy3) was centrifuged at low speed (4000 rpm for 5 min) and washed several times with washing buffer to remove the unbound AuNP-CP2-Cy3. The final nanocomposite was dispersed into DTW.

4.2.10 Preparation of Samples for SERS Experiment

Samples for Raman spectroscopy were prepared on the silicon wafer (single side polished (<111>), N-type, and contains no dopant, thickness 0.5 mm, purchased from Sigma Aldrich, USA). The 2.5 cm × 2.5 cm cut silicon wafers were sequentially washed in an ultrasonic bath in different solvents: UPW, acetone, ethanol, and once again in UPW, for 15 min each. The substrates were finally dried under a nitrogen flow (Mikoliunaite et al., 2015). The 50 µL each of the samples were dropped onto the polished surface of the silicon wafers and dried in the vacuum atmosphere using vacuum pump at ambient condition. Consequently, a thin uniform layer of the sample was formed onto the silicon surface. A schematic presentation of sample preparation is illustrated in the Figure

4.3. The SERS spectra of the prepared samples were acquired using Renishaw Invia Confocal Raman Microscope using a 20x working objective lens and 532 nm laser as the light source. The obtained SERS spectra were chopped to reveal Raman bands with/without applicable baseline correction. All these manipulations were conducted using the Origin Pro 9.1 software.

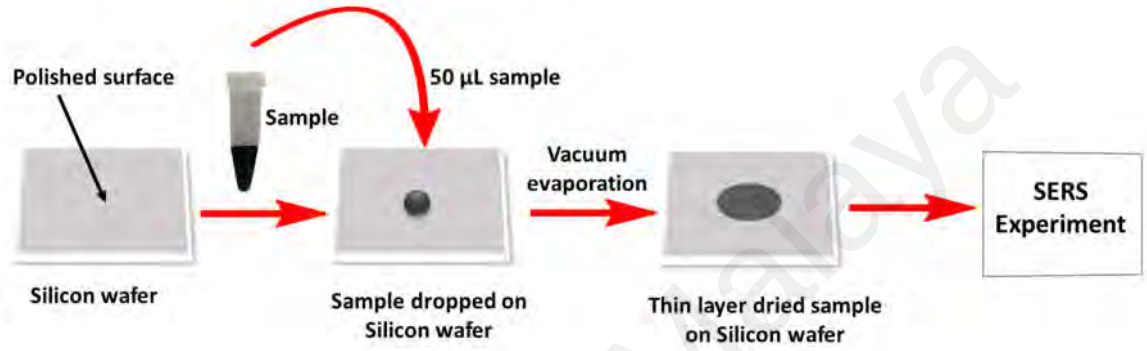

Figure 4. 3: Schematic presentation of SERS sample preparation.

4.3 Results and Discussion

4.3.1 Design and Principle of the Biosensor

The principle of dual platform based (i.e. GO-AuNPs and AuNPs) SERS detection of DNA is illustrated in Figure 4.4. Here employed a 'sandwich' assay strategy which involved the attachment of CP1 on GO-AuNPs composites by the well-established Au-S bonding followed by hybridization with corresponding target sequences (Figure 4.4a). On the other hand, CP2 was immobilized onto another platform (i.e. AuNPs) followed by the attachment of Cy3 Raman tag (Figure 4.4b). The covalently bound Cy3 were in close proximity to the AuNPs surface, thus ensured strong SERS signals to be observed (L. Sun et al., 2007). CP1 and CP2 were thiolated at the 5′ and 3′ end respectively which allowed the facile self-assembly of DNA strands on AuNP surfaces through formation of Au–S bonds (Ning et al., 2020; Zhang et al., 2007). Furthermore, C6 spacer arm was inserted in between the terminal thiol group and nucleotide bases of capture DNA (CP1 and CP2),

to keep the CP sequences in upright conformation and free for hybridization as DNA bases in close proximity to AuNPs surface could face difficulties due to steric effect (Park et al., 2002; Zhang et al., 2007). In the construction of SERS biosensor (Figure 4.4c), a sandwich complex was formed via a binary networking between the two platforms upon mixing together where CP2 immobilized on AuNPs were hybridized with the remainder target sequence attached to GO-AuNPs (Mucic et al, 1998; Sun et al., 2007). The SERS signal finally confirmed the presence of target DNA sequence in the dual platform based fabricated hybridized composite.

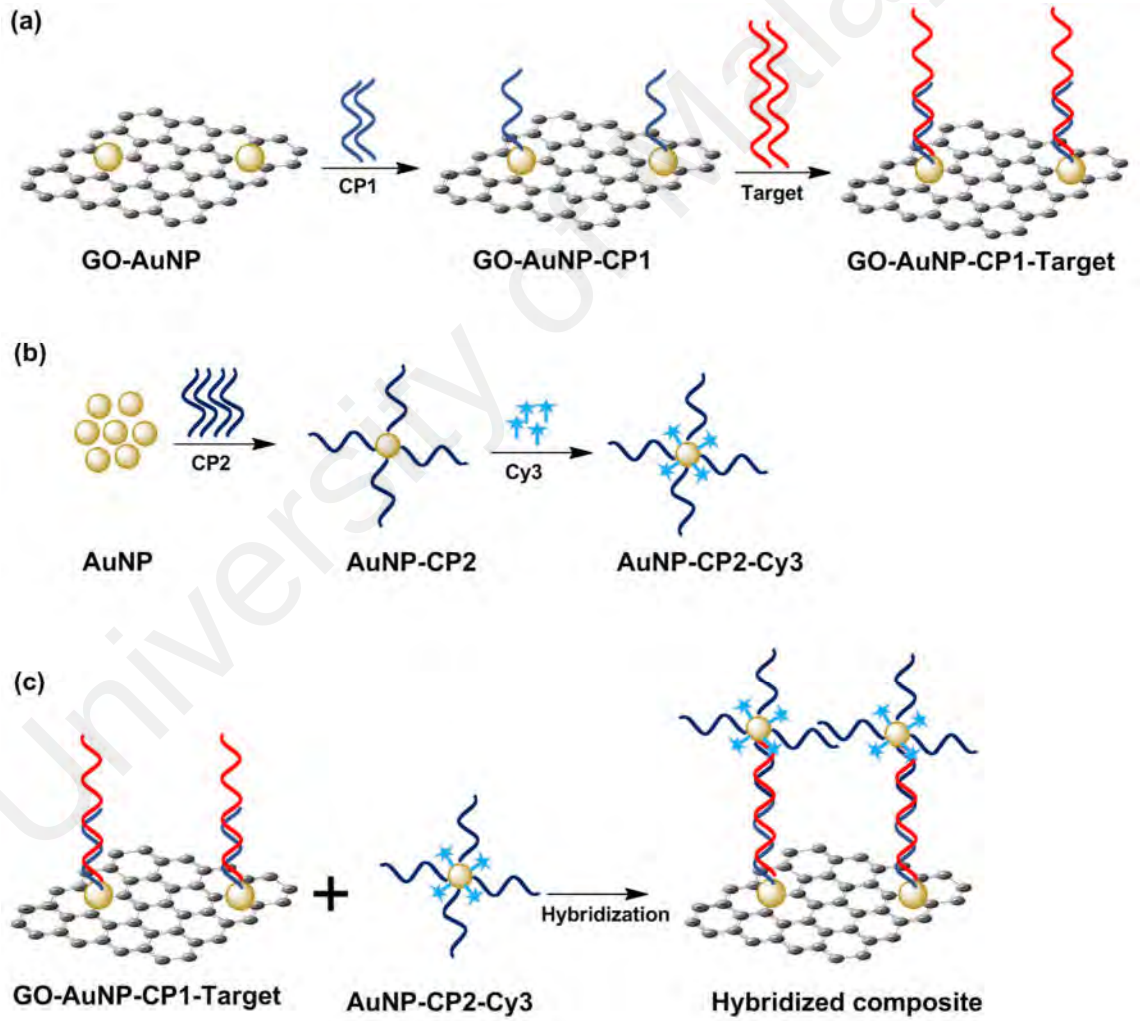

Figure 4. 4: The schematic illustration of SERS sandwich biosensor based on GO-AuNPs and AuNPs dual platforms.

4.3.2 Characterization of GO, AuNPs, and GO-AuNPs nanocomposite

The XRD spectra of GO showed a dominant diffraction peak at 2θ = 10.65° corresponding to an interlayer spacing is 8.30 Å (Figure 4.5a), indicating that the starting graphite flakes had been oxidized to GO (Zeng et al., 2020; Marcano et al., 2010). XRD analysis of the synthesized AuNPs represents the five peaks at 2θ = 38.19° (d-spacing: 2.35 Å), 44.38° (2.04 Å), 56.68° (1.62 Å), 64.70° (1.44 Å) and 77.67° (1.22 Å) (Figure 4.5a), corresponding to the reference code 96-901-1614 of HighScore Plus library, and standard Bragg reflections (crystal planes) of (111), (200), (200), (220), and (311) of Au face centers cubic (fcc) lattice. The intense peak at 56.68° represents the preferential growth in the (200) direction (Kumar et al., 2020). The GO-AuNP composites also showed the four major peaks at 38.10° (d-spacig: 2.36 Å), 44.30° (2.04 Å), 64.70° (1.44 Å) and 77.64° (1.22 Å) confirming the presence of AuNPs on the GO (Figure 4.5a) (Kwak, et al., 2016; Pocklanova et al., 2016).

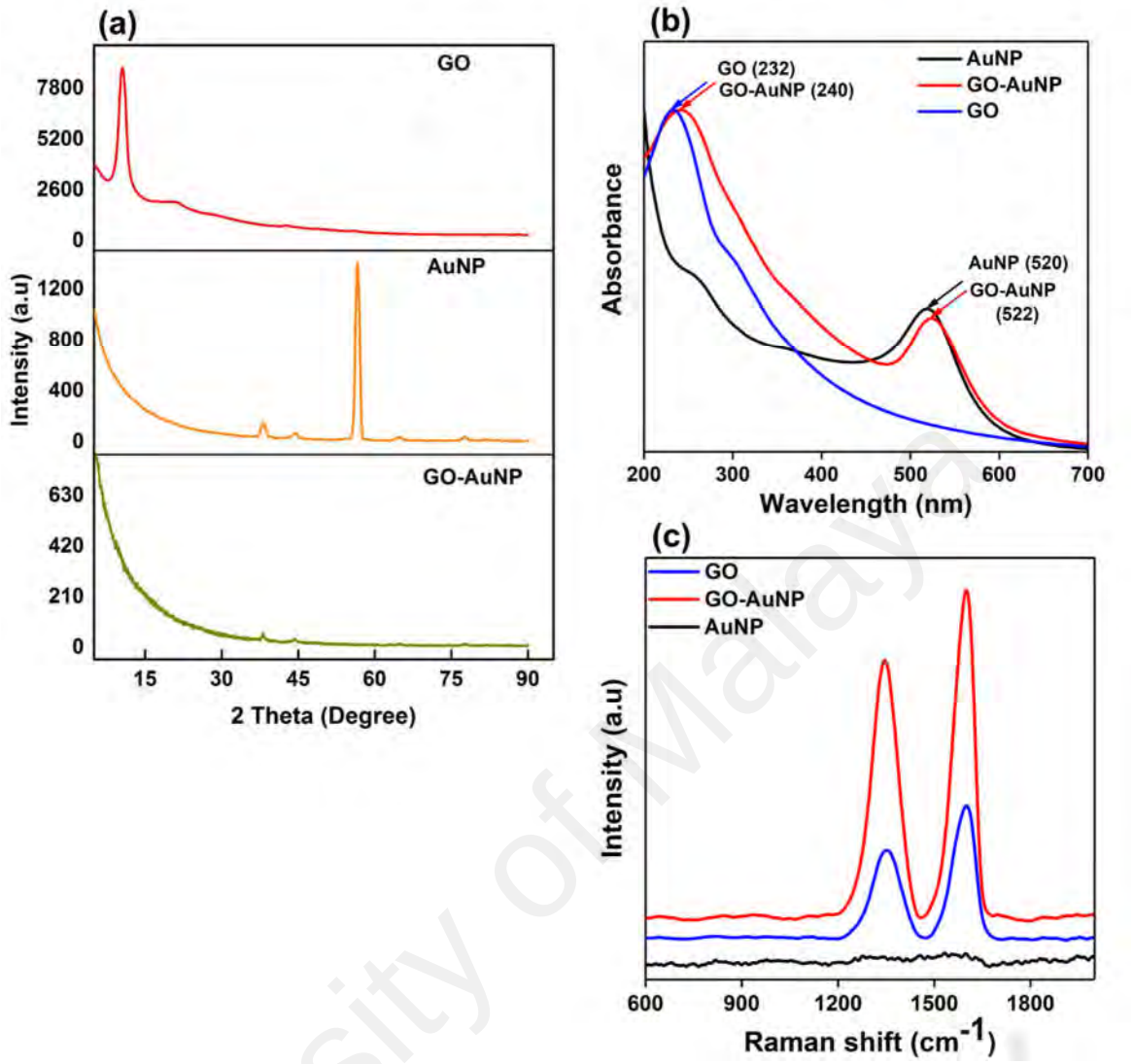

Figure 4. 5: (a) XRD patterns, (b) UV-vis spectra and (c) Raman spectra of GO, and AuNP and GO-AuNP.

The characteristic UV-vis spectrum of GO exhibited a major peak at 232 nm, corresponding to the plasmonic π→π* transitions (C=C bonds) (Figure 4.5b) (Heuer-Jungemann et al., 2015) and confirmed by the presence of flake like structure in HR-TEM images (Figure 4.6a) (Kwak, et al., 2016). The as-prepared burgundy red color AuNPs solution reflected an absorption band at 520 nm in the visible spectrum (Figure 4.5b) (Goncalves et al., 2009). The anticipated shape and diameter of AuNPs were spherical and 13 nm in average which in consequent justified by the HR-TEM examination (Figure 4.6b), hence comply the previous study (Liu & Lu, 2006). GO-AuNPs hybrids showed two peaks at 240 and 522 nm, representing the characteristic absorption peak of GO and

AuNPs respectively, therefore dictating the successful attachment of AuNPs over GO (Figure 4.5b) (Hurtado et al., 2020; Zhang et al., 2012b). The result was consistent with HR-TEM (Figure 4.6c). The AFM study showed that the spherical AuNPs were well distributed without any agglomeration (Figure 4.8a-b) while AFM images of GO-AuNPs represented the spherical shaped AuNPs onto the flat surface of GO (Figure 4.8e-f), thus further confirming the successful attachment of AuNPs onto GO sheet. The synthesized GO was also characterized by the Raman spectra comprising G-band at 1600 cm^{-1} and D-band at 1350 cm^{-1} whereas GO-AuNP composite was characterized by a moderate blue shift (4 cm^{-1}) as the D-band shifted from 1350 cm^{-1} to 1346 cm^{-1} (Figure 4.5c). This shift suggests an interaction between AuNPs and GO substrate and ensures AuNPs were deposited on GO (Subrahmanyam et al., 2010). More importantly, there was a significant increase of Raman spectra for GO-AuNPs in compare to GO (~ 2.5 times higher of G-band value), implies the obvious effect of AuNPs in the synthesized GO-AuNPs which might be due to the electromagnetic SERS enhancement (He et al., 2012; Li et al., 2016c).

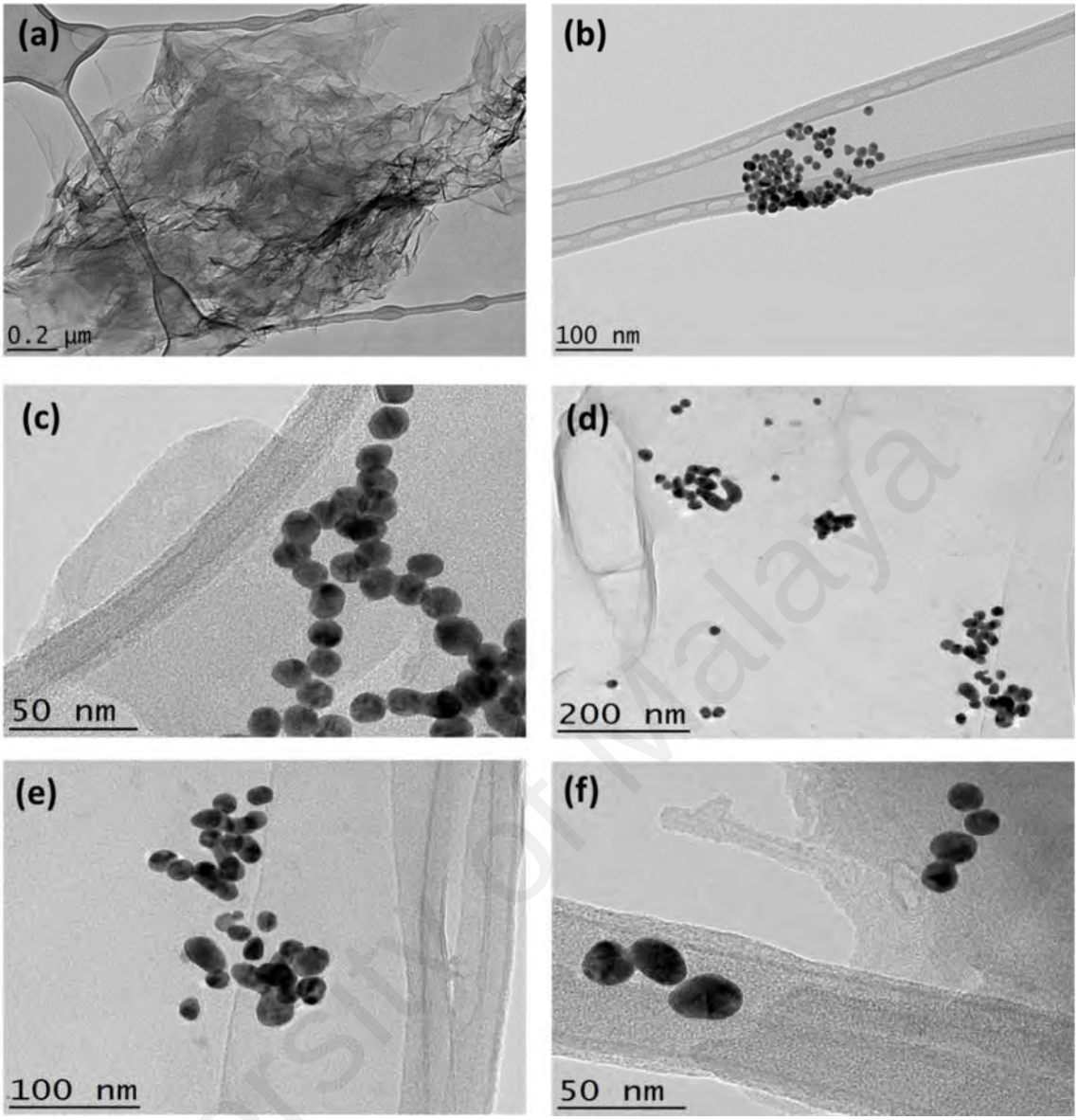

Figure 4. 6: HR-TEM images of (a) GO, (b) AuNP and (c) GO-AuNP on lacy carbon coated copper grid. (d-f) HR-TEM images of hybridized composites by the coupling of two platforms, GO-AuNPs and AuNPs via the hybridization of the CP sequences with the complementary target sequence. As hybridization happened, AuNPs were found mostly aggregated or linked to each other on GO sheets.

4.3.3 Attachment of Capture DNA Probes and Raman Tag to Nanoparticles

The conjugation of 15-mer long ssDNA to AuNPs converted the pristine ruby red AuNPs solution to a pinkish-red solution and this relative reduction of the color density is due to the reduced amount of free AuNPs (Thavanathan et al., 2014). After the attachment of thiolated DNA on AuNPs, the UV-vis spectra showed a peak shifting from 520 to 524 nm (Figure 4.7a), which is due to the increase of AuNPs size through

conjugation with DNA probe, suggesting the successful binding of ssDNA to the AuNPs. Addition of thiolated Cy3 to AuNP-DNA composite, there was a slight red shifting (1 nm) of the peak at 525 nm, indicating further increase of the AuNPs size, and confirms the attachment of Cy3 on AuNP-DNA composites (Figure 4.7a) (Thavanathan et al., 2014). Similarly, absorption spectrum of GO-AuNPs hybrids functionalized with ss-CP1 showed AuNPs characteristic peak shifting from 522 nm to 524 nm (Figure 4.7b), confirming the immobilization of thiolated DNA probe over GO-AuNPs (Wang et al., 2016a). Furthermore, AFM study of AuNPs-DNA indicated the well dispersion of AuNPs (Figure 4.8c-d) which was due to the electrostatic repulsion between AuNPs for oligo functionalization (Csaki et al., 2001). AFM images of GO-AuNPs before and after DNA functionalization also justified with well distribution of AuNPs on GO sheets (Figure 4.8g-h). Moreover, it also demonstrated that AuNPs and GO-AuNPs are stable at gradual increment of NaCl (1 M) during DNA salt-aging process which thus ensures smooth hybridization process.

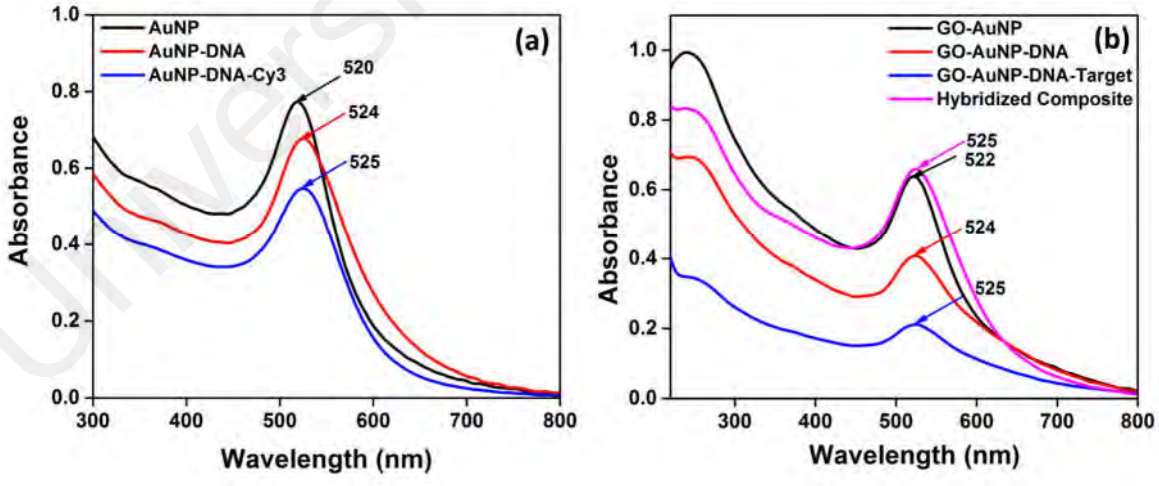

Figure 4. 7: UV-vis absorption spectra of (a) AuNP, AuNPs-ssDNA and AuNP-ssDNA-Cy3 and (b) GO-AuNPs, GO-AuNPs modified with thiolated CP2, followed by corresponding Target and finally the hybridized composite.

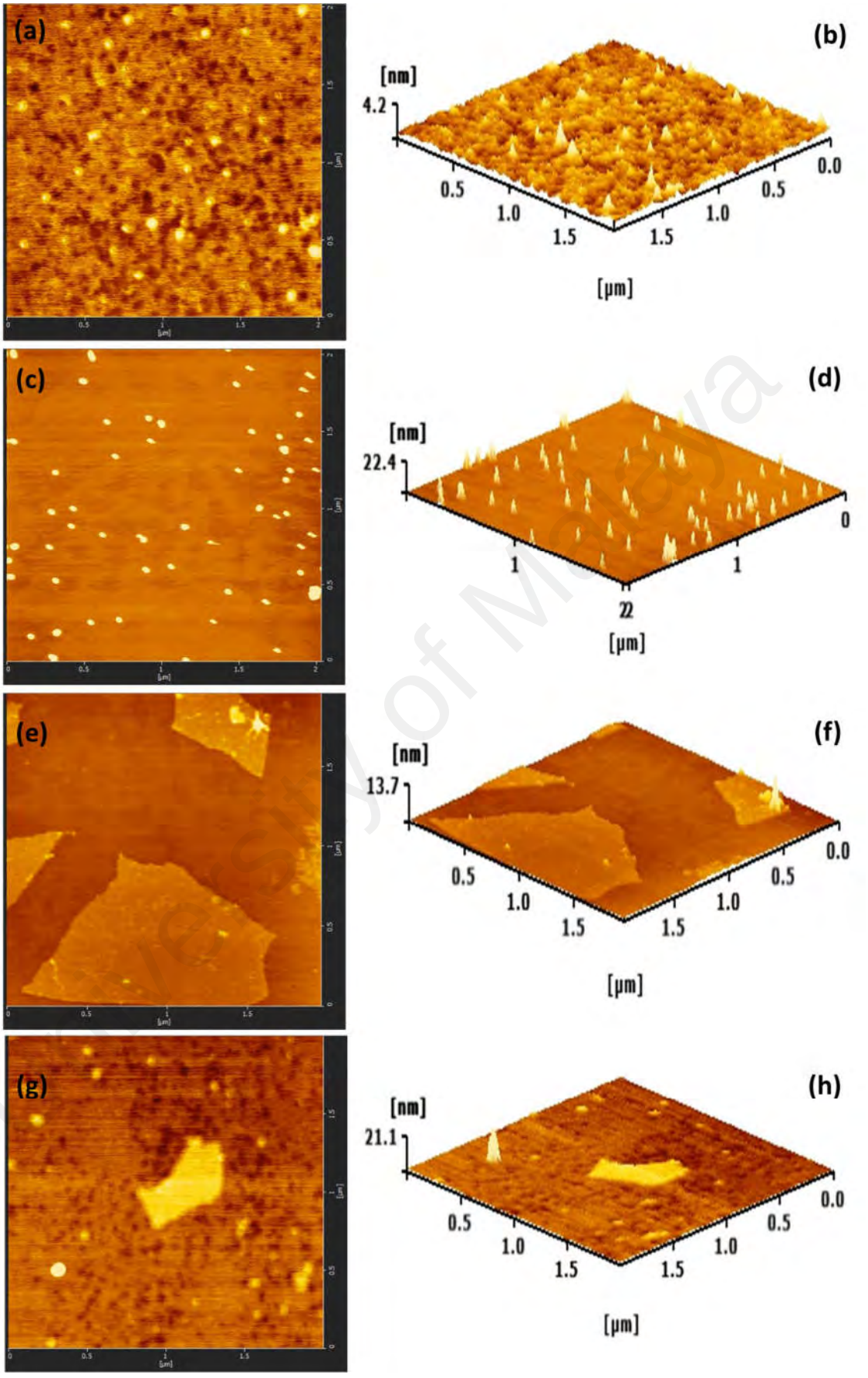

Figure 4. 8: AFM topography 2D and 3D images of AuNPs (a-b), AuNPs-DNA (c-d), GO-AuNPs (e-f), and GO-AuNPs-DNA (g-h) adsorbed on mica surface.

4.3.4 Justification of the Biosensing Strategy

AuNPs were functionalized with CP2 as well as further modified with thiolated Raman dye by Au-S linkage and considered as SP. Raman spectra of AuNPs-Cy3 reflected the fingerprints of Cy3 dye which was characterized by the peaks predominantly at 616, 798, 937, 1121, 1158, 1233, 1270, 1384, 1470, and 1592 cm^{-1} (Figure 4.9a) which conforms another study based on Raman tag incorporation onto AgNPs (Eremina, et al., 2020). Immobilization of Cy3 onto AuNPs produced the spectral fingerprint with greater enhancement of Raman scattering which is due to the combined effect of electromagnetic enhancement and charge transfer mechanism (Jans & Huo, 2012). However, the incorporation of ss-DNA probe to form the composite, AuNPs-CP2-Cy3, had no influence over the Cy3 fingerprint spectra (Eremina, et al., 2020) but a decreased intensity. This reduced intensity is proportional to the less immobilized Cy3 which might be due to prior attachment of ssDNA probe to AuNPs (Figure 4.9a). The unique features in the SP design is that Raman tag was not incorporated in the DNA probe rather directly immobilized onto AuNPs via strong Au-S covalent bonding. Thus, avoided complex manipulation in the probe sequences and keeping the ss-probe sequence completely free for hybridization with corresponding target sequences, which made the process robust (Sun et al., 2007).

The CP1 was immobilized on SERS active GO-AuNPs nanocomposites by Au-S bonding and used as the detection probes subsequently. Attachment of CP1 onto GO-AuNPs followed by hybridization with corresponding target sequences was confirmed by UV-vis spectra with broadened red-shifted plasmon band (Figure 4.7b) (Storhoff et al., 2000). This widening of the peak was due to the increasing of the particle size formed by the GO-AuNPs-CP1-Target composite. The hybridization of GO-AuNPs-CP1-Target with CP2-AuNP-Cy3 was explained by the red shift in the particle SPR from 520 to 525

nm, and wide broadening of the peak with greater intensity at 525 nm position which was due to attachment of more AuNPs composites with the existing GO-AuNPs by the corresponding probe sequences against the target DNA (Figure 4.7b) (Mucic et al., 1998; Storhoff et al., 2000). Moreover, to justify the hybridization process by SERS, GO-AuNPs platform was functionalized with Cy3 both in the absence and presence of ssDNA probe. Only a single peak representing the Cy3 at 1468 cm^{-1} is distinguishable and visible as the other major peaks of Cy3 are overlapped by D and G band of GO (Figure 4.9b) (Prinz et al., 2016). Therefore, as expected the hybridized composites were also found to produce the SERS peak at 1468 cm^{-1} representing the Cy3 attached with AuNPs as well as D-band at 1355 cm^{-1} and G-band at 1590 cm^{-1} characteristic to GO (Figure 4.10a), ensuring the linking of the two platforms via the covalent attachment of the probes and corresponding target.

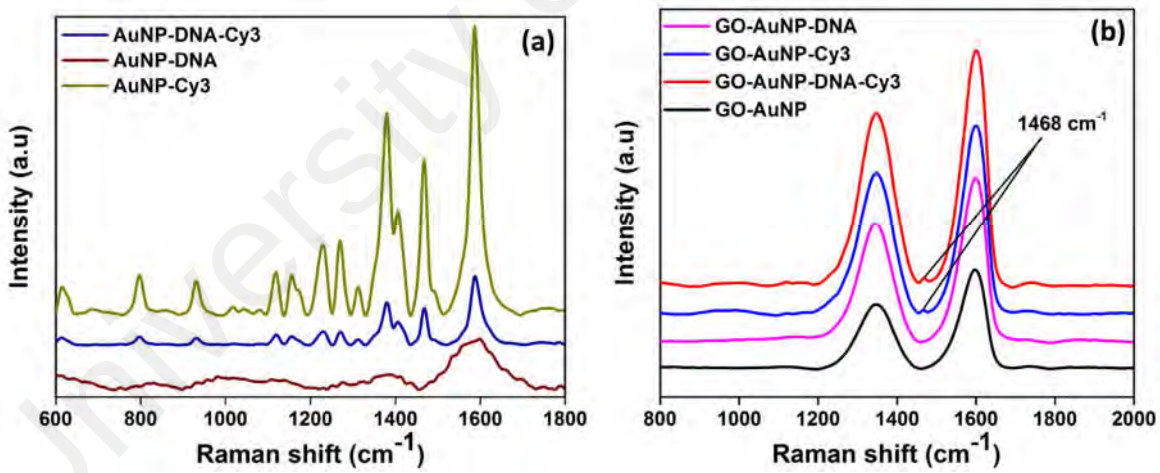

Figure 4. 9: Raman spectra of AuNPs functionalized with DNA, Cy3 and both DNA and Cy3 (a), GO-AuNP and GO-AuNP functionalized with DNA, Cy3 and both DNA and Cy3 (b).

HR-TEM images of the hybridized products also justify that AuNPs were linked with each other in maximum cases which indicates the successful hybridization was happened between the two CP strands via complementary target sequences (Figure 4.6d-f). However, few single AuNPs was also found over the GO sheets, indicating absence of

hybridization which might be due to the lack of either strand of the DNA probe sequences or somehow could not find the complementary sequences to be hybridized. Moreover, to justify the hybridization event happened throughout the reaction systems as well as to validate the preparation of the slide for SERS study, a repeatability study of a hybridized composite was conducted by taking SERS spectra from the randomly selected three different locations on the same slide (Figure 4.10c). The SERS spectra of the three different spots were found identical in appearance and the peak intensity at 1468 cm^{-1} for the three different spectra varied with a good linearity (R^2 = 0.97) with a little relative standard deviation (RSD) value of 5% (Figure 4.10d).

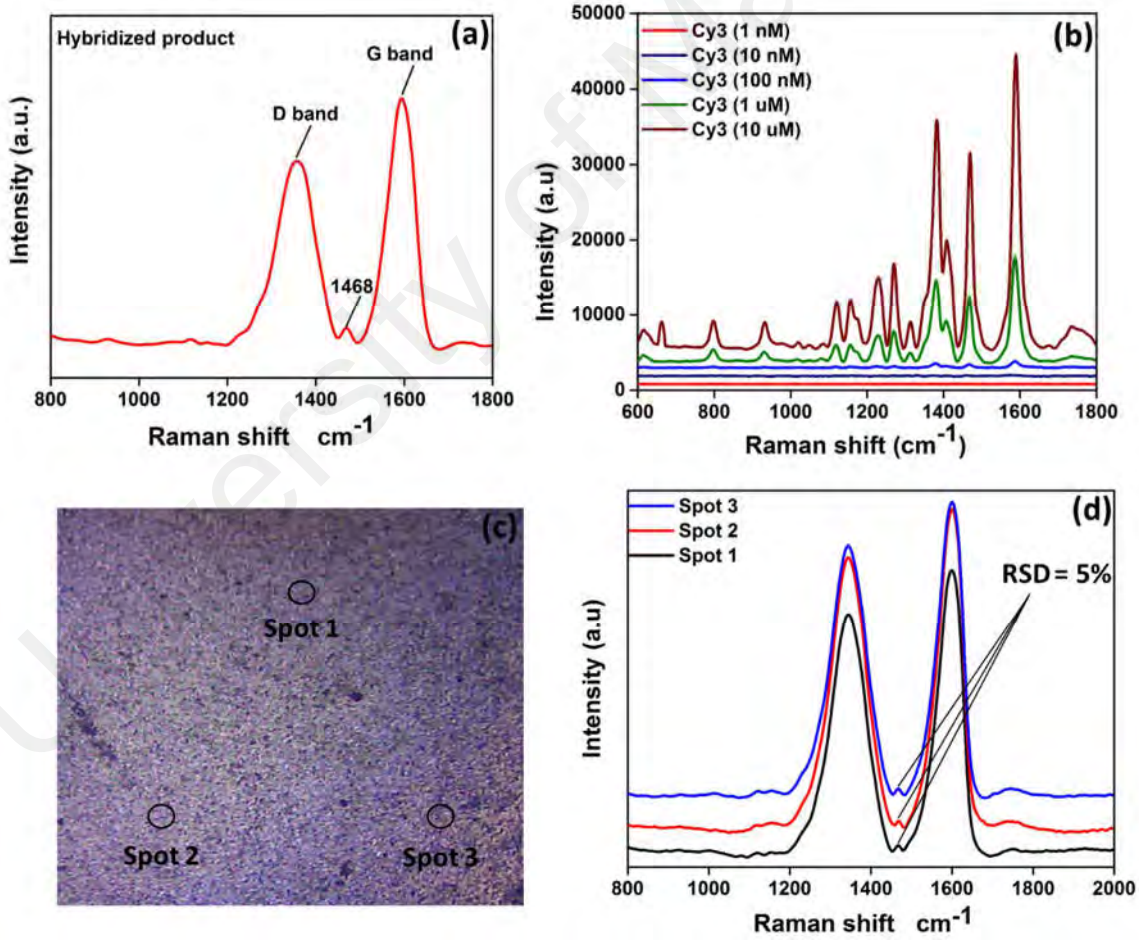

Figure 4.10: (a) SERS spectra of the hybridized composites, representing D and G band of GO at 1355 cm^{-1} and 1590 cm and Cy3 representing peak at 1468 cm^{-1}. (b) Variation of the SERS spectra of Cy3 Raman dye with variable concentration (1 nM to 10 µM). (c) Photographs of the hybridized composites prepared for SERS experiment, in inset the representative spots are marked with black circles, and (d) the corresponding SERS spectra of the hybridized composites

4.3.5 Optimization of Cy3-Cysteamine concentration

To demonstrate the feasibility of the signal control, AuNPs-CP2-Cy3 were prepared by using the fixed concentration (1 μM) of ssDNA and gradual increasing of the Cy3 concentration ranging from 1 nM to 10 μM in steps of 10×. Variations of the Cy3 concentration vs intensity of the peaks are shown in Figure 4.10 (b). It was observed that Cy3 at the minimum concentration of 100 nM needs to be attached to the AuNPs surface to reflect the identical SERS fingerprint of the Cy3 upon laser excitation. It was also evidenced that the Raman intensity was increased with an increase of the Cy3 concentration and there was a steady upward trend of the intensity of Cy3 SERS signal which reached at maximum at 10 μM concentration. Therefore, throughout the study we have used Cy3 at 1 μM concentration as it produced the well distinct and intense peaks of Cy3 dye.

4.3.6 Analytical Performance of the Biosensor

4.3.6.1 Selectivity of the Biosensor

The specificity of the biosensor was solely dependent on the covalent linking of the both platforms via hybridization of split-probe sequences with corresponding target DNA and the appearance of representative Cy3 and GO peaks from the SERS spectra. Detection of MBT target sequence was indicated by the presence of D and G band of GO along with peak at 1468 cm^{-1} position as Cy3 signatory peak. However, due to the use of short-length DNA probes in this sensing approach, there was a possibility of having similar nucleotide sequence in the whole genome sequence of other species than MBT. Thus, to check the similarity in the sequences, the selectivity of the probe and non-target DNA sequences was justified theoretically (Chapter 3). The uniqueness of the 31-mer DNA probe sequence was checked by multiple aligning with cytb gene of MBT and 27 other meat and fish species (Table 3.1) using MEGA5 alignment tool which revealed 100% matching

only with MBT and scored 6-15 nucleotide (19.4-48.4%) mismatching with other non-target species (Table 3.1). In this experiment, the selectivity of the biosensor was evaluated following different control hybridization reactions accomplished by the presence or absence of target DNA sequences and the replacement of target sequence with non-complementary DNA sequences. In detail, substitution of the target sequence was done by i) 31-mer long oligonucleotide sequence with 100% mismatch nucleotide bases, ii) complementary target sequence of the three non-target species (buffalo, horse and cow) having the 6-8 mismatches (Table 3.1), and iii) two other non-target sequences with distinct length – pork (24-mer) and dog (33-mer). In the presence of the corresponding target sequence, GO-AuNP-CP1-Target-CP2-AuNP-Cy3 sandwich composite was formed by the coupling of the two platforms, generated the SERS hot spot and consequently strong SERS signal characterized by Cy3 fingerprint peak at 1468 cm^{-1} along with GO representing G and D band (Figure 4.11a). This SERS spectra therefore indicates a true positive result (Chuong et al., 2017). On the other hand, SERS spectra from the control samples such as hybridized composite with no target sequence (blank sample) generated only GO representing peaks without any existence of Cy3 spectral fingerprint (Figure 4.11a), hence, suggesting no hybridization event due to lack of bridging target sequences. Therefore, the peak intensity at 1468 cm^{-1} for the blank sample is being considered as the baseline signal for Cy3 and the obtained spectra is denoted as the true negative.

The SERS spectra of the hybridized composite achieved in the presence of non-complementary (100% mismatch) and complementary target sequences of the non-target species (cow, buffalo, horse, dog and pig) however, revealed representing GO peaks and in rare cases with very little existence of Cy3 signal (Figure 4.11a). The presence of this very weak Cy3 signal could be considered as false positive, and the intensity is ignored in this study due to the equal or lower signal-to-noise ratio. This little existence of Cy3

spectra was due to some nonspecific interaction between the fabricated GO-AuNPs-CP1-Target and AuNPs-CP2-Cy3 composites, however could not produce intense Cy3 SERS signal due to lack of hot-spot generation. This is because hot spots are generally originated at the interstices between adjacent AuNPs rather than between GO sheet and AuNPs (Chuong et al., 2017). Moreover, due to the dominant presence of the D and G band of GO, all other less intense Cy3 peaks were also minimized (Prinz et al., 2016). A true positive signal is therefore, distinguishable from the false positive by the distinct Cy3 fingerprint peak at 1468 cm^{-1}. Therefore, the results showed that the fabricated sensor is highly efficient to distinguish target and non-target DNA sequences of the closely related species. The selectivity study also confirms that the probe is highly specific for MBT species only and there is no chance for the hybridization with other non-target species.

4.3.6.2 Sensitivity of the Biosensor

The efficiency of the biosensor in terms of the ability to distinguish the corresponding target sequences bearing single-base mismatch and three-base mismatches was verified. As shown in Figure 4.11b, the hybridized composite via the base-mismatch target sequences, generated SERS spectra (i.e. Cy3 representative peak at 1468 cm^{-1}) at lower intensity in comparison to the fully complementary sequence. This is attributed to the fact that mismatched DNA had undergone irregular attachment with the complementary probe sequences due to the base changes in the sequence. The data in Figure 4.11b thus indicates that the higher the number of base mismatches in the sequence, the lower the SERS intensity due to the irregular hybridization. This data clearly suggests that the developed biosensor is sensitive enough to distinguish the DNA with single nucleotide variation. One of the main reasons behind this greater efficiency is probably the use of very short fragment of ssDNA (only 15 and 16 bases long) as the probe sequences for detecting target DNA.

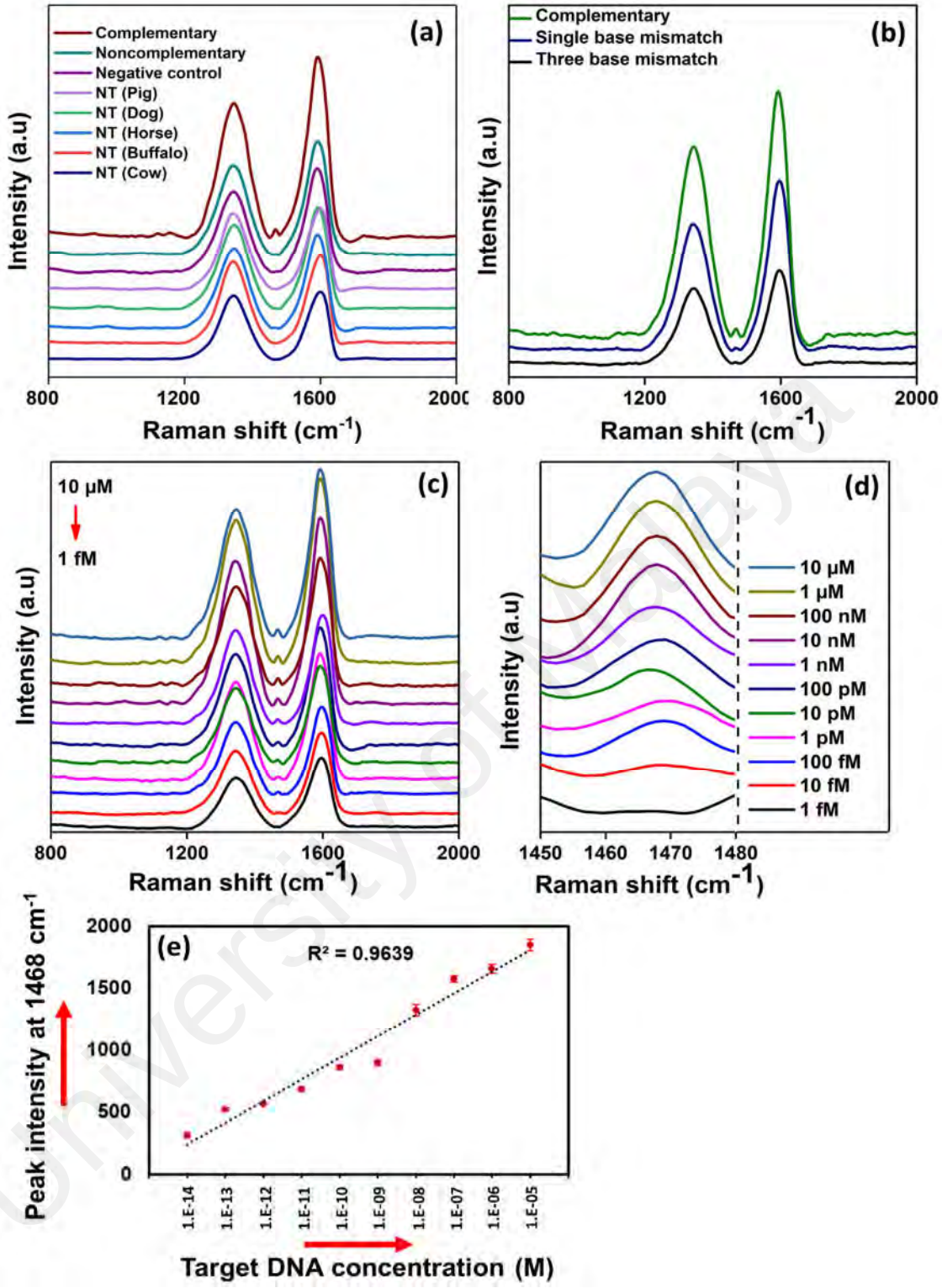

Figure 4.11: (a) SERS spectra of the selectivity study using complementary, non-complementary, negative control (blank) and non-target sequences. (b) SERS spectra of the hybridized composites with corresponding (red), single-base mismatch (dark blue) and three-base mismatches (black) target sequences. (c) Stacked SERS spectra for hybridized composites by 10 µM to 1 fM dilutions of MBT target DNA. (d) SERS spectra of the hybridized composites chopped from 1450 to 1480 cm^{-1} to magnify and distinguish the intensity of 1468 cm^{-1} peak. (e) Linear plot of SERS intensities of 1468 cm^{-1} band vs corresponding target DNA concentration. Error bars represent standard deviations of peak intensities from n=3 repeated measurements.

4.3.6.3 Dynamic Detection Range of the Biosensor

Quantitative detection of the target sequence was performed by measuring the SERS intensity of the representative Cy3 signal from the hybridized compounds formed via the varying concentration of target DNA. Each target DNA sample was ten times diluted from its previous concentration to provide a series of target DNA concentration from 10 μM to 1 fM. The SERS intensity was in downward trend with the decreasing concentration of the target DNA from 10 μM to 1 fM (Figure 4.11c&d). However, there was no/almost indistinguishable Cy3 signal from the hybridized composite for the target concentration below 10 fM. The SERS spectra were background (baseline) corrected, and a standard curve for the intensity of the Cy3 peak at 1468 cm^{-1} position vs target concentrations was plotted (Figure 4.11e). An R^2 value of 0.9639 was obtained from the linear regression analysis of the peak height at 1468 cm^{-1} against the corresponding target DNA concentration. This data suggests that the fabricated biosensor is applicable in detecting target DNA sequence from a wide range of sample concentration. This greater sensitivity of the fabricated biosensor relied on few aspects such as use of GO-AuNPs as the SERS platform where maximum number of AuNPs were being deposited over the large planer surface of GO which in consequent facilitated the covalent binding of CP1 sequences in greater numbers, hence creating more options even for the minute quantity of the target sequences to be hybridized. Even if single CP2 bound to AuNP-Cy3 hybridize with the corresponding unbound portion of target sequence, the Cy3 signal would be strong due to more Cy3 molecules bound over the same AuNP-CP2 composite (Figure 4.4c). Moreover, covalent linking of the CP1 and CP2 via hybridization event brings the two platforms within few nanometer ranges, therefore generates hotspots at the junction of GO-AuNPs and AuNPs which in consequent lead to the strong highly localized enhancement of SERS signal. In addition to the electromagnetic, a minor enhancement due to the resonant charge transfer process between the AuNPs and Cy3 is

also contributed to the detected SERS signal. This CM enhancement might be due to the vibrationally excited state of the adsorbed Cy3 molecule which is caused by two ways - either by exciting electrons from AuNPs to unoccupied molecular orbitals of adsorbed Cy3 and back to the AuNPs or electrons from the occupied molecular orbitals into the Fermi level of AuNPs and back to the adsorbed molecule (Maher, 2012; Radziuk & Moehwald, 2015). Hence to justify the contribution of the hot spots in signal enhancement, SERS spectra of hybridized sandwich composite in the absence of Cy3 was compared to bare GO-AuNPs and the enhancement is about 26% more intense than GO-AuNPs (Figure 4.12). This enhancement is definitely due to the agglomeration of AuNPs over GO-AuNPs via hybridization and hot spot generated at the junctions between AuNPs rather than AuNPs deposition over GO sheet (Chuong et al., 2017). Moreover, functionalization of AuNPs-CP2 with Cy3, followed by hybridization and coupling with GO-AuNPs-CP1-Target, enhances SERS signals further 15% (Figure 4.12) than the hybridized composite without Cy3, therefore, dictates the contribution of chemical enhancement by the adsorbed Cy3 molecule.

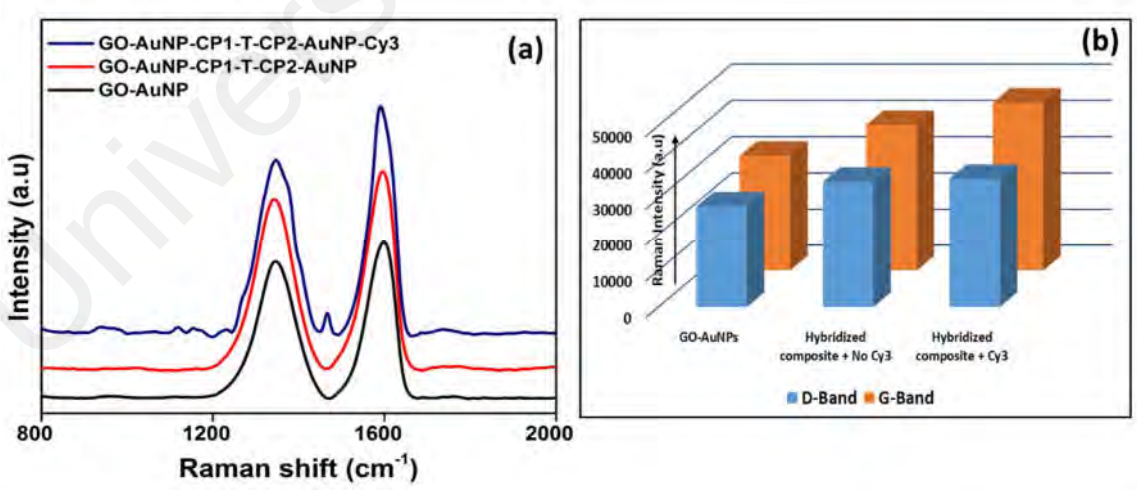

Figure 4.12: (a) SERS spectra of GO-AuNPs (red), coupled dual platforms via hybridization without Cy3 (GO-AuNPs-CP1-T-CP2-AuNP) (red) and hybridized composite with Cy3 (GO-AuNPs-CP1-T-CP2-AuNP-Cy3) (blue), and (b) SERS intensity of D-band and G-band value of bare GO-AuNPs, hybridized composite in absence and presence of Cy3.

The use of SERS active dual nanoparticle platforms, and short-length oligo marker, made the fabricated biosensor viable and amenable for the detection of trace amount of DNA (LOD - 10 fM) present in the sample. The fabricated biosensor showed better capability to detect MBT species in comparison to the some of the PCR based detection techniques involving 120 base pair long amplicon by conventional PCR, PCR-RFLP and SYBR green real-time PCR techniques (Ali et al., 2015a; Ali et al., 2016; Asing et al., 2016). Hence, the detection principle will be efficient enough for the unambiguous tracing of MBT materials in the food chain, or any forensic or archaeological investigations and tracking of trafficking. Moreover, SERS biosensors exhibited better sensitivity than the biosensors fabricated by single platform using Raman label at the terminal end of reporter DNA (He et al., 2012) and even using the dual platforms following sandwich assay procedure (Kang et al., 2010; Zhang et al., 2010). Some of the sandwich assay procedure involved SERS non-active platform hence required further step such as exfoliation of a Gr layer over the hybridized composite (Prinz et al., 2016) or silver enhancement of the hybridized composites (Cao et al., 2002). Therefore, to address these shortcomings as well as to make the sensing way easy, flawless, and convenient, here in this study employed two different SERS-active platforms and only few simple steps involvement to produce multi-component aggregates upon hybridization to get intense SERS intensity via the localized hot spots. Furthermore, Cy3 was directly immobilized onto the AuNPs which also directly contributed on the total enhancement by the charge transfer mechanisms. Hence, the use of different SERS-active substrate and applying the same biosensing principle, it would be possible to establish a multiplex DNA sensor for the simultaneous detection of multiple DNA biomarker sequences from different origin.

4.3.6.4 Application of the SERS DNA Biosensor for Real Sample Analysis

The purity of the extracted genomic DNA of the muscle tissue of MBT species was determined using A260/A280 ratio which was obtained around 1.7, therefore indicates a high purity of DNA (Ali et al., 2015b). In addition, the concentration of the extracted genomic DNA was found ~300 ng/µL. However, the extracted DNA concentration was also converted into nM concentration by applying the Equation 5. To determine the average size, the extracted genomic DNA was electrophoresed at low agarose concentration (2%), along with ready to use XLarge DNA Ladder (GeneDirex, Taiwan) which includes fragments ranging from 250 bp to 25,000 bp.

$$\text{Concentration (nM)} = \frac{(\text{concentration in ng/µL})}{(660\ \text{g/mol} \times \text{average size of the DNA in bp})} \times 10^6 \ldots (5)$$

The SERS biosensing strategy which was already established for the detection and quantification of the corresponding synthetic target DNA of MBT species, was further validated with extracted genomic DNA from the MBT meat sample as well as evaluated the feasibility and efficiency of the fabricated SERS biosensor for real sample analysis. The extracted MBT genomic DNA sample was serially diluted in TE buffer until the established LOD concentration for the synthetic target DNA. The serially diluted DNA suspensions were then heated in a water bath at 95°C for 15 min followed by immediate chilling in ice bath for another 15 min to obtain the ssDNA strands. Finally, the heat treated cold shocked denatured ssDNA solution was ultrasonicated for 20 min to break down the long DNA strands into smaller fragments of DNA (Pandey et al., 2011; Tiwari et al., 2015). The combined effect of the heating-rapid cooling denaturation of genomic DNA to ssDNA and the ultrasonication to obtain the smaller fragments of DNA, therefore increases the hybridization efficiency by the easy access of fragmented target DNA to the immobilized DNA probes (Wang & Son, 2013). The fabricated SERS biosensor thus

showed extraordinary sensitivity in the detection and quantification of real sample as well. The LOD obtained for the real sample was as low as 100 fM (Figure 4.13a), which is 10 times lower than the established LOD (10 fM) for the synthetic target DNA. The statistical curve obtained from the peak intensity at 1468 cm^{-1} vs target DNA concentration also showed a good linearity with R^2 value of 0.9677 (Figure 4.13b). The LOD value is 10 times lower in compare to the synthetic target DNA which is due to the variable length of the corresponding target DNA and the presence of some inhibitory components inherited during the extraction procedure. However, in a broader sense, it dictates that the efficiency of the coupling of two platforms via real sample DNA mediated hybridization is justified to be used for the real-time applications.

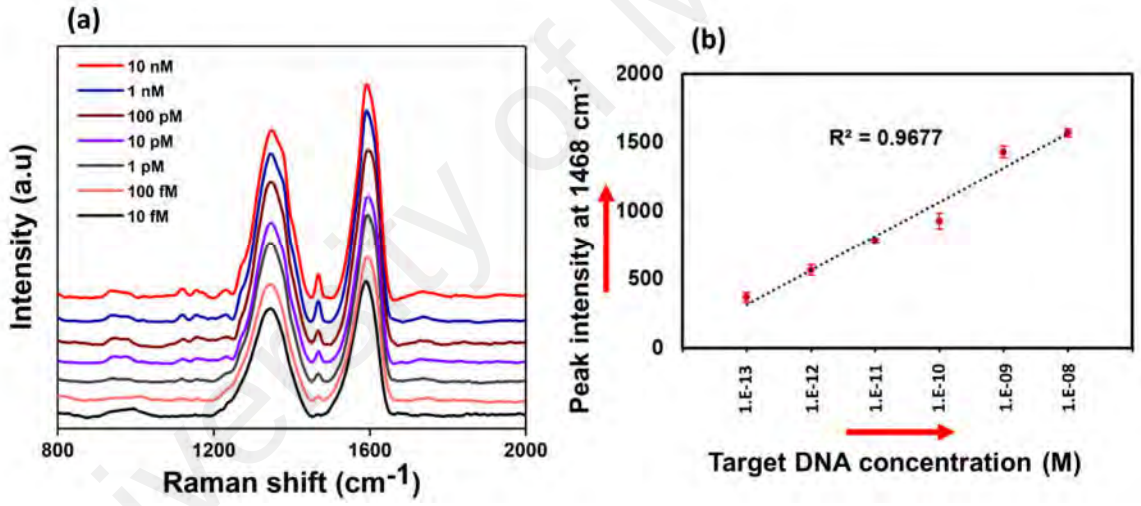

Figure 4.13: (a) The SERS spectra of the hybridized composites coupled by the target DNA extracted from the MBT muscle tissue. The SERS peak at 1468 cm^{-1} dictated the target DNA concentration and observed a gradual decline of the peak intensity with the increment of the target DNA dilution. (b) The linear curve of SERS intensity at 1468 cm^{-1} vs target DNA concentration for the real sample. Error bars represent standard deviations of peak intensities from n=3 repeated measurements.

4.4 Conclusion

In this study, a dual platform-based SERS assay was demonstrated for the efficient and sensitive detection of DNA. To fabricate the device, short-length probe sequences were immobilized onto two different nanostructure platforms to form GO-AuNPs-CP1 and

AuNPs-CP2-Cy3 respectively. The novel features of the sensor are the use of very short-length DNA probe sequences and the linking of the two SERS active platforms via target-probe DNA hybridization to produce a unique and enhanced SERS signal. This huge enhancement is in fact due to the combined effects of electromagnetic enhancement via the hot spot generated by multicomponent assembly as well as the chemical enhancement by the charge transfer mechanism between Cy3 and AuNPs surfaces. Therefore, the presence of target DNA up to 10 fM, was able to combine the two platforms together to generate the unique and distinguishable SERS spectra. The biosensors thus provide the LOD down to 10 fM and could differentiate the target sequences with single nucleotide variation. Furthermore, the fabrication of the biosensor is easy, convenient, involves low-cost SERS substrate and provides extraordinary specificity to discriminate the corresponding sequences of the closely related non-target meat species. The SERS biosensor thus revealed better suitability and efficiency for the detection and quantification of MBT materials in the food chain to remove the ambiguity. There the developed biosensor could be adopted by the regulatory authorities, archaeologists and wildlife protection agencies for the forensic or archaeological authentication even under compromised conditions as well as tracking of the MBT trafficking with greater reliability and confidence. Moreover, this PCR free, short-length split-probe DNA conjugated dual platforms based SERS sensing technology would also be suitable for detecting any short-length DNA biomarkers. Hence, this platform could be considered as a model for the detection of life threatening pathogenic microorganisms, cancers, verification of food adulteration, authentication of species, and forensic applications; and could guide to the multiplex detection strategy.

CHAPTER 5: DUAL PLATFORM AND RAMAN TAG INTERCALATED SHORT-LENGTH DNA PROBE BASED SERS DNA BIOSENSOR FOR THE QUANTITATIVE DETECTION OF PIG SPECIES

5.1 Introduction

Meat adulteration is now getting increasing attention due to the some recent meat scandals which received intense public outrage, global media coverage and consequently huge economic loss (Jaques, 2015; O'mahony, 2013; Whitworth et al., 2017). Apart from the commercial value, adulteration of meat products is a major concern for the adverse health effects due to allergies caused by the undeclared food ingredients, as well as from the cultural and religious point of view (Ali et al., 2017; Premanandh, 2013). Meat adulteration is typically committed by the substitution of high-value meat with cheaper one. Pork which is one of the most commonly available as well as consumed globally with beef and poultry, having similar color and texture with mutton or beef, are generally substituted for these two kinds of meat for pursuing higher economic profit (Griffiths et al., 2014; Liu et al., 2019). Moreover, the halal and kosher global meat markets are now expanding fast along with huge demand for certified products due to the perception of safe and better quality as well as ethnic considerations (Fischer, 2016; Skouridou et al., 2019). Therefore, the development of a sensitive, reliable and rapid method as a first line of defense is of high demand for detecting and deterring the food fraud or accidental cross-contamination especially in processed meat products, which could assist in preventing unfair business competition, boosts up consumer confidences, economic growth and lead to a social harmony.

Different assay techniques mostly based on protein or DNA biomarkers have been utilized to verify the authenticity of the meat products and to know the origin of the species. Pork fat (lard) or protein marker based techniques include HPLC (Giaretta et al.,

2013); electrophoretic methods (Montowska & Pospiech, 2013; Skouridou et al., 2019); FTIR, UV-vis and MS (Kumar et al., 2017); ELISA (Mandli et al., 2018); and recently developed lateral flow devices (Kuswandi et al., 2017). However, requirement of costly instruments, substantial laboratory setup and specialized skilled person for the operation and data interpretation, inability of differentiating closely related species from mixed sample matrices due to cross-species reactions and above all, the thermal instability of lipid and proteins, have therefore lessen the applicability of these mentioned techniques for both raw and process food products (Hossain et al., 2016). In contrast, DNA based detection techniques have shown greater success due to the higher stability, sensitivity and accuracy (Kang & Tanaka, 2018). PCR based DNA detection methods for both qualitative and quantitative evaluation of pork residues in the meat and meat products include species-specific PCR (Lee et al., 2016), PCR-RFLP (Hossain et al., 2016), and real time PCR (Hossain et al., 2017a; Kang & Tanaka, 2018). However, the reduction of amplicon length (≤150 bp) in PCR techniques is often challenging, as it reduces the specificity of the technique and producing artifacts in the final result (Ali et al., 2012c). Hence, short-length DNA linked nanoparticle based different sensing strategies have been getting promising acceptance for their greater efficiency to replace the PCR based techniques.

SERS which is capable of single molecule differentiation due to molecule specific vibrational spectra, considered as one of the most powerful analytical techniques for DNA detection (Kneipp et al., 2006; Xu et al., 2015). High sensitive different SERS DNA biosensing strategies have been reported for diverse applications. One of the efficient techniques is the co-adsorption of Raman tag and DNA probe sequences onto the same platform (Khalil et al., 2019). However, in the co-adsorption process, it is very difficult to maintain the ratio of the immobilized Raman dye and probe sequences on the same nanostructures. Therefore, preparation of SERS label by an alternative but effective way

via intercalating the Raman tag in the DNA probe sequences have been verified (Cao et al., 2002). However, the distance between the intercalated Raman tag and the surface of nanostructured platform has a significant role in the SERS intensity, i.e. the closer the Raman tag the greater the amplification, hence the improved sensitivity (Eremina, et al., 2020; Sun et al., 2011; Zou & Schatz, 2006). Hence, the SERS DNA biosensor adopting a novel design in intercalating Raman tag to the DNA probe sequences along with the platform components would be the best choice to achieve greater sensitivity due to the enhanced SERS signal.

Herein, we report a noble SERS DNA biosensing strategy based on self-assembly of two sensor platforms via the hybridization of complementary target sequences for the trace sensing of pig DNA. In this sensing strategy, GO-AuNR and AuNP were used as the platform while a uniquely designed probe DNA sequence by intercalating ATTO Rho6G was used as SP DNA. However, ATTO Rho6G was intercalated in such a way that upon the attachment of SP sequence, the intercalated Raman tag kept position much adjacent to the AuNPs surface while keeping the nucleotide bases independent for the hybridization (Park et al., 2002; Zhang et al., 2007). Therefore, hybridization of the target DNA with the corresponding two split-probe DNA functionalized onto two different platforms facilitates the covalent coupling of the AuNPs over GO-AuNRs, and enhances the local electromagnetic field due to the 'hot spot' originated between the GO-AuNR and AuNP systems (Hao & Schatz, 2004; Qian et al., 2008). With this approach, the higher the target DNA concentration, the more coupling of the two platforms which consequently lead to intense SERS signal. Therefore, with a greater amplification of the SERS signal, a very low concentration of pork DNA was detected (LOD - 100 aM). Moreover, due to the very short DNA probe sequences, the fabricated biosensor shows excellent sequence specificity and sensitivity to distinguish the DNA sequences of the

closely relevant six non-target species and the target sequence with a single-base mismatch.

5.2 Materials and Methods

5.2.1 Chemicals and Instruments

Graphite powder, $HAuCl_4 \cdot 3H_2O$, trisodium citrate dihydrate (≥99.0%), sodium borohydride ($NaBH_4$) (≥98.0%), TCEP (≥98%), silver nitrate ($AgNO_3$) (≥99.0%), L-ascorbic acid (≥99.0%), cetyltrimethylammonium bromide (CTAB) (≥99.0%), TE buffer (pH 7.4), and sodium chloride (NaCl) (≥99.0%) were purchased from Sigma Aldrich. $KMnO_4$, H_3PO_4 were obtained from R & M Chemicals Ltd.; HCl (37%), H_2SO_4 (95-97%) and ethanol (99.8%) from Friendemann Schmidt and H_2O_2 (35%) was purchased from QReC. UPW (18.2 MΩ cm) was prepared in house and used throughout the study. All the glass wares used in the experiments were cleaned with aqua regia (1:3 mixture of HNO_3 and HCl), followed by through washing with water.

Corning LSE compact centrifuge was used to wash GO, AuNPs, AuNRs and GO-AuNRs while Mini-15K CE Mini Lab High Speed Centrifuge was used for the small volume samples. Ultrasonic homogenizer (TF-650Y) for exfoliating GO, UV–vis spectrophotometer (model: UV-2600, Shimadzu, Japan) for UV-vis spectra and NanoDrop 2000 spectrophotometer for the quantification of DNA as well as for UV-vis absorption spectra of minute volume of sample were used as per requirements. FEI Tecnai F20 TWIN 200 kV transmission electron microscope (FEI Company, Hillsboro, USA) was employed for capturing high resolution images of the synthesized nanocomposites. AFM was performed using AFM5000II Scanning Probe Microscope (Hitachi) in dynamic force (tapping) mode.

5.2.2 Probe sequences, Complementary and Non-complementary Target DNA

Pig (*Sus scrofa*) DNA probe (24-mer) was selected from cytb gene and verified by Hossain et al. (2017) to discriminate the cattle, buffalo and porcine materials in food chain by real-time PCR (Hossain et al., 2017a). The selected probe DNA sequence was divided into 12-mer length of two equal halves. The 5′ terminus of the probe sequence was chemically functionalized with ATTO Rho6G adjacent to the C6 spacer followed by a terminal 5′ thiol modifier. Another part of the probe sequence was functionalized with 3′C3 S-S. The chemically modified oligo DNA was synthesized and purified by Biosynthesis, USA (http://www.biosyn.com/index.aspx) while all other oligonucleotide sequences were obtained from IDT, Singapore (https://sg.idtdna.com/pages). All the oligo sequences used in this study are listed in the Table 5.1. The lyophilized chemically modified oligonucleotide was dissolved in nuclease free water for reconstitution while rest of the oligo sequences were reconstituted as per manufacturer instructions using TE buffer (pH 7.4) and kept as stock solution (100 μM) at -40°C.

Table 5. 1: List of the oligo nucleotide sequences

Name	**Sequence profile**
Probe Sequence	5'-CCTGCCATTCATCATTACCGCCCT-3'
SP sequence	5'-S-S-C6-(ATTO Rho6G)-CCTGCCATTCAT-3'
CP sequence	5'-CATTACCGCCCT-C3-S-S-3'
Target sequence	5'-AGGGCGGTAATGATGAATGGCAGG-3'
Single base mismatch	5'-AGGGCGGTAATTATGAATGGCAGG-3'
Three base mismatches	5'-AGGGCGGTAGCTATGAATGGCAGG-3'
Non-Target (Goat)	5'-AGGGCTGTGATGATGAATGGGAGG-3'
Non-Target (Rat)	5'-AGGGCGGCGATAATGAATGGGAGG-3'
Non-Target (Sheep)	5'-AGGGCTGCGATGATGAATGGGAAA-3'
Non-Target (Cow)	5'-TGTAGGATTAGGCAGATTCCCAGGAGGGAAC-3'
Non-Target (Horse)	5'-TGGAGGATTAGGCAGATTCCTAGGAGGGAGC-3'
Non-Target (Buffalo)	5'-TGCAGGATTAGGCAGATGCCTAGGAGAGAGC-3'

5.2.3 Collection of Meat Samples and Extraction of Genomic DNA

Authentic frozen raw pork samples in triplicates were collected from another research team as mentioned in Section 4.2.3, who have already verified the supplied meat sample by multiplex PCR assay (Hossain et al., 2017a; Hossain et al., 2017b). The total DNA was extracted from the muscle tissue of pork samples using FavorPrep Tissue Genomic DNA Extraction Mini Kit (Favorgen Bitoech Corp, Taiwan) as per manufacturer's instructions and descriptions mentioned in Section 4.2.3. The DNA obtained by the extraction procedure was checked for the concentration and purity by UV-vis absorbance using NanoDrop 2000 spectrophotometer (Thermo Scientific). The absorbance at 260 nm and the ratio of absorption maxima of nucleic acid (A260) and protein (A280) were used to determine the concentration and the purity of the extracted DNA. The purified DNA was kept at -20°C for further use.

5.2.4 Synthesis of Graphene Oxide

GO was synthesized as per protocol described in the Section 4.2.4.

5.2.5 Synthesis of AuNPs

The AuNPs were synthesized following the same procedure described in the Section 4.2.5.

5.2.6 Synthesis of AuNRs and GO-AuNR composite

AuNRs were synthesized in aqueous solution following the seed mediated protocol with minor modifications as reported by Feng et al. (Feng et al., 2015). In brief, the seed solution was prepared by mixing CTAB (3.75 mL, 0.1 M) and $HAuCl_4$ solution (50 µL, 24 mM), followed by the addition and mixing of ice-cold $NaBH_4$ (300 µL, 0.01 M) with slow magnetic stirring for 2 min. The color of the solution was changed from yellow to

light brown within 1-2 min which indicates the formation of Au seeds. The solution was then kept standing at room temperature for at least 2 h. The growth solution was prepared by mixing $HAuCl_4$ (204 µL, 24 mM), CTAB (10 mL, 0.1 M), H_2SO_4 (200 µL, 0.5 M) and $AgNO_3$ (100 µL, 10 mM) in a flask, followed by drop-wise slow addition of ascorbic acid until the solution turned to colorless (0.1 M, around ~ 80 µL). Finally, 24 µL of seed solution was added to the growth solution at room temperature to initiate the formation of AuNRs, hence the color of the solution was gradually changed between 10-20 min. The solution was kept standing under the same condition at room temperature for overnight. The as-synthesized AuNRs was washed twice with UPW to remove the excess surfactant by centrifuging at 11000 rpm for 15 min. Finally the obtained AuNRs precipitate was redispersed in UPW and stored at room temperature for routine use.

On the other hand, GO-AuNRs composite was synthesized via the electrostatic self-assembly reported by Han et al. (X. Han, Fang, Shi, Wang, & Zhang, 2013). Firstly, a 0.5 mg/mL homogenous suspension of GO was prepared by dispersing 10 mg of GO in 20 mL of distilled water followed by ultrasonic agitation. Subsequently, 10 mL of GO (0.5 mg/mL) suspension was added to 10 mL of AuNRs dispersion with ultrasonic agitation for 10 min followed by vigorous stirring for 2 h at room temperature. GO-AuNRs nanocomposite was therefore obtained.

5.2.7 Preparation of Signal Probe conjugated AuNPs

Thiol-modified chemically functionalized SP DNA (1 µM, 100 µL) was incubated with freshly prepared TCEP (10 mM, 10 µL) for at least 1 h at room temperature to reduce the disulfide bonds. Before functionalization, the as-prepared AuNPs (400 µL) was centrifuged at 8000 rpm for 30 min and the obtained AuNPs pellet was re-dispersed in UPW to a final volume of 200 µL. The AuNPs were then functionalized with thiol-active ss-signal DNA probe as per protocol described at the previous study (Section 4.2.7) with

minor modifications. In detail, the TCEP treated ATTO Rho6G intercalated SP DNA were mixed with AuNPs and incubated at room temperature for 16-20 h. The mixture was then treated with Tween 20 solution (0.1% Tween 20 in 10 mM PBS, pH 7.4) and incubated at room temperature for 30 min. This was followed by the salt aging of the suspension with stepwise addition of NaCl (1 M) at an interval of 1 h or more until reach to 100 mM NaCl concentration. During the salt aging process, a certain quantity of DNA is attached to AuNPs after each increment of NaCl and keep stabilize the DNA functionalized AuNPs (AuNP-SP) for the next addition. Moreover, the conformation of the probe DNA onto AuNPs is changed from horizontal to vertical array, and keep accessible the nucleotide bases for the subsequent hybridization process (Feng et al., 2015). The AuNP-SP were allowed to age for another 40 h at room temperature under the same conditions. The main outcome of the prolonged salt-aging process is the decrease of repulsion between the DNAs, to achieve an ultrahigh density of DNA on the AuNPs (Liu & Liu, 2017). The salt-aged AuNP-SP solution was then centrifuged at 8000 rpm for 30 min, followed by discarding the supernatant to remove the unbound, free DNA. The obtained AuNP-SP is resuspended in UPW and the washing procedure is repeated twice to keep the solution as much as possible free from unbound DNA and finally stored in a refrigerator for further use.

5.2.8 Preparation of Capture Probe conjugated GO-AuNR

GO-AuNR were functionalized with the CP DNA as per procedure in the literature with minor modifications (Pal et al., 2011). The thiolated CP sequences were treated with TCEP as per above mentioned procedure and mixed with GO-AuNR in water containing 0.01% sodium dodecyl sulfate and incubated overnight. This was followed by the addition of 10×TBE into the suspension to achieve a final buffer concentration of 1×TBE. After 4-5 h incubation, 1 M NaCl solution was added gradually to reach to a final NaCl

concentration of at least 100 mM by 24 h. The suspension was kept standing overnight at room temperature. The GO-AuNR-CP DNA (GO-AuNR-CP) composite was then washed with 1×TBE buffer by repeated centrifugation at 8000 rpm for 30 min to remove the excess unbound DNA and finally suspended in the 0.1 mM PBS (pH 7.4).

5.2.9 Fabrication of the Sandwich Biosensor and acquisition of SERS Spectra

The corresponding target DNA sequences (100 µL) were added to the AuNP-SP (200 µL) suspension and incubated overnight at room temperature to facilitate the hybridization between the SP sequences and target DNA. The suspension was washed with UPW by repeated centrifugation at 8000 rpm for 30 min to remove the unhybridized target DNA and the obtained partially hybridized composites (AuNP-SP-Target) was finally dispersed in 0.1 mM PBS (pH 7.4). Equal volumes of GO-AuNR-CP and AuNP-SP-Target were then mixed together and incubated overnight at room temperature. During the incubation period, CP sequences are hybridized with the unbound part of the target DNAs, already attached to AuNPs-SP and formed the sandwich structure (GO-AuNR-CP-Target-SP-AuNP). Upon formation of the hybridized composite, purification was carried out by centrifugation at very low speed (1000 rpm for 4 min) to separate the unbound AuNP-SP-Target or GO-AuNR-CP present in the supernatant. Afterward, the dual platform coupled sandwich biosensor composite was dispersed in 0.1 mM PBS (pH 7.4). The samples for SERS experiment were prepared as per procedure described in the Section 4.2.10 by placing 50 µL of the obtained final product (GO-AuNR-CP-Target-SP-AuNP) onto the silicon wafer, followed by vacuum drying. Similarly, the SERS spectra were recorded using Renishaw Invia Confocal Raman Microscope using 532 nm laser excitation and 20x objective lens and the obtained SERS data were analyzed using Origin 2017 software.

5.3 Results and Discussion

5.3.1 Characterization of GO, AuNPs, AuNRs and GO-AuNR

The synthesized GO, AuNPs, AuNR and GO-AuNR were characterized by UV-vis spectroscopy, XRD, Raman spectroscopy and HR-TEM. The crystalline nature of the synthesized AuNPs was confirmed by XRD analysis and the obtained XRD patterns revealed five diffraction peaks at 2θ = 38.25°, 44.40°, 64.68°, 77.69° and 81.84° (Figure 5.1a), which are assigned to the (111), (200), (220), (311) and (222) of lattice plane of FCC AuNPs (JCPDS No. 04-0784). The high intensity diffraction peak at 2θ = 38.18° corresponds to (111) plane indicating its predominant orientation (Kumar et al., 2020). The as-prepared burgundy red color AuNPs showed an absorption band at 519 nm in the UV-vis spectrum (Figure 5.1b) and confirmed by the AFM (Figure 5.3a-b) and HR-TEM images (Figure 5.2a) where AuNPs were observed as spherical in shape with size ranged from 12 to 14 nm in diameter.

The oxidative synthesis of GO from graphite flakes was confirmed by the XRD analysis with a diffraction peak at 2θ = 10.24° corresponding to the (002) reflection plane of GO (Figure 5.1a) (Zeng et al., 2020; Marcano et al., 2010). The UV-vis spectroscopy of the ultrasonicated and well dispersed GO suspension in water showed a characteristic absorption peak at 233 nm (Figure 5.1c), assigned to the π-π* transitions of aromatic CC bonds (Ma et al., 2020), which was further confirmed by the HR-TEM (Figure 5.2b) and AFM topography images (Figure 5.3c-d) of GO. In HR-TEM image, GO was characterized by the typical crumpled and flake structure (Kwak, et al., 2016). On the other hand, UV–vis–NIR absorption spectra of the as-prepared AuNRs showed two absorption peaks at 522 and 827 nm (Figure 5.1c) which are due to the transverse and longitudinal SPR respectively (Han et al., 2013; Zhang et al., 2013a). The TEM image of AuNR exhibited the high quality of AuNRs with uniform shape and size and average

diameter of 12±2 nm and length 55±7 nm (Figure 5.2c). UV-vis and TEM studies of AuNRs therefore correlate and correspond with the previous study (Feng et al., 2015; Guo et al., 2018).

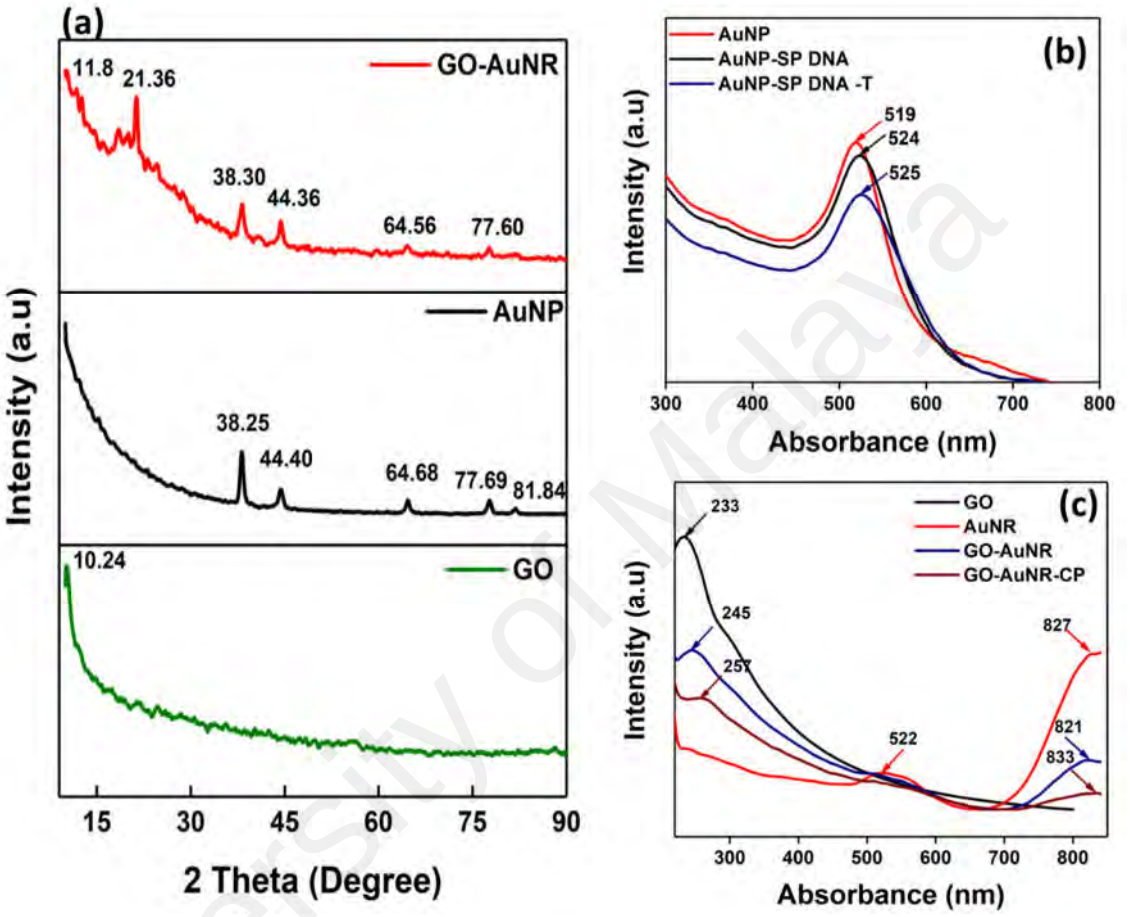

Figure 5. 1: (a) XRD spectra of GO, AuNP and GO-AuNR. UV-vis absorption spectra of (b) AuNPs, AuNPs functionalized with thiolated SP DNA, and AuNP linked SP with partially hybridized target DNA; and (c) GO, AuNR, GO-AuNR, and GO-AuNR functionalized with the CP DNA.

XRD spectra of GO-AuNR hybrid showed peaks at 2θ = 11.8°, 21.36°, 38.30°, 44.36°, 64.56° and 77.60° (Figure 5.1a) where the peak at 2θ =11.8° is attributed to corresponding GO peak and the peak at 2θ = 21.36° indicated the partial reduction of GO which might be due to ultrasonication and prolong vigorous stirring. However, the other diffraction peaks at 38.30° (111), 44.36° (200), 64.56° (220) and 77.60° (311) attributes to the presence of AuNRs over the GO (Tao & Wang, 2018). Moreover, the UV-vis spectrum of GO-AuNR hybrid showed three peaks at 245, 511 and 821 nm, where the peak at 245

nm represents the characteristic but shifted absorption band of GO, and the peaks at 511 and 821 nm represent the transverse and longitudinal plasmon bands of AuNR respectively but shifted a bit in compare to pure AuNRs, hence confirms the formation of GO-AuNR nanocomposites (Figure 5.1b) (Tao & Wang, 2018; Caires, et al., 2015; Moon et al., 2015). The coupling of the AuNRs and GO was further confirmed by the AFM and HR-TEM studies. It was observed in the HR-TEM image that the near-transparent GO is perfectly decorated by a large number of well dispersed AuNRs (Figure 5.2d), which was further verified by the well scattered AuNRs over GO sheets in the AFM study (Figure 5.3e-f). Therefore, the XRD, TEM and AFM characterization study of the *ex situ* synthesized GO-AuNR, ensures the homogenous distribution of the uniform size-ranged AuNR over GO sheets via strong electrostatic attractions (Tao & Wang, 2018; Moon et al., 2015; Han et al., 2013).

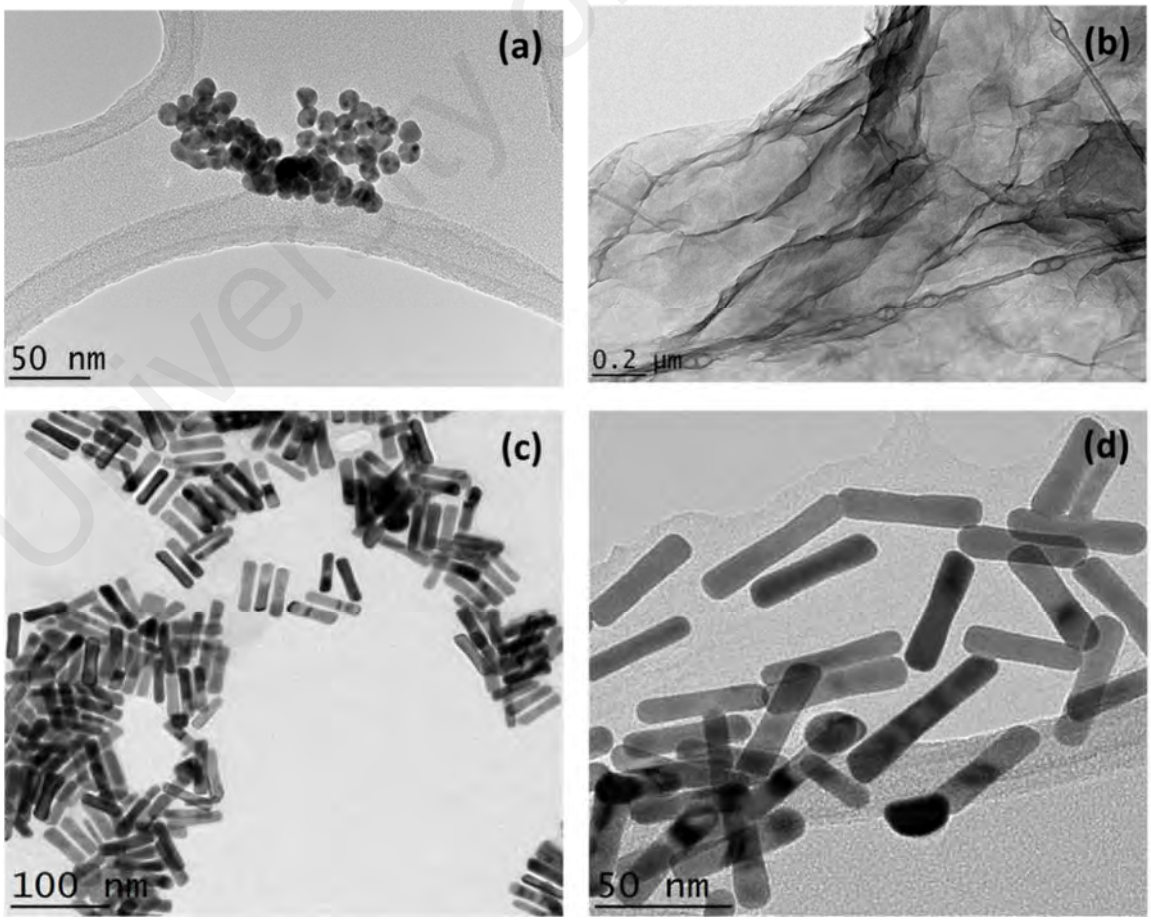

Figure 5. 2: HR-TEM images of (a) AuNPs, (b) GO, (c) AuNR, and (d) GO-AuNR samples prepared on lacy carbon coated copper grid.

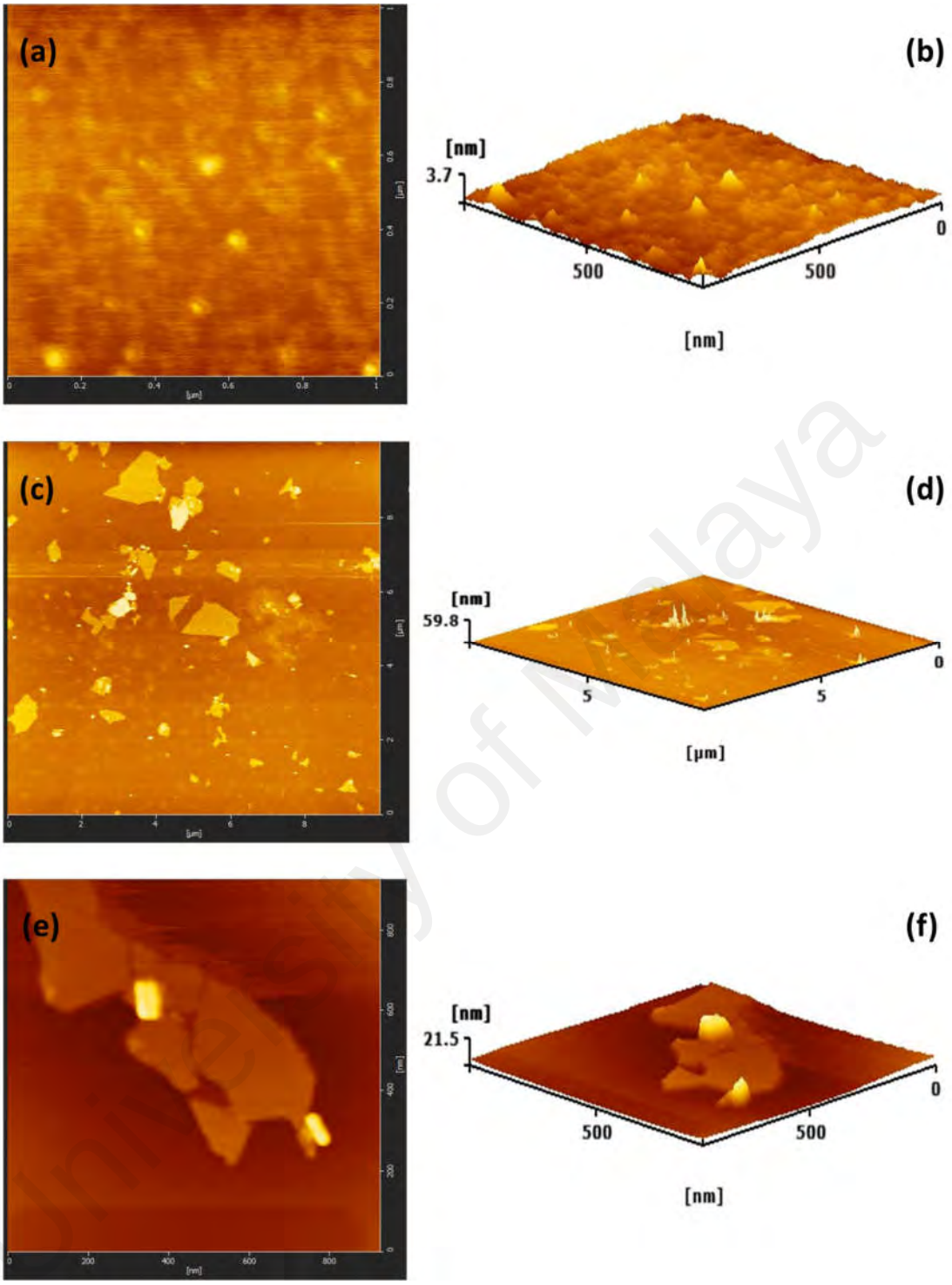

Figure 5. 3: AFM topography 2D and 3D images of AuNPs (a-b), GO (c-d) and GO-AuNR (e-f) adsorbed on mica surface.

5.3.2 Attachment of the DNA Probe Sequences onto Sensor Platforms

Attachment of the 12-mer long SP sequences on the AuNPs surface via the thiol-gold linkage is confirmed by the peak shift from 519 nm to 524 nm in UV-vis spectrum (Figure 5.1b) (Xing, et al., 2020). The 5 nm red shift is due to the increase of the AuNP particle

size via the formation of a single layer of probe sequences, which therefore confirms the successful attachment of DNA onto the AuNPs surface. In addition, there was no significant color changes of the AuNPs solution which also confirms the absence of AuNPs aggregation during the salt aging steps (Thavanathan et al., 2014). The hybridization of the corresponding target DNA with the SP sequences linked to AuNPs showed a further slight shifting (1 nm) in UV-vis spectrum. Similarly, the UV-vis absorption spectrum of the ss capture DNA covalently linked to the GO-AuNR hybrids exhibited a red shifting of the characteristic AuNR peak from 821 to 833 nm (Figure 5.1c), hence confirming the successful attachment of the thiolated DNA to the AuNRs of the hybrid composite.

5.3.3 Principle and Justification of the SERS DNA Biosensing Technique

In the biosensor fabrication, the SP DNA having a unique design by the incorporation of ATTO Rho6G immediate after the C6 spacer, was immobilized onto the AuNPs via the Au-S linkage between the AuNPs and terminal thiol molecule of the SP (Figure 5.4a) (Zhang et al., 2007). Here, the C6 spacer assist the SP sequences to stand at upright position and holds the Raman tag within few nanometers from the AuNPs surface, which ensures the SERS effect via both the electromagnetic and charge transfer mechanism. On the other hand, CP sequences were attached onto the GO-AuNR hybrid via covalent bonding of the terminal thiol molecule of the probe sequences with AuNR of the GO-AuNR hybrid composite (Figure 5.4b). To immobilize the CP sequence, the C3 spacer molecule next to the disulfide bond, keeps the DNA strands at upright conformation by minimizing the steric effects between the nucleotide bases and surfaces of AuNPs (Zhang et al., 2007) and makes the nucleotide bases accessible for the hybridization. Therefore, the partial hybridization of the target sequences with the SP linked to the AuNPs, followed by the formation of the sandwich complex via binary covalent linking between

the CP with the remainder of the free target sequence couples the two platforms together (Figure 5.4c) thereby, enhances the SERS signal due to the multicomponent aggregated hot spots induced electromagnetic and Raman tag contributed chemical enhancement (Mucic et al., 1998; Sun et al., 2007)

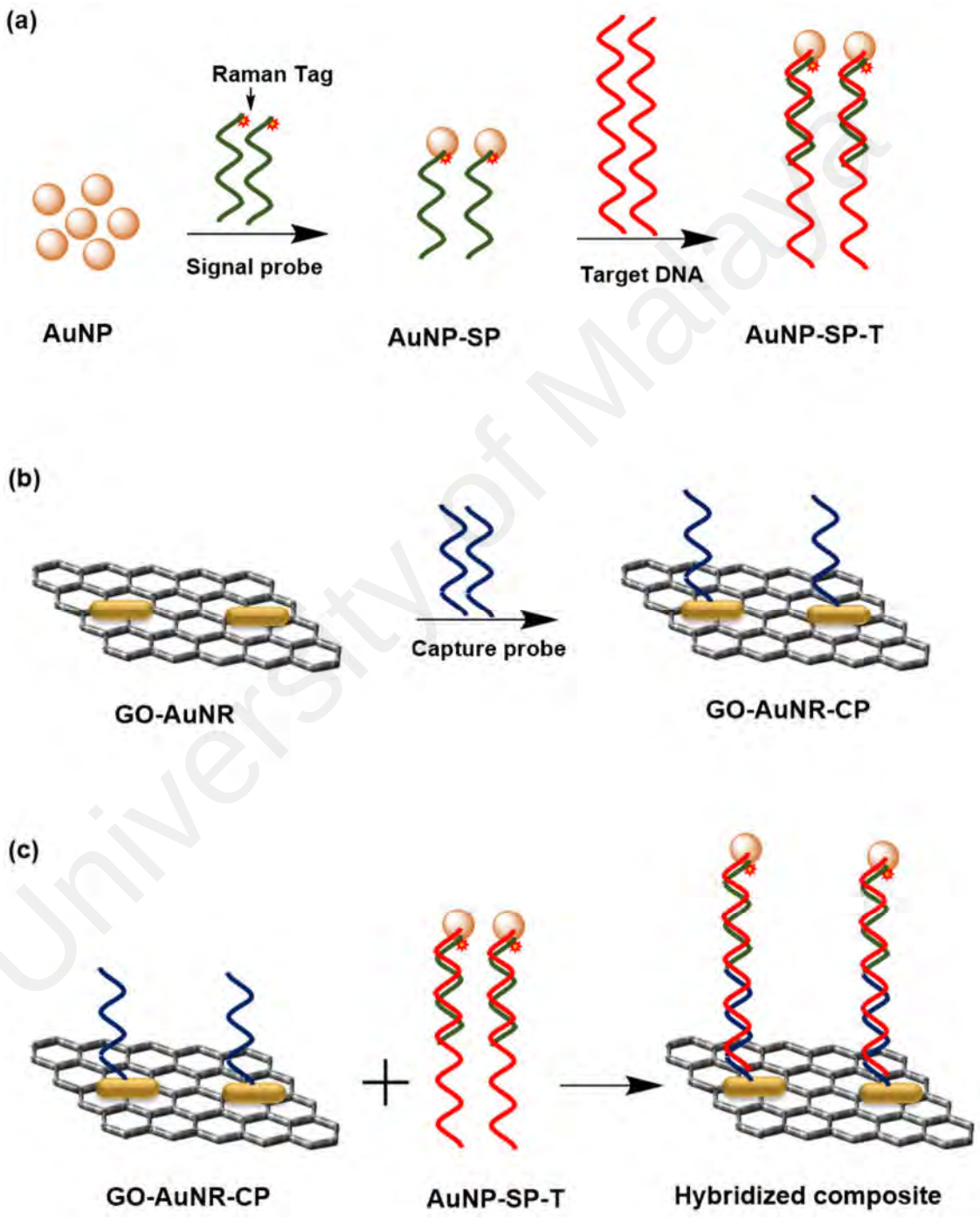

Figure 5. 4: Schematic representation of the SERS DNA biosensing strategy using GO-AuNR and AuNP platforms.

The successful attachment of the SP sequences onto the AuNPs platform was confirmed by the presence of distinct fingerprint SERS spectrum of ATTO Rho6G attributed to the peaks at 774, 1126, 1184, 1359, 1507, 1569 and 1647 cm^{-1} which are identical to the corresponding Raman peaks of pure ATTO Rho6G (Figure 5.5a) as well as the obtained data is in line with another study conducted by using AgNPs functionalized with terminally integrated Rho6G probe sequences (Eremina, et al., 2020). However, the Raman intensity of SP functionalized AuNPs is smaller than the pure ATTO Rho6G dye alone, which is definitely due to the lower number of ATTO Rho6G molecules, as each SP is integrated with only one Raman tag. Moreover, the partial hybridization of the SP sequences with the corresponding target sequences has no impact on the spectral fingerprint, rather a decreased intensity was observed due to loss of few SP sequences by repetitive washing (Figure 5.5a). On the other hand, the Raman spectrum of the CP linked SERS-active GO-AuNR substrate exhibits the GO characteristic D and G band only. However, the SERS spectrum of GO-AuNR immobilized SP sequences was characterized by the D and G band as well as ATTO Rho6G finger print peaks mainly at 1508 cm^{-1} along with few other peaks at 610, 774, 1184 and 1647 cm^{-1} (Figure 5.5b). This unique spectrum therefore, confirms the successful immobilization strategies of probe sequences onto GO-AuNR platform as well as the pattern and position of the ATTO Rho6G finger print peaks. The SERS spectrum of the hybridized composite also revealed the same but intense spectrum like GO-AuNR-SP composite including D band at 1356 cm^{-1}, G band at 1600 cm^{-1} and the dominant ATTO Rho6G representing peak at 1508 cm^{-1}, in addition to the presence of few peaks at 610, 774, 1184 and 1647 cm^{-1} (Figure 5.5b). This confirms the hybridization of the probe DNAs with the corresponding target DNAs and the consequent coupling of the two platforms (Prinz et al., 2016). Hence, based on this biosensing strategy, the intensity of the ATTO Rho6G which represents the fingerprint peaks of the hybridized composites can be correlated to the amount of

corresponding target DNA. Therefore, the peak at 1508 cm^{-1} was selected as the standard for the qualitative and quantitative detection of the target pig DNA throughout the study. Further, the linking of the two platforms was also confirmed by the HR-TEM images of the hybridized products (Figure 5.6a-d), where the AuNPs were attached onto the AuNRs of the GO-AuNRs composites. This indicates the successful hybridization between the complementary target sequences with the two strands of CP and SP sequences.

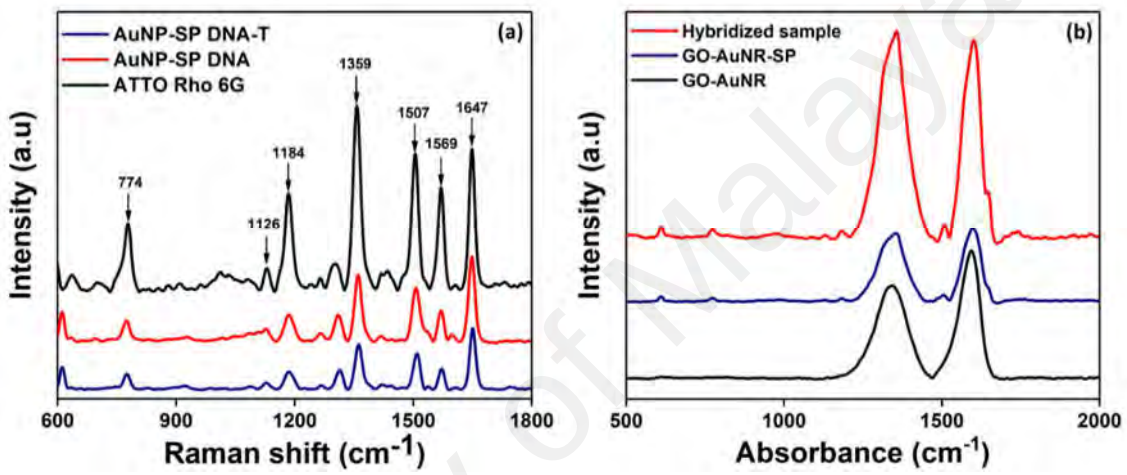

Figure 5. 5: Raman spectra of (a) pure ATTO Rho6G, AuNPs functionalized with SP DNA intercalated with ATTO Rho6G followed by partial hybridization with the corresponding target DNA, and (b) GO-AuNR, GO-AuNR functionalized with SP DNA and the hybridized composite (GO-AuNR-CP-Target- SP-AuNP).

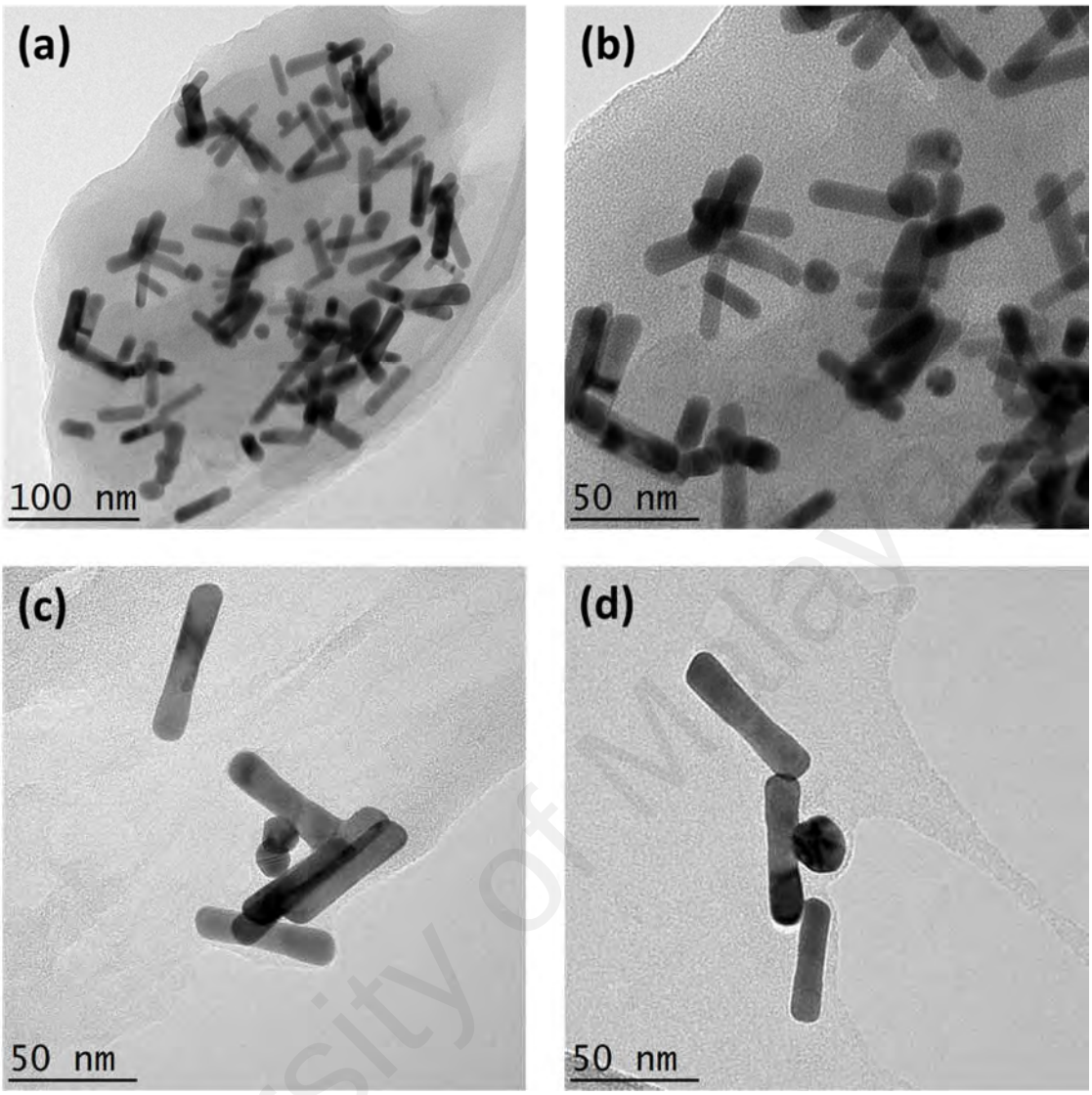

Figure 5. 6: HR-TEM images of the hybridized composites (GO-AuNR-CP-Target- SP-AuNP) at 100 nm (a) and 50 nm (b-d) magnification. The hybridized composites were formed via probe-target hybridization mediated coupling of AuNPs onto the GO-AuNR. In the images, the AuNPs are mostly found attaching to the AuNRs of GO-AuNRs hybrid, indicates the successful hybridization.

5.3.4 Performance of the Dual Platform based SERS DNA Biosensor

The quantitative detection of the target DNA was accomplished by determining the intensity of the representative SERS peak at 1508 cm^{-1} for intercalated ATTO Rho6G in the SP DNA. The quantitative evaluation was performed by varying the concentration of target DNA from 10 aM to 1 μM, which showed a steady upward trend of the SERS signal intensity at 1508 cm^{-1} (Figure 5.7a&b). However, the ATTO Rho6G finger print peak at 1508 cm^{-1} for the hybridized composite of 10 aM target DNA concentration was

found indistinguishable, in contrary the peak intensity of the 100 aM concentration of target DNA was still well distinguished and detectable, therefore is considered as the LOD. Moreover, the peak intensity shows a linear response with the target DNA concentration between 100 am to 1 μM with a correlation coefficient value (R^2) of 0.9828 (Figure 5.7c). Compared to other works of DNA detection, this dual platform based SERS biosensor with a very short-length DNA probe provides a higher sensitivity for detecting minute amount of DNA in the sample. This excellent performance of the fabricated biosensor relies on the use of two different SERS-active platforms and the presence of Raman tag intercalated to DNA probe sequences where ATTO Rho6G is positioned spontaneously within few nanometers of the AuNPs surface due to the unique design of the DNA probes. The SERS signal enhancement is in fact reliant on the distance between the sensor platform and immobilized Raman dye (Eremina, et al., 2020).

GO-AuNRs nanocomposite as the platform have great influence in SERS enhancement owing to the strong light scattering and local-field enhancement properties of AuNRs induced by the anisotropic splitting of the SPR into transverse SPR and longitudinal SPR, and the synergistic effect of GO and AuNR components (J. Guo et al., 2018; Vianna et al., 2016). Moreover, hybridization of the target DNA with the corresponding SP and CP sequences coupled the GO-AuNR and AuNP platforms, promote to generate hot spots at the nanoparticles junction which consequently leads to an increased SERS signal due to the electromagnetic enhancement (Lin et al., 2015). Furthermore, the platforms were attached via linking of the probe-target sequences, hence the ATTO Rho6G integrated to the SP sequences must be aligned in the interstices of the GO-AuNR and AuNPs, where the hot spots actually originate. Hence, the Raman tag contributes directly in the SERS signal enhancement by the chemical charge transfer mechanism between the AuNPs and dye (Maher, 2012; Radziuk & Moehwald, 2015).

The short-length split DNA markers with the direct incorporation of Raman tag is a novel approach which exerts no hindrance on hybridization rather enhances the SERS signal, is therefore significant in DNA detection. The developed biosensor thus exhibited better performance compared to the biosensor fabricated by using the dual platforms, co-adsorption of Raman tag and probe sequences onto the same AuNPs platform and following the same hybridization principle as discussed at the Chapter-4 for detecting MBT (Khalil et al., 2019). Moreover, this sandwich assay biosensor is an efficient platform in terms of selectivity and sensitivity, compared to the biosensors comprising of SERS non-active (Cao et al., 2002; Prinz et al., 2016), SERS active single platform (Eremina, et al., 2020), and even SERS-active dual platforms (J. Huang et al., 2010; Xia et al., 2010). The fabricated SERS biosensor showed greater efficiency towards the detection of pork in compare to the commonly used techniques such as PCR (Kang & Tanaka, 2018; Xu et al., 2018a), colorimetry (Roy et al., 2017), enzyme immunoassay (Mandli et al., 2018) and even electrochemical detection assays (Roy et al., 2016). Hence, to minimize the shortcoming of the previously reported SERS DNA biosensors, and adopting a straightforward, convenient and efficient technique, herein the developed SERS-active dual platforms and Raman tag intercalated oligo probe based SERS DNA biosensors proved as an efficient sensing approach. Furthermore, this is the first-ever reported SERS technique for the detection and quantification of pork species which could be considered as efficient approach for the definite identification of trace pork residues in the food chain or industrial applications as a quality control or screening procedure.

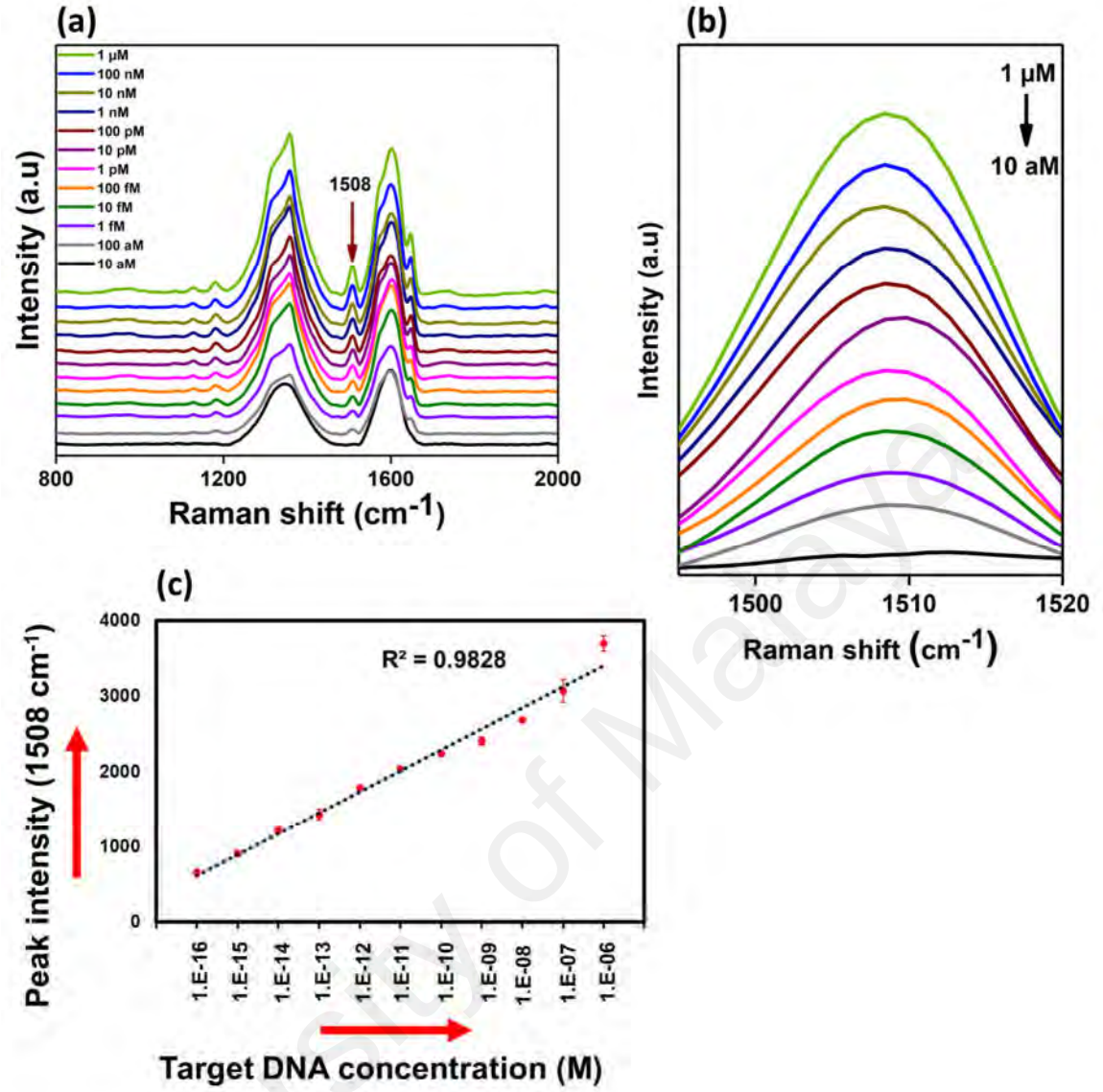

Figure 5. 7: (a) The stacked SERS spectra of the hybridized composites obtained from the target DNA of pork species from 1 µM to 10 aM, (b) the chopped spectra (1490 to 1520 cm^{-1}) of the hybridized composites (1 µM to 10 aM) to magnify and distinguish the intensity of the peak at 1508 cm^{-1} (c) The linear curve of SERS intensity at 1508 cm^{-1} vs target DNA concentration. Error bars represent standard deviations of peak intensities from n=3 repeated measurements.

5.3.5 Selectivity, Specificity and Reproducibility study of the Biosensor

The selectivity of the biosensor was investigated by assessing the hybridization capability of the biosensor with other non-target DNA as the interference factors. Because of the complementary in nature, the target DNA of pig only hybridized with the corresponding probe sequences and formed duplex structures, which was characterized by the appearance of D and G bands of GO with an obvious distinct peak at 1508 cm^{-1}

attributed to the ATTO Rho6G (Figure 5.8a). This intense SERS spectrum is due to the generation of hot spots at the interstices between the GO-AuNR and AuNPs (Chuong et al., 2017) and therefore indicates a positive result. As depicted in Figure 5.8 (a&b), the blank sample (negative control), and interference samples (non-target DNA sequences of goat, rat, sheep, cow, horse, buffalo and canine) at a concentration of 1 μM, produced low Raman intensity for the peak at 1508 cm^{-1}, a signatory peak of hybridization. Therefore, the peak intensity at 1508 cm^{-1} for the blank sample was considered as the baseline signal for the ATTO Rho6G and the obtained spectrum is denoted as the true negative. However, the small presence of ATTO Rho6G signal from the blank, as well as the non-target treated hybridized composite might be due to the non-specific interaction between the fabricated GO-AuNR-CP and AuNP-SP-Target composites (Khalil et al., 2019). The results of interference study showed that in the presence of the corresponding target sequences, the SERS intensity of the ATTO Rho6G signal at 1508 cm^{-1} was much stronger compared to other non-target DNA of variable length and nucleotide mismatches, therefore, indicating excellent selectivity of the biosensor for the detection of pig DNA.

Furthermore, the biosensor was tested to differentiate the target DNA with single nucleotide base mismatch and three-base mismatches. The SERS intensity of the ATTO Rho6G signal at 1508 cm^{-1} from the hybridized composite formed by the single base-mismatch was found more intense than the three-base mismatches (Figure 5.8b). However, both SERS spectra were obviously less intense compared to the complementary target sequences, but more intense compared to the other interference non-target DNA (Figure 5.8b). This is attributed to the hybridization between the single-base mismatch target sequences with the SP and followed by CP sequences. Hence, the chances of hybridization are lowered by the number of mismatch bases. The plots in Figure 5.8 (a&b) indicate a lower occurrence of hybridization, subsequently the lower SERS intensity is

due to the larger number of nucleotide mismatches in the sequences. This excellent specificity of the fabricated biosensor is due to the selection of short-length DNA probe which was further split into produce two very short segments of DNA sequences, thus can easily recognize the complementary nucleotide bases in the target sequences (Khalil et al., 2019). Furthermore, validation of the hybridization procedure, sample preparation for Raman experiment, and the reproducibility study of the SERS DNA biosensors were justified by the SERS spectra from randomly chosen six different points of a slide prepared from the hybridized composite obtained from the 100 pM target DNA concentration. All the SERS figures were found alike (Figure 5.8c) and the RSD value of the corresponding SERS intensity of the representative peak (1508 cm^{-1}) is estimated as 6.65% (Figure 5.8d). Hence, the study proves a good reproducibility of the developed SERS DNA biosensor (Xu et al., 2020).

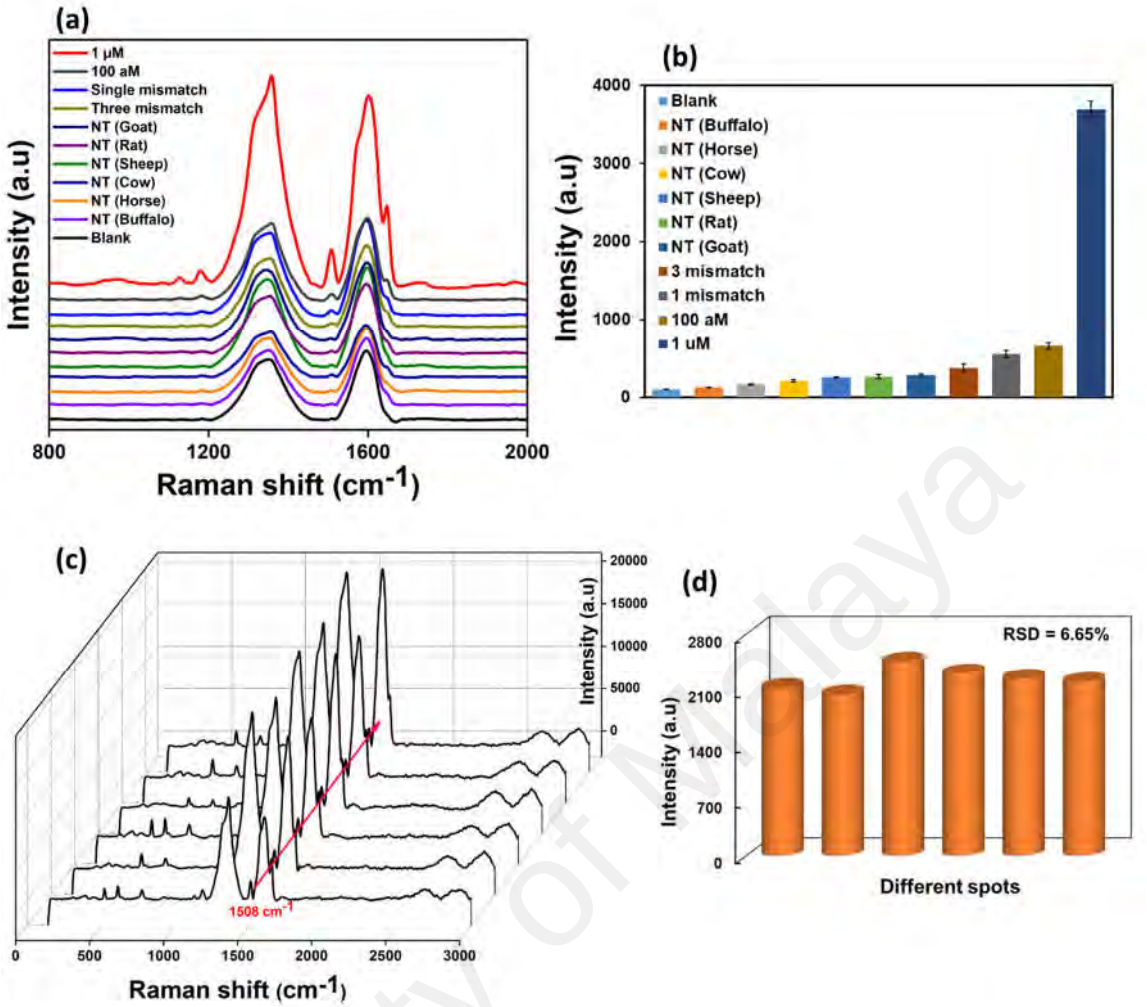

Figure 5. 8: (a) SERS spectra of the selectivity study of the fabricated biosensors using different DNA sequences -complementary (1 μM), LOD concentration (100 aM), 1 μM concentration of blank sample, single mismatch, triple mismatches and interference samples (non-target sequence of goat, rat, sheep, cow, horse and buffalo), and (b) the corresponding intensity of the SERS fingerprint signal at peak position 1508 cm^{-1}. Error bars represent standard deviations of peak intensities from n=3 repeated measurements. (c) SERS spectra of the hybridized composite (100 pM target DNA) from six different spots, and (d) the RSD of the SERS peak intensity at 1508 cm^{-1} for 6 different spots.

5.3.6 Application of the Biosensor for Real Sample Analysis

The purity of the extracted DNA from the pork sample was determined by the A260/A280 ratio and the result was around 1.7, hence reflecting the high purity of DNA (Ali et al., 2015b). The concentration of the extracted DNA was checked by UV-vis absorption at 260 nm and it was found ~60 ng/μL. The value was converted into nM concentration by applying the Equation 5 and knowing the average size of the genomic DNA strands by doing electrophoresis at 2% agarose gel and using XLarge DNA Ladder

(250 to 25k bp) (GeneDirex, Taiwan) as marker. Therefore, to validate the feasibility and efficiency of the fabricated SERS DNA biosensor, the extracted pork DNA sample was diluted until attaining the established LOD concentration for the synthetic target DNA. The serially diluted DNA solution were then heat-treated in a water bath at 95°C for 15 min followed by rapid cooling in ice bath for further 15 min and finally ultrasonication of the heat treated denatured ssDNA solution for 20 min to obtain the small-fragmented ssDNA (Pandey et al., 2011; Tiwari et al., 2015). The fabricated sensor showed extraordinary sensitivity for the detection of corresponding target DNA from real sample. The SERS peak at 1508 cm^{-1} for the DNA concentration from 10 nM to 1 fM were found well distinguished. The LOD was established as 1 fM (Figure 5.9a), which is 10 times lower than the LOD value (100 aM) for the synthetic target DNA. The curve obtained from the peak intensity at 1508 cm^{-1} vs target DNA concentration also showed an excellent linear relationship with an R^2 value of 0.9827 (Figure 5.9b). Therefore, it can be concluded that the efficiency of the coupling of two platforms by the real DNA sample is well-justified for the practical applications.

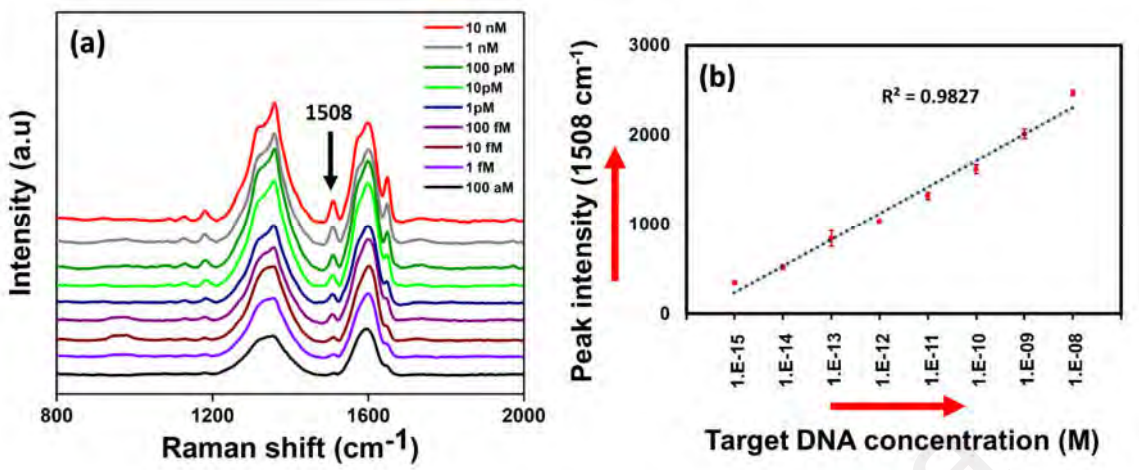

Figure 5. 9: (a) The SERS spectra for the hybridized composites by target DNA (100 aM to 10 nM) from real pork sample. (b) The linear curve of SERS intensity at 1508 cm^{-1} vs target DNA concentration for the real sample. Error bars represent standard deviations of peak intensities from n=3 repeated measurements.

5.4 Conclusion

In this work, 24-mer length probe sequence used for the detection of pork DNA was split into two parts. The 5′ terminal was chemically functionalized with ATTO Rho6G adjacent to the C6 spacer arm with terminal thiol modifier using a novel design and immobilized onto AuNPs surface. On the other hand, 3′ end of the split-probe DNA functionalized with C3-S-S was immobilized onto a SERS active GO-AuNR. Introduction of the complementary target sequences coupled the two platforms together, via the target-probe sequence hybridization and consequently produced an identical, distinguished and enhanced SERS signal. The greater SERS intensity is due to the combined effect of electromagnetic and chemical enhancements at the hot spot region originated at the junction of GO-AuNRs and AuNPs. Therefore, by the combination of the two different platforms and very short-length Raman tagged DNA probe sequences, the fabricated biosensor showed an LOD as low as 100 aM and differentiated the DNA sequences of closely related non-target species (goat, rat, sheep, cow, horse and buffalo) and the single-base mismatch in the complementary target sequences. Moreover, the biosensor was validated for the real sample analysis. The biosensor thus exhibited greater

selectivity, sensitivity as well as sensitivity for the qualitative and quantitative detection of pig DNA, which is a potential application in industries and regulatory agencies. Finally, it is believed that different SERS active sensor platforms, facile fabrication procedure, species-specific Raman tag integrated short-length oligo probe sequences could lead to the fabrication of multiplex biosensors for the detection of a panel of biomarkers for application in diverse fields.

CHAPTER 6: SERS BASED DUPLEX DNA BIOSENSOR FOR THE SIMULTANEOUS QUANTITATIVE DETECTION OF MALAYAN BOX TURTLE AND PIG SPECIES

6.1 Introduction

Reliable, fast, sensitive and multiplex DNA detection is in high demand toward the fundamental molecular biology research to practical applications in diverse fields such as gene profiling, medical diagnostics, drug screening, food safety and adulteration, and forensics (Duan et al., 2015; Li et al., 2005a). Researches on the multiplex DNA detection have been attempted and yet ongoing for the development of a facile, sensitive detection and quantification of DNA of different origin in one assay adopting different principles including PCR, spectrophotometry, fluorescence, electrochemistry, and SERS (Kang et al., 2010). Multiplex PCR which involves simultaneous amplification of target DNA of different species in a single experiment, however less suited and challenging for highly sensitive application due to the inherent complexity and the amplification of target DNA of different-length templates (Ahamad et al., 2017; Hou et al., 2015). Similarly, multiplex real-time PCR is also remarkably promising due to the simultaneous detection and quantification of the multiple target DNA samples in a single assay, however require several pre-processing steps as well as fluorescent dye labeling (Kim et al., 2019). Furthermore, nanoparticle based fluorescence assay has also been considering the preferred techniques since last decade for the simultaneous multiplex DNA detection. Though having greater preferences for its promising sensitivity and selectivity, its application in multiplex detection is being restricted due to the inherent photo bleaching, narrow excitation with broad emission profile, and the most importantly the peak overlapping of different fluorophores (Sun et al., 2007; Zhang et al., 2011). In this context, SERS has gained much interests as an attractive alternative strategy for the quantitative and simultaneous multiplex DNA detection due to its capability of producing

molecule specific vibrational spectra, and inherent fluorescence quenching properties to easily distinguish the different Raman label from a mixture of samples (Braun et al., 2007; He et al., 2012).

Apart from the absence of photo bleaching from Raman dye or Raman scattering compound, narrow Raman bands (spectrum) peak width, availability of large number of Raman labels to choose the best option according to the specific experimental protocol and deliberate application, and finally the highly specific and informative fingerprint signal spectra for each of the Raman labels, SERS is therefore a method of choice in current days for the high-level multiplex detection assay (Braun et al., 2007; Kneipp et al., 2006; Zhang et al., 2010). SERS based multiplex detection assays have been reported for the simultaneous detection of wide variety of analytes such as pathogenic bacteria – *S. typhimurium* and *S. aureus* (Zhang et al., 2015), hazardous pesticides - thiram, tricyclazole, and carbaryl (Kwon et al., 2019), miRNAs (Kim et al., 2019), and most importantly breast cancer cell lines (MCF-7 and BT-20) (Yarbakht et al., 2018).

Hence, the advantageous features of SERS over other detection protocols, have led to the development of wide verities of SERS sensing platforms and detection schemes for the efficient multiplex SERS biosensor. SERS based DNA detection generally involves three component based single or dual platform sandwich assay following either insertion of the Raman tag to the probe sequences (Eremina, et al., 2020; Kang et al., 2010) or co-adsorption of probe sequences and Raman reporter molecules on the same platform (Qian et al., 2008). A single platform based sandwich assay multiplex DNA detection technique generally involves immobilization of the CP sequences onto the sensor platform while Raman tag intercalated SP DNA and/or Raman reporter DNA are kept free, hence the presence of the corresponding target DNA combines both strands and generates Raman tag specific fingerprint spectra (He et al., 2012). In contrary, the dual platform based

SERS multiplex detection techniques involves functionalization of one platform with CP sequences and immobilization of the Raman tag integrated SP (Kang et al., 2010) or co-attachment of Raman tag and SP sequences onto another platform (Khalil et al., 2019), and the consequent linking of the two platforms via corresponding target DNA mediated hybridization. Though different SERS platform component have been reported till now, SERS active GO-AuNPs and AuNPs were chosen for this study due to their strong influence in SERS signal enhancement (Liang et al., 2015).

Herein, in this chapter, a duplex SERS DNA biosensing protocol has been reported for the simultaneous detection of the two different meat species - MBT and pig species. Likewise the strategy as discussed in the Chapter 5, a unique concept in SP DNA designing was executed by intercalating ATTO Rho6G and Cy3 Raman dyes to the pig and MBT specific probe DNA sequences respectively as well as immobilized onto AuNPs separately. On the other hand, CP sequences of both species were immobilized simultaneously to the same GO-AuNPs platform. Therefore, presence of the pig and MBT target sequences, covalent hybridization of the three components (CP-Target-SP) results in the multicomponent agglomeration by the coupling of AuNPs over GO-AuNPs, and consequently results in the enhanced SERS signal due to the combined effect of electromagnetic and chemical enhancements (Hao & Schatz, 2004; Qian et al., 2008). This greater amplification of the SERS signal thus lead to the detection of a very low amount of DNA present in the samples. The obtained LOD for the simultaneous detection of the two different target DNA was established 10 fM. The sensing strategy was validated by the real sample analysis and the obtained LOD was 100 fM. Furthermore, the biosensor exhibited excellent selectivity to the closely related five different non-target species as well as showing specificity to the single nucleotide differentiation. Therefore, the reported simple, straight forward but specific and sensitive DNA sensing strategy

using multicomponent platforms would guide to the fabrication of multiplex DNA biosensor as well as could be applicable for universal application in diverse fields.

6.2 Materials and Methods

6.2.1 Chemicals and Instruments

Gold chloride trihydrate ($HAuCl_4 \cdot 3H_2O$), sodium citrate dihydrate (≥99%), NaCl (≥99.0%) and TCEP (≥98%) and TE buffer solution, pH 7.4 were obtained from Sigma Aldrich. DTW was purchased from Biobasic Canada Inc. and UPW (18.2 MΩ cm) was prepared in house and used throughout the study. All the glass wares used in the experiments were cleaned with aqua regia (1:3 mixture of HNO_3 and HCl), followed by through washing with water. The rest of the chemicals were of analytical reagent grade and used whenever required.

Washing and purification of AuNPs and GO-AuNPs were accomplished using large volume Corning LSE compact centrifuge and Mini-15K CE Mini Lab High Speed Centrifuge was used for the small volume samples. UV–vis spectrophotometer (model: UV-2600, Shimadzu, Japan) for UV spectra of large volume sample and NanoDrop 2000 spectrophotometer for the quantification of DNA as well as for UV-vis absorption spectra of minute volume of sample were used as per requirements. Atomic Force Microscopy (AFM) was performed using AFM5000II Scanning Probe Microscope (Hitachi) in dynamic force (tapping) mode. TEM was performed using lacy carbon coated copper grid with HT7700 transmission electron microscope (Hitachi, Japan) and SERS spectra were recorded using Renishaw Invia Confocal Raman Microscope.

6.2.2 Probe sequences, Complementary and Non-complementary Target DNA.

The detail about selection, design, modification and functionalization of DNA probe sequences of both MBT and pig species were discussed in the Chapter 3. The oligo

sequences used in this study are listed in the Table 6.1. The chemically modified oligo sequences were synthesized and purified by Biosynthesis, USA and the rest of the oligonucleotide sequences were obtained from IDT, Singapore. The lyophilized chemically modified oligonucleotide sequences were reconstituted with nuclease free water and kept as stock solution (100 µM) at -40°C. The other probes and oligo sequences were reconstituted as per manufacturer instructions using TE buffer (pH 7.4) and kept as stock solution (100 µM) at -40°C.

Table 6. 1: List of the oligo nucleotide sequences

Name	**Sequence Profile**
Probe sequence (MBT)	5′-GATCATTACTAGGCACCTGCCTAATCCTTCA -3′
SP sequence (MBT)	5′-S-S-C6-(Cy3)-GATCATTACTAGGCAC-3′
CP sequence (MBT)	5′-CTGCCTAATCCTTCA-C3-S-S-3′
Probe Sequence (Pig)	5′-CCTGCCATTCATCATTACCGCCCT-3′
SP sequence (Pig)	5′-S-S-C6-(ATTO Rho6G)-CCTGCCATTCAT-3′
CP sequence (Pig)	5′-CATTACCGCCCT-C3-S-S-3′
Target DNA (MBT)	5′-TGAAGGATTAGGCAGGTGCCTAGTAATGATC-3′
Target DNA (Pig)	5′-AGGGCGGTAATGATGAATGGCAGG-3′
1-base mismatch (MBT)	5′-TGAAGGATTAGGCAAGTGCCTAGTAATGATC-3′
3-base mismatch (MBT)	5′-TGAAGGATTAGGTGAGTGCCTAGTAATGAT-C3′
1-base mismatch (Pig)	5′-AGGGCGGTAATTATGAATGGCAGG-3′
3-base mismatches (Pig)	5′-AGGGCGGTAGCTATGAATGGCAGG-3′
Non-Target (Goat)	5′-AGGGCTGTGATGATGAATGGGAGG-3′
Non-Target (Sheep)	5′-AGGGCTGCGATGATGAATGGGAAA-3′
Non-Target (Cow)	5′-TGTAGGATTAGGCAGATTCCCAGGAGGGAAC-3′
Non-Target (Horse)	5′-TGGAGGATTAGGCAGATTCCTAGGAGGGAGC-3′
Non-Target (Buffalo)	5′-TGCAGGATTAGGCAGATGCCTAGGAGAGAGC-3′

6.2.3 Collection of Meat Samples and Extraction of Genomic DNA

As mentioned in previous Chapters (Section 4.2.3 and Section 5.2.3) the frozen raw meat samples of MBT and pig species in triplicates were collected from another research team at NANOCAT, University Malaya who have already verified the provided meat sample using different PCR methods (Ali et al., 2015b; Ali et al., 2016; Asing et al., 2016; Hossain et al., 2017a; Hossain et al., 2017b). The total DNA was extracted from muscle tissue of MBT and pork samples separately using FavorPrep Tissue Genomic DNA Extraction Mini Kit (Favorgen Bitoech Corp, Taiwan) and the mentioned protocols described in Section 4.2.3. The concentration and purity of the extracted DNA were confirmed by the UV-vis absorbance at 260 nm and the A260/A280 absorbance ratio respectively.

6.2.4 Synthesis of AuNPs

AuNPs were synthesized as per the procedure mentioned by Frens *et al.* with minor modifications (Frens, 1973). In brief, 100 mL of 0.01% $HAuCl_4.3H_2O$ solution (0.254 mM) was taken in an Erlenmeyer flask, placed on a hot plate with vigorous stirring and heated the solution until complete boiling. 1% sodium citrate solution (38.8 mM, 1.25 mL) was added promptly to the highly stirred-boiling solution and started to develop deep red (bluish) color from the light yellow color in less than 1 min, indicting the formation of gold nuclei and within 3 min developed wine-red color due to the formation of AuNPs colloidal suspension (Xia, et al., 2016). The solution was further allowed to reflux for 20 min at the same condition, after that the heating system was removed and the solution was allowed to cool at room temperature. In this easy synthesis procedure, $HAuCl_4.3H_2O$ is reduced with $C_6H_5Na_3O_7 \cdot 2H_2O$ which acts as both the reducing agent and the stabilizer. During the reduction process the gold atoms are released from the $HAuCl_4.3H_2O$, aggregated to form AuNPs and continued to grow until the total $HAuCl_4$ is reduced

(Balasubramanian et al., 2010). The obtained AuNPs suspension was stored in the refrigerator by wrapping the bottle with aluminum foil.

6.2.5 Synthesis of GO-AuNPs

An aqueous suspension of GO (0.275 mg/mL) was prepared by ultrasonication for 2 h from the previously synthesized GO as mentioned in the section 4.2.4. GO-AuNPs composites were synthesized by the citrate reduction method following the procedure reported in the literature with minor modifications (Chuang et al., 2014). 7.5 mL GO suspension (0.275 mg/mL) was added to the 25 mL $HAuCl_4 \cdot 3H_2O$ solution (0.24 mM) in an Erlenmeyer flask and the mixture was then aged for 30 min with continuous stirring to promote the interaction of Au ions with GO surface. After that, the suspension was heated to 80°C, followed by prompt addition of the sodium citrate (0.085 mM, 470 µL) into it. The reaction was continued for another 4 h at 80°C with continuous stirring, after that allowed to cool down to room temperature. The resulting GO-AuNPs suspension was centrifuged at 6000 rpm for 2 h and washed 3 times with UPW to remove the free AuNPs. Finally the obtained GO-AuNPs was re-suspended in UPW and stored at room temperature.

6.2.6 Preparation of Signal Probe conjugated AuNPs.

As-prepared AuNPs solution (400 µL) was centrifuged at 8000 rpm for 30 min and the obtained AuNPs pellet was redispersed in UPW to prepare a final volume of 200 µL. Both MBT and pork SP DNA sequences (1 µM, 100 µL) were treated separately with freshly prepared TCEP (10 mM, 10 µL) for at least 1 h at room temperature. TCEP was used throughout the study to cleave the disulfide bond and produce the free terminal thiol on DNA, which has certain advantage over DTT by trimming column separation step as well as inherent lesser affinity to AuNPs (Liu & Liu, 2017). AuNPs were then functionalized

with the thiol active SP sequences by following the procedure described at the section 5.2.7 with very minor modifications. In detail, TCEP treated MBT and pork SP sequences were added to AuNPs and incubated for 16 – 20 h, followed by Tween 20 solution (0.1% Tween 20 in 10 mM PBS, pH 7.4) was added in such a way that final Tween 20 concentration reached to 0.01% in the solution and kept standing for further 30 min. This was followed by the salt aging of the suspension with stepwise addition of NaCl (1 M) at an interval of 1 h or more until reach to 100 mM NaCl concentration.

NaCl is added slowly to the solution to screen the charge repulsion while retaining the stability of AuNPs. Initially only a few probe sequences are adsorbed to the AuNPs either via thiol binding or nucleotide bases (Figure 6.1). This initial attachment of DNA also increases the negative charge intensity of the AuNPs and repel the incoming other DNA sequences. Therefore, in salt aging after an increment of NaCl concentration, few more oligo sequences are attached until a new electrostatic repulsion equilibrium has been reached which in consequent increase the stability of AuNPs to further NaCl addition. Moreover, in salt aging process, the terminal thiol group of the probe sequences displaces the DNA adsorbed via nucleotide bases on AuNP, hence assisted to DNA stand up which provides more effective steric stability and make easy availability of DNA sequences for further hybridization (Cutler et al., 2012; Liu & Liu, 2017; Zhang et al., 2013c) (Figure 6.1). The SP conjugated AuNP suspension were further incubated at room temperature for 40 h under the same conditions. During this prolonged salt aging condition the repulsion forces between the DNAs on the AuNPs are reduced, therefore an ultrahigh density is achieved (Liu & Liu, 2017). The salt-aged AuNP-SP solution was centrifuged at 8000 rpm for 30 min, discarded the supernatant to exclude the free unbound probe sequences, and resuspended the pellet in UPW, washed twice with UPW by centrifugation and finally the obtained AuNP-SP solution in UPW is ready for further experiment.

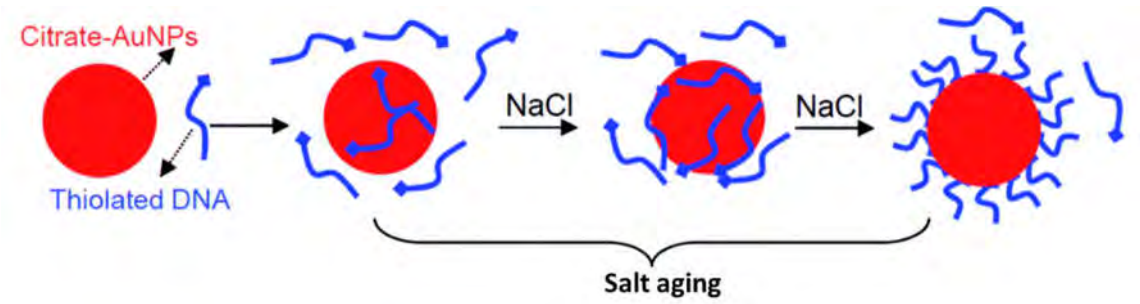

Figure 6. 1: Functionalization of citrate capped AuNPs with thiol-active probe sequences and the impact of salt aging process. Addition of NaCl in small increments facilitate the attachment of DNA strands and provides stability of AuNPs from irreversible aggregation. Reproduced with permission from the Reference (Liu & Liu, 2017).

6.2.7 Preparation of Capture Probe conjugated GO-AuNP

As-prepared GO-AuNPs suspension (200 µL) was centrifuged at 8000 rpm for 30 min and the supernatant was discarded to remove the free AuNPs as well as to wash out any sodium citrate residue present. The obtained GO-AuNP composite was suspended in the equivalent volume of UPW. At the same time, capture strands (1 µM, 100 µL) of both species (MBT and pig) were TCEP treated in separate Eppendorf tube as per above mentioned procedure (Section 6.2.6) to activate the 3′ terminal thiol. Thereafter, both thiol-active capture strands were simultaneously added to the GO-AuNPs suspension with frequent shaking and incubated for 16 h at room temperature. After incubation, the obtained suspension was treated with Tween 20 solution (0.1% Tween 20 in 10 mM PBS, pH 7.4), followed by salt aging process following the exactly same procedure as mentioned above. During the salt aging process, CP sequences attached to AuNPs of GO-AuNPs composite by the similar manner as happened for AuNPs alone. After the salt aging process, the suspension was incubated for another 40 h at room temperature, after that centrifuged at 8000 rpm for 30 min to remove the excess unbound DNA. Finally, GO-AuNP immobilized CP DNA (GO-AuNP-CP (MBT+ pig)) precipitates were dispersed in 0.1 mM PBS (pH 7.4) for further use.

6.2.8 Fabrication of the Sandwich Biosensor and acquisition of SERS spectra

AuNPs functionalized separately with MBT and pig species specific SP sequences (AuNPs-SP (MBT) and (AuNPs-SP (Pig)) (200 µL) were incubated discretely with the corresponding target DNA sequences (100 µL of each species) at room temperature for overnight. During this incubation period, AuNPs bound SP sequences were partially hybridized with a complementary portion of the target DNA sequences. The formed hybridized composites (AuNP-SP-Target) were centrifuged at 8000 rpm for 30 min, washed and purified with UPW by repeated centrifugation and discarding the supernatant containing unhybridized target DNA. The obtained partially hybridized composites (AuNP-SP (MBT)-T and AuNP-SP (Pig)-T were dispersed in 0.1 mM PBS (pH 7.4). Equal volume of (200 µL) AuNP-SP (MBT)-T and AuNP-SP (Pig)-T were added into the GO-AuNP functionalized with both MBT and pig specific CP sequences (GO-AuNP-CP (MBT+ pig)) suspension (200 µL), mixed well manually and incubated overnight at room temperature. Upon mixing together and incubation, CP sequences bound to the same platform (GO-AuNP) were hybridized with unbound portion of the partially hybridized target DNA sequences and coupled to form sandwich composite (GO-AuNP-CP-Target-SP-AuNP). The hybridized composite was purified by centrifugation at low speed (4000 rpm for 5 min) and washed twice with UPW to remove the unbound/free AuNPs-SP-T or GO-AuNP-CP suspended in the supernatant. The obtained final hybridized composite was dispersed in 0.1 mM PBS (pH 7.4). The SERS samples were prepared as per procedure mentioned in the Section 4.2.10 by dropping 50 µL of the each of the sample onto the silicon wafer, followed by vacuum drying at ambient atmosphere. The SERS spectra were also acquired using Renishaw Invia Confocal Raman Microscope using 532 nm laser and 20x objective lens. The obtained SERS spectra were analyzed with/without applicable baseline correction to depict the expected Raman bands using Origin 2017 software.

6.3 Results and Discussion

6.3.1 Principle of the SERS Duplex Biosensor

To fabricate duplex SERS DNA biosensors for the detection of MBT and pig species simultaneously, Raman dye intercalated uniquely designed SP DNA, dual platforms (GO-AuNP and AuNP), and sandwich assay strategy were employed. The complete picture of the duplex SERS DNA biosensing strategy for the simultaneous detection of two different species is demonstrated in Figure 6.2. As a sensing approach, both MBT and pig specific CP sequences were immobilized onto the same GO-AuNP platform by covalent Au-S bonding between the terminal 3′-thiol molecule of the capture DNAs and AuNPs of the GO-AuNP hybrid composite (Figure 6.2a) (Zhang et al., 2007). The C3 spacer arm immediate after the terminal thiol molecule aid to minimize the steric hindrance, keep DNA strands at upright arrangement, hence improve the hybridization efficiency of the GO-AuNP tethered CP sequences with the complementary target DNA strand (Milton et al., 2013; Tjong et al., 2014). On the other hand, Cy3 intercalated SP sequences (MBT) and ATTO Rho6G integrated SP DNA (pig) were immobilized onto AuNPs separately via the covalent Au-S bonding (Figure 6.2b). In SP sequences, the C6 spacer molecules between the nucleotides and the terminal thiol molecule ensures the SP strands in perpendicular presentation and easy accessibility of the nucleotide bases for the hybridization by diminishing the steric effect between the nucleotide bases and AuNP surface (Park et al., 2002; Zhang et al., 2007). In addition, upon attachment of SP sequences to the AuNPs, integrated Raman dyes exist adjacent to the AuNP surface which therefore, confirms enhanced SERS signal by the Raman tag induced charge transfer mechanism. Addition of the corresponding target DNA to the AuNP-SP (MBT) and AuNP-SP (pig) resulted in the partial hybridization by probe-target DNA covalent bonding (Figure 6.2b). Therefore, mixing of the GO-AuNP-CP (MBT+Pig) with AuNP-SP (MBT) and AuNP-SP (Pig) together, a multicomponent sandwich complexes were

formed due to the hybridization of CP sequences with the reminder free partially hybridized target DNA linked to AuNPs (Figure 6.2c). The covalent hybridization takes place between the AuNP-SP-Target with the CP DNA attached either on the same or different neighboring AuNPs of GO-AuNP hybrid. The SERS spectra generated from the hybridized composites indicates the presence of both Cy3 and ATTO Rho6G fingerprint peaks, therefore confirms the presence of the complementary DNA strands of both of the target species. Moreover, the hybridized composite generates enhanced SERS signal due to the enhancement of the confined electromagnetic field by the excitation of the LSPR from the plasmonic AuNPs and more specifically the hot spots originated at the junctions of the strongly coupled AuNPs dimer or agglomerations via linking of the two distinct platforms (Duan et al., 2015; Prinz et al., 2016).

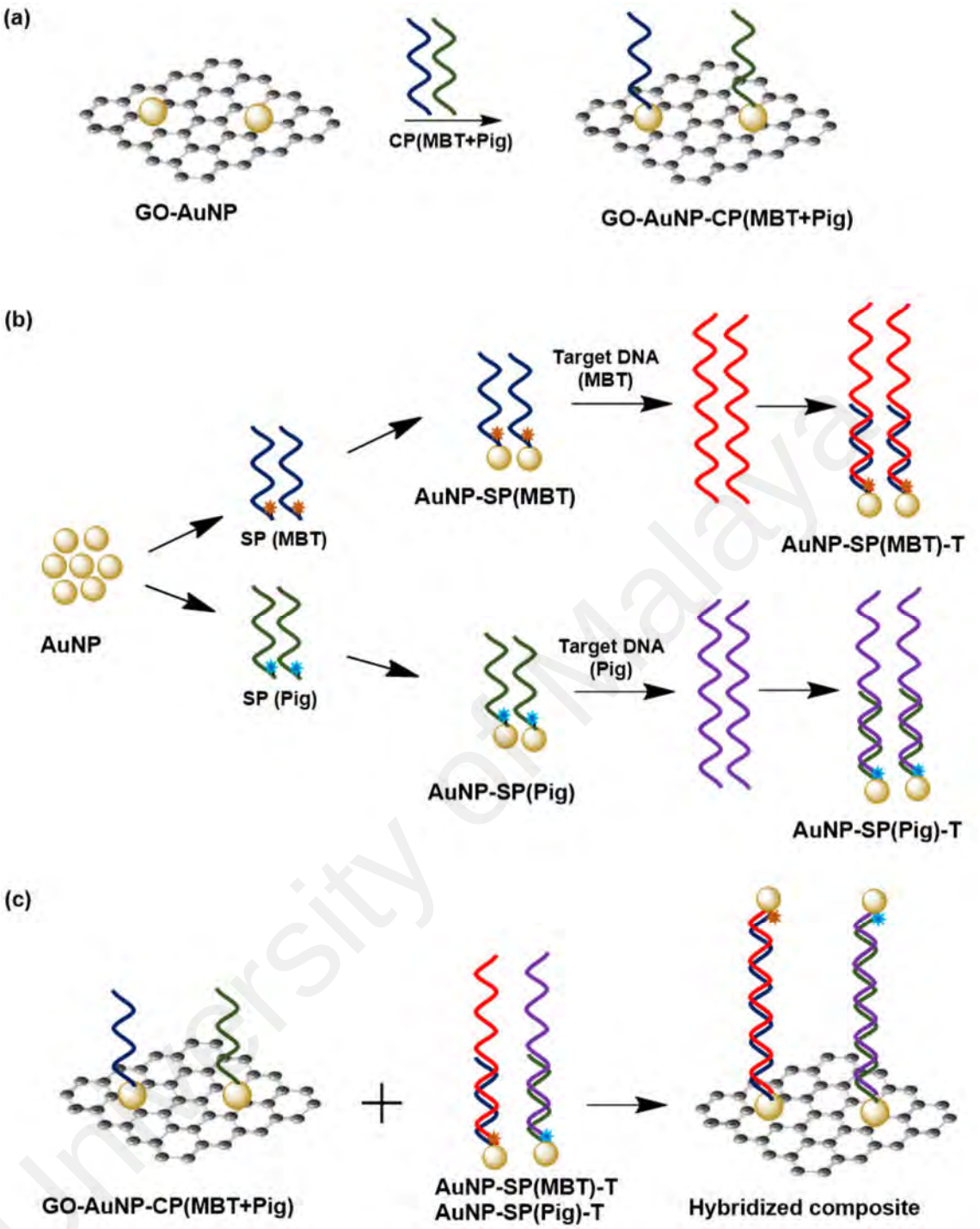

Figure 6. 2: The schematic illustration of dual platform (GO-AuNP and AuNP) and Raman tag intercalated probe sequence based duplex SERS DNA biosensor.

6.3.2 Characterization of GO, AuNPs, and GO-AuNPs nanocomposite

The synthesized GO, AuNPs, and GO-AuNP composite were characterized by UV-vis spectroscopy, Raman spectroscopy, TEM and AFM topography studies. The as-synthesized brilliant red color AuNPs solution produced an absorbance maxima at 521

nm by the UV-vis spectrophotometer (Figure 6.3a). The size and shape of the synthesized AuNPs were verified by TEM study where the AuNPs were found rounded shape with homogenous size distribution between 20±2 nm (Figure 6.3c) and corresponds the study on the revitalizing of the Frens Method (Xia, et al., 2016). The size of the AuNPs was further confirmed by the AFM study (Figure 6.4a-b). The ultrasonicated well dispersed GO aqueous suspension exhibited an absorption peak at 242 nm characteristic to the plasmonic plasmonic $\pi \rightarrow \pi^*$ transitions (C=C bonds) (Figure 6.3a) (Heuer-Jungemann et al., 2015) which was further evaluated by the TEM images of GO representing few-layered wrinkled GO sheets (Figure 6.3d). On the other hand, the UV-vis spectrum of GO-AuNP hybrid composite generated two peaks at 246 nm and 524 nm (Figure 6.3a), representing the characteristic but shifted absorption of peak of GO and AuNPs respectively. This shift is related to the changes of the dielectric constant of the medium due to the attachment of AuNPs onto the GO surface of the GO-AuNP composite. Furthermore, the broader absorption peak at 246 nm compared to AuNPs due to d-transition of AuNPs and formation of new electronic levels in the valence and conduction bands of GO, and finally missing of the shoulder at 303 nm related to the sp3 transitions of GO in the nanohybrid composites, clearly evidenced a strong interaction between GO sheets and AuNPs (Hernández-Sánchez et al., 2018).

The TEM study of GO-AuNPs also revealed that AuNPs were nearly spherical and mostly dispersed singly over the single to few layered transparent GO sheet. The average size of the AuNPs anchored to GO sheets was approximately 27±5 nm. There was no AuNPs found on other area of the lacy carbon copper grid except the GO sheet (Figure 6.3e-f). Moreover, the AFM topography images of the GO-AuNPs hybrid also exhibited the same feature like TEM, though the number of AuNPs over the GO sheet is very low (Figure 6.4c-d). These characterization studies therefore strongly indicates that the AuNPs were strongly attached to the GO sheets. In addition, the Raman spectra of the

synthesized GO and GO-AuNPs were characterized by the characteristic G-band at 1595 cm^{-1} and D-band at 1345 cm^{-1} of the GO (Figure 6.3b). The D-band is the defect induced features and corresponds to breathing mode of k-point phonons of A_{1g} symmetry while G-band refers to the first order scattering of E_{2g} phonon of C sp^2 atoms (Chuang et al., 2014). However, the Raman intensity of the GO-AuNPs was greatly increased (around 2 times) in compare to the GO which indicated the citrate reduction of the gold salt to AuNPs over the GO sheets, as well as electromagnetic effect of the plasmonic AuNPs on the overall enhancement (Cheng et al., 2013; Liang et al., 2015; Li et al., 2016c).

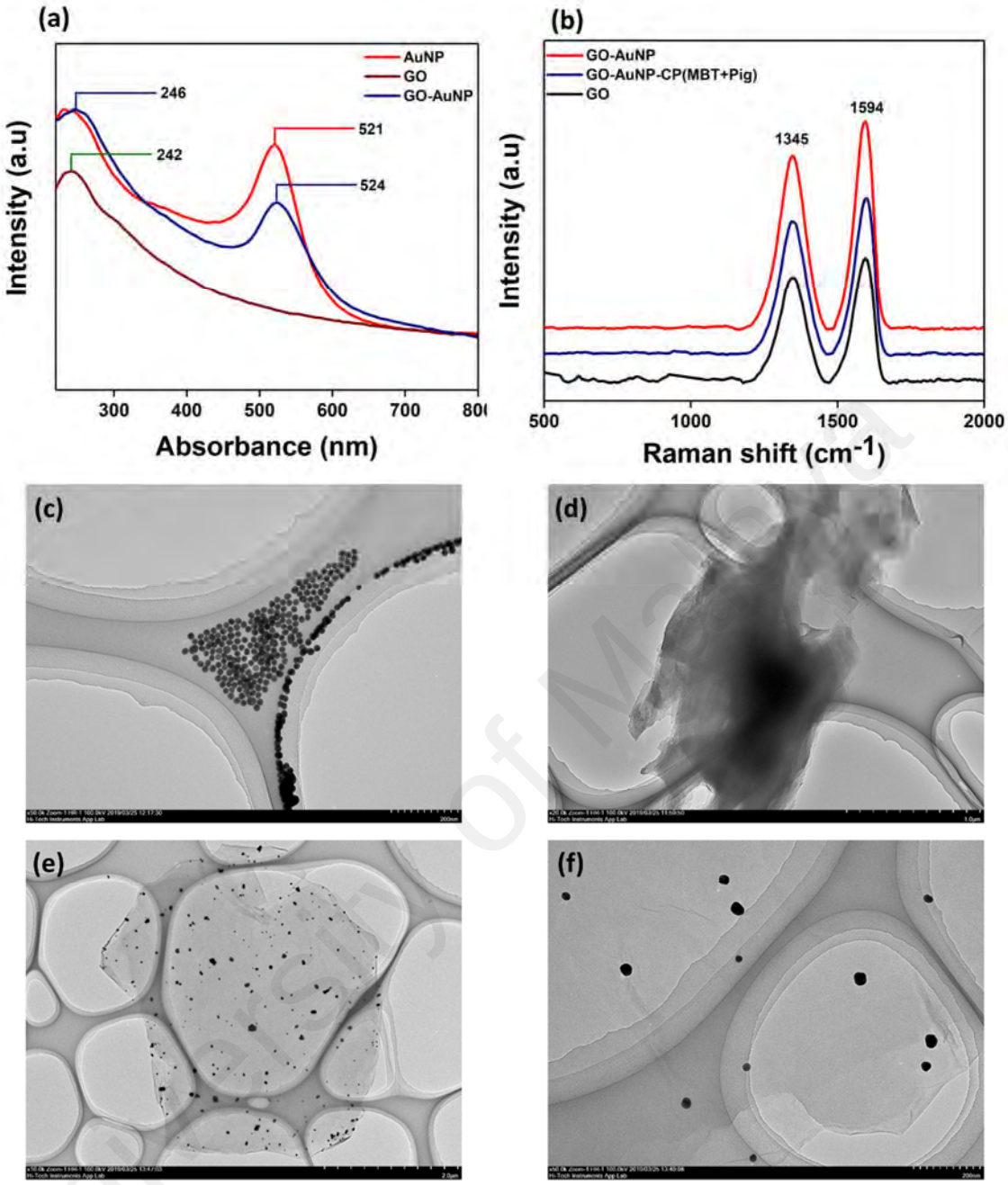

Figure 6. 3: (a) UV-vis absorption spectra of AuNP, GO and GO-AuNPs. (b) Raman spectra of GO, GO-AuNPs and GO-AuNPs functionalized with CP DNA. TEM images of (c) AuNP, (d) GO, and (e-f) GO-AuNP at 2 µM and 200 nm on lacy carbon copper grid.

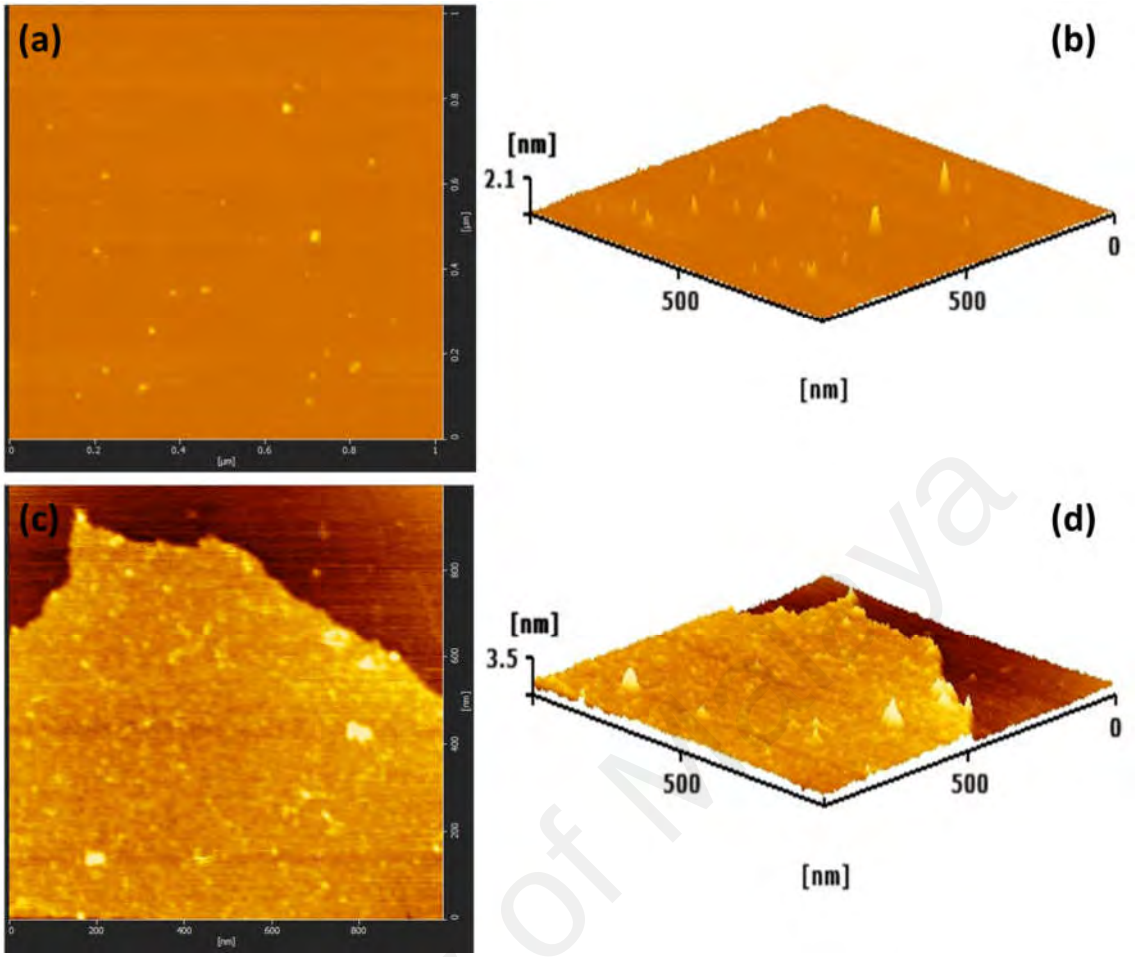

Figure 6. 4: AFM topography 2D and 3D images of (a-b) AuNPs and (c-d) GO-AuNP adsorbed on mica surface.

6.3.3 Attachment of DNA Probe Sequences onto the Sensor platform

The 16-mer long MBT and 12-mer long pig SP sequences were immobilized onto the AuNPs by Au-S linkage and formed a dense layer of probe sequences via salt aging process. The attachment of SP DNA onto the AuNPs was visually observed by the conversion of ruby red color to slightly pinkish-red color solution which is the indicative of the reduced number of free AuNPs as well as ensures no agglomeration of AuNPs by the NaCl salt aging process (Thavanathan et al., 2014). Attachment of SP sequences was also observed by the UV-vis peak shifting from 521 nm to 524 nm for both SP sequences (Figure 6.5a) which was due to the raising of the AuNPs size via the formation of a dense layer of probe sequences, therefore suggesting the successful binding of ssDNA to the AuNPs. Moreover, the addition of the corresponding target DNA to the AuNP-SP(MBT)

and AuNP-SP (pig) suspension facilitated the partial hybridization by probe-target bonding which therefore resulted in further UV-vis peak shifting of 1 nm and 2 nm, respectively (Figure 6.5a). In the same way, UV-vis absorption spectrum of the GO-AuNPs hybrid composite functionalized with the CP sequences of both MBT and pig species, exhibited an identical GO-AuNP spectrum with a peak shifting from 524 nm to 527 nm characteristic to AuNPs (Figure 6.5b), therefore justifying the successful attachment of thiol-terminated capture DNA by Au-S chemisorption process over GO-AuNPs (Wang et al., 2016a).

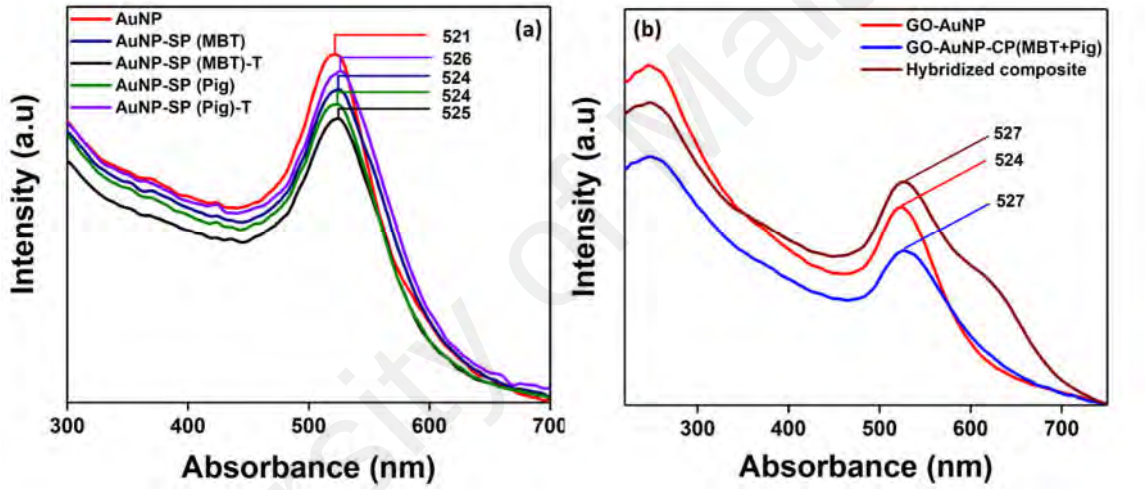

Figure 6. 5: (a) UV-vis absorption spectra of AuNP, AuNPs functionalized with Raman tag integrated SP sequences and AuNP-SP with partially hybridized target DNA. (b) UV-vis spectra of GO-AuNP, GO-AuNPs modified with both MBT and pig CP sequences and the hybridized composite.

6.3.4 Justification of the Duplex Biosensing strategy

The 16-mer MBT and 12-mer pig split-probe sequences were chemically functionalized with the Raman dye - Cy3 and ATTO Rho6G respectively (Table 3.4 and Figure 3.3), therefore termed as the SP sequence throughout this Chapter. Both Cy3 and ATTO Rho6G dyes have identical Raman fingerprint spectra as mentioned in the section 3.3. Hence, intercalation of these Raman tags in the oligonucleotide sequences was also justified by the presence of the respective dye specific fingerprint spectra. In this context,

the SERS spectra of the AuNP-SP(MBT) and AuNP-SP(Pig) were found to produce the SERS spectra comprising of the dominant peaks at 1231, 1270, 1382, 1468, and 1589 cm^{-1} attributed to the fingerprint spectrum of Cy3 in MBT sequences and 610, 1360, 1506, 1570, and 1648 cm^{-1} corresponds the SERS spectrum of ATTO Rho6G in pig SP sequences (Figure 6.6a and Table 6.2) (Eremina, et al., 2020). Immobilization of both SP sequences onto the AuNPs also exhibited all the mentioned major peaks including some other minor peaks (Figure 6.6a and Table 6.2). Thus, the existence of these Raman tag specific fingerprint peaks by SERS study not only proved the presence of the integrated Raman tag to the respective probe sequences but also confirmed the successful attachment of the SP sequences to the AuNP surface via Au-S thiol linkage.

Table 6. 2: SERS peak profiles of the signal probes immobilized onto AuNP, GO-AuNP and hybridized composite.

Sensor composition	**Representative SERS peaks**
AuNP-SP (MBT)	615, 797, 931, 1120, 1155, 1231, 1270, 1311, 1382, 1408, 1468, 1589
AuNP-SP (Pig)	610, 774, 1130, 1184, 1310, 1360, 1506, 1570, 1648
AuNP-SP(MBT +Pig)	612, 774, 934, 1132, 1190, 1215, 1272, 1312, 1360, 1392,1438, 1478, 1508, 1538, 1590
GO-AuNP-SP (MBT)	689, 1130, 1211, 1350, 1476, 1595
GO-AuNP-SP (Pig)	610, 772, 1128, 1182, 1356, 1506, 1599, 1644
Hybridized composite	612, 774, 934, 1132, 1181, 1217, 1360, 1478, 1508, 1600, 1648

On the other hand, the GO-AuNP hybrid were also functionalized with the SP sequences to justify the origin, presence and intensity of the integrated Raman tag specific peaks. The SERS spectrum of the GO-AuNP-SP(MBT) presented the major peaks at 1130, 1211, and 1476 cm^{-1} including GO representing D band at 1350 cm^{-1} and G band at 1595 cm^{-1} (Figure 6.6b) while GO-AuNP-SP (Pig) revealed major peaks at 610, 772,

1182, and 1506 cm^{-1} including at 1356 and 1599 cm^{-1} characteristic to graphitic D and G bands, respectively (Figure 6.6c). In both cases, few major peaks were diminished by the dominant presence and intensity of the D and G band of GO-AuNP (Prinz et al., 2016). In contrast, the SERS spectrum of the GO-AuNPs hybrid linked to CP sequences generated the GO characteristic D and G bands only (Figure 6.3b). However, the coupling of GO-AuNPs-CP(MBT+Pig) with AuNPs-SP(MBT) and AuNPs-SP(Pig) via hybridization with the corresponding target DNAs generated a multicomponent agglomerated hybridized composite. Hence, as expected, the SERS spectrum of the hybridized composites revealed GO representing D band at 1360 cm^{-1}, G band at 1600 cm^{-1} including Cy3 representative peaks at 1132, 1217 and 1478 cm^{-1} and ATTO Rho6G representing peaks at 612, 774, 1181, and 1508 cm^{-1} in addition to the presence of few minor peaks (Figure 6.6d and Table 6.2) (Prinz et al., 2016). It is to be noted that there was a little shifting of the dominant peaks of the hybridized composites in compare to the SP DNA immobilized onto single platform. The presence of both Cy3 and ATTO Rho6G representative Raman peaks as well as D and G band of GO from the hybridized composites confirms the coupling of the platforms, hence hybridization of the split-probe DNAs linked to different sensor platforms via the corresponding MBT and pig target DNAs. Moreover, it was also dictated the feasibility and suitability of the simultaneous detection of the two different target DNAs using multi-component platforms. Though the hybridized composite revealed the strong presence of several Cy3 and ATTO Rho6G representative peaks, peak at 1478 cm^{-1} as representative of Cy3 and peak at 1508 cm^{-1} characteristic to ATTO Rho6G were selected as standard peaks due to their presence in between the D and G bands, for the simultaneous presence and quantitative detection of both MBT and pig species throughout the study. Thus, according to the sensing strategy, the intensity of these two selected Raman peaks at 1478 cm^{-1} (Cy3) and 1508 cm^{-1} (ATTO Rho6G) were correlated with concentration of the MBT and pig target DNA respectively.

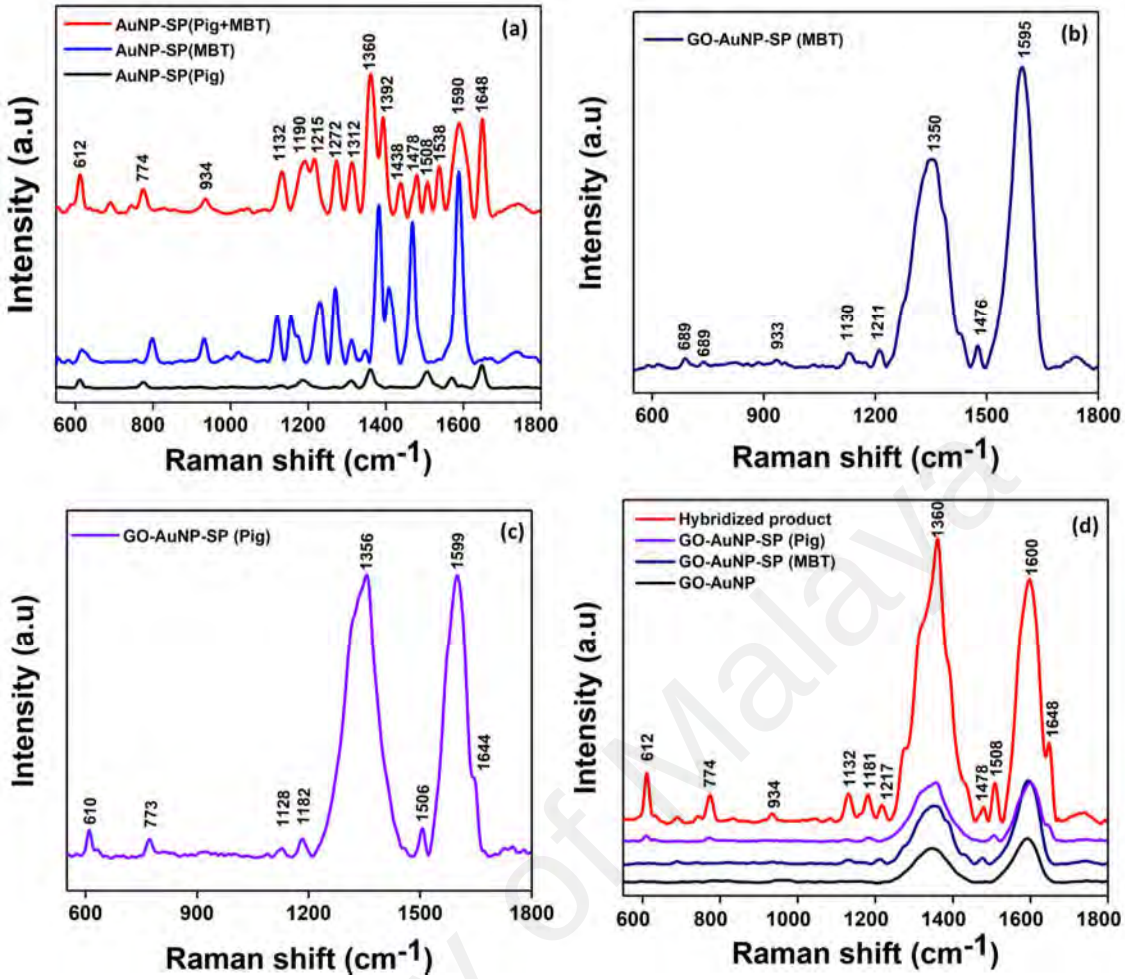

Figure 6. 6: SERS spectra of (a) AuNPs functionalized with SP sequences of MBT, pig and both MBT and pig species; (b) GO-AuNP immobilized with MBT SP DNA; (c) GO-AuNP functionalized with Pig SP sequences; and (d) the stacked SERS spectra of GO-AuNP, GO-AuNP functionalized with SP sequences of MBT and pig, and the hybridized composite.

The linking of GO-AuNP-CP(MBT+Pig) with AuNP-SP(MBT) and AuNP-SP(Pig) via hybridization with the complementary MBT and pig target DNA sequences were also explained by the red shift of LSPR peak from 524 (GO-AuNP) to 527 nm with broadening of the peak while no shifting in compare to GO-AuNP-CP(MBT+Pig) rather enhanced intensity due to the increased AuNP concentration (Figure 6.5b) (Khalil et al., 2019). Moreover, UV-vis absorption spectrum of hybridized composite revealed a new peak at ~ 620 nm which is attributed to the strong plasmonic coupling between the AuNPs via CP-Target DNA-SP hybridization (Zhou et al., 2017). Moreover, the TEM images of the hybridized composite further confirmed the bridging of the AuNPs over the GO sheets

either forming dimer predominantly or AuNPs aggregate by covalent linking of CP and SP sequences via corresponding target DNAs (Figure 6.7a-d). In addition, it was also estimated that the inter-distance between the linked AuNPs was also very little around 1 nm to few nanometers, therefore dictating the successful hybridization event (Zhou et al., 2017). It is also to be mentioned that the hybridization event was happened onto GO sheet of GO-AuNPs as there was no AuNPs found outside the GO sheet in the TEM images from low to high magnification. However, in the TEM images of the hybridized composite, few single AuNPs were also found on the GO sheets which indicate a non-specific adsorption of AuNPs over the GO sheet of the GO-AuNP composite. This was due to the failure of hybridization, due to the absence of DNA probe sequences or the absence of complementary target sequences to be hybridized (Khalil et al., 2019).

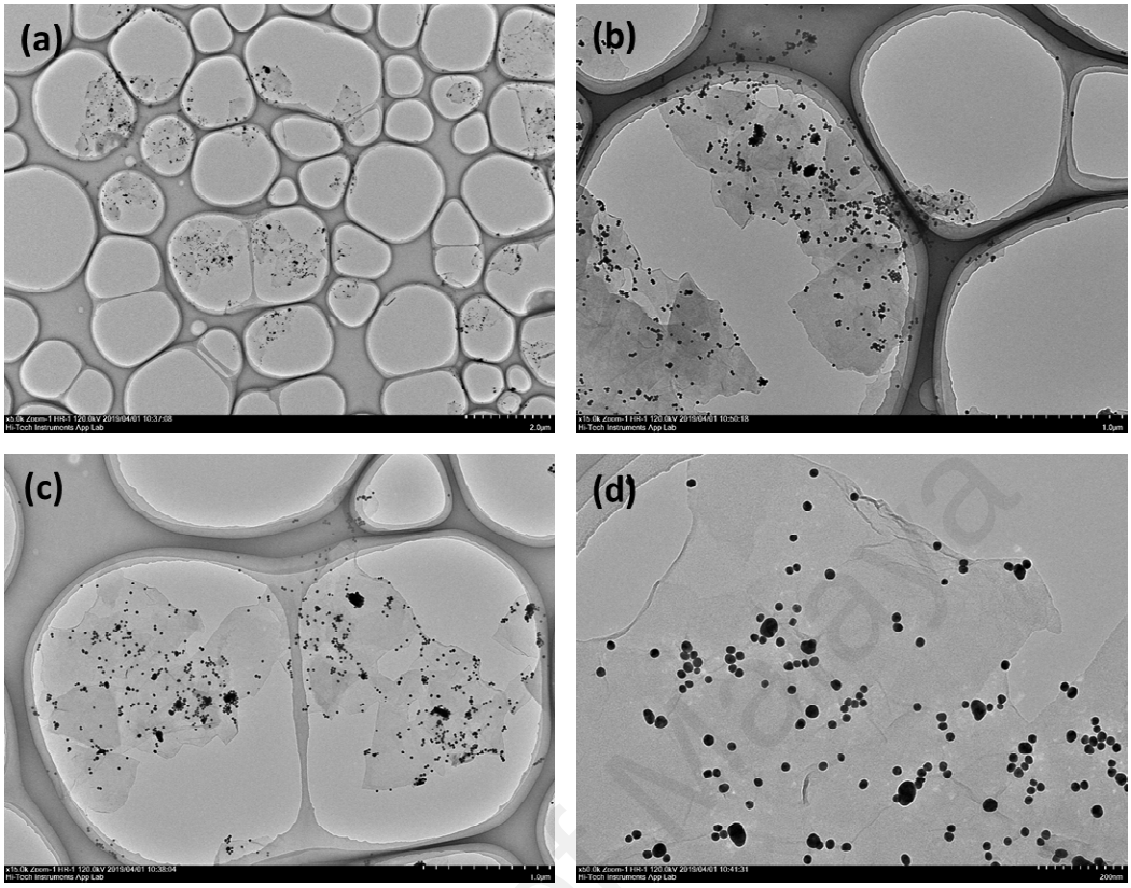

Figure 6. 7: TEM images of the hybridized composites at 2 μM (a), 1 μM (b-c) and 200 nm (d) magnifications. The hybridized composites were formed via probe-target hybridization mediated coupling of AuNPs onto the GO-AuNP. In the images, the AuNPs are found onto GO sheets as well as mostly linked to each other, dictates the successful hybridization.

6.3.5 Analytical Performance of the Duplex SERS DNA Biosensor

6.3.5.1 Reproducibility, Selectivity and Specificity of the Biosensor

The duplex sensing hybridization protocol relied on the assembly of three components - GO-AuNP-CP(MBT+Pig), AuNP-SP(MBT) and AuNP-SP(Pig) via probes-target hybridization. Therefore, the efficiency of the biosensor was largely dependent on the hybridization mediated homogenous coupling of the sensor platforms. Hence, to justify the homogenous hybridization proficiency, SERS sample was prepared from the 10 pM target DNA mediated hybridized composite onto the Si wafer, and the spectra were captured by laser excitation onto the randomly selected five different positions of the slide. The five SERS spectra from the five different spots of the slides were observed

identical in terms of feature, peak location and intensity. All the five peaks exhibited the D-band, G-band and the Cy3 and ATTO Rho6G fingerprint peaks at 1478 cm^{-1} and 1508 cm^{-1} along with some other peaks (Figure 6.8a). The RSD value of the SERS intensity of the corresponding Cy3 and ATTO Rho6G peaks at 1478 cm^{-1} and 1508 cm^{-1} were around 6% and 13% respectively (Figure 6.8b), thus indicates a promising reproducibility of the fabricated biosensor (Xu et al., 2020). However, to achieve an optimum repeatability or reproducibility using target DNA sequences of different origin for simultaneous multiplex detection in one assay as well as to obtain a homogenous layer of hybridized composite from the aqueous suspension are definitely a challenging task for practical multiplex SERS sensor (Kang et al., 2010). Moreover, the correlation between the signal intensity of both Raman tag specific peaks depends on the hot spots generated by the equal assembly of the two SP sequences immobilized AuNPs via hybridization, as well as the acquisition of the SERS spectra from the locations of equally distributed hot spots of between or among the plasmonic nanostructure. The obtained RSD therefore dictates the hybridization reaction occurred uniformly throughout the system with a considerable variation.

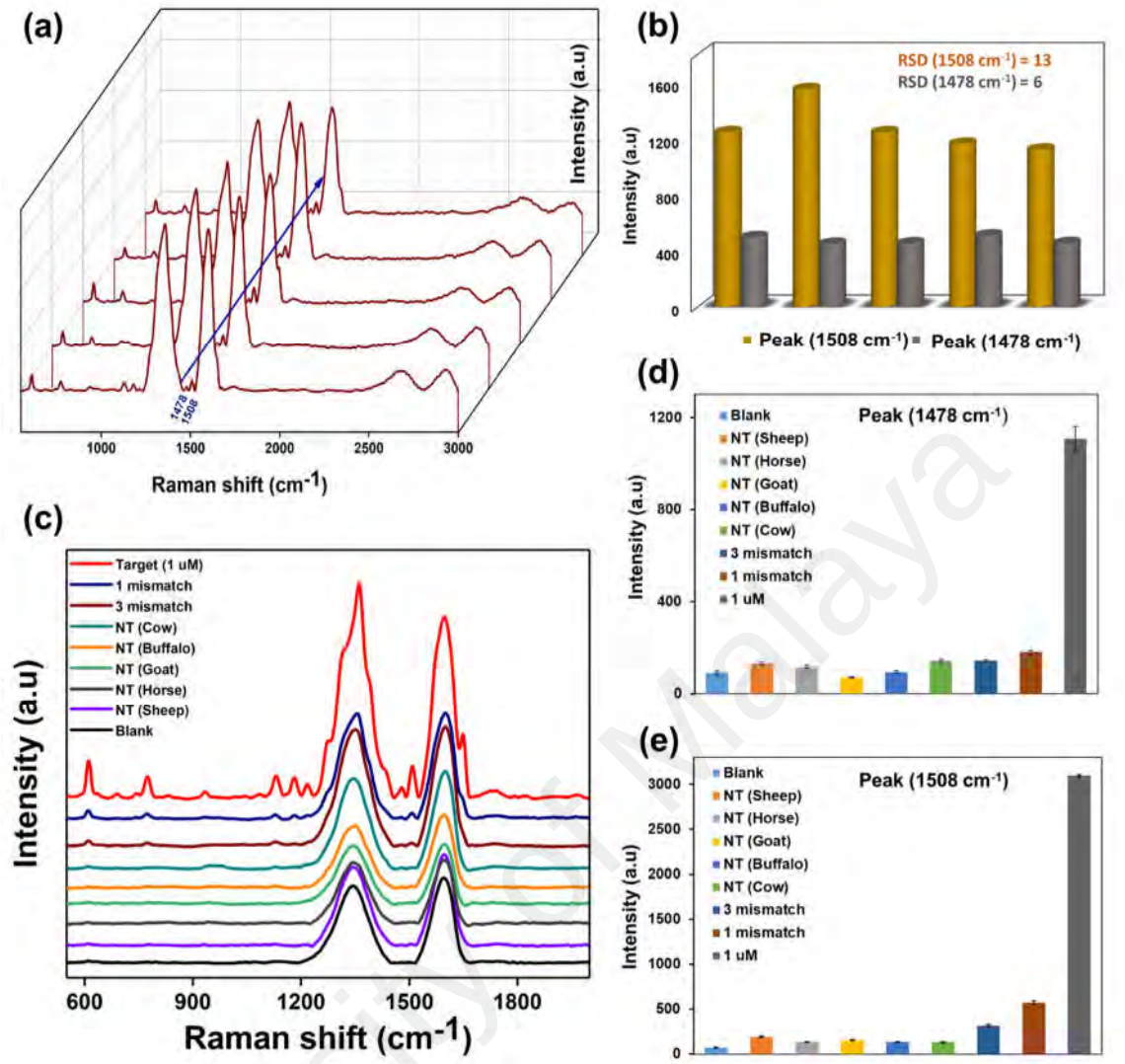

Figure 6. 8: (a) SERS spectra of the hybridized composite (10 pM target DNA concentration) from five different spots, and (b) the RSD of the intensity of SERS peaks at 1478 cm^{-1} and 1508 cm^{-1} for the five different spots. (c) SERS spectra of the selectivity study of the fabricated biosensors using different DNA sequences - 1 µM concentration of complementary, single base-mismatch, triple base-mismatches, interference samples (non-target DNA sequences of cow, buffalo, goat, horse and sheep) and blank sample; and the corresponding intensity of the SERS fingerprint peak at (d) 1478 cm^{-1} and (e) 1508 cm^{-1}. Error bars in (d) & (e) represent standard deviations of peak intensities from n=3 repeated measurements.

The specificity of the fabricated sensing device or strategy is totally dependent on the recognition of the corresponding target DNA sequences by the immobilized CP and SP sequences onto two different nanostructures. In the presence of the corresponding target DNA, AuNP-SP(MBT) and AuNP-SP(Pig) were connected with CP sequences of both MBT and pig species, therefore formed a multicomponent aggregated hybridized composite. The SERS spectra of the hybridized composite is therefore characterized by

the D and G band of GO, representing the CP functionalized GO-AuNPs platform as well as the peaks at 1478 and 1508 cm^{-1} dictating the AuNPs functionalized with Cy3 and ATTO Rho6G intercalated MBT and Pig SP sequences respectively (Figure 6.8c). The hybridized composite produced an intense SERS spectrum due to the generation of hot spots at the interstices of the AuNPs formed hybridization mediated coupling of the sensor platforms. This intense SERS spectrum comprising of peaks at 1350 cm^{-1} (D band), 1600 cm^{-1} (G band), 1478 cm^{-1} (Cy3 for MBT) and 1508 cm^{-1} (ATTO Rho6G for pig) is therefore referred to a spectrum of a true positive result (Chuong et al., 2017). The biosensing strategy was also evaluated using different control reactions including the mixing of GO-AuNPs-CP(MBT+Pig) with AuNP-SP(MBT) and AuNPs-SP(Pig) in the absences of any target DNA (negative control) as well as replacement of the target DNAs with non-target DNA sequences of closely related five different species including goat, sheep, cow, horse and buffalo. The SERS spectra of the negative control sample and hybridized composites via non-target DNA sequences exhibited strong D and G band along with minor presence of the representative Cy3 and ATTO Rho6G peaks (Figure 6.8c-e). This little existence of the Raman tag specific fingerprint peaks though did not distinctly reveal in the stacked SERS spectra (Figure 6.8c), however in maximum instances very close to signal-to-noise ratio, hence considered at insignificant signal. However, the weak signal of the Cy3 and ATTO Rho6G peak in the hybridized product due to the nonspecific adsorption of the AuNP-SP(MBT) and AuNPs-SP(Pig) onto the GO sheet of GO-AuNP-CP(MBT+Pig) composites. Hence, the results of the selectivity study prove that the fabricated biosensor was selective enough to discriminate the nucleotide sequences of the corresponding target and other non-target sequences.

The biosensing strategy was further evaluated using synthetic corresponding target DNA distinguished with only one nucleotide and three nucleotide bases in the sequence composition. In this context, the SP and CP immobilized sensor platforms were mixed in

the presence of 1 μM concentration of one nucleotide and three nucleotide mismatch target DNA sequences and evaluated the hybridization efficiency. The hybridized composites displayed the similar SERS spectra containing D and G-bands with Cy3 and ATTO Rho6G specific peaks at 1478 cm^{-1} and 1508 cm^{-1} as that of SERS spectra of the hybridized composite via complementary target DNA (Figure 6.8c). However, the intensity of the selected peaks of Cy3 and ATTO Rho6G was observed too small in comparison to the equal-concentration corresponding target DNA mediated hybridization product. This low intensity was due to the very low frequency of hybridization or irregular binding of mismatch sequences with the complementary SP and CP sequences. In contrary, the peaks intensity was found a bit higher from the negative control and other non-target DNA coupled hybridized products (Figure 6.8d-e). This results thus suggest that hybridization efficiency in general is decreased with the increase of the nucleotide sequence variation in the target sequence. Hence, the duplex SERS DNA biosensor owns the potentiality to differentiate the DNA sequences even with single nucleotide change.

6.3.5.2 Sensitivity of the Biosensor

The sensitivity of the fabricated split-probe and multicomponent assembly based duplex SERS biosensor for the simultaneous quantification of the target DNA of the MBT and pig species was evaluated. For quantification, a gradual dilution from 1 μM to 1 fM of the target DNA sequences was prepared and each of the target DNA solution was added to the respective SP functionalized AuNPs suspension, followed by incubation and simultaneous mixing with the GO-AuNP functionalized with both of the capture DNA probes (Figure 6.2). The SERS spectrum of the highest target DNA concentration (1 μM) produced a well distinct, intense peaks at 612, 774, 934, 1132, 1181, 1217, 1478, 1508, and 1648 cm^{-1} representative of the both signal Raman tag along with D and G-band at 1360 and 1600 cm^{-1} respectively (Figure 6.9a). However, the quantitative evaluation of

the hybridized composite was done by assessing the SERS intensity of the selected fingerprint peaks at 1478 cm^{-1} and 1508 cm^{-1}, representative of Cy3 and ATTO Rho6G dye intercalated to SP sequences of MBT and pig species. The plotted SERS intensity showed a steady declining trend from the high to low concentration of target DNA (1 μM - 1 fM). The SERS spectra of the hybridized composite achieved via target DNA concentration from 1 μM to 10 fM exhibited well distinct peaks while at 1 fM concentration for both of target DNA, peak at 1508 cm^{-1} was still distinguishable while the peak at 1478 cm^{-1} showed almost no or indistinguishable mark, justified by the magnified view of stacked SERS spectra (Figure 6.9b). Hence, in terms of the simultaneous detection of both species, the lowest LOD was estimated 10 fM (Figure 6.9 a&b). The linear curve of the peak height at 1478 and 1508 cm^{-1} vs target DNA concentration was also plotted which showed a linear response and the correlation coefficient (R^2) value were found 0.9528 (Figure 6.9c) and 0.976 (Figure 6.9d) respectively. These linear curves therefore suggest the strong relationship between the peak intensities with the target DNA concentrations, hence approves the feasibility of the quantitative detection of the DNA.

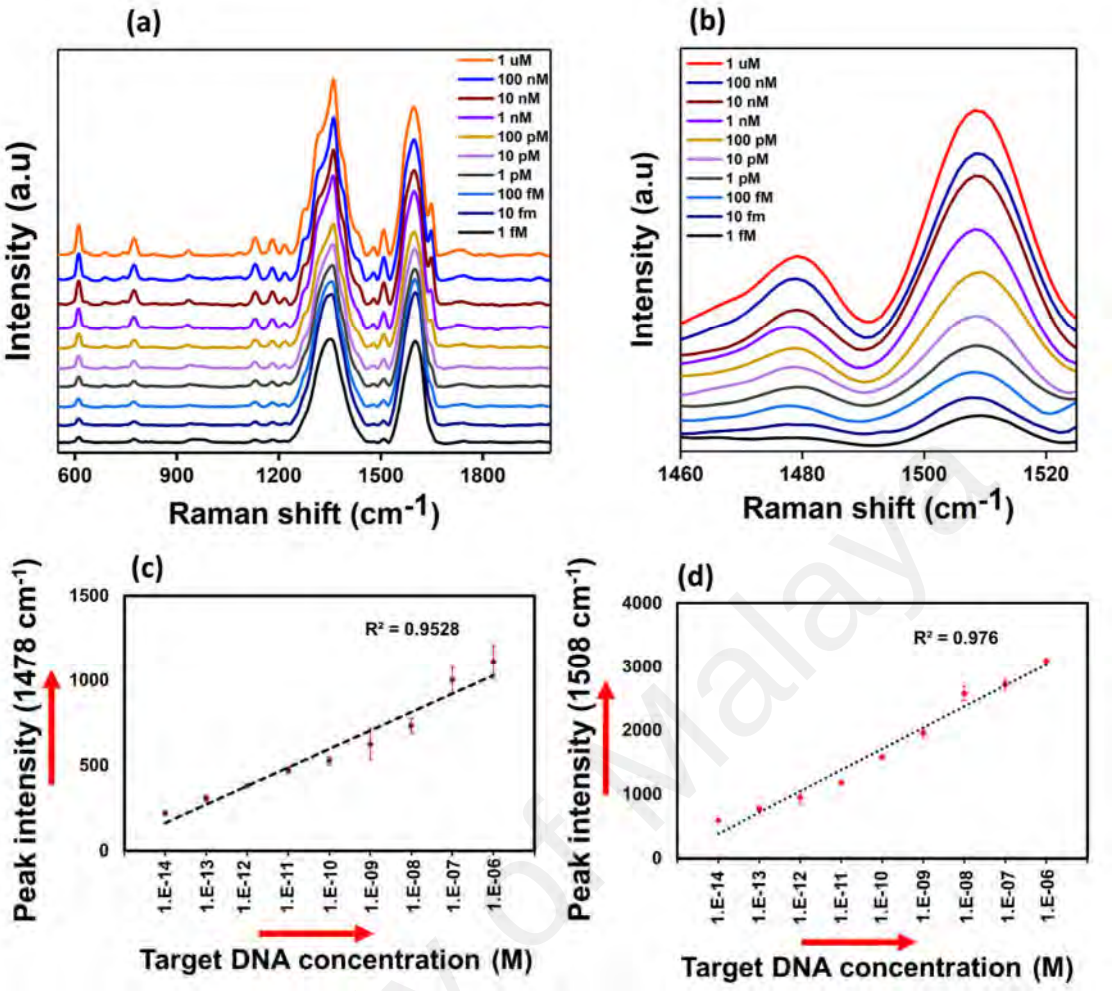

Figure 6. 9: (a) The SERS spectra representing all the produced peaks of the hybridized composite obtained from the serially diluted target DNA (1 µM to 1 fM) of both MBT and pig species. (b) The SERS spectra were chopped from 1460 to 1525 cm^{-1} to reveal and magnify the fingerprint peaks of Cy3 at 1478 cm^{-1} and ATTO Rho6G at 1508 cm^{-1}. Linear curve of SERS intensities at (c) 1478 cm^{-1} and (d) 1508 cm^{-1} band vs corresponding target DNA concentration. Error bars in (c) & (d) represent standard deviations of peak intensities from n=3 repeated measurements.

This greater efficiency of the SERS sensing assay was the cumulative impact of the few determinants. For example, using the GO-AuNPs as the sensor platform which have already proved to contribute in Raman signal enhancement by the electromagnetic enhancement due to the combining of two individual components. Moreover, AuNPs over the planar GO sheet not only protect from the GO from self-aggregating but also facilitate the chemisorption of the signal DNA probes by Au-S bonding, then creating greater possibility to link with the corresponding target DNA sequences. Therefore, addition of the AuNP-SP(MBT)-T and AuNP-SP(Pig)-T to the GO-AuNP-CP(MBT+Pig), more

AuNPs were attached onto the GO-AuNPs via probe-target hybridization. The composite thus formed by the hybridization mediated multi-component networking, generates the hot spots between or among the adjacent AuNPs (Chuong et al., 2017; Duan et al., 2015), lead to an increased SERS intensity by the hot spot induced electromagnetic enhancement (Lin et al., 2015). In addition, AuNPs functionalized with the signal probe sequences intercalated with Raman dye immediate after the C6 spacer also contributed in SERS signal enhancement by the charge transfer mechanism between the Raman tag and plasmonic AuNPs surface (Maher, 2012; Radziuk & Moehwald, 2015). Therefore, the combined effect of the electromagnetic and chemical enhancement had a cumulative impact on the SERS intensity of the hybridized composite, leading to reveal even the minor Raman peaks distinctly. Hence, attachment of the two platforms even by the low quantity of target DNA and the consequent amplification of the less intense SERS signal into well distinct peaks guided to the excellent sensitivity of the biosensor (Maher, 2012; Radziuk & Moehwald, 2015).

The fabricated duplex SERS DNA biosensor showed greater sensitivity (several times of magnitude) than the commonly employed multiplex PCR or multiplex real time-PCR technique (Hossain et al., 2017a; Hossain et al., 2017b). Moreover, this SERS-active multi-component nanoplatform based duplex DNA biosensor showed better performances than the biosensors comprising of SERS non-active (Cao et al., 2002; Prinz et al., 2016), SERS-active single platform (He et al., 2012), and even SERS active dual platforms with the sandwich assay procedure (Kang et al., 2010; Zhang et al., 2010). Furthermore, a novel unique probe design was adopted in this experiment by inserting Raman tag immediate after the C6-spacer into the DNA probe, therefore upon immobilization onto AuNPs, contribute directly in SERS signal enhancement which thus supersede the sensitivity of some of the approaches involving Raman tag attachment at the terminal end (Eremina, et al., 2020). However, despite excellent sensitivity,

nanoparticle based SERS signaling is greatly dependent on the formation of hot spots at the junctions or interstices which in fact is very difficult to experimentally control for the reproducible detection sensitivity (Sanchez-Cortes et al., 1995; Zhang et al., 2010).

6.3.5.3 Application of the SERS DNA Biosensor for Real Sample Analysis

The purity of the extracted genomic DNA from the MBT and pork samples was determined by the A260/A280 ratio which was found between 1.7 – 1.9, reflecting the extracted DNA samples were highly purified (Ali et al., 2015b). In addition, the concentration of the extracted DNA samples was also estimated to ~300 ng/µL for MBT and ~60 ng/µL for pork. The DNA samples were prepared in nM concentration by determining the average size of the genomic DNA strands via electrophoresis in 2% agarose gel using XLarge DNA Ladder (250 to 25k bp) (GeneDirex, Taiwan) as the marker and applying the Equation 5. The DNA samples were then serially diluted from the initially adjusted 10 nM concentration to 10 fM which is the established LOD for the synthetic target DNAs. However, the serially diluted genomic DNA samples were denatured and fragmented into small pieces ssDNA by the heat treatment at 95°C for 15 min followed by prompt cooling in ice-cold water for 15 min and finally ultrasonication for 15 min at room temperature (Pandey et al., 2011; Tiwari et al., 2015). The established duplex SERS DNA sensing strategy was therefore validated for the real sample analysis following the same protocol as described for the synthesized target DNAs. The biosensor exhibited excellent performance in the simultaneous detection and quantification of the target DNA from MBT and pork real samples which was expedited by the post-extraction process of the DNA by denaturing and fragmenting to small pieces, hence ensuring easy access to the probe DNAs immobilized to sensor platforms (Wang & Son, 2013). The biosensor showed a good sensitivity and the obtained LOD was 100 fM which is a 10 times lower than the LOD of synthetic target DNA samples. The linear regression analysis

of the peaks intensity vs the target DNA concentration showed a good linear response with an R^2 value of 0.9064 and 0.9555 for the peaks at 1478 cm^{-1} and 1508 cm^{-1}, respectively. The established LOD and the corresponding R^2 value for target DNA from real sample of both target species were lower than the synthetic target DNAs which might be due to the fragmented DNA strands of variable length, a lower instances of the renaturation of the genomic DNA as the denatured both strands present in the sample solution and the hindrance of the hybridization kinetics due to the presence of multiple-length dual species target DNA (Wang & Son, 2013). However, in overall consideration the duplex SERS DNA biosensor was proved as robust and compatible for the simultaneous detection of two different species via real sample extracted target DNA mediated multicomponent assembly.

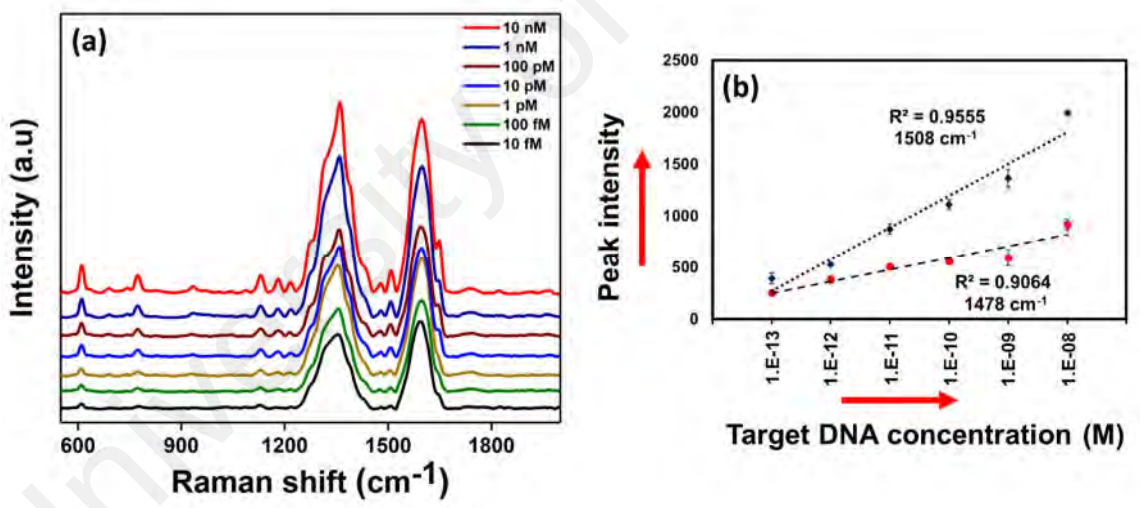

Figure 6. 10: (a) The SERS spectra of the hybridized composite obtained by the addition of a gradually diluted (10 nM to 10 fM) extracted target DNA of both MBT and pork samples. The Cy3 and ATTO Rho6G representing peaks at 1478 cm^{-1} and 1508 cm^{-1} perhaps confirming the presence of both species, showed a steady downward trend with the decreasing target DNA concentration. (b) The linear curve of SERS intensity at 1478 cm^{-1} and 1508 cm^{-1} vs the target DNA concentrations where error bars represent standard deviations of peak intensities from n=3 repeated measurements.

6.4 Conclusion

In this study, a highly sensitive and selective SERS DNA biosensor was developed for the simultaneous detection and quantification of two different meat species. In this context, Cy3 and ATTO Rho6G directly were inserted into 5′terminal of split-probe sequences and immobilized onto AuNPs while 3′terminal of split-probe (CP) of MBT and pig species were immobilized onto GO-AuNPs. In the presence of the corresponding target DNA sequences, covalent linking among the sensor platforms resulted in the multi-component agglomeration and huge SERS signal enhancement which therefore facilitated to amplify the small signal to a well-distinct spectrum. Hence, the biosensor exhibited an outstanding sensitivity to detect the target DNA as low as 10 fM. This low sensitivity is due to the novel feature of Raman tag integration in the probe sequences as well as the use of multicomponent platforms to generate electromagnetic hot spots at the junctions of AuNPs. Moreover, the biosensor exhibited high specificity towards the nucleotide base differences in the target DNA and proved to differentiate the target DNA sequences with single nucleotide variation as well as target DNA sequences of the closely related five non-target species. Furthermore, the duplex SERS biosensor was validated for the real sample analysis and the obtained LOD (100 fM) was also promising. Hence, the duplex sensing strategy was proved and validated for the simultaneous and sensitive detection of DNA of different meat species. This study is therefore one-step ahead on the way to guide the multiplex detection in a single experiment by a single laser excitement to detect a panel of meat species or even could be adopted for versatile applications such as detection food adultering organisms, food poisoning causing bacteria, identification of cancer causing antigen, forensic applications and many more.

CHAPTER 7: CONCLUSION AND RECOMMENDATIONS

Till date lots of approaches have been reported for the DNA probe designing and functionalization in SERS biosensing application. In this study, short-length DNA probe sequences of linear fashion functionalized with alkyl spacer and terminal thiol molecule were employed to fabricate the biosensor. Herein this study, for the first time reported the PCR free SERS DNA biosensing technique for the detection of meat species. In this dissertation, a convenient, facile and easy fabrication of the SERS DNA biosensors using low-cost SERS-active substrates and short-length DNA biomarkers were reported with extraordinary performances. Three different SERS DNA sensing strategies were established utilizing different compositions and combination of SERS active platforms such as GO-AuNPs, GO-AuNR and AuNPs. In addition, two different Raman tag attachment strategies have been adopted – (i) direct attachment of Raman tag along with DNA probe sequences on to the same sensor platform, and (ii) the direct integration of Raman tag to the nucleotide sequences of DNA probe followed by immobilization onto the AuNP platform. In this context, two different Raman dyes such as Cy3 and ATTO Rho6G of distinctive Raman spectral profile were selected and used to intercalate in SP sequences of the MBT and pig species. Moreover, in this dissertation, SERS DNA biosensors for single as well as simultaneous dual species detection techniques have been developed.

In the first sensing protocol, SERS-active dual platforms - GO-AuNPs and AuNPs and co-attachment approach for Raman tag (Cy3) immobilization along with DNA probe on AuNPs were employed for the detection of MBT species. The noble features of the sensor are the use of very short-length probe sequences and the linking of the two SERS active platforms via target-probe DNA hybridization to produce a unique and enhanced SERS signal. This huge enhancement is in fact due to the combined effects of electromagnetic

enhancement via the hot spots, generated by the dual-platform assembly as well as the chemical enhancement by the charge transfer mechanism between Cy3 and AuNPs surfaces. Here, the hybridization aided linking of the two different platforms resulted the huge enhancement of the SERS signal which facilitated to achieve an LOD of 10 fM, thus showed greater efficiency than the conventional and most widely used PCR based detection systems. Moreover, the sensing system showed outstanding performances in discriminating the DNA sequences of the closely related meat species as well as three and even a single nucleotide variations in the corresponding target DNA sequences. Furthermore, the developed dual platform based SERS DNA biosensor was validated with DNA samples extracted from the MBT muscle tissue samples with an LOD of 100 fM. However, though the Raman tag was directly immobilized onto the AuNPs which in consequent contributed to SERS signal enhancement by charge transfer mechanism, one of the utmost limitations of the this strategy is that there is no control over the proportion of the DNA probes and Raman tags on the same AuNP platform.

In the second approach, a different platform components – GO-AuNR and AuNPs as well as Raman tag (ATTO Rho6G) intercalated uniquely designed SP sequences were used to explore the role of Raman tag in the intercalated DNA probe. Moreover, the use of GO-AuNR as a sensor platform and its contribution in the SERS signal enhancement was also evaluated. The hybridization mediated coupling of the two platforms produced an intense SERS signal which is due to the direct contribution of the intercalated Raman tag in probe sequences as well as stronger light scattering properties and electron transfer ability of AuNR of GO-AuNR composite. The biosensor thus facilitated the detection of very low amount of corresponding target sequences and the established LOD was 100 am. The obtained LOD is 100-fold greater than the Raman tag and SP co-attachment mediated sensing strategy used for the detection of MBT. Moreover, the biosensor was also justified for the real sample analysis with sensitivity down to 1 fM. It is the first ever

reported a noble DNA designing by incorporating Raman tag directly in the nucleotide sequences as well as a SERS sensing approach for the detection of pork meat.

Subsequently, to take the SERS sensing strategy one-step forward, an assay technique for the simultaneous and quantitative detection of MBT and pig species were conducted by using GO-AuNP and AuNP as the platforms, as well as using Cy3 and ATTO Rho6G tagged SP sequences for MBT and pig species respectively. Presence of the complementary target DNA sequences produced a multi-component aggregated hybridized composites via probe-target covalent binding which in consequent produced intense and distinct SERS spectra comprising of both Cy3 and ATTO Rho6G fingerprint peaks. The SERS spectra of the hybridized composite depicted the clearly distinct fingerprints peaks for both of the target species. The advantage of using these multicomponent based SERS assay is that the linking of the platforms produced large number of hot spots at the junctions, hence produced strong SERS signal by the combined effect of electromagnetic and chemical enhancement. This dual sensing strategy also showed excellent performances in terms of sensitivity with LOD 10 fM, selectivity by differentiating the DNA sequences of the closely related species, and specificity by identifying and distinguishing single and three nucleotide base-mismatches.

The fabricated biosensors proved to be suitable and efficient enough for the sensitive and quantitative detection of MBT and pig species singly as well as simultaneously. Hence, all the three set objectives of this thesis were achieved. Hence, these simple, facile, cost-effective, highly specific and sensitive SERS DNA sensing techniques could be useful for the detection of the raw meat species. Moreover, the strategies could be application for the verification of food adulterants from the processed food products due to use of very short-length DNA probe sequences, where the DNA are generally denatured or degraded into small pieces, thus could be easily identified and traceable.

Moreover, the assay protocols could be applied as universal sensing strategies in detecting life threatening microorganisms, cancer diagnostic, forensic applications even for compromised samples; could be adopted by the regulatory authorities for tracing the target analytes from minute amount of sample, archaeologists and wildlife protection agencies to track the trafficking of the animals to be extinct.

The multiplex biosensors with greater sensitivity and selectivity have great demand, therefore future work should consider to develop an integrated SERS biosensor for simultaneously detecting a panel of target analytes by a single laser shot, which would immensely improve its usability. Furthermore, the future work should focus on developing a portable sensing system so that on-site detection of the analyte with minimum sample processing could be possible. However, I believe the developed strategies would be applicable for the detection DNA extracted from any kind of samples as the method is justified for both the synthetic as well as DNA from real samples. Hence, it is to be concluded that this promising sensing technology can undoubtedly result in concrete innovations through combined efforts of multidisciplinary teams uniting chemists, biochemists, material scientists, physicists, biologists, and engineers.

REFERENCES

Abalde-Cela, S., Carregal-Romero, S., Coelho, J. P., and Guerrero-Martinez, A. (2016). Recent progress on colloidal metal nanoparticles as signal enhancers in nanosensing. *Advances in Colloid and Interface Science, 233*, 255-270.

Abbas, O., Zadravec, M., Baeten, V., Mikuš, T., Lešić, T., Vulić, A., Prpić, J., Jemeršić, L and Pleadin, J. (2018). Analytical methods used for the authentication of food of animal origin. *Food Chemistry, 246*, 6-17.

Aboud, M. J., Gassmann, M., and McCord, B. R. (2010). The development of mini pentameric STR loci for rapid analysis of forensic DNA samples on a microfluidic system. *Electrophoresis, 31*(15), 2672-2679.

Ahamad, M. N. U., Ali, M. E., Hossain, M. M., Asing, A., Sultana, S., and Jahurul, M. (2017). Multiplex PCR assay discriminates rabbit, rat and squirrel meat in food chain. *Food Additives & Contaminants: Part A 34*(12), 2043-2057.

Ahmad, A. N., Abidin, U. F. U. Z., Othman, M., and Rahman, R. A. (2018). Overview of the halal food control system in Malaysia. *Food Control, 90*, 352-363.

Ahmed, H., El-Nasser, M. A., Mohammed, D., & Mohamed, M. (2011). Identification of meat species in some raw meat products in Assiut city, Egypt. In *Animal hygiene and sustainable livestock production. Proceedings of the XVth International Congress of the International Society for Animal Hygiene, Vienna, Austria,* (2), 973-975.

Aida, A. A., Man, Y. C., Wong, C., Raha, A., and Son, R. (2005). Analysis of raw meats and fats of pigs using polymerase chain reaction for Halal authentication. *Meat Science, 69*(1), 47-52.

Alamprese, C., Casale, M., Sinelli, N., Lanteri, S., and Casiraghi, E. (2013). Detection of minced beef adulteration with turkey meat by UV–vis, NIR and MIR spectroscopy. *LWT-Food Science and Technology, 53*(1), 225-232.

Al Amin, M., Rahman, M. M., Razimi, M. S. A., Chowdhury, Z. Z., Hussain, M. N. M., and Desa, M. N. M. (2020). Screening of commercial meat products from supermarket chains for feline derivatives using SP-PCR-RLFP and lab-on-a-chip. *Journal of Food Composition and Analysis*, 103565.

Albrecht, M. G., and Creighton, J. A. (1977). Anomalously intense Raman spectra of pyridine at a silver electrode. *Journal of the American Chemical Society, 99*(15), 5215-5217.

Ali, M. E., Kashif, M., Uddin, K., Hashim, U., Mustafa, S., and Man, Y. B. C. (2012a). Species authentication methods in foods and feeds: the present, past, and future of halal forensics. *Food Analytical Methods, 5*(5), 935-955.

Ali, M. E., Hashim, U., Dhahi, T. S., Mustafa, S., Man, Y. B. C., and Latif, M. A. (2012b). Analysis of pork adulteration in commercial burgers targeting porcine-specific

mitochondrial cytochrome b gene by TaqMan probe real-time polymerase chain reaction. *Food Analytical Methods, 5*(4), 784-794.

Ali, M. E., Hashim, U., Mustafa, S., and Man, Y. B. C. (2012c). Swine-specific PCR-RFLP assay targeting mitochondrial cytochrome B gene for semiquantitative detection of pork in commercial meat products. *Food Analytical Methods, 5*(3), 613-623.

Ali, M., Hashim, U., Mustafa, S., Man, Y., and Islam, K. N. (2012d). Gold nanoparticle sensor for the visual detection of pork adulteration in meatball formulation. *Journal of Nanomaterials, 2012*, 1.

Ali, M. E., Ahamad, M. N. U., Asing, Hossain, M. A. M., and Sultana, S. (2018). Multiplex polymerase chain reaction-restriction fragment length polymorphism assay discriminates of rabbit, rat and squirrel meat in frankfurter products. *Food Control, 84*, 148-158.

Ali, M. E., Al Amin, M., Hamid, S. B. A., Hossain, M. M., and Mustafa, S. (2015a). Lab-on-a-chip-based PCR-RFLP assay for the confirmed detection of short-length feline DNA in food. *Food Additives Contaminants: Part A, 32*(9), 1373-1383.

Ali, M. E., Asing, Hamid, S. B. A., Razzak, M. A., Rashid, N. R. A., Al Amin, M., and Mustafa, S. (2015b). A suitable method to detect potential fraud of bringing Malayan box turtle (Cuora amboinensis) meat into the food chain. *Food Additives & Contaminants: Part A, 32*(8), 1223-1233.

Ali, M. E., Razzak, M. A., Hamid, S. B. A., Rahman, M. M., Amin, M. A., Rashid, N. R. A., and Asing. (2015c). Multiplex PCR assay for the detection of five meat species forbidden in Islamic foods. Food chemistry, 177, 214-224.

Ali, M. E., Hamid, S. B. A., Hossain, M. M., Mustafa, S., Kader, M. A., and Zaidul, I. (2016). Lab-on-a-Chip-based PCR-RFLP assay for the detection of Malayan box turtle (Cuora amboinensis) in the food chain and traditional Chinese medicines. *PLOS ONE, 11*(10), e0163436.

Ali, M. E., Razzak, M. A., and Hamid, S. B. A. (2014). Multiplex PCR in species authentication: probability and prospects – a review. *Food Analytical Methods, 7*(10), 1933-1949.

Alwan, A. M., Wali, L. A., and Yousif, A. A. (2018). Optimization of AgNPs/mesoPS active substrates for ultra–low molecule detection process. *Silicon*, 10(5), 2241-2251.

Anonym. (2018). Sus scrofa Invasive Species Compendium. (Accessed on 29 June 2019). Retrieved from https://www.cabi.org/isc/datasheet/119688#tosummaryOfInvasiveness.

Aristoy, M. C., and Toldrá, F. (2004). Histidine dipeptides HPLC-based test for the detection of mammalian origin proteins in feeds for ruminants. *Meat Science, 67*(2), 211-217.

Armenteros, M., Heinonen, M., Ollilainen, V., Toldrá, F., and Estévez, M. (2009). Analysis of protein carbonyls in meat products by using the DNPH-method, fluorescence spectroscopy and liquid chromatography–electrospray ionisation–mass spectrometry (LC–ESI–MS). *Meat Science, 83*(1), 104-112.

Arslan, A., Ilhak, O. I., and Calicioglu, M. (2006). Effect of method of cooking on identification of heat processed beef using polymerase chain reaction (PCR) technique. *Meat Science, 72*(2), 326-330.

Arya, M., Shergill, I. S., Williamson, M., Gommersall, L., Arya, N., and Patel, H. R. (2005). Basic principles of real-time quantitative PCR. *Expert review of molecular diagnostics, 5*(2), 209-219.

Asal, M., Özen, Ö., Şahinler, M., and Polatoğlu, İ. (2018). Recent Developments in Enzyme, DNA and Immuno-Based Biosensors. *Sensors*, *18*(6), 1924.

Asensio, L., González, I., García, T., and Martín, R. (2008). Determination of food authenticity by enzyme-linked immunosorbent assay (ELISA). *Food Control, 19*(1), 1-8.

Asing, Ali, E., Hamid, S. B. A., Hossain, M., Ahamad, M. N. U., Hossain, S. A., Naquiah, N., and Zaidul, I. (2016). Duplex real-time PCR assay using SYBR Green to detect and quantify Malayan box turtle (Cuora amboinensis) materials in meatballs, burgers, frankfurters and traditional Chinese herbal jelly powder. *Food Additives & Contaminants: Part A, 33*(11), 1643-1659.

Azimzadeh, M., Rahaie, M., Nasirizadeh, N., Ashtari, K., and Naderi-Manesh, H. (2016). An electrochemical nanobiosensor for plasma miRNA-155, based on graphene oxide and gold nanorod, for early detection of breast cancer. *Biosensors and Bioelectronics, 77*, 99-106.

Balasubramanian, S. K., Yang, L., Yung, L. Y. L., Ong, C. N., Ong, W. Y., and Liya, E. Y. (2010). Characterization, purification, and stability of gold nanoparticles. *Biomaterials*, *31*(34), 9023-9030.

Ballin, N. Z., Vogensen, F. K., and Karlsson, A. H. (2009). Species determination – Can we detect and quantify meat adulteration? *Meat Science, 83*(2), 165-174.

Bansal, S., Singh, A., Mangal, M., Mangal, A. K., and Kumar, S. (2017). Food adulteration: Sources, health risks, and detection methods. *Critical Reviews in Food Science and Nutrition*, 57(6), 1174-1189.

Bantz, K. C., Meyer, A. F., Wittenberg, N. J., Im, H., Kurtuluş, Ö., Lee, S. H., Lindquist, N.C., Oh, S.-H., and Haynes, C. L. (2011). Recent progress in SERS biosensing. *Physical Chemistry Chemical Physics, 13*(24), 11551-11567.

Barhoumi, A., and Halas, N. J. (2010). Label-free detection of DNA hybridization using surface enhanced Raman spectroscopy. *Journal of the American Chemical Society, 132*(37), 12792-12793.

Barhoumi, A., Zhang, D., Tam, F., and Halas, N. J. (2008). Surface-enhanced Raman spectroscopy of DNA. *Journal of the American Chemical Society, 130*(16), 5523-5529.

Bayraç, C., Eyidoğan, F., and Öktem, H. A. (2017). DNA aptamer-based colorimetric detection platform for Salmonella Enteritidis. *Biosensors and Bioelectronics, 98*, 22-28.

Bell, S. E., and Sirimuthu, N. M. (2006). Surface-enhanced Raman spectroscopy (SERS) for sub-micromolar detection of DNA/RNA mononucleotides. *Journal of the American Chemical Society, 128*(49), 15580-15581.

Benvidi, A., Firouzabadi, A. D., Moshtaghiun, S. M., Mazloum-Ardakani, M., and Tezerjani, M. D. (2015). Ultrasensitive DNA sensor based on gold nanoparticles/reduced graphene oxide/glassy carbon electrode. *Analytical biochemistry, 484*, 24-30.

Bernama. (2016). Wildlife Crime Unit seizes 1,070 tortoises in two raids. Malaymail. (Accessed on 27 June 2019). Retrieved from https://www.malaymail.com/news/malaysia/2016/07/26/wildlife-crime-unit-seizes-1070-tortoises-in-two-raids/1170039.

Bhardwaj, N., Bhardwaj, S. K., Bhatt, D., Lim, D. K., Kim, K.-H., and Deep, A. (2019). Optical detection of waterborne pathogens using nanomaterials. *TrAC Trends in Analytical Chemistry, 113*, 280-300.

Bonne, K., and Verbeke, W. (2008). Religious values informing halal meat production and the control and delivery of halal credence quality. *Agriculture and Human Values, 25*(1), 35-47.

Boon, E. M., and Barton, J. K. (2002). Charge transport in DNA. *Current opinion in structural biology, 12*(3), 320-329.

Bottero, M. T., and Dalmasso, A. (2011). Animal species identification in food products: evolution of biomolecular methods. *The Veterinary Journal, 190*(1), 34-38.

Bourguiba-Hachemi, S., and Fathallah, M. D. (2016). DNA testing of meat foods raises issues beyond adulteration. *Sky J. Food Sci, 5*, 001-007.

Braun, G., Lee, S. J., Dante, M., Nguyen, T.-Q., Moskovits, M., and Reich, N. (2007). Surface-enhanced Raman spectroscopy for DNA detection by nanoparticle assembly onto smooth metal films. *Journal of the American Chemical Society, 129*(20), 6378-6379.

Brown, B. (2013). Findus beef lasagne contained up to 100% horsemeat. *BBC News.* (Accessed on 27 June 2019). Retrieved from*:* https://www.bbc.com/news/uk-21375594.

Cai, R., Yin, F., Zhang, Z., Tian, Y., and Zhou, N. (2019). Functional chimera aptamer and molecular beacon based fluorescent detection of Staphylococcus aureus with strand displacement-target recycling amplification. *Analytica Chimica Acta, 1075,* 128-136.

Caires, A., Alves, D., Fantini, C., Ferlauto, A., and Ladeira, L. (2015). One-pot in situ photochemical synthesis of graphene oxide/gold nanorod nanocomposites for surface-enhanced Raman spectroscopy. *RSC Advances, 5*(58), 46552-46557.

Calvo, J., Zaragoza, P., and Osta, R. (2001). Random amplified polymorphic DNA fingerprints for identification of species in poultry pate. *Poultry Science, 80*(4), 522-524.

Cammà, C., Di Domenico, M., and Monaco, F. (2012). Development and validation of fast Real-Time PCR assays for species identification in raw and cooked meat mixtures. *Food Control, 23*(2), 400-404.

Cao, Y. C., Jin, R., and Mirkin, C. A. (2002). Nanoparticles with Raman spectroscopic fingerprints for DNA and RNA detection. *Science, 297*(5586), 1536-1540.

Cawthorn, D.-M., Steinman, H. A., and Hoffman, L. C. (2013). A high incidence of species substitution and mislabelling detected in meat products sold in South Africa. *Food Control, 32*(2), 440-449.

Cha, T. W., Boiadjiev, V., Lozano, J., Yang, H., and Zhu, X. Y. (2002). Immobilization of oligonucleotides on poly(ethylene glycol) brush-coated Si surfaces. *Analytical biochemistry, 311*(1), 27-32.

Chaubey, A., and Malhotra, B. D. (2002). Mediated biosensors. *Biosensors and Bioelectronics, 17*(6), 441-456.

Che Man, Y. B., Aida, A. A., Raha, A. R., and Son, R. (2007). Identification of pork derivatives in food products by species-specific polymerase chain reaction (PCR) for halal verification. *Food Control, 18*(7), 885-889.

Chen, C., Liu, W., Tian, S., and Hong, T. (2019). Novel Surface-Enhanced Raman Spectroscopy Techniques for DNA, Protein and Drug Detection. *Sensors, 19*(7), 1712.

Chen, F.-C., and Hsieh, Y. (2000). Detection of pork in heat-processed meat products by monoclonal antibody-based ELISA. *Journal of AOAC International, 83*(1), 79-85.

Chen, H., Müller, M. B., Gilmore, K. J., Wallace, G. G., and Li, D. (2008). Mechanically strong, electrically conductive, and biocompatible graphene paper. *Advanced Materials, 20*(18), 3557-3561.

Chen, K., Wu, L., Jiang, X., Lu, Z., and Han, H. (2014). Target triggered self-assembly of Au nanoparticles for amplified detection of Bacillus thuringiensis transgenic sequence using SERS. *Biosensors and Bioelectronics, 62*, 196-200.

Chen, T.-H., Chang, H.-C., and Lue, K.-Y. (2009). Unregulated trade in turtle shells for Chinese traditional medicine in East and Southeast Asia: the case of Taiwan. *Chelonian Conservation and Biology, 8*(1), 11-18.

Chen, X., Lin, Y.-H., Li, J., Lin, L.-S., Chen, G.-N., and Yang, H.-H. (2011). A simple and ultrasensitive electrochemical DNA biosensor based on DNA concatamers. *Chemical Communications, 47*(44), 12116-12118.

Cheng, S., Zheng, B., Wang, M., Lam, M. H.-W., and Ge, X. (2013). Double-functionalized gold nanoparticles with split aptamer for the detection of adenosine triphosphate. *Talanta, 115*, 506-511.

Chou, C.-C., Lin, S.-P., Lee, K.-M., Hsu, C.-T., Vickroy, T. W., and Zen, J.-M. (2007). Fast differentiation of meats from fifteen animal species by liquid chromatography with electrochemical detection using copper nanoparticle plated electrodes. *Journal of Chromatography B, 846*(1), 230-239.

Chou, I.-H., Benford, M., Beier, H. T., Coté, G. L., Wang, M., Jing, N., Komeoka, J, and Good, T. A. (2008). Nanofluidic biosensing for β-amyloid detection using surface enhanced Raman spectroscopy. *Nano letters, 8*(6), 1729-1735.

Chuah, L.-O., He, X. B., Effarizah, M. E., Syahariza, Z. A., Shamila-Syuhada, A. K., and Rusul, G. (2016). Mislabelling of beef and poultry products sold in Malaysia. *Food Control, 62*, 157-164.

Chuang, M.-K., Lin, S.-W., Chen, F.-C., Chu, C.-W., and Hsu, C.-S. (2014). Gold nanoparticle-decorated graphene oxides for plasmonic-enhanced polymer photovoltaic devices. *Nanoscale, 6*(3), 1573-1579.

Chuong, T. T., Pallaoro, A., Chaves, C. A., Li, Z., Lee, J., Eisenstein, M., Stucky, G.D., Moskovits, M. and Soh, H. T. (2017). Dual-reporter SERS-based biomolecular assay with reduced false-positive signals. *Proceedings of the National Academy of Sciences, 114*(34), 9056-9061.

Coghlan, M. L., Maker, G., Crighton, E., Haile, J., Murray, D. C., White, N. E., Byard, R.W., Bellgard, M.I., Mullaney, I. and Trengove, R. (2015). Combined DNA, toxicological and heavy metal analyses provides an auditing toolkit to improve pharmacovigilance of traditional Chinese medicine (TCM). *Scientific reports, 5*, 17475.

Connor, E. E., Mwamuka, J., Gole, A., Murphy, C. J., and Wyatt, M. D. (2005). Gold nanoparticles are taken up by human cells but do not cause acute cytotoxicity. *Small, 1*(3), 325-327.

Cota-Rivas, M., and Vallejo-Cordoba, B. (1997). Capillary electrophoresis for meat species differentiation. *Journal of Capillary Electrophoresis, 4*(4), 195-199.

Covaci, A., Voorspoels, S., Schepens, P., Jorens, P., Blust, R., and Neels, H. (2008). The Belgian PCB/dioxin crisis—8 years later: An overview. *Environmental Toxicology and Pharmacology, 25*(2), 164-170.

Csaki, A., Möller, R., Straube, W., Köhler, J., and Fritzsche, W. J. N. A. R. (2001). DNA monolayer on gold substrates characterized by nanoparticle labeling and scanning force microscopy. *29*(16), e81-e81.

Cutler, J. I., Auyeung, E., and Mirkin, C. A. (2012). Spherical nucleic acids. *Journal of the American Chemical Society, 134*(3), 1376-1391.

Darling, J. A., and Blum, M. J. (2007). DNA-based methods for monitoring invasive species: a review and prospectus. *Biological Invasions, 9*(7), 751-765.

Das, G., Patra, N., Gopalakrishnan, A., Zaccaria, R. P., Toma, A., Thorat, S., Di Fabrizio, E., Diaspro, A., and Salerno, M. (2012). Fabrication of large-area ordered and reproducible nanostructures for SERS biosensor application. *Analyst, 137*(8), 1785-1792.

De Mey, E., Drabik-Markiewicz, G., De Maere, H., Peeters, M. C., Derdelinckx, G., Paelinck, H., and Kowalska, T. (2012). Dabsyl derivatisation as an alternative for dansylation in the detection of biogenic amines in fermented meat products by reversed phase high performance liquid chromatography. *Food Chemistry, 130*(4), 1017-1023.

Delgado, C. L. (2003). Rising consumption of meat and milk in developing countries has created a new food revolution. *The Journal of nutrition*, 133(11), 3907S-3910S.

Dehghani, Z., Hosseini, M., and Mohammadnejad, J. (2019). A fluorescence nanobiosensor for detection of Campylobacter jejuni DNA in milk based on Au/Ag bimetallic nanoclusters. *Journal of Food Measurement and Characterization*, 1-8.

Di Pietrantonio, F., Cannatà, D., and Benetti, M. (2019). Biosensor technologies based on nanomaterials. In *Functional Nanostructured Interfaces for Environmental and Biomedical Applications*, 181-242: Elsevier.

Di Pinto, A., Forte, V. T., Conversano, M. C., and Tantillo, G. M. (2005). Duplex polymerase chain reaction for detection of pork meat in horse meat fresh sausages from Italian retail sources. *Food Control, 16*(5), 391-394.

Diao, W., Tang, M., Ding, S., Li, X., Cheng, W., Mo, F., Yan, X., Ma, H., and Yan, Y. (2018). Highly sensitive surface plasmon resonance biosensor for the detection of HIV-related DNA based on dynamic and structural DNA nanodevices. *Biosensors and Bioelectronics, 100*, 228-234.

Ding, W., Song, C., Li, T., Ma, H., Yao, Y., and Yao, C. (2019). TiO_2 nanowires as an effective sensing platform for rapid fluorescence detection of single-stranded DNA and double-stranded DNA. *Talanta, 199*, 442-448.

Dooley, J. J., Paine, K. E., Garrett, S. D., and Brown, H. M. (2004). Detection of meat species using TaqMan real-time PCR assays. *Meat Science, 68*(3), 431-438.

Dooley, J. J., Sage, H. D., Clarke, M.-A. L., Brown, H. M., and Garrett, S. D. (2005). Fish species identification using PCR− RFLP analysis and lab-on-a-chip capillary electrophoresis: application to detect white fish species in food products and an interlaboratory study. *Journal of agricultural food chemistry, 53*(9), 3348-3357.

Drummond, T. G., Hill, M. G., and Barton, J. K. (2003). Electrochemical DNA sensors. *Nature biotechnology, 21*(10), 1192.

Duan, B., Zhou, J., Fang, Z., Wang, C., Wang, X., Hemond, H. F., Chan-Park, M.B., and Duan, H. (2015). Surface enhanced Raman scattering by graphene-nanosheet-gapped plasmonic nanoparticle arrays for multiplexed DNA detection. *Nanoscale, 7*(29), 12606-12613.

Duan, N., Chang, B., Zhang, H., Wang, Z., & Wu, S. (2016a). Salmonella typhimurium detection using a surface-enhanced Raman scattering-based aptasensor. *International journal of food microbiology, 218*, 38-43.

Duan, N., Yan, Y., Wu, S., and Wang, Z. (2016b). Vibrio parahaemolyticus detection aptasensor using surface-enhanced Raman scattering. *Food Control, 63*, 122-127.

Elghanian, R., Storhoff, J. J., Mucic, R. C., Letsinger, R. L., and Mirkin, C. A. (1997). Selective colorimetric detection of polynucleotides based on the distance-dependent optical properties of gold nanoparticles. *Science, 277*(5329), 1078-1081.

Ellis, D. I., Broadhurst, D., Clarke, S. J., and Goodacre, R. (2005). Rapid identification of closely related muscle foods by vibrational spectroscopy and machine learning. *Analyst, 130*(12), 1648-1654.

Eremina, O. E., Zatsepin, T. S., Farzan, V. M., Veselova, I. A., and Zvereva, M. I. (2020). DNA detection by dye labeled oligonucleotides using surface enhanced Raman spectroscopy. *Mendeleev Communications*, 30(1), 18-21.

Esteki, M., Regueiro, J., and Simal-Gándara, J. (2019). Tackling Fraudsters with Global Strategies to Expose Fraud in the Food Chain. *Comprehensive Reviews in Food Science and Food Safety, 18*(2), 425-440.

Estévez, M., Morcuende, D., Ventanas, S., and Cava, R. (2003). Analysis of volatiles in meat from Iberian pigs and lean pigs after refrigeration and cooking by using SPME-GC-MS. *Journal of Agricultural Food Chemistry, 51*(11), 3429-3435.

Fajardo, V., González, I., Martín, I., Rojas, M., Hernández, P. E., García, T., and Martín, R. (2008). Real-time PCR for detection and quantification of red deer (Cervus elaphus), fallow deer (Dama dama), and roe deer (Capreolus capreolus) in meat mixtures. *Meat Science, 79*(2), 289-298.

Fajardo, V., González, I., Rojas, M., García, T., and Martín, R. (2010). A review of current PCR-based methodologies for the authentication of meats from game animal species. *Trends in Food Science & Technology, 21*(8), 408-421.

Fan, Z., Kanchanapally, R., & Ray, P. C. (2013). Hybrid graphene oxide based ultrasensitive SERS probe for label-free biosensing. *The Journal of Physical Chemistry Letters, 4*(21), 3813-3818.

FAO. (2014). Animal production and health. Food and Agricuture Organization of the United Nations. Accessed on 22 June 2019. Retrieved from http://www.fao.org/ag/againfo/themes/en/meat/backgr_sources.html

Faulds, K., Jarvis, R., Smith, W. E., Graham, D., and Goodacre, R. (2008). Multiplexed detection of six labelled oligonucleotides using surface enhanced resonance Raman scattering (SERRS). *Analyst, 133*(11), 1505-1512.

Faulds, K., Smith, W. E., and Graham, D. (2004). Evaluation of surface-enhanced resonance Raman scattering for quantitative DNA analysis. *Analytical chemistry, 76*(2), 412-417.

Felisiak, K., Szymczak, M., and Kołakowski, E. (2019). Identification of non-protein nitrogen compounds separated by CZE without derivatization from TCA extract from salted herring meat. *Journal of Food Composition and Analysis, 77*, 108-114.

Feng, L., Xuan, Z., Ma, J., Chen, J., Cui, D., Su, C., Guo, J., and Zhang, Y. (2015). Preparation of gold nanorods with different aspect ratio and the optical response to solution refractive index. *Journal of Experimental Nanoscience, 10*(4), 258-267.

Ferraro, J. R. (2003). Introductory raman spectroscopy: Elsevier.

Fischer, J. J. G. (2016). Markets, religion, regulation: Kosher, halal and Hindu vegetarianism in global perspective. *69*, 67-70.

Fleischmann, M., Hendra, P. J., and McQuillan, A. J. (1974). Raman spectra of pyridine adsorbed at a silver electrode. *Chemical Physics Letters, 26*(2), 163-166.

Flores-Manguia, M. E., Bermudez-Almada, M. C., and Vazquez-Moreno, L. (2000). A research note: Detection of adulteration in processed traditional meat products. *Journal of Muscle Foods, 11*(4), 319-325.

Fojta, M., Havran, L., Billova, S., Kostecka, P., Masarik, M., and Kizek, R. (2003). Two-surface strategy in electrochemical DNA hybridization assays: detection of osmium-labeled target DNA at carbon electrodes. *Electroanalysis: An International Journal Devoted to Fundamental Practical Aspects of Electroanalysis, 15*(5-6), 431-440.

Formenty, P., Odugleh-Kolev, A., Grein, T., Abela-Rider, B., Merianos, A., Drager-Dayal, R., Drury, P., Eremin, S., Pessoa-Da-Silva, C., and Slattery, R. (2011). From forecasting to control of emerging infectious diseases of zoonotic origin: linking animal and human health systems. In *Animal health and biodiversity: preparing for the future. Compendium of the OIE Global Conference on Wildlife, Paris, France,* (pp. 59-70).

Fortunati, S., Rozzi, A., Curti, F., Giannetto, M., Corradini, R., and Careri, M. (2019). Novel amperometric genosensor based on peptide nucleic acid (PNA) probes immobilized on carbon nanotubes-screen printed electrodes for the determination of trace levels of non-amplified DNA in genetically modified (GM) soy. *Biosensors and Bioelectronics, 129*, 7-14.

Frens, G. (1973). Controlled nucleation for the regulation of the particle size in monodisperse gold suspensions. *Nature physical science, 241*(105), 20.

FSN. (2015). Meat and Poultry Products Recalled for Misbranding, Labeling Problems. Food Safety News, Accessed on 23 June 2019, Retrieved from https://www.foodsafetynews.com/2015/10/co-firm-recalls-meat-and-poultry-products-for-misbranding-labeling-problems/#.WLgQbfmGPIU

FSN. (2016). Colorado company recalls beef products linked to E. coli illness. Food Safety News. (Accessed on 23 June 2019). Retrieved from https://www.foodsafetynews.com/2016/07/colorado-company-recalls/#more-129532.

FSN. (2018). Ready-to-eat and raw meat and poultry products recalled for not listing allergens. Food Safety News. (Accessed on 23 June 2019). *Retrieved from* https://www.foodsafetynews.com/2018/11/ready-to-eat-and-raw-meat-and-poultry-products-recalled-for-not-listing-allergens/.

Fund, T. C. (2002). A global action plan for conservation of tortoises and freshwater turtles. *Strategy and funding prospectus, 2007*, 30.

Gao, Y., and Torrente-Murciano, L. (2020). Mechanistic insights of the reduction of gold salts in the Turkevich protocol. *Nanoscale*, 12(4), 2740-2751.

Gauss, C. B. L., Dubey, J. P., Vidal, D., Ruiz, F., Vicente, J., Marco, I., Lavin, S., Gortazaar, C. and Almería, S. (2005). Seroprevalence of Toxoplasma gondii in wild pigs (Sus scrofa) from Spain. *Veterinary Parasitology, 131*(1), 151-156.

Gayo, J., and Hale, S. A. (2007). Detection and quantification of species authenticity and adulteration in crabmeat using visible and near-infrared spectroscopy. *Journal of agricultural food chemistry, 55*(3), 585-592.

Giaretta, N., Di Giuseppe, A. M. A., Lippert, M., Parente, A., and Di Maro, A. (2013). Myoglobin as marker in meat adulteration: A UPLC method for determining the presence of pork meat in raw beef burger. *Food Chemistry, 141*(3), 1814-1820.

Giljohann, D. A., Seferos, D. S., Daniel, W. L., Massich, M. D., Patel, P. C., and Mirkin, C. A. (2010). Gold nanoparticles for biology and medicine. *Angewandte Chemie International Edition, 49*(19), 3280-3294.

Gingerich, J. L. (2006). *Florida's fabulous mammals*: World Publications.

Girish, P., Anjaneyulu, A., Viswas, K., Anand, M., Rajkumar, N., Shivakumar, B., and Bhaskar, S. (2004). Sequence analysis of mitochondrial 12S rRNA gene can identify meat species. *Meat Science, 66*(3), 551-556.

Girish, P., Haunshi, S., Vaithiyanathan, S., Rajitha, R., and Ramakrishna, C. (2013). A rapid method for authentication of Buffalo (Bubalus bubalis) meat by Alkaline Lysis method of DNA extraction and species specific polymerase chain reaction. *Journal of food science technology, 50*(1), 141-146.

Goncalves, G., Marques, P. A., Granadeiro, C. M., Nogueira, H. I., Singh, M., and Gracio, J. (2009). Surface modification of graphene nanosheets with gold nanoparticles: the role of oxygen moieties at graphene surface on gold nucleation and growth. *Chemistry of Materials, 21*(20), 4796-4802.

Graham-Rowe, D. (2011). Endangered and in demand. *Nature, 480*(Suppl. 7378), S101.

Grasselli, J. G., Snavely, M. K., and Bulkin, B. J. (1981). *Chemical applications of Raman spectroscopy*: John Wiley & Sons Inc.

Green, A. D., Buhlmann, K. A., Hagen, C., Romanek, C., and Gibbons, J. W. (2010). Mercury contamination in turtles and implications for human health. *Journal of environmental health*, *72*(10), 14-23.

Grieshaber, D., MacKenzie, R., Voeroes, J., and Reimhult, E. (2008). Electrochemical biosensors-sensor principles and architectures. *Sensors, 8*(3), 1400-1458.

Griffiths, A. M., Sotelo, C. G., Mendes, R., Pérez-Martín, R. I., Schröder, U., Shorten, M., Silva, H.A., Verrez-Bagnis, V. and Mariani, S. (2014). Current methods for seafood authenticity testing in Europe: Is there a need for harmonisation?. *Food Control*, *45*, 95-100.

Guo, J., Ning, T., Han, Y., Sheng, Y., Li, C., Zhao, X., Lu, Z., Man, B., Jiao, Y. and Jiang, S. (2018). Preparation, characterization, and nonlinear optical properties of hybridized graphene@ gold nanorods nanocomposites. *Applied Surface Science, 433*, 45-50.

Guo, L., Ya, M., Hai, X., Guo, Y.-S., Li, C.-D., Xu, W.-L., Liao, C.-S., Feng, W. and Cai, Q. (2019). A simultaneous triplex TaqMan real-time PCR approach for authentication of caprine and bovine meat, milk and cheese. *International Dairy Journal, 95*, 58-64.

Gupta, V. K., Yola, M. L., Qureshi, M. S., Solak, A. O., Atar, N., and Üstündağ, Z. (2013). A novel impedimetric biosensor based on graphene oxide/gold nanoplatform for detection of DNA arrays. *Sensors and Actuators B: Chemical, 188*, 1201-1211.

Guven, B., Boyaci, I. H., Tamer, U., Acar-Soykut, E., and Dogan, U. (2015). Development of rolling circle amplification based surface-enhanced Raman spectroscopy method for 35S promoter gene detection. *Talanta, 136*, 68-74.

Ha, N.-R., Jung, I.-P., La, I.-J., Jung, H.-S., and Yoon, M.-Y. (2017). Ultra-sensitive detection of kanamycin for food safety using a reduced graphene oxide-based fluorescent aptasensor. *Scientific reports, 7*, 40305.

Hajihosseini, S., Nasirizadeh, N., Hejazi, M. S., and Yaghmaei, P. (2016). A sensitive DNA biosensor fabricated from gold nanoparticles and graphene oxide on a glassy carbon electrode. *Materials Science and Engineering: C, 61*, 506-515.

Hakonen, A., Andersson, P. O., Schmidt, M. S., Rindzevicius, T., and Käll, M. (2015). Explosive and chemical threat detection by surface-enhanced Raman scattering: A review. *Analytica Chimica Acta*.

Halperin, A., Buhot, A., and Zhulina, E. (2006). Hybridization at a surface: the role of spacers in DNA microarrays. *Langmuir, 22*(26), 11290-11304.

Han, J., Liu, Y., and Guo, R. (2009). Facile synthesis of highly stable gold nanoparticles and their unexpected excellent catalytic activity for Suzuki− Miyaura cross-

coupling reaction in water. *Journal of the American Chemical Society, 131*(6), 2060-2061.

Han, J., Wu, J., and Du, J. (2019). Fluorescent DNA Biosensor for Single-Base Mismatch Detection Assisted by Cationic Comb-Type Copolymer. *Molecules, 24*(3), 575.

Han, X., Fang, X., Shi, A., Wang, J., and Zhang, Y. J. A. b. (2013). An electrochemical DNA biosensor based on gold nanorods decorated graphene oxide sheets for sensing platform. *443*(2), 117-123.

Hanzaee, K. H., and Ramezani, M. R. (2011). Intention to halal products in the world markets. *Interdisciplinary Journal of Research in Business, 1*(5), 1-7.

Hao, E., and Schatz, G. C. (2004). Electromagnetic fields around silver nanoparticles and dimers. *The Journal of chemical physics, 120*(1), 357-366.

Happer, C., and Wellesley, L. (2019). Meat consumption, behaviour and the media environment: a focus group analysis across four countries. *Food Security, 11*(1), 123-139.

Hernández-Sánchez, D., Villabona-Leal, G., Saucedo-Orozco, I., Bracamonte, V., Pérez, E., Bittencourt, C., and Quintana, M. (2018). Stable graphene oxide–gold nanoparticle platforms for biosensing applications. *Physical Chemistry Chemical Physics*, 20(3), 1685-1692.

Hart, S. M., Banal, J. L., Bathe, M., and Schlau-Cohen, G. S. (2020). Identification of Non-Radiative Decay Pathways in Cy3. *The Journal of Physical Chemistry Letters*.

Haunshi, S., Basumatary, R., Girish, P. S., Doley, S., Bardoloi, R. K., and Kumar, A. (2009). Identification of chicken, duck, pigeon and pig meat by species-specific markers of mitochondrial origin. *Meat Science, 83*(3), 454-459.

He, S., Liu, K.-K., Su, S., Yan, J., Mao, X., Wang, D., He, Y., Li, L.-J., Song, S. and Fan, C. (2012). Graphene-based high-efficiency surface-enhanced Raman scattering-active platform for sensitive and multiplex DNA detection. *Analytical chemistry, 84*(10), 4622-4627.

Heise, C., and Bier, F. F. (2005). Immobilization of DNA on microarrays. In *Immobilisation of DNA on Chips II* (pp. 1-25): Springer.

Hellberg, R. S. R., and Morrissey, M. T. (2011). Advances in DNA-based techniques for the detection of seafood species substitution on the commercial market. *JALA: Journal of the Association for Laboratory Automation, 16*(4), 308-321.

Henchion, M., McCarthy, M., Resconi, V. C., and Troy, D. (2014). Meat consumption: Trends and quality matters. *Meat Science, 98*(3), 561-568.

Hering, K., Cialla, D., Ackermann, K., Dörfer, T., Möller, R., Schneidewind, H., Mattheis, R., Fritzsche, W., Rösch, P. and Popp, J. (2008). SERS: a versatile tool in chemical and biochemical diagnostics. *Analytical and bioanalytical chemistry, 390*(1), 113-124.

Heuer-Jungemann, A., Kiessling, L., Stratakis, E., Kymakis, E., El-Sagheer, A. H., Brown, T., and Kanaras, A. G. (2015). Programming the assembly of gold nanoparticles on graphene oxide sheets using DNA. *Journal of Materials Chemistry C, 3*(36), 9379-9384.

Hicks, C. J. (2001). SERS: Surface Enhanced Raman Spectroscopy. *MSU CEM, 924*.

Hird, H., Chisholm, J., Sánchez, A., Hernandez, M., Goodier, R., Schneede, K., Boltz, C. and Popping, B. (2006). Effect of heat and pressure processing on DNA fragmentation and implications for the detection of meat using a real-time polymerase chain reaction. *Food Additives and Contaminants, 23*(7), 645-650.

Hossain, M. A. M., Ali, M. E., Sultana, S., Asing, Bonny, S. Q., Kader, M. A., and Rahman, M. A. (2017a). Quantitative Tetraplex Real-Time Polymerase Chain Reaction Assay with TaqMan Probes Discriminates Cattle, Buffalo, and Porcine Materials in Food Chain. *Journal of Agricultural and Food Chemistry, 65*(19), 3975-3985.

Hossain, M. A. M., Ali, M. E., Hamid, S. B. A., Asing, Mustafa, S., Desa, M. N. M., and Zaidul, I. S. M. (2017b). Targeting double genes in multiplex PCR for discriminating bovine, buffalo and porcine materials in food chain. *Food Control, 73*, 175-184.

Hossain, M. M., Ali, M. E., Abd Hamid, S. B., Mustafa, S., Mohd Desa, M. N., and Zaidul, I. (2016). Double gene targeting multiplex polymerase chain reaction–restriction fragment length polymorphism assay discriminates beef, buffalo, and pork substitution in frankfurter products. *Journal of Agricultural and Food Chemistry, 64*(32), 6343-6354.

Hou, B., Meng, X., Zhang, L., Guo, J., Li, S., and Jin, H. (2015). Development of a sensitive and specific multiplex PCR method for the simultaneous detection of chicken, duck and goose DNA in meat products. *Meat Science, 101*, 90-94.

Hsu, Y. C., Pestka, J., and Smith, D. (1999). ELISA to quantify triose phosphate isomerase to potentially determine processing adequacy in ground beef. *Journal of food science, 64*(4), 623-628.

Hu, C., Rong, J., Cui, J., Yang, Y., Yang, L., Wang, Y., and Liu, Y. (2013). Fabrication of a graphene oxide–gold nanorod hybrid material by electrostatic self-assembly for surface-enhanced Raman scattering. *Carbon, 51*, 255-264.

Huang, H., Bai, W., Dong, C., Guo, R., and Liu, Z. (2015). An ultrasensitive electrochemical DNA biosensor based on graphene/Au nanorod/polythionine for human papillomavirus DNA detection. *Biosensors and Bioelectronics, 68*, 442-446.

Huang, J., Zhang, L., Chen, B., Ji, N., Chen, F., Zhang, Y., and Zhang, Z. (2010). Nanocomposites of size-controlled gold nanoparticles and graphene oxide: formation and applications in SERS and catalysis. *Nanoscale, 2*(12), 2733-2738.

Huang, R., He, N., and Li, Z. (2018). Recent progresses in DNA nanostructure-based biosensors for detection of tumor markers. *Biosensors and Bioelectronics, 109*, 27-34.

Hurtado, R. B., Cortez-Valadez, M., Aragon-Guajardo, J., Cruz-Rivera, J., Martínez-Suárez, F., and Flores-Acosta, M. (2020). One-step synthesis of reduced graphene oxide/gold nanoparticles under ambient conditions. *Arabian Journal of Chemistry*, 13(1), 1633-1640.

Immoos, C. E., Lee, S. J., and Grinstaff, M. W. (2004). DNA-PEG-DNA triblock macromolecules for reagentless DNA detection. *Journal of the American Chemical Society, 126*(35), 10814-10815.

Indrasti, D., Che Man, Y. B., Mustafa, S., and Hashim, D. M. (2010). Lard detection based on fatty acids profile using comprehensive gas chromatography hyphenated with time-of-flight mass spectrometry. *Food Chemistry, 122*(4), 1273-1277.

Isola, N. R., Stokes, D. L., and Vo-Dinh, T. (1998). Surface-enhanced Raman gene probe for HIV detection. *Analytical chemistry, 70*(7), 1352-1356.

Iwobi, A., Sebah, D., Kraemer, I., Losher, C., Fischer, G., Busch, U., and Huber, I. (2015). A multiplex real-time PCR method for the quantification of beef and pork fractions in minced meat. *Food Chemistry, 169*, 305-313.

Iwobi, A. N., Huber, I., Hauner, G., Miller, A., and Busch, U. (2011). Biochip technology for the detection of animal species in meat products. *Food Analytical Methods, 4*(3), 389-398.

Jans, H., and Huo, Q. (2012). Gold nanoparticle-enabled biological and chemical detection and analysis. *Chemical Society Reviews, 41*(7), 2849-2866.

Jaques, T. (2015). Cadbury and pig DNA: when issue management intersects with religion. *Corporate Communications: An International Journal, 20*(4), 468-482.

Jarvis, R. M., and Goodacre, R. (2008). Characterisation and identification of bacteria using SERS. *Chemical Society Reviews, 37*(5), 931-936.

Jasuja, K., and Berry, V. (2009). Implantation and growth of dendritic gold nanostructures on graphene derivatives: electrical property tailoring and Raman enhancement. *ACS Nano, 3*(8), 2358-2366.

Jasuja, K., Linn, J., Melton, S., and Berry, V. (2010). Microwave-reduced uncapped metal nanoparticles on graphene: tuning catalytic, electrical, and Raman properties. *The Journal of Physical Chemistry Letters, 1*(12), 1853-1860.

Jaswir, I., Mirghani, M. E. S., Hassan, T. H., & Said, M. Z. M. (2003). Determination of Lard in Mixture of Body Fats of Mutton and Cow by Fourier Transform Infrared Spectroscopy. *Journal of Oleo Science, 52*(12), 633-638.

Jin, B., Wang, S., Lin, M., Jin, Y., Zhang, S., Cui, X., Gong, Y., Li, A., Xu, F. and Lu, T. J. (2017). Upconversion nanoparticles based FRET aptasensor for rapid and ultrasenstive bacteria detection. *Biosensors and Bioelectronics, 90*, 525-533.

Jin, P., Ding, H., Li, P., Fan, L., and Fu, C. (2014). Analysis of meat products adulterated in Suzhou area in 2013. *Chineses journal of food hygiene, 26*, 168-172.

Jin, R., Cao, Y. C., Thaxton, C. S., and Mirkin, C. A. (2006). Glass-bead-based parallel detection of DNA using composite Raman labels. *Small, 2*(3), 375-380.

Johnson, R. (2014). Food fraud and "economically motivated adulteration" of food and food ingredients. Congressional Research Service Report.

Jones, K. E., Patel, N. G., Levy, M. A., Storeygard, A., Balk, D., Gittleman, J. L., and Daszak, P. (2008). Global trends in emerging infectious diseases. *Nature, 451*(7181), 990.

Joshi, M., and Deshpande, J. (2010). Polymerase chain reaction: methods, principles and application. *International Journal of Biomedical Research, 2*(1), 81-97.

Jung, C., Mun, H. Y., Li, T., and Park, H. G. (2008). A simple gold nanoparticle-mediated immobilization method to fabricate highly homogeneous DNA microarrays having higher capacities than those prepared by using conventional techniques. *Nanotechnology, 20*(3), 035607.

Kahraman, M., Aydın, Ö., and Çulha, M. (2009). Oligonucleotide-mediated Au–Ag core–shell nanoparticles. *Plasmonics, 4*(4), 293.

Kambhampati, P., Child, C., Foster, M. C., and Campion, A. (1998). On the chemical mechanism of surface enhanced Raman scattering: experiment and theory. *The Journal of chemical physics, 108*(12), 5013-5026.

Kandjani, A. E., Mohammadtaheri, M., Thakkar, A., Bhargava, S. K., and Bansal, V. (2014). Zinc oxide/silver nanoarrays as reusable SERS substrates with controllable 'hot-spots' for highly reproducible molecular sensing. *Journal of colloid and interface science, 436*, 251-257.

Kane, D. E., and Hellberg, R. S. (2016). Identification of species in ground meat products sold on the U.S. commercial market using DNA-based methods. *Food Control, 59*, 158-163.

Kang, T., Yoo, S. M., Yoon, I., Lee, S. Y., and Kim, B. (2010). Patterned multiplex pathogen DNA detection by Au particle-on-wire SERS sensor. *Nano letters, 10*(4), 1189-1193.

Kang, T. S., and Tanaka, T. (2018). Comparison of quantitative methods based on SYBR Green real-time qPCR to estimate pork meat adulteration in processed beef products. *Food Chemistry, 269*, 549-558.

Karahalil, E. (2020). Principles of halal-compliant fermentations: Microbial alternatives for the halal food industry. *Trends in Food Science & Technology*, 98, 1-9.

Karesh, W., and Machalaba, C. (2012). Animal health and biodiversity: preparing for the future. Compendium of the OIE Global Conference on Wildlife, Paris, France. In *Animal health and biodiversity: preparing for the future. Compendium of the OIE Global Conference on Wildlife, Paris, France.*

Kennedy, J., Delaney, L., McGloin, A., and Wall, P. G. (2009). Public perceptions of the dioxin crisis in Irish pork.

Kerman, K., Vestergaard, M. d., Nagatani, N., Takamura, Y., and Tamiya, E. (2006). Electrochemical genosensor based on peptide nucleic acid-mediated PCR and asymmetric PCR techniques: electrostatic interactions with a metal cation. *Analytical chemistry, 78*(7), 2182-2189.

Khalil, I., Julkapli, N., Yehye, W., Basirun, W., and Bhargava, S. (2016). Graphene–gold nanoparticles hybrid—synthesis, functionalization, and application in a electrochemical and surface-enhanced raman scattering biosensor. *Materials, 9*(6), 406.

Khalil, I., Rahmati, S., Muhd Julkapli, N., and Yehye, W. A. (2018). Graphene metal nanocomposites — Recent progress in electrochemical biosensing applications. *Journal of Industrial and Engineering Chemistry, 59*, 425-439.

Khalil, I., Yehye, W. A., Julkapli, N. M., Rahmati, S., Sina, A. A. I., Basirun, W. J., and Johan, M. R. (2019). Graphene oxide and gold nanoparticle based dual platform with short DNA probe for the PCR free DNA biosensing using surface-enhanced Raman scattering. *Biosensors and Bioelectronics, 131*, 214-223.

Khan, M. S., Vishakante, G. D., and Siddaramaiah, H. (2013). Gold nanoparticles: a paradigm shift in biomedical applications. *Advances in Colloid and Interface Science, 199*, 44-58.

Khansili, N., Rattu, G., and Krishna, P. M. (2018). Label-free optical biosensors for food and biological sensor applications. *Sensors and Actuators B: Chemical, 265*, 35-49.

Kiefer, W. (2011). *Surface enhanced Raman spectroscopy: analytical, biophysical and life science applications*: John Wiley & Sons.

Kiefer, W., and Schlücker, S. (2011). *Surface enhanced Raman spectroscopy: analytical, biophysical and life science applications*: John Wiley & Sons.

Kim, J. E., Choi, J. H., Colas, M., Kim, D. H., and Lee, H. (2016). Gold-based hybrid nanomaterials for biosensing and molecular diagnostic applications. *Biosensors and Bioelectronics, 80*, 543-559.

Kim, W. H., Lee, J. U., Song, S., Kim, S., Choi, Y. J., and Sim, S. J. (2019). A label-free, ultra-highly sensitive and multiplexed SERS nanoplasmonic biosensor for miRNA detection using a head-flocked gold nanopillar. *Analyst, 144*(5), 1768-1776.

Kneipp, K., Kneipp, H., and Bohr, H. G. (2006). Single-molecule SERS spectroscopy. In *Surface-Enhanced Raman Scattering* (pp. 261-277): Springer.

Kneipp, K., Wang, Y., Kneipp, H., Perelman, L. T., Itzkan, I., Dasari, R. R., and Feld, M. S. (1997). Single molecule detection using surface-enhanced Raman scattering (SERS). *Physical review letters, 78*(9), 1667.

Kong, X.-k., Chen, Q.-w., and Sun, Z.-y. (2013). Enhanced SERS of the complex substrate using Au supported on graphene with pyridine and R6G as the probe molecules. *Chemical Physics Letters, 564*, 54-59.

Kosuda, K., Bingham, J., Wustholz, K., and Van Duyne, R. (2010). Nanostructures and surface-enhanced Raman spectroscopy. *Handbook of Nanoscale Optics and Electronics*, 309.

Kowitt, B. (2016). Analysis of Burger Market Finds Unwanted Ingredients: Rat and Human DNA. (Accessed on 23 June 2019), Retrieved from https://fortune.com/2016/05/10/burger-market-analysis-rat-human-dna/.

Krishnan, S. K., Singh, E., Singh, P., Meyyappan, M., and Nalwa, H. S. (2019). A review on graphene-based nanocomposites for electrochemical and fluorescent biosensors. *RSC Advances, 9*(16), 8778-8881.

Kumar, A., Das, N., Satija, N. K., Mandrah, K., Roy, S. K., and Rayavarapu, R. G. (2020). A novel approach towards synthesis and characterization of non-cytotoxic gold nanoparticles using taurine as capping agent. *Nanomaterials*, 10(1), 45.

Kumar, D., Singh, S., Karabasanavar, N. S., Singh, R., and Umapathi, V. (2014). Authentication of beef, carabeef, chevon, mutton and pork by a PCR-RFLP assay of mitochondrial cytb gene. *Journal of food science technology, 51*(11), 3458-3463.

Kumar, S., Gandhi, K., and Kumar, R. (2007). Modeling of formation of gold nanoparticles by citrate method. *Industrial & Engineering Chemistry Research, 46*(10), 3128-3136.

Kumar, Y., and Karne, S. C. (2017). Spectral analysis: A rapid tool for species detection in meat products. *Trends in food science & technology*, *62*, 59-67.

Kung, C.-C., Lin, P.-Y., Buse, F. J., Xue, Y., Yu, X., Dai, L., and Liu, C.-C. (2014). Preparation and characterization of three dimensional graphene foam supported platinum–ruthenium bimetallic nanocatalysts for hydrogen peroxide based electrochemical biosensors. *Biosensors and Bioelectronics, 52*, 1-7.

Kuswandi, B., Gani, A. A., and Ahmad, M. J. F. b. (2017). Immuno strip test for detection of pork adulteration in cooked meatballs. *19*, 1-6.

Kwak, M., Lee, S., Kim, D., Park, S.-K., and Piao, Y. (2016). Facile synthesis of Au-graphene nanocomposite for the selective determination of dopamine. *Journal of Electroanalytical Chemistry*, 776, 66-73.

Kwon, G., Kim, J., Kim, D., Ko, Y., Yamauchi, Y., and You, J. (2019). Nanoporous cellulose paper-based SERS platform for multiplex detection of hazardous pesticides. *Cellulose, 26*(8), 4935-4944.

Laestadius, L. I., and Wolfson, J. A. (2019). Unsustainable societal demands on the food system. In *Environmental Nutrition* (pp. 75-100). Academic Press.

Larson, G., Dobney, K., Albarella, U., Fang, M., Matisoo-Smith, E., Robins, J., Lowden, S., Finlayson, H., Brand, T. and Willerslev, E. (2005). Worldwide phylogeography of wild boar reveals multiple centers of pig domestication. *Science, 307*(5715), 1618-1621.

Le Ru, E. C., and Etchegoin, P. G. (2012). Single-molecule surface-enhanced Raman spectroscopy. *Annual Review of Physical Chemistry, 63*, 65-87.

Lee, J.-H., Kim, M.-R., Jo, C.-H., Jung, Y.-K., Kwon, K., and Kang, T. S. (2016). Specific PCR assays to determine bovine, porcine, fish and plant origin of gelatin capsules of dietary supplements. *Food Chemistry, 211*, 253-259.

Lee, J., Shim, S., Kim, B., and Shin, H. S. (2011). Surface-Enhanced Raman Scattering of Single-and Few-Layer Graphene by the Deposition of Gold Nanoparticles. *Chemistry-A European Journal, 17*(8), 2381-2387.

Lee, J. U., Lee, W., Yoon, S. S., Kim, J., and Byun, J. H. (2014). Site-selective immobilization of gold nanoparticles on graphene sheets and its electrochemical properties. *Applied Surface Science, 315*, 73-80.

Lee, T. (2008). Over-the-counter biosensors: Past, present, and future. *Sensors, 8*(9), 5535-5559.

Leinonen, I., Iannetta, P. P. M., Rees, R. M., Russell, W., Watson, C., and Barnes, A. (2019). Lysine supply is a critical factor in achieving sustainable global protein economy. *Frontiers in Sustainable Food Systems, 3*, 27.

Li, N., Wang, J., Shen, Q., Li, F., Xu, J., and Jiang, T. (2016a). Survey of duck, chicken and pork component in lamb or beef slices sold in Beijing. *Chineses journal of food hygiene, 26*, 227-232.

Li, C., Zheng, B., Zhang, T., Zhao, J., Gu, Y., Yan, X., Li, Y., Liu, W., Feng, G., and Zhang, Z. (2016b). Petal-like graphene–Ag composites with highly exposed active edge sites were designed and constructed for electrochemical determination of metronidazole. *RSC Advances, 6*(51), 45202-45209.

Li, Y., Yang, J., Zhou, Y.-z., Zhong, T., Zheng, S.-h., and Zeng, W.-w. (2016c). Facile synthesis of gold nanoparticles-graphene oxide films and their excellent surface-enhanced Raman scattering activity. *Monatshefte für Chemie-Chemical Monthly, 147*(4), 677-683.

Li, H., and Rothberg, L. (2004). Colorimetric detection of DNA sequences based on electrostatic interactions with unmodified gold nanoparticles. *Proceedings of the National Academy of Sciences of the United States of America, 101*(39), 14036-14039.

Li, W., Li, Y., Wu, Y., Liao, J., Qi, T., Li, H., Li, J., Zhang, X., and Qian, Z. (2015a). A Nonenzymatic Electrochemical Immunosensor for Ultrasensitive Detection of Tumor Biomarkers Based on Palladium Nanoparticles Conjugated Reduced Graphene Nanosheets. *Journal of biomedical nanotechnology, 11*(11), 2050-2056.

Li, J.-J., An, H.-Q., Zhu, J., and Zhao, J.-W. (2015b). Improve the surface enhanced Raman scattering of gold nanorods decorated graphene oxide: The effect of CTAB on the electronic transition. *Applied Surface Science, 347*, 856-860.

Li, M., Zhang, J., Suri, S., Sooter, L. J., Ma, D., and Wu, N. (2012). Detection of adenosine triphosphate with an aptamer biosensor based on surface-enhanced Raman scattering. *Analytical chemistry, 84*(6), 2837-2842.

Li, Y., Ding, X., Li, D., Wu, H., Huang, W., and Ding, S. (2019a). A homogeneous fluorescent biosensing strategy for highly sensitive detection of DNA based on a programmed entropy-driven strand displacement reaction and DNAzyme for dual recycling amplification. *Analytical Methods, 11*(12), 1613-1619.

Li, T. T., Jalbani, Y. M., Zhang, G. L., Zhao, Z. Y., Wang, Z. Y., Zhao, X. Y., and Chen, A. L. (2019b). Detection of goat meat adulteration by real-time PCR based on a reference primer. *Food Chemistry, 277*, 554-557.

Li, X.-H., Zhang, X.-L., Wu, J., Lin, N., Sun, W.-M., Chen, M., Ou, Q.-S., and Lin, Z.-Y. (2019c). Hyperbranched rolling circle amplification (HRCA)-based fluorescence biosensor for ultrasensitive and specific detection of single-nucleotide polymorphism genotyping associated with the therapy of chronic hepatitis B virus infection. *Talanta, 191*, 277-282.

Li, Y.-J., Xiang, J., and Zhou, F. (2007). Sensitive and label-free detection of DNA by surface plasmon resonance. *Plasmonics, 2*(2), 79-87.

Li, Y., Cu, Y. T. H., and Luo, D. (2005). Multiplexed detection of pathogen DNA with DNA-based fluorescence nanobarcodes. *Nature biotechnology, 23*(7), 885.

Liang, J., Zhou, J., Tan, J., Wang, Z., and Deng, L. (2019). Aptamer-Based Fluorescent Determination of Salmonella paratyphi A Using Phi29-DNA Polymerase-Assisted Cyclic Amplification. *Analytical Letters, 52*(6), 919-931.

Liang, X., Liang, B., Pan, Z., Lang, X., Zhang, Y., Wang, G., Yin, P., and Guo, L. (2015). Tuning plasmonic and chemical enhancement for SERS detection on graphene-based Au hybrids. *Nanoscale*, 7(47), 20188-20196.

Lin, T.-W., Wu, H.-Y., Tasi, T.-T., Lai, Y.-H., and Shen, H.-H. (2015). Surface-enhanced Raman spectroscopy for DNA detection by the self-assembly of Ag nanoparticles onto Ag nanoparticle–graphene oxide nanocomposites. *17*(28), 18443-18448.

Ling, X., Xie, L., Fang, Y., Xu, H., Zhang, H., Kong, J., Dresselhaus, M. S. and Liu, Z. (2009). Can graphene be used as a substrate for Raman enhancement? *Nano letters, 10*(2), 553-561.

Liu, B., and Liu, J. (2017). Methods for preparing DNA-functionalized gold nanoparticles, a key reagent of bioanalytical chemistry. *Analytical Methods, 9*(18), 2633-2643.

Liu, C., Jiang, D., Xiang, G., Liu, L., Liu, F., and Pu, X. (2014b). An electrochemical DNA biosensor for the detection of mycobacterium tuberculosis, based on signal

amplification of graphene and a gold nanoparticle–polyaniline nanocomposite. *Analyst, 139*(21), 5460-5465.

Liu, H., Chen, X., Huang, L., Wang, J., and Pan, H. (2014a). Palladium Nanoparticles Embedded into Graphene Nanosheets: Preparation, Characterization, and Nonenzymatic Electrochemical Detection of H2O2. *Electroanalysis, 26*(3), 556-564.

Liu, J., and Lu, Y. (2006). Preparation of aptamer-linked gold nanoparticle purple aggregates for colorimetric sensing of analytes. *Nature protocols, 1*(1), 246.

Liu, M., Zheng, C., Cui, M., Zhang, X., Yang, D.-P., Wang, X., and Cui, D. (2018). Graphene oxide wrapped with gold nanorods as a tag in a SERS based immunoassay for the hepatitis B surface antigen. *Microchimica Acta, 185*(10), 458.

Liu, R., Wang, Q., Li, Q., Yang, X., Wang, K., and Nie, W. (2017). Surface plasmon resonance biosensor for sensitive detection of microRNA and cancer cell using multiple signal amplification strategy. *Biosensors and Bioelectronics, 87*, 433-438.

Liu, R., Wang, X., Wang, X., Shi, Y., Shi, C., Wang, W., and Ma, C. (2019). A simple isothermal nucleic acid amplification method for the effective on-site identification for adulteration of pork source in mutton. *Food Control, 98*, 297-302.

Lowenstein, J. M., Reuther, J. D., Hood, D. G., Scheuenstuhl, G., Gerlach, S. C., and Ubelaker, D. H. (2006). Identification of animal species by protein radioimmunoassay of bone fragments and bloodstained stone tools. *Forensic Science International, 159*(2-3), 182-188.

Lu, G., Li, H., Liusman, C., Yin, Z., Wu, S., and Zhang, H. (2011). Surface enhanced Raman scattering of Ag or Au nanoparticle-decorated reduced graphene oxide for detection of aromatic molecules. *Chemical Science, 2*(9), 1817-1821.

Lucarelli, F., Tombelli, S., Minunni, M., Marrazza, G., and Mascini, M. (2008). Electrochemical and piezoelectric DNA biosensors for hybridisation detection. *Analytica Chimica Acta, 609*(2), 139-159.

Lynch, H., Berardy, A., & Wharton, C. (2019). Food production and dietary patterns. In *Environmental Nutrition* (pp. 101-122). Academic Press.

Ma, K., Wang, R., Jiao, T., Zhou, J., Zhang, L., Li, J., Bai, Z., and Peng, Q. (2020). Preparation and aggregate state regulation of co-assembly graphene oxide-porphyrin composite Langmuir films via surface-modified graphene oxide sheets. *Colloids and Surfaces A: Physicochemical and Engineering Aspects*, 584, 124023.

Ma, Q., Li, P., Gao, Z., and Li, S. F. Y. (2019). Rapid, sensitive and highly specific label-free fluorescence biosensor for microRNA by branched rolling circle amplification. *Sensors and Actuators B: Chemical, 281*, 424-431.

Ma, X., and Miao, P. (2019). Silver nanoparticle@ DNA tetrahedron-based colorimetric detection of HIV-related DNA with cascade strand displacement amplification. *Journal of Materials Chemistry B*, *7*(16), 2608-2612.

Ma, X., Qu, Q., Zhao, Y., Luo, Z., Zhao, Y., Ng, K. W., and Zhao, Y. (2013). Graphene oxide wrapped gold nanoparticles for intracellular Raman imaging and drug delivery. *Journal of Materials Chemistry B, 1*(47), 6495-6500.

Mackin, K. M. (2019). Meat and Poultry Wrap, Salad Products recalled for Listeria in facility. Food Safety News. (Accessed on 23 June 2019). Retrieved from https://www.foodsafetynews.com/2019/04/meat-and-poultry-wrap-salad-products-recalled-for-listeria-in-facility/.

Maede, D. (2006). A strategy for molecular species detection in meat and meat products by PCR-RFLP and DNA sequencing using mitochondrial and chromosomal genetic sequences. *European Food Research Technology, 224*(2), 209-217.

Mafra, I., Ferreira, I. M., and Oliveira, M. B. P. (2008). Food authentication by PCR-based methods. *European Food Research Technology, 227*(3), 649-665.

Maher, R. C. (2012). SERS hot spots. In *Raman spectroscopy for nanomaterials characterization* (pp. 215-260). Springer, Berlin, Heidelberg.

Mandli, J., Fatimi, I. E., Seddaoui, N., and Amine, A. (2018). Enzyme immunoassay (ELISA/immunosensor) for a sensitive detection of pork adulteration in meat. *Food Chemistry, 255*, 380-389.

Mane, B. G., Mendiratta, S. K., and Tiwari, A. K. (2012). Beef specific polymerase chain reaction assay for authentication of meat and meat products. *Food Control, 28*(2), 246-249.

Manikandan, M., Abdelhamid, H. N., Talib, A., and Wu, H.-F. (2014). Facile synthesis of gold nanohexagons on graphene templates in Raman spectroscopy for biosensing cancer and cancer stem cells. *Biosensors and Bioelectronics, 55*, 180-186.

Manzanares Palenzuela, C. L., Pourrahimi, A. M., Sofer, Z. k., and Pumera, M. (2019). Mix-and-Read No-Wash Fluorescence DNA Sensing System Using Graphene Oxide: Analytical Performance of Fresh Versus Aged Dispersions. *ACS Omega, 4*(1), 1611-1616.

Marbaix, H., Budinger, D., Dieu, M., Fumière, O., Gillard, N., Delahaut, P., Mauro, S., and Raes, M. (2016). Identification of Proteins and Peptide Biomarkers for Detecting Banned Processed Animal Proteins (PAPs) in Meat and Bone Meal by Mass Spectrometry. *Journal of Agricultural and Food Chemistry, 64*(11), 2405-2414.

Marcano, D. C., Kosynkin, D. V., Berlin, J. M., Sinitskii, A., Sun, Z., Slesarev, A., Alemany, L.B., Lu, W., and Tour, J. M. (2010). Improved Synthesis of Graphene Oxide. *ACS Nano, 4*(8), 4806-4814.

Marikkar, J., Ghazali, H., Man, Y. C., Peiris, T., and Lai, O. (2005). Distinguishing lard from other animal fats in admixtures of some vegetable oils using liquid chromatographic data coupled with multivariate data analysis. *Food Chemistry, 91*(1), 5-14.

Martin, R., Azcona, J. I., Casas, C., Hernandez, P. E., and Sanz, B. (1988). Sandwich ELISA for detection of pig meat in raw beef using antisera to muscle soluble proteins. *Journal of food protection, 51*(10), 790-798.

Martins, T. D., Ribeiro, A. C. C., de Camargo, H. S., da Costa Filho, P. A., Cavalcante, H. P. M., and Dias, D. L. (2013). New insights on optical biosensors: techniques, construction and application. *State of the Art in Biosensors—General Aspects*, 112-139.

Mathew, V. N. (2014). Acceptance on halal food among non-Muslim consumers. *Procedia-Social and Behavioral Sciences, 121*, 262-271.

Mazorra-Manzano, M. A., Torres-Llanez, M. J., González-Córdova, A. F., and Vallejo-Cordoba, B. (2012). A capillary electrophoresis method for the determination of hydroxyproline as a collagen content index in meat products. *Food Analytical Methods, 5*(3), 464-470.

Merkoçi, A. (2010). Nanoparticles-based strategies for DNA, protein and cell sensors. *Biosensors and Bioelectronics, 26*(4), 1164-1177.

Meyer-Rochow, V. B. (2009). Food taboos: their origins and purposes. *Journal of ethnobiology and ethnomedicine, 5*(1), 18.

Mikoliunaite, L., Rodriguez, R. D., Sheremet, E., Kolchuzhin, V., Mehner, J., Ramanavicius, A., and Zahn, D. R. (2015). The substrate matters in the Raman spectroscopy analysis of cells. *Scientific reports*, 5, 13150.

Milton, J. A., Patole, S., Yin, H., Xiao, Q., Brown, T., and Melvin, T. (2013). Efficient self-assembly of DNA-functionalized fluorophores and gold nanoparticles with DNA functionalized silicon surfaces: the effect of oligomer spacers. *Nucleic acids research, 41*(7), e80-e80.

Montowska, M., Alexander, M. R., Tucker, G. A., and Barrett, D. A. (2014). Rapid detection of peptide markers for authentication purposes in raw and cooked meat using ambient liquid extraction surface analysis mass spectrometry. *Analytical chemistry, 86*(20), 10257-10265.

Montowska, M., Alexander, M. R., Tucker, G. A., and Barrett, D. A. (2015). Authentication of processed meat products by peptidomic analysis using rapid ambient mass spectrometry. *Food Chemistry, 187*, 297-304.

Montowska, M., & Pospiech, E. (2007). Species identification of meat by electrophoretic methods. *Acta Scientiarum Polonorum Technologia Alimentaria, 6*(1), 5-16.

Montowska, M., & Pospiech, E. (2013). Species-specific expression of various proteins in meat tissue: proteomic analysis of raw and cooked meat and meat products

made from beef, pork and selected poultry species. *Food chemistry*, *136*(3-4), 1461-1469.

Moon, H., Kumar, D., Kim, H., Sim, C., Chang, J.-H., Kim, J.-M., Kim, H., and Lim, D.-K. (2015). Amplified photoacoustic performance and enhanced photothermal stability of reduced graphene oxide coated gold nanorods for sensitive photoacoustic imaging. *ACS Nano*, 9(3), 2711-2719.

Mucic, R. C., Storhoff, J. J., Mirkin, C. A., and Letsinger, R. L. (1998). DNA-Directed Synthesis of Binary Nanoparticle Network Materials. *Journal of the American Chemical Society, 120*(48), 12674-12675.

Muench, F., Solomonov, A., Bendikov, T., Molina-Luna, L., Rubinstein, I., and Vaskevich, A. (2019). Empowering Electroless Plating to Produce Silver Nanoparticle Films for DNA Biosensing Using Localized Surface Plasmon Resonance Spectroscopy. *ACS Applied Bio Materials, 2*(2), 856-864.

Murray, I., Aucott, L. S., and Pike, I. H. (2001). Use of discriminant analysis on visible and near infrared reflectance spectra to detect adulteration of fishmeal with meat and bone meal. *Journal of Near Infrared Spectroscopy, 9*(4), 297-311.

Murugaiah, C., Noor, Z. M., Mastakim, M., Bilung, L. M., Selamat, J., and Radu, S. (2009). Meat species identification and Halal authentication analysis using mitochondrial DNA. *Meat Science, 83*(1), 57-61.

Nakyinsige, K., Man, Y. B. C., & Sazili, A. Q. (2012). Halal authenticity issues in meat and meat products. *Meat Science, 91*(3), 207-214.

Nejad, F. P., Tafvizi, F., Ebrahimi, M. T., and Hosseni, S. E. (2014). Optimization of multiplex PCR for the identification of animal species using mitochondrial genes in sausages. *European Food Research and Technology, 239*(3), 533-541.

Ngo, H. T., Wang, H.-N., Burke, T., Ginsburg, G. S., and Vo-Dinh, T. (2014b). Multiplex detection of disease biomarkers using SERS molecular sentinel-on-chip. *Analytical and bioanalytical chemistry, 406*(14), 3335-3344.

Ngo, H. T., Wang, H.-N., Fales, A. M., Nicholson, B. P., Woods, C. W., and Vo-Dinh, T. (2014a). DNA bioassay-on-chip using SERS detection for dengue diagnosis. *Analyst, 139*(22), 5655-5659.

Ngo, H. T., Wang, H.-N., Fales, A. M., and Vo-Dinh, T. (2013). Label-free DNA biosensor based on SERS molecular sentinel on nanowave chip. *Analytical chemistry, 85*(13), 6378-6383.

Ngo, H. T., Wang, H.-N., Fales, A. M., and Vo-Dinh, T. (2016). Plasmonic SERS biosensing nanochips for DNA detection. *Analytical and bioanalytical chemistry, 408*(7), 1773-1781.

Nguyen, H., Park, J., Kang, S., and Kim, M. (2015). Surface plasmon resonance: a versatile technique for biosensor applications. *Sensors, 15*(5), 10481-10510.

Nguyen, T. H., Zhang, Z., Mustapha, A., Li, H., and Lin, M. (2014). Use of graphene and gold nanorods as substrates for the detection of pesticides by surface enhanced Raman spectroscopy. *Journal of Agricultural and Food Chemistry, 62*(43), 10445-10451.

Nhari, R. R., Hanish, I., Mokhtar, N. K., Hamid, M., and El Sheikha, A. (2019). Authentication approach using enzyme-linked immunosorbent assay for detection

Ni, F., Sheng, R., and Cotton, T. M. (1990). Flow-injection analysis and real-time detection of RNA bases by surface-enhanced Raman spectroscopy. *Analytical chemistry, 62*(18), 1958-1963.

Nie, S., and Emory, S. R. (1997). Probing single molecules and single nanoparticles by surface-enhanced Raman scattering. *Science, 275*(5303), 1102-1106.

Niemz, A., Ferguson, T. M., and Boyle, D. S. (2011). Point-of-care nucleic acid testing for infectious diseases. *Trends in biotechnology, 29*(5), 240-250.

Ning, T., Liao, F., Cui, H., Yin, Z., Ma, G., Cheng, L., Hong, N., Xiong, F., and Fan, H. (2020). A homogeneous electrochemical DNA sensor on the basis of a self-assembled thiol layer on a gold support and by using tetraferrocene for signal amplification. *Microchimica Acta*, 187(6).

Nizar, N. N. A., Marikkar, J. M. N., and Hashim, D. M. (2013). Differentiation of lard, chicken fat, beef fat and mutton fat by GCMS and EA-IRMS techniques. *Journal of Oleo Science, 62*(7), 459-464.

Nizar, N. N. A., Zainal, I. H., Bonny, S. Q., Pulingam, T., Vythalingam, L. M., and Ali, M. E. (2018). DNA and nanobiosensor technology for the detection of adulteration and microbial contamination in religious food. *In Preparation and Processing of Religious and Cultural Foods* (pp. 409-431): Elsevier.

Nizar, N. N. A., Hossain, M., Sultana, S., Ahamad, M. N., Johan, M. R., and Ali, M. E. (2019). Quantitative duplex real-time polymerase chain reaction assay with TaqMan probe detects and quantifies Crocodylus porosus in food chain and traditional medicines. *Food Additives & Contaminants: Part A*, 1-11.

Nurjuliana, M., Man, Y. C., Hashim, D. M., and Mohamed, A. (2011). Rapid identification of pork for halal authentication using the electronic nose and gas chromatography mass spectrometer with headspace analyzer. *Meat Science, 88*(4), 638-644.

Nurrulhidayah, A., Che Man, Y., Amin, I., Arieff Salleh, R., Farawahidah, M., Shuhaimi, M., and Khatib, A. (2015). FTIR-ATR spectroscopy based metabolite fingerprinting as a direct determination of butter adulterated with lard. *International journal of food properties, 18*(2), 372-379.

O'mahony, P. (2013). Finding horse meat in beef products—a global problem. *QJM: An International Journal of Medicine, 106*(6), 595-597.

O'Mullane, A. P., Ippolito, S. J., Sabri, Y. M., Bansal, V., and Bhargava, S. K. (2009). Premonolayer oxidation of nanostructured gold: An important factor influencing electrocatalytic activity. *Langmuir, 25*(6), 3845-3852.

OECD-FAO. (2017). *OECD-FAO agricultural outlook 2017-2026*: OECD Publishing.

OECD. (2019). Meat consumption. (Accessed on 28 June 2019). Retrieved from https://data.oecd.org/agroutput/meat-consumption.htm

Pal, D., Boby, N., Kumar, S., Kaur, G., Ali, S. A., Reboud, J., Shrivastava, S., Gupta, P.K., Cooper, J.M. and Chaudhuri, P. (2017). Visual detection of Brucella in bovine biological samples using DNA-activated gold nanoparticles. *PLOS ONE, 12*(7), e0180919.

Pal, S., Deng, Z., Wang, H., Zou, S., Liu, Y., & Yan, H. (2011). DNA directed self-assembly of anisotropic plasmonic nanostructures. *Journal of the American Chemical Society, 133*(44), 17606-17609.

Pan, H.-z., Yu, H.-w., Wang, N., Zhang, Z., Wan, G.-c., Liu, H., Guan, X., and Chang, D. (2015). Electrochemical DNA biosensor based on a glassy carbon electrode modified with gold nanoparticles and graphene for sensitive determination of Klebsiella pneumoniae carbapenemase. *Journal of biotechnology, 214*, 133-138.

Pandey, C. M., Sumana, G., and Malhotra, B. D. (2011). Microstructured cystine dendrites-based impedimetric sensor for nucleic acid detection. *Biomacromolecules, 12*(8), 2925-2932.

Papetti, A., and Colombo, R. (2019). High-performance capillary electrophoresis for food quality evaluation. In *Evaluation Technologies for Food Quality* (pp. 301-377). Woodhead Publishing.

Park, C., Park, H., Lee, H. J., Lee, H. S., Park, K. H., Choi, C.-H., and Na, S. (2019). Double amplified colorimetric detection of DNA using gold nanoparticles, enzymes and a catalytic hairpin assembly. *Microchimica Acta, 186*(1), 34.

Park, S.-J., Taton, T. A., and Mirkin, C. A. (2002). Array-based electrical detection of DNA with nanoparticle probes. *Science, 295*(5559), 1503-1506.

Pearson, A., O'Mullane, A. P., Bhargava, S. K., and Bansal, V. (2012). Comparison of nanostructures obtained from galvanic replacement in water and an ionic liquid for applications in electrocatalysis and SERS. *Electrochemistry Communications, 25*, 87-90.

Peng, H.-P., Hu, Y., Liu, P., Deng, Y.-N., Wang, P., Chen, W., Liu, A.-L., Chen. Y.-Z., and Lin, X.-H. (2015). Label-free electrochemical DNA biosensor for rapid detection of mutidrug resistance gene based on Au nanoparticles/toluidine blue–graphene oxide nanocomposites. *Sensors and Actuators B: Chemical, 207*, 269-276.

Peng, X., Zhang, Y., Lu, D., Guo, Y., and Guo, S. (2019). Ultrathin Ti_3C_2 nanosheets based "off-on" fluorescent nanoprobe for rapid and sensitive detection of HPV infection. *Sensors and Actuators B: Chemical, 286*, 222-229.

Perumal, V., and Hashim, U. (2014). Advances in biosensors: Principle, architecture and applications. *Journal of Applied Biomedicine, 12*(1), 1-15.

Phillips, R. L., Miranda, O. R., You, C. C., Rotello, V. M., and Bunz, U. H. (2008). Rapid and Efficient Identification of Bacteria Using Gold-Nanoparticle–Poly (para-phenyleneethynylene) Constructs. *Angewandte Chemie International Edition, 47*(14), 2590-2594.

Picariello, G., De Martino, A., Mamone, G., Ferranti, P., Addeo, F., Faccia, M., SpangnaMusso, S., and Di Luccia, A. (2006). Proteomic study of muscle sarcoplasmic proteins using AUT-PAGE/SDS-PAGE as two-dimensional gel electrophoresis. *Journal of Chromatography B, 833*(1), 101-108.

Plowman, B., Ippolito, S. J., Bansal, V., Sabri, Y. M., O'Mullane, A. P., and Bhargava, S. K. (2009). Gold nanospikes formed through a simple electrochemical route with high electrocatalytic and surface enhanced Raman scattering activity. *Chemical Communications*(33), 5039-5041.

Pocklanova, R., Rathi, A. K., Gawande, M. B., Datta, K. K. R., Ranc, V., Cepe, K., Petr, M., Varma, R.S., Kvitek, L., and Zboril, R. (2016). Gold nanoparticle-decorated graphene oxide: Synthesis and application in oxidation reactions under benign conditions. *Journal of Molecular Catalysis A: Chemical, 424*, 121-127.

Pohanka, M., and Skládal, P. (2008). Electrochemical biosensors--principles and applications. *Journal of Applied Biomedicine, 6*(2).

Prabowo, B. A., Alom, A., Secario, M. K., Masim, F. C. P., Lai, H.-C., Hatanaka, K., and Liu, K.-C. (2016). Graphene-based portable SPR sensor for the detection of Mycobacterium tuberculosis DNA strain. *Procedia Engineering, 168*, 541-545.

Premanandh, J. (2013). Horse meat scandal–A wake-up call for regulatory authorities. *Food control*, *34*(2), 568-569.

Prinz, J., Matković, A., Pešić, J., Gajić, R., and Bald, I. (2016). Hybrid Structures for Surface-Enhanced Raman Scattering: DNA Origami/Gold Nanoparticle Dimer/Graphene. *Small, 12*(39), 5458-5467.

Qian, X., Zhou, X., and Nie, S. (2008). Surface-enhanced Raman nanoparticle beacons based on bioconjugated gold nanocrystals and long range plasmonic coupling. *Journal of the American Chemical Society, 130*(45), 14934-14935.

Qian, Y., Fan, T., Yao, Y., Shi, X., Liao, X., Zhou, F., and Gao, F. (2018). Label-free and Raman dyes-free surface-enhanced Raman spectroscopy for detection of DNA. *Sensors and Actuators B: Chemical, 254*, 483-489.

Qin, P., Qu, W., Xu, J., Qiao, D., Yao, L., Xue, F., and Chen, W. (2019). A sensitive multiplex PCR protocol for simultaneous detection of chicken, duck, and pork in beef samples. Journal of food science and technology, 56(3), 1266-1274.

Qiu, C., Zhou, H., Cao, B., Sun, L., and Yu, T. (2013). Raman spectroscopy of morphology-controlled deposition of Au on graphene. *Carbon, 59*, 487-494.

Qiu, C., and Hou, M. (2020). Association between Food Preferences, Eating Behaviors and Socio-Demographic Factors, Physical Activity among Children and Adolescents: A Cross-Sectional Study. *Nutrients*, 12(3), 640.

Qlark Jr, L. (1956). Monitor and control of blood and tissue oxygen tensions. *ASAIO Journal, 2*(1), 41-48.

Quinto, C. A., Tinoco, R., and Hellberg, R. S. (2016). DNA barcoding reveals mislabeling of game meat species on the U.S. commercial market. *Food Control, 59*, 386-392.

Rady, A., and Adedeji, A. (2018). Assessing different processed meats for adulterants using visible-near-infrared spectroscopy. *Meat Science, 136*, 59-67.

Radziuk, D., and Moehwald, H. (2015). Prospects for plasmonic hot spots in single molecule SERS towards the chemical imaging of live cells. *Physical Chemistry Chemical Physics, 17*(33), 21072-21093.

Rahman, M. (2015). Development of canine biomarker based detection and quantification assays for determining food adulteration and halal authentication/Md. Mahfujur Rahman (*Doctoral dissertation, University of Malaya*).

Rahmati, S., Julkapli, N. M., Yehye, W. A., and Basirun, W. J. (2016). Identification of meat origin in food products–A review. *Food Control, 68*, 379-390.

Rao, Q., and Hsieh, Y.-H. P. (2007). Evaluation of a commercial lateral flow feed test for rapid detection of beef and sheep content in raw and cooked meats. *Meat Science, 76*(3), 489-494.

Rashid, J. I. A., and Yusof, N. A. (2017). The strategies of DNA immobilization and hybridization detection mechanism in the construction of electrochemical DNA sensor: A review. *Sensing and Bio-Sensing Research, 16*, 19-31.

Regenstein, J. M., Chaudry, M. M., and Regenstein, C. E. (2003). The kosher and halal food laws. *Comprehensive Reviews in Food Science and Food Safety, 2*(3), 111-127.

Regenstein, J. M. (2020). Kosher and Halal: How They Affect Muslim and Jewish Dietary Practices. *Handbook of Eating and Drinking: Interdisciplinary Perspectives*, 593-614.

Rischkowsky, B., and Pilling, D. (2007). *The state of the world's animal genetic resources for food and agriculture.* Food & Agriculture Org.

Rohman, A., and Che Man, Y. (2010). FTIR spectroscopy combined with chemometrics for analysis of lard in the mixtures with body fats of lamb, cow, and chicken. *International Food Research Journal, 17*(3), 519-526.

Rohman, A., Sismindari, Erwanto, Y., and Che Man, Y. B. (2011). Analysis of pork adulteration in beef meatball using Fourier transform infrared (FTIR) spectroscopy. *Meat Science, 88*(1), 91-95.

Rojas, M., Gonzalez, I., Pavon, M. A., Pegels, N., Lago, A., Hernandez, P. E., Garcia, T., and Martin, R. (2010). Novel TaqMan real-time polymerase chain reaction assay for verifying the authenticity of meat and commercial meat products from game birds. *Food Additives and Contaminants, 27*(6), 749-763.

Roy, S., Mohd-Naim, N. F., Safavieh, M., and Ahmed, M. U. (2017). Colorimetric nucleic acid detection on paper microchip using loop mediated isothermal amplification and crystal violet dye. *ACS sensors*, *2*(11), 1713-1720.

Roy, S., Rahman, I. A., Santos, J. H., and Ahmed, M. U. (2016). Meat species identification using DNA-redox electrostatic interactions and non-specific adsorption on graphene biochips. *Food Control, 61*, 70-78.

Saez, R., Sanz, Y., and Toldra, F. (2004). PCR-based fingerprinting techniques for rapid detection of animal species in meat products. *Meat Science, 66*(3), 659-665.

Saidur, M. R., Aziz, A. R. A., and Basirun, W. J. (2017). Recent advances in DNA-based electrochemical biosensors for heavy metal ion detection: A review. *Biosensors and Bioelectronics, 90*, 125-139.

Sanchez-Cortes, S., Garcıa-Ramos, J., Morcillo, G., and Tinti, A. (1995). Morphological study of silver colloids employed in surface-enhanced Raman spectroscopy: Activation when exciting in visible and near-infrared regions. *Journal of colloid and interface science, 175*(2), 358-368.

Sans, P., and Combris, P. (2015). World meat consumption patterns: An overview of the last fifty years (1961–2011). *Meat Science, 109*, 106-111.

Sassolas, A., Leca-Bouvier, B. D., and Blum, L. J. (2008). DNA biosensors and microarrays. *Chemical reviews, 108*(1), 109-139.

Sattarahmady, N., Tondro, G. H., Gholchin, M., and Heli, H. (2015). Gold nanoparticles biosensor of Brucella spp. genomic DNA: Visual and spectrophotometric detections. *Biochemical Engineering Journal, 97*, 1-7.

Saud, S., Li, G., Sun, Y., Khan, M. I., Rehman, A. U., Uzzaman, A., Liu, W., Ding, C., Xiao, H., and Wang, Y. (2019). A facile isoelectric focusing of myoglobin and hemoglobin used as markers for screening of chicken meat quality in China. *Electrophoresis*.

Scallan, E., Hoekstra, R. M., Angulo, F. J., Tauxe, R. V., Widdowson, M.-A., Roy, S. L., Jones, J.L., and Griffin, P. M. (2011). Foodborne illness acquired in the United States—major pathogens. *Emerging infectious diseases*, 17(1), 7.

Schatz, G. C., Young, M. A., and Van Duyne, R. P. (2006). Electromagnetic mechanism of SERS. In *Surface-enhanced Raman scattering* (pp. 19-45): Springer.

Scheijen, J. L. J. M., Clevers, E., Engelen, L., Dagnelie, P. C., Brouns, F., Stehouwer, C. D. A., and Schalkwijk, C. G. (2016). Analysis of advanced glycation endproducts in selected food items by ultra-performance liquid chromatography tandem mass spectrometry: Presentation of a dietary AGE database. *Food Chemistry, 190*, 1145-1150.

Schlücker, S. (2009). SERS microscopy: nanoparticle probes and biomedical applications. *ChemPhysChem, 10*(9-10), 1344-1354.

Schoppe, S. (2008). The Southeast Asian Box Turtle Cuora amboinensis (Daudin, 1802) in Malaysia. In *NDF Workshop Case Studies, Doc. WG*.

Selvakannan, P., Ramanathan, R., Plowman, B. J., Sabri, Y. M., Daima, H. K., O'Mullane, A. P., bansal, V., and Bhargava, S. K. (2013). Probing the effect of charge transfer enhancement in off resonance mode SERS via conjugation of the probe dye between silver nanoparticles and metal substrates. *Physical Chemistry Chemical Physics, 15*(31), 12920-12929.

Shahrokhian, S., and Salimian, R. (2018). Ultrasensitive detection of cancer biomarkers using conducting polymer/electrochemically reduced graphene oxide-based biosensor: Application toward BRCA1 sensing. *Sensors and Actuators B: Chemical, 266*, 160-169.

Sharma, D. K., Ott, A., O'Mullane, A. P., and Bhargava, S. K. (2011). The facile formation of silver dendritic structures in the absence of surfactants and their electrochemical and SERS properties. *Colloids and Surfaces A: Physicochemical and Engineering Aspects, 386*(1), 98-106.

Shendure, J., and Ji, H. (2008). Next-generation DNA sequencing. *Nature biotechnology*, 26(10), 1135-1145.

Shiohara, A., Wang, Y., and Liz-Marzán, L. M. (2014). Recent approaches toward creation of hot spots for SERS detection. *Journal of Photochemistry Photobiology C: Photochemistry Reviews, 21*, 2-25.

Si, Y., and Samulski, E. T. (2008). Exfoliated graphene separated by platinum nanoparticles. *Chemistry of Materials, 20*(21), 6792-6797.

Skarpeid, H.-J., Moe, R. E., and Indahl, U. G. (2001). Detection of mechanically recovered meat and head meat from cattle in ground beef mixtures by multivariate analysis of isoelectric focusing protein profiles. *Meat Science, 57*(3), 227-234.

Skarpeid, H. J., Kvaal, K., and Hildrum, K. I. (1998). Identification of animal species in ground meat mixtures by multivariate analysis of isoelectric focusing protein profiles. *Electrophoresis, 19*(18), 3103-3109.

Skouridou, V., Tomaso, H., Rau, J., Bashammakh, A. S., El-Shahawi, M. S., Alyoubi, A. O., and O'Sullivan, C. K. (2019). Duplex PCR-ELONA for the detection of pork adulteration in meat products. *Food Chemistry, 287*, 354-362.

Sonntag, M. D., Klingsporn, J. M., Zrimsek, A. B., Sharma, B., Ruvuna, L. K., and Van Duyne, R. P. (2014). Molecular plasmonics for nanoscale spectroscopy. *Chemical Society Reviews, 43*(4), 1230-1247.

Steel, A. B., Herne, T. M., and Tarlov, M. J. (1998). Electrochemical quantitation of DNA immobilized on gold. *Analytical chemistry, 70*(22), 4670-4677.

Stiles, P. L., Dieringer, J. A., Shah, N. C., and Van Duyne, R. P. (2008). Surface-enhanced Raman spectroscopy. *Annu. Rev. Anal. Chem., 1*, 601-626.

Storhoff, J. J., Lazarides, A. A., Mucic, R. C., Mirkin, C. A., Letsinger, R. L., and Schatz, G. C. (2000). What Controls the Optical Properties of DNA-Linked Gold Nanoparticle Assemblies? *Journal of the American Chemical Society, 122*(19), 4640-4650.

Subrahmanyam, K. S., Manna, A. K., Pati, S. K., and Rao, C. N. R. (2010). A study of graphene decorated with metal nanoparticles. *Chemical Physics Letters, 497*(1), 70-75.

Sultana, S., Hossain, M. M., Naquiah, N. N. A., and Ali, M. E. (2018). Novel multiplex PCR-RFLP assay discriminates bovine, porcine and fish gelatin substitution in Asian pharmaceuticals capsule shells. *Food Additives & Contaminants: Part A, 35*(9), 1662-1673.

Sun, L., Yu, C., and Irudayaraj, J. (2007). Surface-enhanced Raman scattering based nonfluorescent probe for multiplex DNA detection. *Analytical chemistry, 79*(11), 3981-3988.

Sun, W., Wang, X., Lu, Y., Gong, S., Qi, X., Lei, B., Sun, Z., and Li, G. (2015a). Electrochemical deoxyribonucleic acid biosensor based on electrodeposited graphene and nickel oxide nanoparticle modified electrode for the detection of salmonella enteritidis gene sequence. *Materials Science and Engineering: C, 49*, 34-39.

Sun, X., Jia, M., Guan, L., Ji, J., Zhang, Y., Tang, L., and Li, Z. (2015b). Multilayer graphene–gold nanocomposite modified stem-loop DNA biosensor for peanut allergen-Ara h1 detection. *Food Chemistry, 172*, 335-342.

Sun, Y.-H., Kong, R.-M., Lu, D.-Q., Zhang, X.-B., Meng, H.-M., Tan, W., Shen, G.-L., and Yu, R.-Q. (2011). A nanoscale DNA–Au dendrimer as a signal amplifier for the universal design of functional DNA-based SERS biosensors. *Chemical Communications, 47*(13), 3840-3842.

Szabo, A., Febel, H., Sugar, L., and Romvari, R. (2007). Fatty acid regiodistribution analysis of divergent animal triacylglycerol samples–a possible approach for species differentiation. *Journal of food lipids, 14*(1), 62-77.

Talemi, R. P., and Mousavi, S. M. (2017). A novel colorimetric DNA biosensor for genetic assay purpose based on gold nanoparticles self-assembled onto a functionalized glass surface. *Journal of the Taiwan Institute of Chemical Engineers, 76*, 44-50.

Tamura, K., Peterson, D., Peterson, N., Stecher, G., Nei, M., and Kumar, S. (2011). MEGA5: molecular evolutionary genetics analysis using maximum likelihood, evolutionary distance, and maximum parsimony methods. *Molecular biology and evolution, 28*(10), 2731-2739.

Tao, G., and Wang, J. (2018). Gold nanorod@ nanoparticle seed-SERSnanotags/graphene oxide plasmonic superstructured nanocomposities as an "on-off" SERS aptasensor. *Carbon, 133*, 209-217.

Taylor, L. H., Latham, S. M., and Woolhouse, M. E. (2001). Risk factors for human disease emergence. *Philosophical Transactions of the Royal Society of London. Series B: Biological Sciences, 356*(1411), 983-989.

Thavanathan, J., Huang, N. M., and Thong, K. L. (2014). Colorimetric detection of DNA hybridization based on a dual platform of gold nanoparticles and graphene oxide. *Biosensors and Bioelectronics, 55*, 91-98.

Thévenot, D. R., Toth, K., Durst, R. A., and Wilson, G. (2001). Electrochemical biosensors: recommended definitions and classification. *Analytical Letters*, *34*(5), 635-659.

Thienes, C. P., Masiri, J., Benoit, L. A., Barrios-Lopez, B., Samuel, S. A., Krebs, R. A., Cox, D.P., Dobritsa, A.P., Nadala, C., and Samadpour, M. (2019). Quantitative Detection of Beef Contamination in Cooked Meat Products by ELISA. *Journal of AOAC International, 102*(3), 898-902.

Tien, H.-W., Huang, Y.-L., Yang, S.-Y., Wang, J.-Y., and Ma, C.-C. M. (2011). The production of graphene nanosheets decorated with silver nanoparticles for use in transparent, conductive films. *Carbon, 49*(5), 1550-1560.

Tiwari, I., Gupta, M., Pandey, C. M., and Mishra, V. (2015). Gold nanoparticle decorated graphene sheet-polypyrrole based nanocomposite: its synthesis, characterization and genosensing application. *Dalton Transactions, 44*(35), 15557-15566.

Tiwari, V. S., Oleg, T., Darbha, G. K., Hardy, W., Singh, J., and Ray, P. C. (2007). Non-resonance SERS effects of silver colloids with different shapes. *Chemical Physics Letters, 446*(1-3), 77-82.

Tjong, V., Tang, L., Zauscher, S., and Chilkoti, A. (2014). "Smart" DNA interfaces. *Chemical Society Reviews, 43*(5), 1612-1626.

Tondro, G., Vais, R. D., and Sattarahmady, N. (2018). An optical genosensor for Enterococcus faecalis using conjugated gold nanoparticles-rRNA oligonucleotide. *Sensors and Actuators B: Chemical, 263*, 36-42.

Turna, J., Marcela, B., and Domenico, P. (2010). Polymerase chain reaction–restriction fragment length polymorphism (PCR-RFLP) as a molecular discrimination tool for raw and heat-treated game and domestic animal meats. *Journal of Food and Nutrition Research, 49*(3), 134-139.

USDA-FAS. (2018a). World Per Capita Pork Consumption. Pork Checkoff. (Accessed on 12 June 2020). Retrieved from https://www.pork.org/facts/stats/u-s-pork-exports/world-per-capita-pork-consumption/.

USDA-FAS. (2018b). Top 10 Pork-Producing Countries. Pork Checkoff. (Accessed on 12 June 2020). Retrieved from https://www.pork.org/facts/stats/u-s-pork-exports/top-10-pork-producing-countries/.

Vallejo-Cordoba, B., and Cota-Rivas, M. (1998). Meat species identification by linear discriminant analysis of capillary electrophoresis protein profiles. *Journal of Capillary Electrophoresis, 5*(5-6), 171-175.

Vallejo-Cordoba, B., González-Córdova, A. F., Mazorra-Manzano, M. A., and Rodríguez-Ramírez, R. (2005). Caillary electrophoresis for the analysis of meat authenticity. *Journal of separation science, 28*(9-10), 826-836.

Ventura, R. J., Ching, P. K., de los Reyes, V. C., Sucaldito, M. N., and Tayag, E. (2015). Chelonitoxism outbreak caused from consuming turtle, Eastern Samar, Philippines, August 2013. *Western Pacific surveillance and response journal: WPSAR, 6*(2), 12.

Vianna, P. G., Grasseschi, D., Costa, G. K., Carvalho, I. C., Domingues, S. H., Fontana, J., and de Matos, C. (2016). Graphene oxide/gold nanorod nanocomposite for stable surface-enhanced Raman spectroscopy. *ACS Photonics*, *3*(6), 1027-1035.

Vikrant, K., Bhardwaj, N., Bhardwaj, S. K., Kim, K.-H., and Deep, A. (2019). Nanomaterials as efficient platforms for sensing DNA. *Biomaterials, 214*, 119215.

Vindas, K., Leroy, L., Garrigue, P., Voci, S., Livache, T., Arbault, S., Sojic, N., Buhot, A., and Engel, E. (2019). Highly parallel remote SPR detection of DNA hybridization by micropillar optical arrays. *Analytical and bioanalytical chemistry*, 1-11.

Vo-Dinh, T. (2008). Nanobiosensing using plasmonic nanoprobes. *IEEE Journal of Selected Topics in Quantum Electronics*, *14*(1), 198-205.

von Bargen, C., Dojahn, J., Waidelich, D., Humpf, H.-U., and Brockmeyer, J. (2013). New sensitive high-performance liquid chromatography–tandem mass spectrometry method for the detection of horse and pork in halal beef. *Journal of Agricultural and Food Chemistry, 61*(49), 11986-11994.

Wabuyele, M. B., and Vo-Dinh, T. (2005). Detection of human immunodeficiency virus type 1 DNA sequence using plasmonics nanoprobes. *Analytical chemistry, 77*(23), 7810-7815.

Walker, M. J., Burns, M., and Burns, D. T. (2013). Horse meat in beef products - species substitution 2013. *Journal of the Association of Public Analysts, 41*, 67-106.

Wang, H.-N., Fales, A. M., and Vo-Dinh, T. (2015c). Plasmonics-based SERS nanobiosensor for homogeneous nucleic acid detection. *Nanomedicine: Nanotechnology, Biology and Medicine, 11*(4), 811-814.

Wang, H.-N., and Vo-Dinh, T. (2009). Multiplex detection of breast cancer biomarkers using plasmonic molecular sentinel nanoprobes. *Nanotechnology, 20*(6), 065101.

Wang, J., Shi, A., Fang, X., Han, X., and Zhang, Y. (2014). Ultrasensitive electrochemical supersandwich DNA biosensor using a glassy carbon electrode modified with gold particle-decorated sheets of graphene oxide. *Microchimica Acta, 181*(9-10), 935-940.

Wang, J., Shi, A., Fang, X., Han, X., and Zhang, Y. (2015a). An ultrasensitive supersandwich electrochemical DNA biosensor based on gold nanoparticles decorated reduced graphene oxide. *Analytical biochemistry, 469*, 71-75.

Wang, Q., Li, Q., Yang, X., Wang, K., Du, S., Zhang, H., and Nie, Y. (2016a). Graphene oxide–gold nanoparticles hybrids-based surface plasmon resonance for sensitive detection of microRNA. *Biosensors and Bioelectronics, 77*, 1001-1007.

Wang, Q., Liu, R., Yang, X., Wang, K., Zhu, J., He, L., and Li, Q. (2016b). Surface plasmon resonance biosensor for enzyme-free amplified microRNA detection based on gold nanoparticles and DNA supersandwich. *Sensors and Actuators B: Chemical, 223*, 613-620.

Wang, Q., Zhang, B., Lin, X., and Weng, W. (2011). Hybridization biosensor based on the covalent immobilization of probe DNA on chitosan–mutiwalled carbon nanotubes nanocomposite by using glutaraldehyde as an arm linker. *Sensors and Actuators B: Chemical, 156*(2), 599-605.

Wang, Q., Zou, L., Yang, X., Liu, X., Nie, W., Zheng, Y., Cheng, Q, and Wang, K. (2019). Direct quantification of cancerous exosomes via surface plasmon resonance with dual gold nanoparticle-assisted signal amplification. *Biosensors and Bioelectronics, 135*, 129-136.

Wang, W., He, D., Duan, J., Wang, S., Peng, H., Wu, H., Fu, M., Wang, Y., and Zhang, X. (2013). Simple synthesis method of reduced graphene oxide/gold nanoparticle and its application in surface-enhanced Raman scattering. *Chemical Physics Letters, 582*, 119-122.

Wang, X., Li, G., Liu, L., Cheng, Y., Zheng, W., Wu, S., Wu, F., and Sun, W. (2015b). Application of titanium dioxide nanowires and electroreduced graphene oxide modified electrodes for the electrochemical detection of specific tlh gene sequence from Vibrio parahaemolyticus. *Analytical Methods, 7*(6), 2623-2629.

Wang, X., and Son, A. (2013). Effects of pretreatment on the denaturation and fragmentation of genomic DNA for DNA hybridization. *Environmental Science: Processes & Impacts, 15*(12), 2204-2212.

Wang, Y., Ni, Z., Hu, H., Hao, Y., Wong, C. P., Yu, T., Thong, J. T., and Shen, Z. X. (2010). Gold on graphene as a substrate for surface enhanced Raman scattering study. *Applied Physics Letters, 97*(16), 163111.

Wang, Y., Yan, B., and Chen, L. (2012b). SERS tags: novel optical nanoprobes for bioanalysis. *Chemical reviews, 113*(3), 1391-1428.

Wang, Z., Zhang, J., Yin, Z., Wu, S., Mandler, D., and Zhang, H. (2012a). Fabrication of nanoelectrode ensembles by electrodepositon of Au nanoparticles on single-layer graphene oxide sheets. *Nanoscale, 4*(8), 2728-2733.

Watanabe, H., Hayazawa, N., Inouye, Y., and Kawata, S. (2005). DFT vibrational calculations of rhodamine 6G adsorbed on silver: analysis of tip-enhanced Raman spectroscopy. *The Journal of Physical Chemistry B*, 109(11), 5012-5020.

Wei, H., Li, B., Li, J., Wang, E., and Dong, S. (2007). Simple and sensitive aptamer-based colorimetric sensing of protein using unmodified gold nanoparticle probes. *Chem. Commun.*(36), 3735-3737.

Whitworth, E., Druckman, A., and Woodward, A. (2017). Food scares: a comprehensive categorisation. *British Food Journal*, *119*(1), 131-142.

WJC. (2018). Operation Dragon: New evidence of the scale of corruption in the illegal turtle and tortoise trade in Southeast Asia. Wildlife Justice Commission. Accessed on 27 June 2019. Retrieved from https://wildlifejustice.org/operation-dragon-new-evidence-of-the-scale-of-corruption-in-the-illegal-turtle-and-tortoise-trade-in-southeast-asia/.

Woodhouse, A. (2015). US$6m turtle meat shipment bound for Hong Kong seized in Pakistan. *South China* Morning Post. (Accessed on 27 June 2019). Retrieved from https://www.scmp.com/news/hong-kong/article/1732213/us6m-turtle-meat-shipment-bound-hong-kong-seized-pakistan.

Wu, Z.-S., Zhou, G., Yin, L.-C., Ren, W., Li, F., and Cheng, H.-M. (2012). Graphene/metal oxide composite electrode materials for energy storage. *Nano Energy, 1*(1), 107-131.

Xia, F., White, R. J., Zuo, X., Patterson, A., Xiao, Y., Kang, D., Gong, X., Plaxco, K.W., and Heeger, A. J. (2010). An electrochemical supersandwich assay for sensitive and selective DNA detection in complex matrices. *Journal of the American Chemical Society, 132*(41), 14346-14348.

Xia, H., Xiahou, Y., Zhang, P., Ding, W., and Wang, D. (2016). Revitalizing the Frens method to synthesize uniform, quasi-spherical gold nanoparticles with deliberately regulated sizes from 2 to 330 nm. *Langmuir*, 32(23), 5870-5880.

Xing, X.-J., Xiao, W.-L., Liu, X.-G., Zhou, Y., Pang, D.-W., and Tang, H.-W. (2016). A fluorescent aptasensor using double-stranded DNA/graphene oxide as the indicator probe. *Biosensors and Bioelectronics, 78*, 431-437.

Xing, Y., Han, J., Wu, X., Pierce, D. T., and Zhao, J. X. (2020). Aggregation-based determination of mercury (II) using DNA-modified single gold nanoparticle, T-Hg (II)-T interaction, and single-particle ICP-MS. *Microchimica Acta*, 187(1), 56.

Xu, C., Lan, L., Yao, Y., Ping, J., Li, Y., and Ying, Y. (2018b). An unmodified gold nanorods-based DNA colorimetric biosensor with enzyme-free hybridization chain reaction amplification. *Sensors and Actuators B: Chemical, 273*, 642-648.

Xu, H., Michael, Y. S., Cromer, R., Penn, S. G., Holland, E., Chakarova, G., & Natan, M. J. (2012). Portable SERS sensor for sensitive detection of food-borne pathogens. In *Raman Spectroscopy for Nanomaterials Characterization* (pp. 531-551): Springer.

Xu, L.-J., Lei, Z.-C., Li, J., Zong, C., Yang, C. J., and Ren, B. (2015). Label-free surface-enhanced Raman spectroscopy detection of DNA with single-base sensitivity. *Journal of the American Chemical Society, 137*(15), 5149-5154.

Xu, Q., Lou, X., Wang, L., Ding, X., Yu, H., and Xiao, Y. (2016). Rapid, Surfactant-Free, and Quantitative Functionalization of Gold Nanoparticles with Thiolated DNA under Physiological pH and Its Application in Molecular Beacon-Based Biosensor. *ACS applied materials & interfaces, 8*(40), 27298-27304.

Xu, R., Wei, S., Zhou, G., Ren, J., Liu, Z., Tang, S., Cheung, P.C. and Wu, X. (2018a). Multiplex TaqMan locked nucleic acid real-time PCR for the differential identification of various meat and meat products. *Meat science*, *137*, 41-46.

Xu, W., Mao, N., & Zhang, J. (2013a). Graphene: A Platform for Surface-Enhanced Raman Spectroscopy. *Small, 9*(8), 1206-1224.

Xu, W., Xiao, J., Chen, Y., Chen, Y., Ling, X., and Zhang, J. (2013b). Graphene-Veiled Gold Substrate for Surface-Enhanced Raman Spectroscopy. *Advanced Materials, 25*(6), 928-933.

Xu, W., Zhao, A., Zuo, F., Khan, R., Hussain, H. M. J., and Li, J. (2020). A highly sensitive DNAzyme-based SERS biosensor for quantitative detection of lead ions in human serum. *Analytical and Bioanalytical Chemistry*.

Xue, T., Liang, W., Li, Y., Sun, Y., Xiang, Y., Zhang, Y., Dai, Z., Duo, Y., Wu, L., and. Qi, K. (2019). Ultrasensitive detection of miRNA with an antimonene-based surface plasmon resonance sensor. *Nature communications, 10*(1), 28.

Yáñez-Sedeño, P., Agüí, L., Villalonga, R., and Pingarrón, J. M. (2014). Biosensors in forensic analysis. A review. *Analytica Chimica Acta, 823*, 1-19.

Yarbakht, M., Nikkhah, M., Moshaii, A., Weber, K., Matthäus, C., Cialla-May, D., and Popp, J. (2018). Simultaneous isolation and detection of single breast cancer cells using surface-enhanced Raman spectroscopy. *Talanta, 186*, 44-52.

Yola, M. L., Eren, T., and Atar, N. (2014). A novel and sensitive electrochemical DNA biosensor based on Fe@ Au nanoparticles decorated graphene oxide. *Electrochimica Acta, 125*, 38-47.

Yoo, E.-H., and Lee, S.-Y. (2010). Glucose biosensors: an overview of use in clinical practice. *Sensors, 10*(5), 4558-4576.

Zeng, Q., Liu, Y., Liu, Q., Liu, P., He, Y., and Zeng, Y. (2020). Preparation and modification mechanism analysis of graphene oxide modified asphalts. *Construction and Building Materials*, 238, 117706.

Zhang, D., Yan, Y., Li, Q., Yu, T., Cheng, W., Wang, L., Ju, H., and Ding, S. (2012a). Label-free and high-sensitive detection of Salmonella using a surface plasmon resonance DNA-based biosensor. *Journal of biotechnology, 160*(3-4), 123-128.

Zhang, H., Harpster, M. H., Park, H. J., Johnson, P. A., and Wilson, W. C. (2010). Surface-enhanced Raman scattering detection of DNA derived from the West Nile virus genome using magnetic capture of Raman-active gold nanoparticles. *Analytical chemistry, 83*(1), 254-260.

Zhang, H., Ma, X., Liu, Y., Duan, N., Wu, S., Wang, Z., and Xu, B. (2015). Gold nanoparticles enhanced SERS aptasensor for the simultaneous detection of Salmonella typhimurium and Staphylococcus aureus. *Biosensors and Bioelectronics, 74*, 872-877.

Zhang, H., Song, Z., Pan, F., and He, F. (2019). A surface-confined DNA assembly enabled target recycling amplification for multiplexed electrochemical DNA detection. *Journal of Electroanalytical Chemistry, 833*, 290-296.

Zhang, J., Song, S., Wang, L., Pan, D., and Fan, C. (2007). A gold nanoparticle-based chronocoulometric DNA sensor for amplified detection of DNA. *Nature protocols, 2*(11), 2888-2895.

Zhang, J., Sun, Y., Xu, B., Zhang, H., Gao, Y., Zhang, H., & Song, D. (2013a). A novel surface plasmon resonance biosensor based on graphene oxide decorated with gold nanorod–antibody conjugates for determination of transferrin. *Biosensors and Bioelectronics, 45*, 230-236.

Zhang, L., Jiang, C., & Zhang, Z. (2013b). Graphene oxide embedded sandwich nanostructures for enhanced Raman readout and their applications in pesticide monitoring. *Nanoscale, 5*(9), 3773-3779.

Zhang, Q., Ren, Q., Miao, Y., Yuan, J., Wang, K., Li, F., Han, D., and Niu, L. (2012b). One-step synthesis of graphene/polyallylamine–Au nanocomposites and their electrocatalysis toward oxygen reduction. *Talanta, 89*, 391-395.

Zhang, T., Wang, Y.-J., Guo, W., Luo, D., Wu, Y., Kučerová, Z., Stejskal, V., Opit, G., Cao, Y., Li, F.-J and Li, Z.-H. (2016). DNA barcoding, species-specific PCR and real-time PCR techniques for the identification of six Tribolium pests of stored products. *Scientific reports*, 6(1), 1-11.

Zhang, X., Gouriye, T., Göeken, K., Servos, M. R., Gill, R., & Liu, J. (2013c). Toward fast and quantitative modification of large gold nanoparticles by thiolated DNA: scaling of nanoscale forces, kinetics, and the need for thiol reduction. *The Journal of Physical Chemistry C, 117*(30), 15677-15684.

Zhang, Y., and Jiang, W. (2012). Decorating graphene sheets with gold nanoparticles for the detection of sequence-specific DNA. *Electrochimica Acta, 71*, 239-245.

Zhang, Z., Wen, Y., Ma, Y., Luo, J., Jiang, L., and Song, Y. (2011). Mixed DNA-functionalized nanoparticle probes for surface-enhanced Raman scattering-based multiplex DNA detection. *47*(26), 7407-7409.

Zhao, P., Li, N., and Astruc, D. (2013). State of the art in gold nanoparticle synthesis. *Coordination Chemistry Reviews, 257*(3-4), 638-665.

Zhao, X.-H., Ma, Q.-J., Wu, X.-X., and Zhu, X. (2012). Graphene oxide-based biosensor for sensitive fluorescence detection of DNA based on exonuclease III-aided signal amplification. *Analytica Chimica Acta, 727*, 67-70.

Zhong, Z., Patskovskyy, S., Bouvrette, P., Luong, J. H., and Gedanken, A. (2004). The surface chemistry of Au colloids and their interactions with functional amino acids. *The Journal of Physical Chemistry B, 108*(13), 4046-4052.

Zhou, W., Li, Q., Liu, H., Yang, J., and Liu, D. (2017). Building electromagnetic hot spots in living cells via target-triggered nanoparticle dimerization. *ACS Nano, 11*(4), 3532-3541.

Zhu, J., Gao, J., Li, J.-J., and Zhao, J.-W. (2014). Improve the surface-enhanced Raman scattering from rhodamine 6G adsorbed gold nanostars with vimineous branches. *Applied Surface Science, 322*, 136-142.

Zhu, X., Zheng, H., Wei, X., Lin, Z., Guo, L., Qiu, B., and Chen, G. (2013). Metal–organic framework (MOF): a novel sensing platform for biomolecules. *Chemical Communications, 49*(13), 1276-1278.

Zong, C., Chen, C.-J., Zhang, M., Wu, D.-Y., and Ren, B. (2015). Transient electrochemical surface-enhanced Raman spectroscopy: a millisecond time-resolved study of an electrochemical redox process. *Journal of the American Chemical Society*, *137*(36), 11768-11774.

Zou, S., and Schatz, G. C. (2006). Coupled plasmonic plasmon/photonic resonance effects in SERS. In *Surface-Enhanced Raman Scattering* (pp. 67-85): Springer.

LIST OF PUBLICATIONS AND PAPERS PRESENTED

List of Publications:

1. **Khalil, Ibrahim**, Wageeh A. Yehye*, Nurhidayatullaili Muhd Julkapli, Abu Ali Ibn Sina, Shahrooz Rahmati, Wan Jefrey Basirun, and Ali Seyfoddin. (2000). Dual platform based sandwich assay surface-enhanced Raman scattering DNA biosensor for the sensitive detection of food adulteration. Analyst, 145, 1414-1426.
2. **Khalil, Ibrahim**, Wageeh A. Yehye*, Nurhidayatullaili Muhd Julkapli, Shahrooz Rahmati, Abu Ali Ibn Sina, Wan Jefrey Basirun, and Mohd Rafie Johan. (2019). Graphene oxide and gold nanoparticle based dual platform with short DNA probe for the PCR free DNA biosensing using surface-enhanced Raman scattering. Biosensors and Bioelectronics 131, 214-223.
3. **Khalil, Ibrahim**, Shahrooz Rahmati, Nurhidayatullaili Muhd Julkapli*, and Wageeh A. Yehye. (2018). Graphene metal nanocomposites—Recent progress in electrochemical biosensing applications. Journal of industrial and engineering chemistry 59, 425-439.
4. **Khalil, Ibrahim**, Nurhidayatullaili Julkapli, Wageeh Yehye*, Wan Basirun, and Suresh Bhargava (2016). Graphene–gold nanoparticles hybrid—synthesis, functionalization, and application in a electrochemical and surface-enhanced Raman scattering biosensor. Materials 9 (6), 406.

Poster Presentation:

1. **Khalil, Ibrahim**, Wageeh A. Yehye, Nurhidayatullaili Muhd Julkapli, Shahrooz Rahmati, and Wan Jefrey Basirun. (2018). Nanoparticle Based Surface Enhance Raman Scattering (SERS) DNA Biosensor for the Sensitive Detection of Meat Adulteration. UMRC 2018 Poster Competition.
2. **Khalil, Ibrahim**, Wageeh A. Yehye, Nurhidayatullaili Muhd Julkapli, Shahrooz Rahmati, and Wan Jefrey Basirun. (2018). Graphene oxide and Gold nanoparticle based dual platform with short DNA probe for the fabrication of Efficient Surface Enhance Raman Scattering DNA Biosensor. CAM Postgraduate Symposium 2018.